The role of gut tissue in arthritis: unravelling glycomic and inflammatory networks underlying immunoregulation

Piaopiao Pan

A thesis submitted in fulfilment of the requirements for the degree of Doctor of Philosophy

School of Infection and Immunity,

College of Medical, Veterinary & Life Sciences,

University of Glasgow

January 2024

Abstract

Rheumatoid arthritis (RA) is a systemic autoimmune chronic disease, which affects not only joints, but skin, lungs, and heart as well. The pathogenesis of RA is complex and is not fully understood yet. Extensive research has focused on RA treatment, and induction of oral tolerance may be a promising therapeutic strategy. Collagen-derived products have been used to induce oral tolerance and undenatured type II collagen (UC-II), which preserves the physiological structure of collagen fibres, has shown an enhanced ability to induce tolerance, although its protective mechanism is not yet fully understood.

The intestinal mucosal site is a dynamic and multifunctional interface that is essential for nutrient absorption, immunological defence, microbiota interaction, and overall digestive and metabolic health. Its proper function is vital for maintaining overall well-being and preventing various gastrointestinal disorders. Recent studies found that dysbiosis at the intestinal mucosal site is associated with RA onset. Most research on the mucosal therapeutic potential in RA has focused on the modulation of immune and tolerogenic responses in the gut, while less attention has been given to stromal cells within the local microenvironment.

Glycans, covering all cell membranes, are pivotal to a wide range of biological functions including cell communication, cell adhesion, and cell signalling. They are a hidden player in the immunological regulation of health and inflammation. The role of glycosylation in intestinal homeostasis and microbial composition has increasingly gained attention over the past few years. Alterations in glycosylation have been observed in many intestinal diseases. However, whether glycosylation profiles in the gut change in RA remains unknown. There are still many gaps in our understanding of gut pathology and of how intestinal glycosylation may affect oral tolerance during RA.

In this study, we thus, hypothesized that the protective effects of UC-II are associated not only with the induction of oral tolerance but also with the restoration of gut tissue integrity. Here, we used the mouse Collagen-Induced Arthritis (CIA) model as a surrogate for RA and investigated UC-II-mediated protective mechanisms, combined with transcriptomic and glycomic analysis of gut tissue including stromal cells to explore the glycan-related pathways. Overall,

this work highlights the role of gut tissue in experimental arthritis, aiming to understand glycomic and inflammatory networks underlying oral tolerance induction by UC-II. This study will pave the way for novel therapeutic interventions targeting glycosylation/microbiota-related pathways in RA.

Table of Contents

List of Tables

List of Figures

Acknowledgements

I wish to express my unreserved gratitude to my supervisors Dr. Miguel A. Pineda, Prof. Simon Milling, and Prof. Margaret M. Harnett for all your support and guidance throughout the years.

I would like to express my deepest and sincerest gratitude to Miguel, none of these would be possible without your efforts and help since the very beginning. Thank you, Miguel, for always being there to encourage me every time I met challenges and difficulties, especially when I started my PhD during the pandemic. I will never forget the crazy night we spent together for animal experiments. Not only your academic knowledge but also your personality that inspired me so much. You have been a great friend to me and I am really lucky to have worked with you. I also would like to express my thanks to Maggie and Simon, for your invaluable guidance and suggestions throughout my PhD. I never deem I am a lucky person due to the incredibly hard road to my PhD, but I am so lucky to have you all by my side.

Thanks to all who helped me during my PhD. Many thanks to Prof. Stuart Haslam and Aristotelis Antonopoulos for their help with the MS experiment and analysis. Many thanks to Diane Vaughan for excellent training in flow cytometry and cell sorting. Thanks to Fiona McMonagle for the help with histology, and to Leandro and Susan for enhancing my microscopy knowledge. I would also like to express my thanks to Aneesah, Yilin, and Caglar for their assistance at the bench. I really enjoyed working and being friends with you. Also my thanks to Simon's lab and Kevin's lab members and the lovely people in level 4 who helped me with experiments.

I also wish to offer my thanks to my friends Kun, Xiang, Yiyi, Shutong, Zhaoyang, Jinyuan, Geng, Jiangfan, and Nawshin for your accompany, made my life in Glasgow so fantastic. Special thanks to Chang Liu for your support and understanding of my decisions and please accept my sincere apologies for breaking my promise. I cherish all my memories with you all.

Special thanks to Dr. Tao Zhang for your support, accompaniment, and meticulous love. You have lightened my life. I also want to thank my parents for their love and support, and my apologies for being away and letting you be concerned about me for all these years.

The funding of Lonza and the University of Glasgow is also gratefully acknowledged.

In honour of all the mice that are sacrificed in science.

To all scientific researchers who dedicated days and nights to protect humanity from disease.

Author's Declaration

"I declare that, except where explicit reference is made to the contribution of others, that this dissertation is the result of my own work and has not been submitted for any other degree at the University of Glasgow or any other institution."

Printed Name: PIAOPIAO PAN

Signature: _____

Abbreviation

AAL	Aleuria aurantia lectin
ACPAs	Antibodies to citrullinated protein antigens
AIA	Adjuvant-induced arthritis
AMPs	Antimicrobial peptides
APCs	Antigen presenting cells
Asn	Asparagine
BMP	Bone morphogenetic proteins
C-II	Collagen type II
CCL	Chemokine ligand
CFA	Complete Freund's adjuvant
CIA	Collagen-induced arthritis
ConA	Concanavalin A
CRD	Carbohydrate recognition domain
CTL	Cytotoxic T lymphocyte
DCs	Dendritic cells
DMARDs	Disease-modifying antirheumatic drugs
Dol-P	Dolichol-phosphate
EAE	Experimental autoimmune encephalomyelitis
ECM	Extracellular matrix
ELISA	Enzyme-linked immunosorbent assay
Env	Envelope
ER	Endoplasmic reticulum
Fab	Antigen-binding fragment
FAE	Follicular-associated epithelia
FBS	Fetal bovine serum
Fcγbp	Fc-γ binding protein
FLS	Fibroblast-like synoviocytes
Fut	Fucosyltransferase
GAGs	Proteoglycans and glycosaminoglycans
GalNAc	N-acetylgalactosamine
GALT	Gastrointestinal associated lymphoid tissue
GBPs	Glycan binding proteins
GI	Gastrointestinal

GlcNAc	N-acetylglucosamine
GO	Gene Ontology
GSLs	Glycosphingolipids
H&E	Haematoxylin and eosin
HLA	Human leukocyte antigen
HSPH1	Heat shock protein family H member 1
IBD	Inflammatory bowel disease
IBS	Irritable bowel syndrome
ID injection	Intradermal injection
IECs	Intestinal epithelial cells
IEL	Intraepithelial layer
IgG	Immunoglolbulin G
IL	Interleukin
ILCs	Innate lymphoid cells
KEGG	Kyoto Encyclopedia of Genes and Genomes
KGF	Keratinocyte growth factor
KikGR	Kikume green-red
M cell	Microfold cells
MAA II	Maackia aurensis lectin II
MFI	mean fluorescence intensity
MHC	Major histocompatibility complex
MMP3	Matrix metalloproteinases 3
MS	Mass spectrometry
Myd88	Myeloid differentiation priamary response 88
NBF	neutral buffered formalin
NF-κB	Nuclear factor kappa B
NSAIDs	Non-steroidal anti-inflammatory drugs
PBS	Phosphate buffered saline
PCA	Principal component analysis
PDGFRα	Platelet-derived growth factor receptors alpha
PDPN	Podopanin
PHA	Phytohaemagglutinin
PNA	Peanut agglutinin
PPs	Peyer's patches
PRRs	Pattern Recognition Receptors

PRRs	Pattern recognition receptors
PTPN22	Phosphatase non-receptor 22
qPCR	Quantitative polymerase chain reaction
RA	Rheumatoid arthritis
RANKL	Receptor activator of nuclear factor κB ligand
RCA I	Ricinus Communis Agglutiniin I
RegIII	Regenerating islet-derived protein 3
RELMß	Resistin-like molecule ß
RF	Rheumatoid factor
SCWIA	Streptococcal cell wall induced arthritis
SED	Subepithelial dome
Ser	Serine
Siglecs	Sialic acid-binding immunoglobulin-type lectins
SNA	Sambuccus nigra agglutinin
SpA	Spondylarthritis
TGF-b	Transforming growth factor-beta
Thr	Threonine
TLR	Toll-like receptor
TNF-a	Tumour necrosis factor-alpha
UC	Ulcerative colitis
UEA I	Ulex Europaeus Agglutinin I

Chapter 1 General introduction

1.1 Rheumatoid arthritis

Rheumatoid arthritis (RA) is an autoimmune condition affecting articular joints and leads to inflammation of the synovium a highly specialized tissue that lines along the spaces of diarthrodial joints (Figure 1-1). It is one of the most prevalent forms of inflammatory arthritis, causing inflammation, pain, and stiffness in the joints. In developed countries, approximately 0.5-1.0% of adults suffer from RA, and women are 2-3 times more likely to have arthritis than men (Brennan-Olsen et al., 2017). While it primarily targets the joints, RA can also impact other organs and systems in the body (Figure 1-1). If insufficiently treated, RA can lead to accumulating joint damage and irreversible disability.

1.1.1 The pathogenesis of RA

The pathogenesis of RA is a complex and multifaceted process involving various genetic and environmental factors (Smolen et al., 2018). While the exact cause of RA remains unknown, certain genetic factors, particularly related to the immune system, have been identified as contributing to an increased risk of developing the disease (Figure 1-2). For example, variations in the human leukocyte antigen (HLA) genes, especially the HLA-DRB1 gene, are among the most significant genetic risk factors for RA (Mcinnes et al., 2011). Variations in the enzyme tyrosine phosphatase non-receptor 22 (PTPN22) gene have also been linked to an increased risk of RA. This gene is involved in regulating immune cell signalling that leads to T-cell activation. For example, it can act as a negative regulator of T-cell activation by dephosphorylating key tyrosine residues in signalling molecules (Tizaoui et al., 2021, Bottini et al., 2006). Thus, mutations in the PTPN22 gene can result in hyperactive T cells and increase the likelihood of immune system cells attacking the body's own tissues (Tizaoui et al., 2021). Certain PTPN22 variants can lead to dysregulated immune responses and an increased susceptibility to autoimmune diseases, providing a second genetic link to RA (Vang et al., 2005).

Apart from genetic factors, it is also known that environmental effects can play a key role in disease initiation and progression. For example, smoking can induce post-translational modifications leading to major histocompatibility complex (MHC) presentation of modified self-proteins to T cells. As a result, autoimmune responses are initiated, including the production of self-reactive antibodies against immunoglobulin G (Rheumatoid Factor, RF), antibodies to citrullinated protein antigens (ACPAs) (Holers, 2013, Muller et al., 2015) or the cartilage component collagen type II (C-II) (Cook et al., 1996). RF can be detected in 60-80% of RA patients. Autoantibodies like RF can be useful as diagnostic tools for various rheumatic and non-rheumatic autoimmune disorders (Smolen, 2002). Other environmental factors such as infections, microbiota, hormonal factors, diet, obesity, occupational exposures and stress, are likely responsible for disease onset in susceptible individuals (Mcinnes et al., 2011, Smolen et al., 2018).

Although RA is a systemic disease and a variety of immunological events occur outside the joint, the synovium is the main target tissue (Figure 1-2). A healthy synovium is a delicate structure with an intimal lining composed of macrophage-like synoviocytes and fibroblast-like synoviocytes (FLS) and a sublining membrane composed of fibroblasts, adipocytes, blood vessels and scattered immune cells. Two key pathogenetic changes in the synovium are evident in RA. First, the intimal lining greatly expands owing to an increase and activation of both synoviocyte types (Mcinnes et al., 2011), which are a prominent source of cytokines and proteases. The second change is the infiltration of adaptive immune cells into the synovial sublining (Ziff, 1974). Progression of RA pathogenesis is mainly due to the immune-mediated destruction of bone and cartilage such as synovial lining hyperplasia, inflammation, cell infiltration and formation of the pannus, an abnormal layer of tissue formed by macrophages and fibroblast that invades and degrades bone and cartilage (Dennis Jr, 2014).

Cytokines regulate a broad range of inflammatory responses and play a crucial role in the pathogenesis of RA (Figure 1-2c). The pro-inflammatory cytokines, tumour necrosis factor-alpha (TNF-α), produced by macrophages and T cells, is one of the major cytokines driving inflammation in RA (Mcinnes et al., 2007). TNF-α leads to the destruction of joint tissues, contributing to joint pain and swelling. Interleukin-1 (IL-1) (both α and ß), another cytokine implicated in RA, promotes the production of matrix metalloproteinases (MMPs), which degrade joint cartilage

and bone (Figure 1-2c) (Dayer et al., 2017). interleukin-17 (IL-17) is produced by a subset of T cells known as Th17 cells. It promotes inflammation and induces the production of other pro-inflammatory cytokines, as well as chemokines that attract immune cells to the joints (Hu et al., 2011, Moseley et al., 2003). While anti-inflammatory cytokines, such as interleukin-10 (IL-10) and transforming growth factor-beta (TGF-ß), aim to suppress the inflammatory response. TGF-ß can promote tissue repair and regeneration, but it can also contribute to fibrosis and joint damage if dysregulated (Gonzalo-Gil et al., 2014).

While genetics play a role in RA susceptibility, environmental factors also play significant roles in the development and progression of RA (Figure 1-2). Understanding the interplay between these is vital for developing targeted therapies and personalized approaches to manage RA and improve the quality of life for individuals affected by this chronic autoimmune disease.

1.1.2 Treatment of RA

Although there is no cure for RA, the treatment of RA has evolved significantly over the years, and nowadays, there are various effective approaches to managing the disease. The primary goals of standard RA treatments are to reduce inflammation, relieve pain, prevent joint damage, improve physical function, and enhance the overall quality of life for individuals living with the condition.

The first choice usually involves non-steroidal anti-inflammatory drugs (NSAIDs) such as ibuprofen, naproxen and diclofenac. They are widely used in RA especially in the very early phase of RA to alleviate symptoms (Scheiman, 2016) and are often used in combination with disease-modifying antirheumatic drugs (DMARDs) to provide symptomatic relief. DMARDs are a cornerstone of treatment. These drugs work to slow down the progression of the disease and prevent joint damage by targeting the underlying autoimmune response. Methotrexate is often the first line DMARD used due to its proven effectiveness and relatively good safety profile. Other DMARDs, such as sulfasalazine, leflunomide, and hydroxychloroquine, may also be prescribed alone or in combination with methotrexate or other DMARDs. Biologic DMARDs, such as TNF-α inhibitors (e.g., adalimumab, etanercept) (Nam et al., 2017, Fleischmann et al., 2017), IL-6 inhibitors (e.g., tocilizumab) (Smolen

et al., 2017), and other targeted therapies, are used for more severe or refractory cases of RA.

Glucocorticoids are potent anti-inflammatory and anti-allergic drugs that can rapidly and significantly improve the symptoms of arthritis. Short-term use of glucocorticoids may be prescribed to rapidly reduce inflammation during RA flare-ups, but glucocorticoids can cause a broad spectrum of adverse effects over a long period, such as skin atrophy, osteoporosis, disturbed glucose tolerance, hypertension, elevated intraocular pressure, cataract development and a higher risk of infections (Strehl et al., 2016).

The treatment of RA typically not only involves a combination of medication, but lifestyle changes (balanced diet, avoiding smoking, managing stress and etc) (Stamp et al., 2005, Smolen et al., 2018), and sometimes surgical interventions. Despite the relative success of these drugs in the clinic, there are still patients who do not respond to them. This could be because some RA phenotypes may rely on non-haematopoietic cells and also adverse effects of current drugs, suggesting that some pathological pathways in RA remain unknown. In addition, whilst most research has been focused on systemic responses and latterly, the joint, the role of inflammation in distant locations such as the gut mucosa has been studied less over the past decades. In recent years, however, gut mucosal immune responses associated with RA have attracted attention and may provide a breakthrough for novel therapeutic approaches.

1.2 Mucosal immunology in the gut

The intestine contains a high density of immune system cells, and it is one of the most pivotal organs in the body since it is the place where food (foreign antigen) is digested, and a huge number of microorganisms can enter our body. Increasingly, attention has been focused on the immunology of the intestine as its dysregulation is associated with many diseases such as inflammatory bowel disease (IBD), irritable bowel syndrome (IBS), celiac disease, and food allergy (Zhang et al., 2014, Canavan et al., 2014, Caio et al., 2019).

1.2.1 The anatomy of the intestine

The intestine can be divided into the small intestine and the large intestine (also known as colon). The small intestine comprises the duodenum, jejunum, and ileum (Figure 1-3a). The small intestine is characterized by finger-like projections facing lumen known as villi (Figure 1-3b), which increase the surface area to have a better digestion and absorption of food and nutrients. Villi are absent in the cecum and colon. The surface epithelium is continuously renewed by immature cells from crypts of Lieberkühn, where the intestinal stem cells reside and proliferate to replenish the epithelial layer (Mowat et al., 2014). Although the entire small intestine contains dispersed lymphoid tissue, immune system cells accumulate in specific areas, the Peyer's patches (PPs) that are only found in ileum. PPs provide the main anatomical difference between ileum and jejunum. The cecum is located between the ileum and colon, and is where most of water, vitamins and vital salts contained in the stool are absorbed. The colon can be divided into the ascending colon, transverse colon, descending colon, and sigmoid colon. The colon is characterised by elongated crypts, reaching deep into the mucosa, and it has a high density of bacteria.

Cross-sectionally, the intestine can be divided into several layers: the mucosa (epithelial layer and lamina propria), muscularis mucosae (a thin muscle layer), the submucosa (area of connective tissue), and muscle layer (Figure 1-3b) (Mowat et al., 2014). Most immune responses occur in the mucosa as it contains many innate and adaptive immune cells.

1.2.2 The mucus barrier

The first contact of bacteria, food or antigens in our intestine is the mucus barrier, and its integrity is one of the first lines of protection of the gastrointestinal tract to maintain health. The mucus, covering the intestinal epithelial surface, is a complex aqueous fluid which contains specific mucus proteins called mucins (Bansil et al., 2018). The mucus is secreted by goblet/mucous cells in the epithelium (Figure 1-3b). There are two layers of mucus in the colon, while only a single layer in the small intestine (Birchenough et al., 2015). The mucus in the ileum is embedded with antibodies and antimicrobial peptides produced by Paneth cells (Figure 1-3b), which slows down bacterial penetration to maintain gut

integrity (Bansil et al., 2018). While in the colon, mucus has antimicrobial roles, forming a highly charged gel that acts as a physical barrier. Bacteria can only be found in the outer mucus layer but normally, they do not penetrate the inner layer. Instead of the killing mechanisms employed by the small intestine, bacteria are kept at a distance in the colon (Mowat et al., 2014).

Mucin, a complex glycoprotein, is the product of approximately 20 mucin genes. These genes give rise to a protein structure characterized by numerous sequential repetitions of Serine and Threonine (referred to as ST repeats). These ST repeats serve as a scaffold for the attachment of oligosaccharides, forming covalent O-linked bonds (Bansil et al., 2018). The function of mucin glycan is to bind water conferring moisturising and lubricant properties, therefore offering epithelial cells with protection against dehydration and mechanical stress (Cornick et al., 2015, Cone, 2009). The MUC2 mucin is the major component of mucin in the gut and contains two long central regions called PTS domains that become rigid, outstretched rods after O-glycosylation (Birchenough et al., 2015). MUC2 has been reported to deliver tolerogenic signals by enhancement of IL-10 secretion by dendritic cells (DCs), to induce Tregs and maintain gut homeostasis (Meimei Shan, 2013).

Furthermore, mucus is the place where microbiota interact with the gut tissue under healthy conditions (Paone et al., 2020). The gut microbiota composition influences mucus properties and vice versa (Jakobsson et al., 2015, Bergstrom et al., 2013). While how gut microbiota influence the mucus is still a hot topic, recent studies suggest that some bacteria are able to induce/change the expression of host glycosylation, and consequently affect mucin properties (Pelaseyed et al., 2020, Schroeder, 2019). When the mucus composition is dysregulated, gut microbiota can invade into the intestinal epithelium, resulting in many intestinal diseases. For example, $MUC2^{-/-}$ mice showed more severe colitis due to increases in proinflammatory cytokines like TNFα and IL-1ß, demonstrating a critical role for MUC2 (Van Der Sluis et al., 2006). Therefore, the mucus barrier, as the first place to protect our intestine, is important for gut homeostasis.

1.2.3 The intestinal epithelium

The intestinal epithelium is located underneath the mucus layer and comprises mostly intestinal epithelial cells (IECs), including goblet cells, Paneth cells, enteroendocrine cells, enterocytes, and M cells (Figure 1-3b). IECs are continuously replaced every 4-5 days by differentiation of stem cells in the crypt. IECs provide the first line of defence against pathogenic luminal stimuli and promote an effective immune response. The intestinal epithelial barrier is formed by highly adapted IECs, which are regulated by tight junctions, and maintained by occludin and claudin proteins (Bansil et al., 2018).

1.2.3.1 Goblet cells

Goblet cells comprise around 10% of all IECs and are responsible for the secretion of mucins, a protective substance that helps lubricate and protect the intestinal lining (Kim et al., 2010). Furthermore, goblet cells also synthesize and secrete bioactive molecules like trefoil peptides, resistin-like molecule ß (RELMß) and Fc-γ binding protein (Fcγ bp), which contribute to mucus formation (Kim et al., 2010). Inflammatory Th2 responses, with increased levels of cytokines such as IL-4, IL-5, IL-9, and especially IL-13, have a major impact on the regulation of goblet cell function (Birchenough et al., 2015). Additionally, the Th17-associated cytokine IL-22 plays a key role in the regulation of goblet cell differentiation, with IL-22 deficient mice failing to produce Muc2 expression (Turner et al., 2013).

1.2.3.2 Paneth cells

Paneth cells exist only in the small intestine, especially in the ileum (R.Pabst, 1987, Mowat et al., 2014). Paneth cells can live for long period of times up to two months, differentiating from stem cells and migrating to the bottom of crypts (Kong, 2018). Paneth cells are crucial for combatting bacterial invasion, since these cells can secrete antimicrobial peptides (AMPs) and proteins like defensins and lysozyme, which help protect against infections and maintain the balance of gut bacteria. Paneth cells are reported to directly sense enteric bacteria via cell-autonomous MyD88-dependent toll-like receptor (TLR) activation, triggering expression of multiple antimicrobial factors (Bevins et al., 2011, Clevers et al., 2013).

1.2.3.3 Enterocytes

Enterocytes are the predominant cells in the intestinal epithelium. These cells are responsible for absorbing nutrients, electrolytes, and water from the digested food. They have numerous finger-like projections called microvilli that increase their surface area for efficient absorption. In addition, these cells are important in secreting immunoglobulins (Kong, 2018). Enterocytes are connected by tight junctions, which are specialized protein complexes that form a barrier between cells. These junctions regulate the passage of molecules between cells and help maintain the integrity of the intestinal lining.

1.2.3.4 Enteroendocrine cells

Enteroendocrine cells can produce hormones that regulate various processes in the digestive system, including controlling appetite, digestion, and insulin and cholecystokinin secretion. Their secretions are primarily regulated by chyme: the larger the amount of chyme present, the greater the secretions (Rindi et al., 2004). Enteroendocrine cells also play a role in the communication between the gut and the brain, influencing feelings of hunger and satiety and helping regulate food intake.

1.2.4 The intestinal immune system

Gut-associated lymphoid tissue (GALT) and the mesenteric draining lymph nodes are the principal locations responsible for regulating immune responses in the gut. However, many other immune system cells and structures are distributed throughout the intestine, for example, Peyer's patches (PPs) in the small intestine, immune cells residing in the intraepithelial layer and immune cells in the lamina propria.

1.2.4.1 Peyer's patches

Peyer's patches (PPs) are highly organized lymphoid aggregates that form a dome-like structure along the intestinal wall (Figure 1-4). In areas where PPs are not present, such as the colon, isolated lymphoid follicles are found to exert similar immune mechanisms. PPs are key sites for the crosstalk between T and B cells that coordinates immune responses to pathogens whilst promoting tolerance to

harmless microbes and food antigens. In addition, PPs are also the place where the production of IgA antibodies by plasma cells and the induction of memory T cell responses happens (Masahata et al., 2014).

PPs are similar to secondary lymphoid organs. Their structure can be divided into three broad areas: first, an antigen capture area enriched in antigen-presenting cells (APCs) referred to as the subepithelial dome (SED); second, T cell zone; third, B cell zone, where dendritic/B/T cell interactions take place (Figure 1-4) (De Silva et al., 2015). There is a specific area called follicular-associated epithelia (FAE) directly beneath the epithelial cell layer. The area between lymphoid follicle and FAE is called SED, where contains T cells, plasma B cells, dendritic cells (DCs), and macrophages.

When antigens reach the PPs, they are directly transferred from intestinal lumen across the FAE via microfold (M) cells. M cells are specialised epithelial cells residing in the FAE and are able to sample antigens or microorganisms and transport them across the epithelium for uptake and activation by the underlying DCs. M cells express a wide range of receptors on their surface, which allow them to bind various luminal antigens (Mabbott et al., 2013). The number of M cells increases rapidly after microbial change, a mechanism used by some species of bacteria and viruses to gain entry into the body. For example, *Enterohaemorrhagic Escherichia coli* (EHEC) binds to the M cell surface via an outer membrane adhesin, named intimin, resulting in close adherence to the tissue and causing attaching/effacing lesions of the intestinal epithelium (Phillips A.D., 2000).

1.2.4.2 Lymphoid cells of intraepithelial layer

The lymphocytes that are distributed throughout the epithelial cell layer, at all mucosal sites, are known as intraepithelial lymphocytes (IEL). The majority of IEL are T cells. Remarkably, the frequency of IEL is up to 10-15% of all epithelial cells (Fergusont, 1977). IELs can be divided into those that are restricted by classic MHC molecules (CD4+αß T cells and CD8αß+ αßT cells) and those that are restricted by non-classical MHC molecules (CD8αα+ αß T cells, all γδT cells, and double positive/negative cells), which develop independently of the thymus (Cheroutre et al., 2011, Hayday et al., 2008, Williams, 2011, Olivares-Villagomez et al., 2018). T cells with autoreactive T cell receptors are generated due to defective T

cell selection in the thymus (central tolerance), this selection is the principal but not the only mechanism for control of autoimmunity. Autoreactive T cells that have escaped central or peripheral tolerance may become activated inappropriately when exposed to self-antigens in the periphery. There are autoreactive T cell receptors on IELs as some IELs do not undergo thymic education. The expression of autoreactive TCRs may be associated with the maintenance of tolerance to self-antigens in the intestines (Williams, 2011).

IELs play an important role in maintaining gut health and immune surveillance, with the main function being to provide immune defence against infection. Cytokines expressed by IELs are key modulators of the intestinal mucosal barrier, for example, TGF-ß and keratinocyte growth factor (KGF), can protect the barrier integrity and inhibit the mitosis of IECs (Qiu et al., 2013). However, pro-inflammatory cytokines secreted by IELs can have the potential to initiate or propagate gut inflammation or lead to an aberrant immune response. For example, the imbalance of Th1 (IFN-γ, TNF and IL-2) and Th2-like cytokines (IL-4, IL-6, and IL-10), results in the increase of apoptosis of epithelial cells and permeability of epithelial barrier, and consequently bacterial translocation in the gut. Additionally, the dysregulation of Th2 cytokines will also cause changes in O-glycosylation in mucins, which affects the function of mucin (Qiu et al., 2013). Also, inappropriate activation of cytotoxic T lymphocyte (CTL) related genes of IELs are associated with the induction of chronic inflammatory disorders such as celiac disease and IBD (Meresse et al., 2006, Tang et al., 2009). Moreover, IELs are pivotal to the process of bacterial modulation, for example, TCRγδ IELs exhibit unique microbiota-dependent patterns of behaviour by changing their expression of antimicrobial genes and glycolysis (Hoytema Van Konijnenburg et al., 2017, Ismail et al., 2011a).

1.2.4.3 Immune system cells in the lamina propria

The lamina propria lies beneath the epithelial layer and is composed of an extracellular matrix (ECM) containing fibroblasts and blood vessels, and also several types of cells, including $CD4^+$T cells and $CD8^+$T cells, DCs, Innate lymphoid cells (ILCs), macrophages and eosinophils.

When antigens pass through the epithelium, they encounter a variety of lymphocytes, the majority of which are T cells. Unlike peripheral T cells, $CD4^+$T cells and $CD8^+$T cells display an effector memory phenotype in the lamina propria as evidenced by the expression of CD45RO (Williams, 2011). Additionally, T cells in the lamina propria are oligoclonal, suggesting they can only recognize a relatively small diversity of antigens (Guo et al., 2008). In addition, the large numbers of plasma cells in the healthy lamina propria are responsible for IgA secretion (Per Brandtzaeg, 2005), whilst DCs, which are important for tolerance induction and gut homeostasis, are discussed more fully in subsequent sections (Chatper 1.5). Briefly, these cells can sample antigens for presentation to Th cells or migrate to do this in mesenteric lymph nodes. Alternatively, they can migrate to germinal centres within follicular regions of PPs and provide antigens for B cells. Certain ILCs also have important roles in intestinal immunity and inflammation. Thus, ILC3 is one of the sources of IL-22, which influences the local environment by inducing tissue repair and secretion of antimicrobial peptides (Vonarbourg et al., 2010) and appears to be associated with bacterial defence (Kastele et al., 2021, Klose et al., 2013).

Macrophages, however, are the most abundant leukocytes in the healthy intestinal lamina propria. They are essential for intestinal homeostasis by their function of phagocytosis and degradation of microorganisms (Ueda et al., 2010). Interestingly, apart from immune system cells in the lamina propria are important in the immune responses, recent studies found that stromal cells like intestinal fibroblasts can act as a signal hub to affect the behaviour of IECs and IELs, playing an essencial role in the intestinal immunological regulations. (Karpus et al., 2019, Dang et al., 2021, Chalkidi et al., 2022).

1.2.4.4 Mesenteric lymph nodes

Mesenteric lymph nodes are a group of lymph nodes located in the mesentery, which is a fold of tissue that attaches the intestines to the abdominal wall. Mesenteric lymph nodes reflect the constant exposure of the intestine to environmental materials by draining the intestine. Notably, distinct nodes drain different segments of the intestine (Van Den Broeck et al., 2006). When antigens are detected in the intestine, immune cells in the mesenteric lymph nodes become activated, which leads to Ag-presentation by DCs to T cells and the production of

antibodies. Overall, mesenteric lymph nodes are vital for monitoring, detecting, and responding to threats in the gastrointestinal tract, preventing infections and maintaining gut health.

Given the complexity of intestinal components and interactions between the mucosal barrier and IECs, IELs, and immune cells in the lamina propria, dysregulation of this network and/or the influence of environmental factors can impact on microbial composition and consequently, affect intestinal homeostasis.

1.3 The gut-joint axis as an immunoregulatory mechanism

1.3.1 Intestinal dysbiosis in RA

The exact cause of RA remains elusive, but both genetic and environmental factors can play a role. The gut microbiome, one of the environmental factors, which consists of trillions of microorganisms residing in the digestive tract, has been the subject of increasing interest in relation to various autoimmune and inflammatory conditions, including RA. Recent studies of preclinical and early stage of the onset of arthritis indicate that alteration of intestinal microbial composition accelerates the development of RA, which is known as the "gut-joint axis" (Matei et al., 2021, Gracey et al., 2020, Scher et al., 2013). Such evidence corroborates the idea that the pathogenesis of RA might begin at the mucosal site and then transition to the synovial joints (Holers et al., 2018), given therefore the foundations for the 'gut-joint axis' theory (Zaiss et al., 2021).

In healthy gut tissue, the mucus layer produced by intestinal epithelial cells provides a physical barrier against the translocation of microorganisms and their by-products. However, intestinal dysbiosis is associated with the loss of integrity of this barrier, and loss of tight junctions between cells, which makes gut more 'leaky' (Gracey et al., 2020). This type of leaky gut allows the antigens and harmful microbiome to transit into the gut more easily, which could trigger inflammation in the gut. Previous studies reported an increase of *Collinsella aerofaciens, Lactobacillus,* and *Prevotella copri* in RA patients (Chen et al., 2016, Scher et al., 2013, Alpizar-Rodriguez et al., 2019, Zhao et al., 2022, Zhang et al., 2015). While a decrease of *Bacteroidetes* and *Bifidobacteria* was noticed in the

composition of bacteria in the RA patients (Figure 1-5) (Scher et al., 2013, Jussi Vaahtovuo Evelina Munukka, 2008). Mice treated with antibiotics before inducing RA have less severity of disease and less pro-inflammatory cytokines and anti-collagen antibodies in the serum (Jubair et al., 2018). Moreover, studies on ES-62, a helminth-derived immunoregulatory product, showed the capability to reduce mucosal inflammation, leading to a reduction in the joint inflammation (Pineda et al., 2012, Mcinnes et al., 2003). Thus, intestinal dysbiosis, along with reduced barrier function, can initiate and perpetuate intestinal inflammation, which has been observed in early stage of RA. However, how intestinal dysbiosis specifically promotes synovial inflammation is still unclear.

1.3.2 Mechanisms of the gut-joint axis

Although the role of the gut-joint axis in RA has not yet been fully demonstrated, two potential mechanisms are popular right now. First, autoantibodies can be generated in the inflamed intestine; second, activated immune system cells in the intestinal tissue can traffic to the joints (Figure 1-5) (Zhao et al., 2022, Zaiss et al., 2021, Holers et al., 2018).

First, in the inflamed intestine, the crosstalk between immune system cells becomes upregulated in the mucosal barrier, involving anti-microbial peptides, macrophages, dendritic cells, Tregs and Th17 cells and other components (Belkaid et al., 2014). On encountering the invasion in the gut of harmful bacteria, some immune cells are activated, such as Th17 cells. Likewise, (mainly) tissue-resident ILC3s, can contribute to the mucosal immune response via secretion of IL-17 and IL-22 (Valle-Noguera et al., 2020, Withers et al., 2017). IL-22 can stimulate the production of RegIII lectins in response to harmful bacteria. Furthermore, bacterial antigens also promote the activation of autoreactive B and T cells in the lymphoid tissues, resulting in an imbalance between regulatory T cells and T helper 17 cells, leading to the expansion of inflammatory responses. These inflammatory responses can also activate B cells, increasing the production of autoreactive IgA antibodies (ACPAs and RF) (Zhao et al., 2022, Holers et al., 2018), which have also been found in the serum before the onset of clinical RA (Figure 1-5) (Nielen et al., 2004, Rantapaa-Dahlqvist et al., 2003). Collectively, the immune response at gut mucosal surfaces generate antibodies (autoreactive or

those involved in molecular mimicry) in response to bacterial stimuli, therefore promoting the onset of RA.

Second, some human studies support the idea of cell migration from the intestine to the joints. For example, gut-activated B cells adhere efficiently to both gut and synovial high endothelial venules but not to high endothelial venules in peripheral lymph nodes, indicating the B cells activated in the gut might be able to traffic to and enter the joints (Marko Salmi et al., 1995). Moreover, identical T cell clones have been found in the joints and gut tissue in spondylarthritis (SpA) studies, whilst the synovium contains T cells expressing the gut homing receptor αEß7 integrin in RA patients (May et al., 2000, C Trollmo, 1997). Furthermore, a recent study used photoactivatable transgenic Kaede and Kikume green-red (KikGR) mice to label IEL and found IEL trafficking from the distal colon to the joint *in situ,* under inflammation conditions of both the gut and joint in SpA model (Lefferts et al., 2022), suggesting cell migration from the intestine to the joints. Overall, the studies support the idea that immune system cells activated in the gut migrate to the joints and tertiary lymphoid organs. Thus, autoreactive cells migrated from gut could activate macrophages, resulting in pro-inflammatory cytokines such as IL-1ß, IL-6, IL-17 and TNF-α in the joints. Fibroblasts activated by these cytokines could produce MMPs and receptor activators of nuclear factor κB ligand (RANKL) to drive the destruction of bone and cartilage tissue, leading to the development of RA (Figure 1-5).

Pathogenic responses associated with the gut-joint axis could be promoted by multiple factors. The role of gut microbiota-derived biological meditators, such as short-chain fatty acids, bile acids, and tryptophan metabolites, which can regulate the integrity of the intestinal barrier and immune balance, have been reported (Xu et al., 2022). Moreover, a study shows that these mediators can also have effects on bone destruction by inhibiting osteoclast differentiation (Xu et al., 2022). Besides, it was reported butyrate suppresses ILC3 activation, therefore inhibiting the inflammatory response in the intestine (Kim et al., 2017). It is possible that environmental factors, such as diet, and habits like smoking can play a role as well since the microbiota is the bridge of gut-joint axis hypothesis, which is consistent with the reported pathogenic role of these factors in RA.

1.4 Collagen-induced arthritis (CIA) mouse model

Although the pathophysiology of RA has been extensively investigated, there is still a lack of understanding of the fundamental mechanisms initiating RA. Challenges such as limited sample availability at early disease stages or the heterogeneity of the disease have limited the translation of such basic science into more effective therapeutics. Thus, to bypass these problems researchers are conducting studies using animal models of arthritis (Williams, 2004). The rodent models are used widely because of their homogeneity of the genetic background and ease of handling, as well as the wealth of phenotyping reagents, compared to other animal species. Many rodent arthritis models are available nowadays, for example, collagen-induced arthritis (CIA), adjuvant-induced arthritis (AIA) and streptococcal cell wall induced arthritis (SCWIA) models etc (Choudhary et al., 2018).

The CIA mouse model was first described in 1980 (Courtenay et al., 1980) and it is used extensively because it shares many pathological and immunological features with human RA, making it a valuable research tool for RA investigation (Kannan et al., 2005). For example, CIA is strongly associated with major histocompatibility complex class II genes (q haplotype in the case of the usual DBA/1J hosts), and the development of arthritis is accompanied by a robust T- and B-cell response to type II collagen (Choudhary et al., 2018). Besides, another important similarity between RA and CIA is the presence of pro-inflammatory mediators in the inflamed joints, including cytokines (IL-1ß, TNFα, IL-17) and MMPs (Marinova-Mutafchieva et al., 1997, Sandya et al., 2009). Hence, CIA provides a useful autoimmune animal model to study RA.

DBA1/J mice overexpress the TCR-ß gene from a T-cell clone that recognizes mouse type II collagen in the context of H-2^q, resulting in chronic arthritis (Campbell et al., 2000). Thus to induce CIA, mice are immunized with type II chicken (or bovine) collagen emulsified in complete Freund's adjuvant (CFA), followed by a boost of type II chicken collagen in PBS, scheduled 21 days after the first injection, to break tolerance and initiate inflammatory responses in the joint (Choudhary et al., 2018).

Although CIA model is largely similar to RA, they also differ in certain aspects. For example, the murine CIA is self-resolving (after 60 days), while RA is long-term chronic inflammation. In addition, the joint pathology of RA is chronic and symmetrical, whereas that of CIA is transient and asymmetrical (Luan et al., 2021). Therefore, researchers must consider the differences when designing experiments although CIA model is currently the closest to the pathogenesis of human RA.

1.5 Oral tolerance

Oral tolerance is a fascinating immunological phenomenon in which the immune system becomes tolerant to certain antigens after being exposed to them through the oral route, typically through ingestion (Garside, 1999). The process of oral tolerance takes place in the small intestine where food is absorbed. Oral (auto) antigen exposure is therefore an attractive approach for the treatment of autoimmune and inflammatory diseases (Ping Zhu, 2007, Toussirot, 2002, E.Trentham, 1998). Interestingly, contrary to the heterogenous pool of antigens recognised by ACPAs or Rheumatoid Factor, type II collagen being a single molecule constitutes a good target for clinical interventions based on oral tolerance mechanisms. Experimentally, responses against collagen can be studied in vivo using the CIA model, in which intradermal injections of type II collagen and Freud's adjuvant break tolerance and initiate inflammatory responses in the joint. Antibodies against type II collagen (CII) are important in the development of experimental arthritis and CII-specific B and T-cells have been identified in rheumatoid synovium and synovial fluid. Thus, collagen and collagen-derived products have been investigated to induce oral tolerance with therapeutic goals in RA (Zhu et al., 2007, E.Trentham, 1998).

1.5.1 Cellular and immune pathways of oral tolerance

Although the phenomenon of immunological hyporesponsiveness following oral administration of antigen has been known for more than 50 years, the mechanisms underlying oral tolerance induction have still not been fully elucidated. Research into the mechanism of oral tolerance has revealed that several distinct types of T regulator cells (Tregs) can mediate this phenomenon by releasing IL-10 and TGF-β (Weiner et al., 2011). It has also been shown that this effect is transitory in

nature requiring that the food, or antigen, be consumed continuously to maintain the tolerogenic state (Weiner et al., 2011). Several steps are involved in the mechanisms of oral tolerance. First, the antigen that reaches the intestinal epithelium is transported by different routes dependent on its properties, such as size solubility, and doses, which could lead to the induction of tolerance or immunity (Figure 1-6) (Tordesillas et al., 2018). Microfold or M cells are flattened epithelial cells overlying the Peyer's patches, which are organized lymphoid structures distributed along the mucosal tissue. M cells are specialized in the uptake of particular antigens such as viruses and bacteria. Sampling through M cells has been associated with induction of IgA production (Toussirot, 2002), which contributes to immune exclusion by neutralizing antigens in the lumen. The second step, which is a key component of oral tolerance, is the activation of Tregs/clonal deletion by DCs (Weiner, 1997, Toussirot, 2002), especially by CD103+DCs (Weiner et al., 2011). The functional properties of DCs are a result of interactions with commensal bacteria, TGF-β and IL-10 from gut epithelial cells, and their expression of retinoic acid, which is provided in the form of vitamin A in the diet and appears to be constitutively expressed by gut DCs (Coombes et al., 2007, Daniel Mucida, 2007). Recently, an increasing interest exists in defining tolerance-inducing receptors on DCs for new targeting strategies aimed at developing tolerance, including antigen-carbohydrate conjugates (Castenmiller et al., 2021). For example, the siglecs expressed on DCs are affecting the ability of effective antigen uptake, processing and presentation, thereby being associated with tolerogenic immune responses (Crespo et al., 2013, Lubbers et al., 2018). Macrophages are stimulated to produce TGF-β after uptaking apoptotic epithelial cells or apoptotic T cells following high-dose tolerance (Figure 1-6). Finally, activated Tregs release anti-inflammatory cytokines interact with other immune cells and suppress Th1/Th17 response to induce tolerance. Unlike normal T cells activated by antigen or costimulation, Tregs are primed in the absence of "danger or inflammation" signals in the oral tolerance. The combination of Treg-mediated suppression and the production of anti-inflammatory cytokines creates an environment of immune tolerance specific to the ingested antigen. This leads to a state in which the immune system no longer recognizes the antigen as a threat and avoids mounting an aggressive immune attack.

1.5.2 Factors affecting oral tolerance

Far from being a simple process, many factors can influence the development and efficacy of oral tolerance. For example, repeated feeding of low doses of antigen induces active suppression, but high doses lead to anergy, indicating that there are mechanisms completely unrelated to the antigen that we do not understand yet. Nevertheless, the gut microbiota plays a vital role in immune regulation, with a balanced and diverse gut microbiota promoting oral tolerance by influencing immune responses and promoting the development of regulatory T cells (Tordesillas et al., 2018). By contrast, an absence of microbiota is associated with food allergy. Specifically, loss of *Clostridiale* bacterial species promoted food allergy, whilst therapy with *Clostridiales* and *Bacteroidales* commensal bacteria restored tolerance in food allergy by activation of a MyD88-RORγt axis in nascent iTreg cells (Stephen-Victor et al., 2019).

Another factor that affects oral tolerance is the interaction of immune cells with tissue glycans (Rabinovich, 2010). Glycans play an important role in T cell activity and function, including T cell differentiation, T cell signalling and proliferation, T cell self-renewal and T cell homeostasis. An interesting example of glycan-mediated immunoregulation is the attachment of fucose to core N-glycans by the enzyme fucosyltransferase 8 (FUT 8). FUT8 fucosylation of the TCR is associated with hyperactivation of CD4+ T cells (T cells autoreactivity), whereas similar modification of the co-inhibitory receptors (CTLA-4 and PD-1) by FUT8 results in immune tolerance (Pereira et al., 2018). Moreover, glycans in the mucus enhance gut homeostasis and oral tolerance by forming a galectin-3/Dectin-1/FcγRIIB receptor complex, which can activate ß-catenin, a transcription factor that interferes with DC expression of inflammatory but not tolerogenic cytokines (Meimei Shan, 2013). Other factors include dietary components or medications, inflammatory conditions in the gut, and environmental factors: thus further study is needed to understand the multi-factorial process of oral tolerance.

Thus, the manipulation of oral tolerance has various clinical applications in the field of immunology and medicine, particularly for autoimmune diseases, like RA (Weiner, 1997, Toussirot, 2002, Pinheiro-Rosa et al., 2021). For example, repeated oral administrations of type II collagen (CII) exert anti-inflammatory activities. Here DCs in the GALT take up CII, presenting it to induce Tregs and

hence, systemic immune tolerance to CII (Park et al., 2009). In addition, it is possible to suppress allograft rejection by feeding allogeneic cells or relevant MHC peptides (Higgins et al., 1988). Another application is to prevent colitis by feeding autologous colonic protein extract (Hyun et al., 2006).

Despite the immense promise of oral tolerance in animals, this approach has not fully translated to the clinic yet (Weiner et al., 2011). There are still some limitations, for example, the immune system may sometimes break down this tolerance and react against dietary antigens, leading to food allergies or intolerances (Bowman et al., 2008). Adverse effects have also been found during specific oral tolerance induction (Barbi et al., 2012a, Barbi et al., 2012b). Moreover, factors including microbiota composition and dietary habits can also affect the effectiveness of oral tolerance. Therefore, further investigation is required to get a better understanding of oral tolerance and improve its effectiveness.

1.6 Undenatured type II collagen (UC-II)

As described above, oral administration of CII can be used to induce oral tolerance for RA treatment. In this study, undenatured type II collagen (UC-II), was used in the CIA model to study its potential application to RA.

Undenatured type II collagen (UC-II) is a patented form of collagen with undenatured (native) collagen from the cartilage of chicken sternum that preserves the physiological structure of collagen fibres (Figure 1-7) (Lugo et al., 2013). Unlike the production of denatured collagen molecules, the undenatured collagen manufacturing process maintains the intact glycosylation and protein tertiary structure (Bagchi et al., 2002) that is required to shape the protein's characteristic triple helix (Figure 1-7) (Bann et al., 2000). The preservation of this structure is key because it determines the three-dimensional epitopes presented to immune cells in the Peyer's Patches of the gut (Corthay et al., 1998, Bagchi D., 2002). Furthermore, by resisting the hydrolytic action of human gastric fluid (Bagchi et al., 2002), preservation of the triple helix domains allows a more efficient presentation of epitopes and subsequent regulatory responses.

Supporting these findings, some studies have indicated that undenatured collagen reduces pain and joint stiffness in osteoarthritis, both in experimental models and patients (Bagi et al., 2017, Lugo et al., 2016, Rui et al., 2021, Sahin et al., 2023). Mechanistically, oral collagen administration promotes regulatory T cell function, increasing IL-4, IL-10 and TGFß levels (Rui et al., 2021), whilst down-regulating inflammatory cytokines (IL-2, TNF, IL-6, IL-1) and regulating metabolites, like ß-hydroxybutyrate (Stabile et al., 2022, Orhan et al., 2021, Varney et al., 2021). Thus, undenatured collagen has also shown efficacy in ameliorating pain in joint disease (Bagchi et al., 2002), although the precise immunological basis of protection remains unclear and limits use in the clinic to date.

Perhaps surprisingly, less attention has been given to the structural aspects of the gastrointestinal regions where the described effector mechanisms take place. Recent studies suggest that preserving the structure of the gut tissue, and the cues present in its microenvironment, play a crucial role in regulating immune responses and the balanced resolution of inflammation. As described above, the gut-joint axis theory indicates that damage to gut integrity and resulting inflammation could result in the imbalance and dysregulation of the microbiome, thereby inducing systemic inflammation. Indeed, the breakdown of the protective barrier in the gut has been linked to the development of arthritis (Doonan et al., 2019, Matei et al., 2021), indicating that restoration of gut barrier integrity could be a promising approach to treat RA. Furthermore, there is a hypothesis suggesting that rheumatoid arthritis (RA) might originate in mucosal regions before progressing to more remote synovial joints (Holers et al., 2018).

Research found that oral tolerance is associated with gut integrity by interaction with microbiota (Tordesillas et al., 2018). The introduction of *Clostridia* species to germ-free mice increases the production of IL-22 by RORγt+ innate lymphoid cells and T cells within the lamina propria of the intestine. This elevation in IL-22 levels plays a role in decreasing the permeability of the intestine to oral antigens (Stefka et al., 2014). However, whether administration of collagens could contribute to intestinal integrity by interacting with microbiota is still unknown. Therefore, a deeper understanding of the alterations in the microenvironment of the gut mucosal area resulting from oral administration of collagens (such as UC-II) is still needed for us to comprehend, and ultimately utilise, the induction of oral tolerance in RA.

1.7 Glycobiology in inflammation

1.7.1 Overview of glycobiology

Glycobiology is a subject which studies the structures and functions of glycans, or carbohydrates (Cummings et al., 2014). Carbohydrates are not limited to their roles as energy sources, they are involved in cell recognition, communication, adhesion, and signalling. This reflects that every living cell is endowed with a rich and diverse sugar coat – its glycocalyx, which comprises glycoproteins, glycolipids, and proteoglycans (Figure 1-8) (Varki, 2011). Indeed, glycosylation is one of the most important processes involved in modification of proteins and lipids, and cell surface glycoconjugates and includes N-linked glycosylation and O-linked protein glycosylation, and modification of lipids and glycosaminoglycans. Regulatory functions of glycans are often mediated by their interactions with complementary glycan binding proteins (GBPs), which contain a carbohydrate recognition domain (CRD) (Figure 1-9) (Schnaar, 2016, Zaia, 2011). GBPs can "read" the glycan information that is encoded by enzymes involved in glycan biosynthesis, glycosyltransferases (adding glycans) and glycosidases (removing glycans). GBPs not only recognize self glycans but the glycans of pathogens as well, playing important roles in immunity and infection.

1.7.1.1 N-linked glycosylation

N-linked glycosylation refers to the attachment of N-acetylglucosamine (GlcNAc) to the nitrogen of an asparagine (Asn) side chain. These Asn-linked glycoconjugates contain a core structure of GlcNAc(2)-mannose(3), with potential additional monosaccharides to be introduced or removed in varying amounts to increase structural diversity (Figure 1-8) (Reily et al., 2019). N-glycans are found in most living organisms, being crucial to regulating intracellular and extracellular functions. N-glycans are first synthesised in the Endoplasmic reticulum (ER) membrane on the lipid carrier dolichol-phosphate (Dol-P), and then transferred into the Golgi to finish the process, which involves the addition of GlcNAc, galactose, sialic acid and fucose (Varki A, 2022). These complex N-glycans are essential for maintaining basic cellular functions, for example, to retain growth factor and cytokines receptors at the cell surface, through interactions with GBPs such as galectins, or cytokines such as transforming growth factor-ß. In fact,

dysregulation of N-glycosylation can lead to a variety of diseases related to immunity, neuronal cell migration or inflammation (Varki A, 2022).

1.7.1.2 O-linked glycosylation

Glycosylation occurring on amino acids with functional hydroxyl groups, normally Serine (Ser) and Threonine (Thr), is defined as O-linked glycosylation. In general, GlcNAc and N-acetylgalactosamine (GalNAc) are the most common sugars linked to Ser or Thr (Reily et al., 2019). Mucins are the class of glycoproteins carrying the greatest number of O-GalNAc glycans, which are also called mucin-type O-glycans (Bennett et al., 2012, Varki A, 2022). In fact, O-GalNAc glycans are not only found in mucins, but also at single sites on most secreted and membrane-bound proteins. Thus, O-GalNAc glycans are involved in almost every aspect of biology, including cell-cell communication, cell adhesion, signal transduction, immune surveillance, epithelial cell protection, and host-pathogen interactions (Varki A, 2022). The O-GalNAc glycans of mucins have four major core structures (Figure 1-8). Like N-glycans, each core can be extended by additional modifications. Core 1 and core 2 are the most common, while core 3 and 4 are less common, being mostly restricted to mucins in gastrointestinal tissues (Varki A, 2022). On the other hand, GlcNAc linked to Ser or Thr is typically found on intracellular glycoproteins present in nuclear, mitochondrial and cytoplasmic compartments (Reily et al., 2019). O-GlcNAc is therefore involved in cell signalling, playing a key role in modulating cell cycle and stress responses (Van Der Laarse et al., 2018).

1.7.1.3 Glycosphingolipids

Glycosphingolipids (GSLs), a subclass of glycolipids found in the cell membranes of organisms from bacteria to humans, are the major glycolipids of animals (Varki A, 2022). GSLs have a ceramide lipid portion as their backbone and one or more sugar molecules are attached to the ceramide through a glycosidic linkage, forming a glycan structure. GSLs act as recognition molecules on the cell surface, participating in processes like immune response, cell adhesion, and cell signalling pathways (Varki A, 2022, Zhang et al., 2019a). Moreover, the glycosphingolipids on the red blood cells' surface play an important role in determining the blood type (A, B, AB, or O) (Kościelak, 2012).

1.7.1.4 Proteoglycans and glycosaminoglycans

Proteoglycans and glycosaminoglycans (GAGs) are two closely related types of molecules found in the extracellular matrix and on the surface of cells. Proteoglycans are characterized by the presence of long sugar repeats, and these extended sugar chains are GAGs. GAGs have many types like hyaluronic acid, heparan sulfate, keratan sulfate, chondroitin sulfate and dermatan sulfate, which contribute to tissue hydration and resilience (Varki A, 2022, Jianjun Li, 2010). Together, proteoglycans and GAGs play important roles in tissue structure, resilience, lubrication, and cell signalling in various biological contexts (Iozzo et al., 2015).

1.7.1.5 Methods in functional glycomics

Characterization of complex glycan structures and analysis of the interaction of glycans with other molecules are essential in the field of glycobiology and glycomics. Given the distinct nature of glycans, specific techniques have been optimised for glycosciences. Among them, Mass Spectrometry (MS) has emerged as a highly sensitive and powerful technique for glycan structural analysis (Morris, 2001) MS-based experiments provide detailed information, but they require time and resources. A different technique to this is found in glycan microarray and lectin microarray approaches, which can be useful when investigating the interactions between glycans and other molecules (Wang et al., 2008). The enormous body of data generated by such approaches has now resulted in the development of glycome-targeted bioinformatics. For example, SimGlycan™ is a desktop tool designed for the challenges of glycan structure prediction from glycan mass spectrometry data and in addition, it can also predict novel glycans by providing the ability to generate the glycan structure (Jianjun Li, 2010).

1.7.2 Glycobiology of immune responses

1.7.2.1 Glycans in immunity

Like every other cell, immune system cells, express a distinct set of cell surface-associated glycoproteins and glycolipids, together with GBPs, allowing them to sense signals in the environment. GBPs on innate immune system cells can recognize glycans found on the surface of microorganisms, acting as pattern

recognition receptors (PRRs). Glycan recognition has been exploited for vaccine development. For example, the advancements made in the development of HIV-1 vaccines have been significantly influenced by a deeper comprehension of the HIV-1 envelope (Env) glycoprotein, as well as a more thorough recognition of how its glycan makeup impacts both immune responses and the evasion of the immune system (Kwong et al., 2018, Ward et al., 2017). Moreover, glycans regulate adaptive immunity, affecting B and T cell differentiation dependent on glycoproteins, like CD43, CD45, and GBPs, like selectins, galectins and siglecs. For example, galectin-1 is an important mediator of T cell apoptosis and is involved in the homeostasis of T effector cell function (Nancy L. Perillo et al., 1995, Gabriel A. Rabinovich, 1998). T cell-mediated immunity also is regulated by galectin-3 and galectin-9 (Johnson et al., 2013). Additionally, glycans are also important for the function of class I and class II major histocompatibility complex proteins (MHC class I and MHC class II), chemokine receptors and cytokine receptors (Rabinovich et al., 2012). Thus, the loss of complex N-glycans on MHC II results in significant disruption to the presentation of bacterial polysaccharides to T cells (Ryan et al., 2011, Johnson et al., 2013). Remarkably, the majority of cytokines and chemokines are glycosylated proteins and N-glycans attached to Fc portion of IgG can modulate antibody activities (Kaneko Y, 2006). Moreover, glycosylation of key components of the gut microenvironment, including mucus, cells and GBPs, is important in immunological regulation (Chapter 1.7.3). Collectively, glycans and GBPs are key players in shaping and directing immunological pathways required in specific tissues and pathophysiological conditions.

1.7.2.2 Glycosylation in diseases

Dysregulation of glycosylation can result in disease development, not least because it is directly involved in immunity driven by PRRs, but also in subsequent adaptive and inflammatory responses (Groux-Degroote et al., 2020). For example, the glycoproteins, P-selectin and E-selectin mobilized by vascular endothelial cells to the cell surface facing the vessel lumen, can initiate the recruitment of neutrophils and cause inflammation (Schnaar, 2016). E-selectin is up-regulated in all inflammatory skin diseases (Varki A, 2022). Moreover, changes also affect the migration of immune system cells to the site of inflammation. Increases in sialyl Lewis structure, N-glycan branching or exposure of the mucin-type O-glycan (Tn

antigen) have been observed in cancer cells (Pinho et al., 2015). Furthermore, GnT5-deficient mice have an increased capacity to develop experimental autoimmune encephalomyelitis (EAE) and glomerulonephritis (Demetriou M, 2001).

Changes in sialylation, galactosylation, and fucosylation of IgGs, can all play a role in disrupting immune regulation and leading to a range of autoimmune and persistent inflammatory disorders. For example, IgG from patients with RA exhibit alterations in glycosylation, both within the Fc region and the antigen-binding fragment (Fab) region (Adrian Youings, 1996). Moreover, truncated O-glycans in IgA can lead to antibody deposition in the inflamed kidney (Hiki et al., 2001). Additionally, extracellular matrix function is also affected by glycosylation, like abnormal glycosylation of plasma fibrinogen was found in liver disorders (Varki A, 2022).

1.7.3 Glycosylation in the gut

The gastrointestinal (GI) tract, along with its mucosal lining, constitutes an intricate environment comprising the microbiota, both resident and recruited immune system cells, and a dynamic mucus layer and epithelium that can adapt to various stimuli. The mucus barrier is enriched with glycans, especially O-linked glycans in mucins, which play a homeostatic role in the gut (Bergstrom et al., 2013). Moreover, mucins regulate interactions with the microbiota (Moran et al., 2011), and sialylation of mucus protecting mucosal barrier from bacterial degradation, a process governed by ST6GALNAC1 (ST6) sialyltransferase. Supporting this, ST6-deficient mice tend to have more susceptibility to IBD (Yao et al., 2022).

Underneath the mucus layer, a second line of defence is presented by the epithelial glycocalyx, Mucin type O-glycans dominate the intestinal epithelial cells (IECs) glycome. The glycosylation of IECs can also regulate gut microbial composition (Meimei Shan, 2013, Kostopoulos et al., 2021, Goto et al., 2016) and alterations of IEC glycosylation results in many intestinal inflammatory conditions, like IBD (Kudelka et al., 2020), ulcerative colitis (UC), and Crohn's disease (Kelm et al., 2020, Groux-Degroote et al., 2020, Reily et al., 2019, Go et al., 1994). For example, an increase of Galaß1-3-GalNAc was observed in IECs of patients with

UC (Moore, 1988). Additionally, increased fucosylation of the epithelial layer shows a reduction of *Enterococcus faecalis* colonization, while promoting the growth of commensal microbes such as *Porphyromonadaceae*, *Ruminococcaceae*, and *Bacteroides* species (Goto et al., 2014, Pham et al., 2014). Interestingly, intestinal immune cells regulate epithelial fucosylation, a monosaccharide which conditions microbiome composition. IL-22 produced by ILC3 induces epithelial expression of α1-2 fucosylation (viaby fucosyltransferase 2(FUT2)) in mice. Dysregulation of FUT2 is associated with infection and chronic inflammatory disease in the gut (Goto et al., 2016, Brazil et al., 2021, Wang et al., 2017b). These examples illustrate how, intestinal epithelial glycans contribute to the integration of host, microbial, and environmental cues to maintain mucosal homeostasis.

Apart from the glycosylation of mucus barrier and epithelial cells, the dysregulation of glycosylation of immune system cells, such as neutrophils and T cells, in the intestine can also contribute to intestinal inflammation (Brazil et al., 2021). Studies to date highlight the importance of glycosylation in the intestine, especially epithelial cells, however, the enormous diversity of glycans coupled with glycosylation of many cell types in the gut makes uncovering the functions of specific glycans extremely challenging. Further investigations are needed to fully understand how glycosylation in the gut regulates and maintains intestinal homeostasis.

1.8 Summary and research objectives

Despite extensive RA research, disease pathogenesis is still not fully understood, and there is still an unmet need to develop novel and effective therapies. Therapies based on induction of tolerance hold therapeutic potential, although their use in the clinic to date is still limited. This could be improved with a better understanding of the role of the gut tissue in RA pathogenesis. Glycans and glycosylation-dependent networks are being increasingly recognised as key molecules in local immunity, as they integrate genetic and environmental factors. In the gut, tissue glycosylation may affect not only immunological functions, but also host-microbiome interactions and inflammatory responses. However, although glycans have been extensively described as modulators of inflammation, whether gut-dependent pathology in RA is mediated by changes in tissue

glycosylation has not been yet demonstrated. For example, do potential changes in intestinal glycosylation affect the induction of tolerance? Are glycans involved in the described gut-mediated pathology in arthritis? What causes the alteration of glycosylation under chronic inflammatory conditions?

Therefore, in this research, we investigated the molecular mechanisms underlying gut inflammation in experimental arthritis with the following aims:

- to evaluate the protective effect of UC-II in experimental models of RA and to provide further insight into the cellular and molecular mechanisms triggered.

- to describe the glycosylation profile of the small and large intestine in health and to identify changes in the gut glycosylation in the gut during experimental arthritis.

- to investigate the interactions among cell types in the gut and define glycan-related pathways of regulation of intestinal integrity and homeostasis.

By addressing these objectives, we will attempt to draw a clearer picture of the glycomic and inflammatory networks underlying gut function and induction of oral tolerance. Ultimately, we will have a better understanding of the role of gut tissue in RA, contributing to the identification of novel pathophysiological pathways and clinical targets.

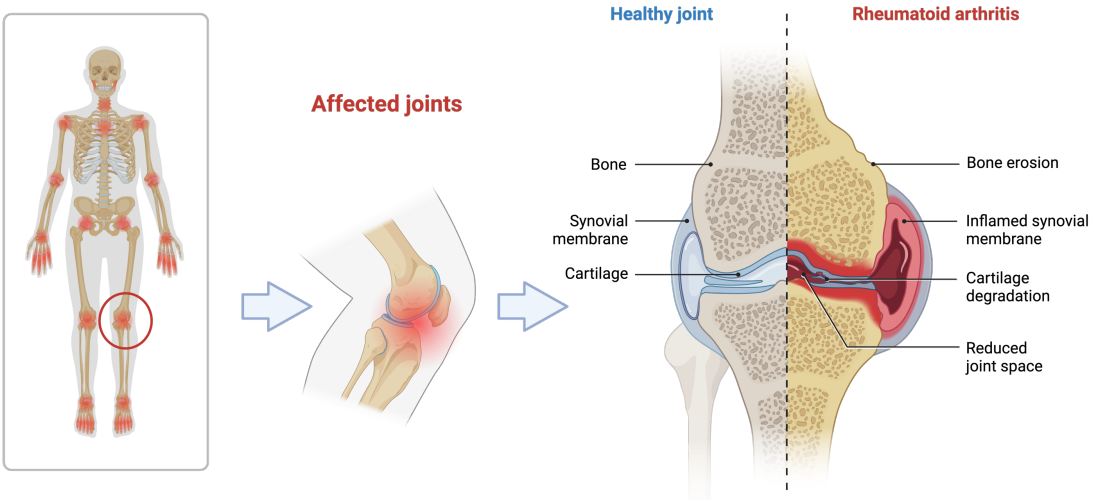

Figure 1-1 Rheumatoid arthritis compared to healthy joint.

Bone, synovial membrane and cartilage changes in the joint during systemic rheumatoid arthritis compared to healthy joints. Created by Biorender.

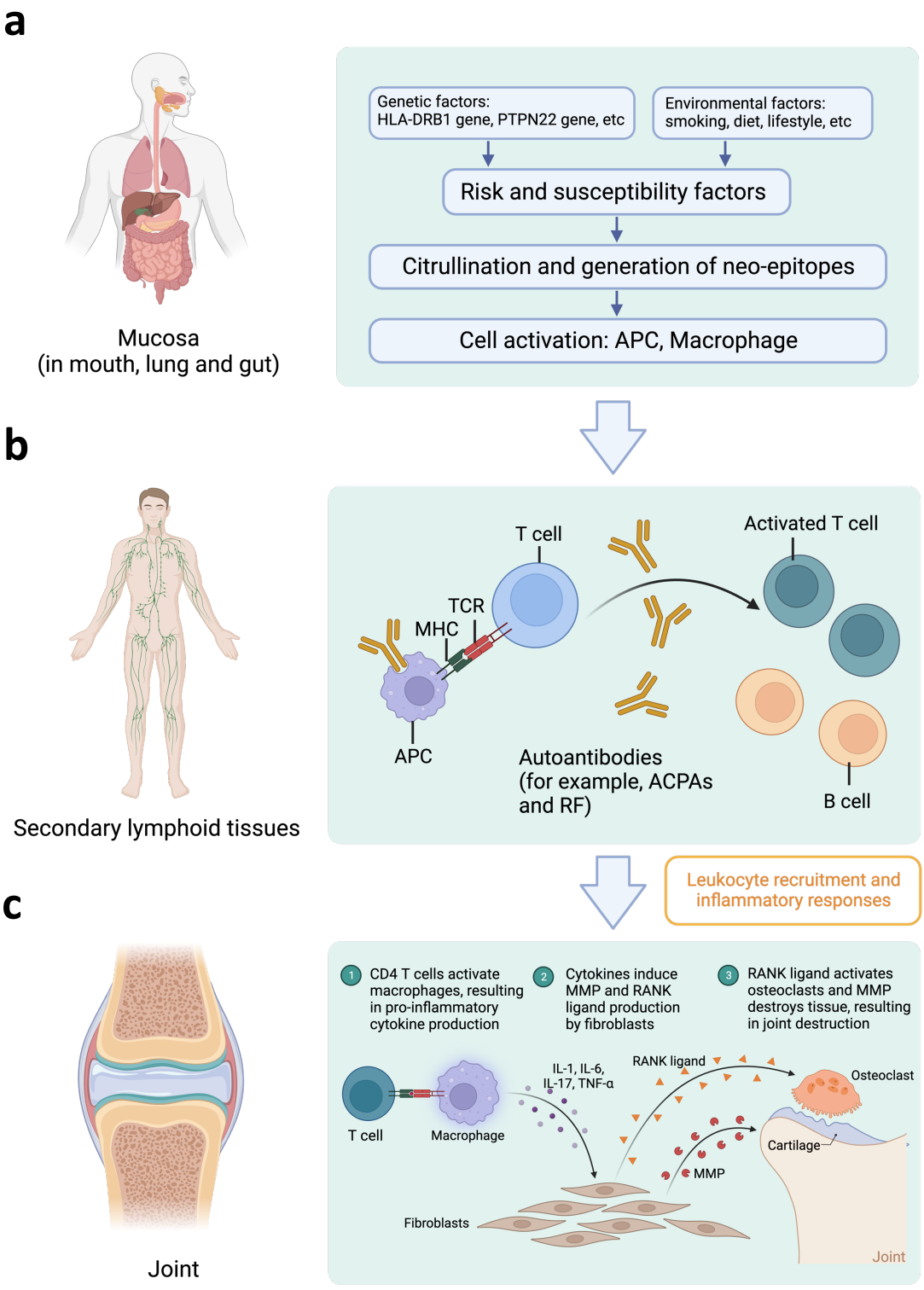

Figure 1-2 Mechanisms involved in initiation and progression of rheumatoid arthritis.

a) Genetic and environmental factors can trigger neo-epitopes generation that can be recognised by the adaptive immune system. **b)** These altered peptides are presented by antigen-presenting cells (APCs), activate an adaptive immune response in lymphoid tissues and elicit autoantibody formation. **c)** Stromal cells, APCs and macrophages can be activated locally and produce a range of inflammatory factors. Paracrine and autocrine actions of cytokines, along with persistent adaptive immune responses, can perpetuate the disease and ultimately lead to cartilage and bone destruction. ACPAs, anti-citrullinated protein antibodies; MHC, major histocompatibility complex; MMP, matrix metalloproteinase; RANKL, receptor activator of nuclear factor-κB ligand; RF, rheumatoid factor; TCR, T cell receptor; TNF-α, tumour necrosis factor α.

Adapted from (Smolen et al., 2018; Zhao et al., 2022), created by Biorender.

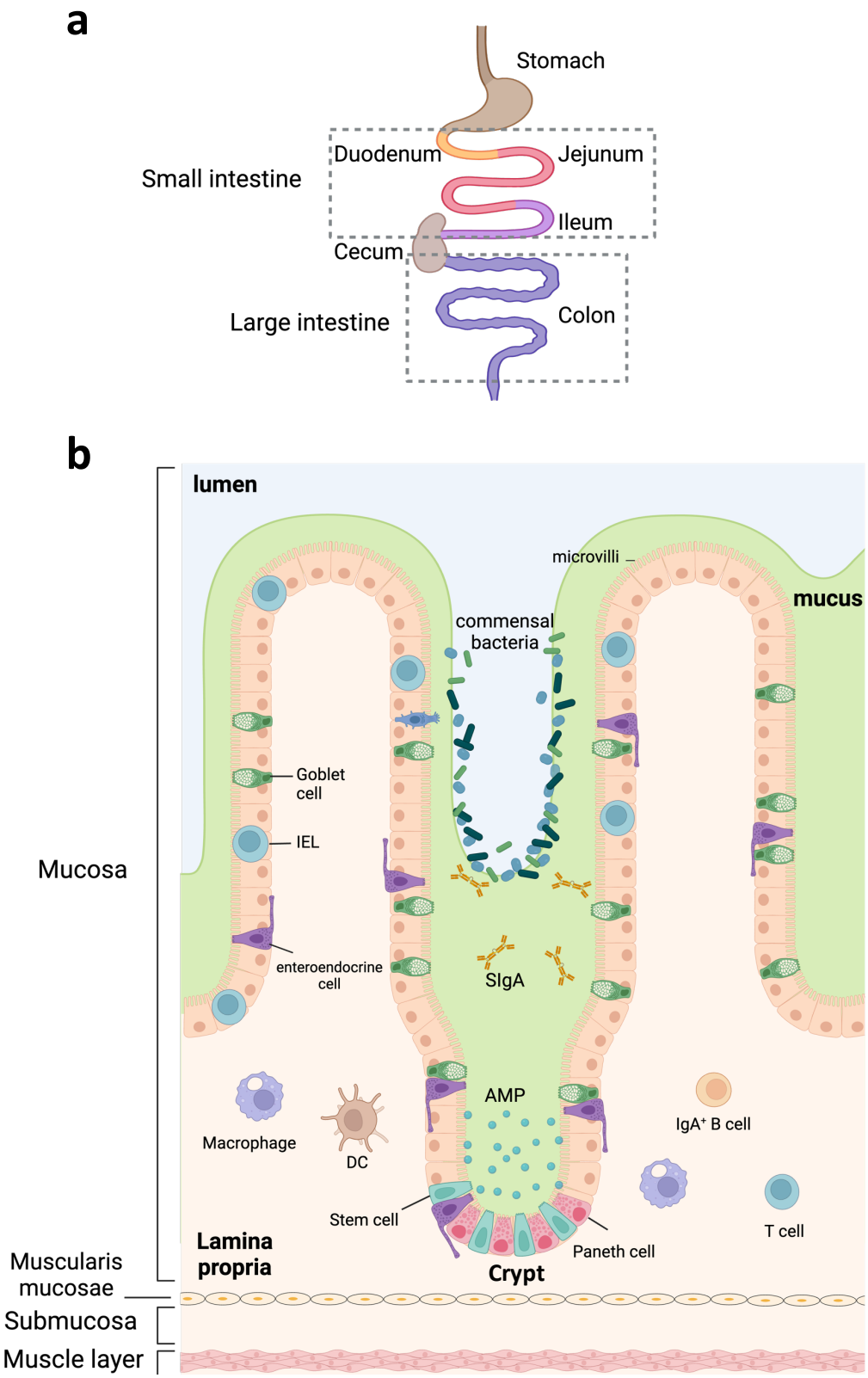

Figure 1-3 Anatomy of the intestinal mucosa and its immune apparatus.

a) Diagram of the gastrointestinal tract. **b)** The intestine can be divided into mucosa, muscularis, submucosa and muscle layer cross-sectionally. Intestinal epithelial cells (IECs) are produced from stem cells near the bottom of the crypts. Paneth cells migrate downwards to the crypt. The central part of the villus comprises the lamina propria, where most immune cells are found, whereas the intraepithelial lymphocytes (IELs) are found lying between epithelial cells. DC, dendritic cell; SIgA, secretory immunoglobulin A; AMP, antimicrobial peptides.

Adapted from (Mowat and Agace, 2014), created by Biorender.

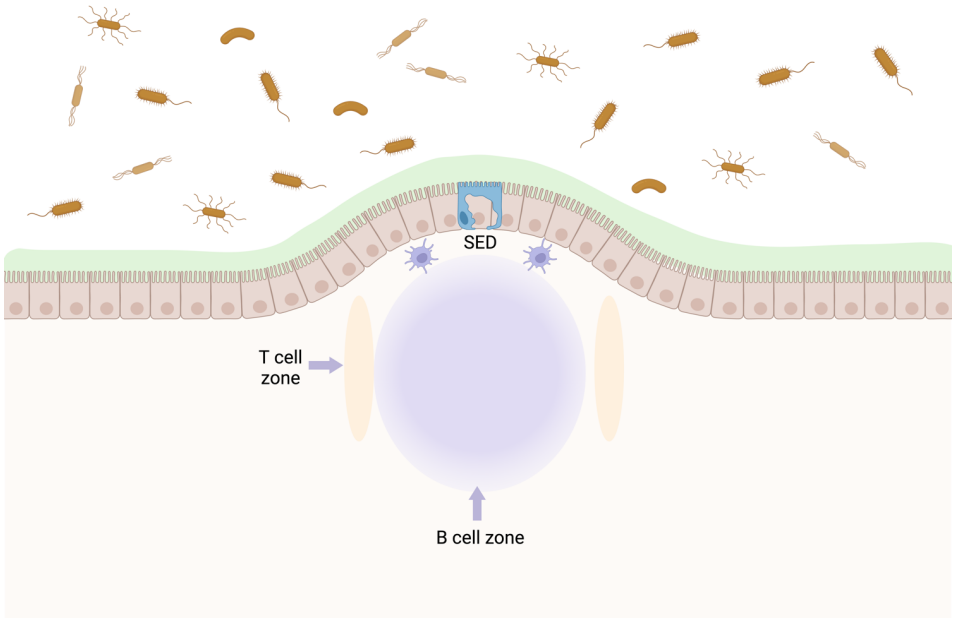

Figure 1-4 Microanatomy of a Peyer's patch (PPs)

Bacteria or antigen transfer into follicular-associated epithelia (FAE) via microfold (M) cells. The area beneath M cells are subepithelial dome (SED), where contains dendritic cells (DCs). T cell zone and B cell zone are below the SED, where interaction of immune cells take place.

Adapted from (Williams, 2011), created by Biorender.

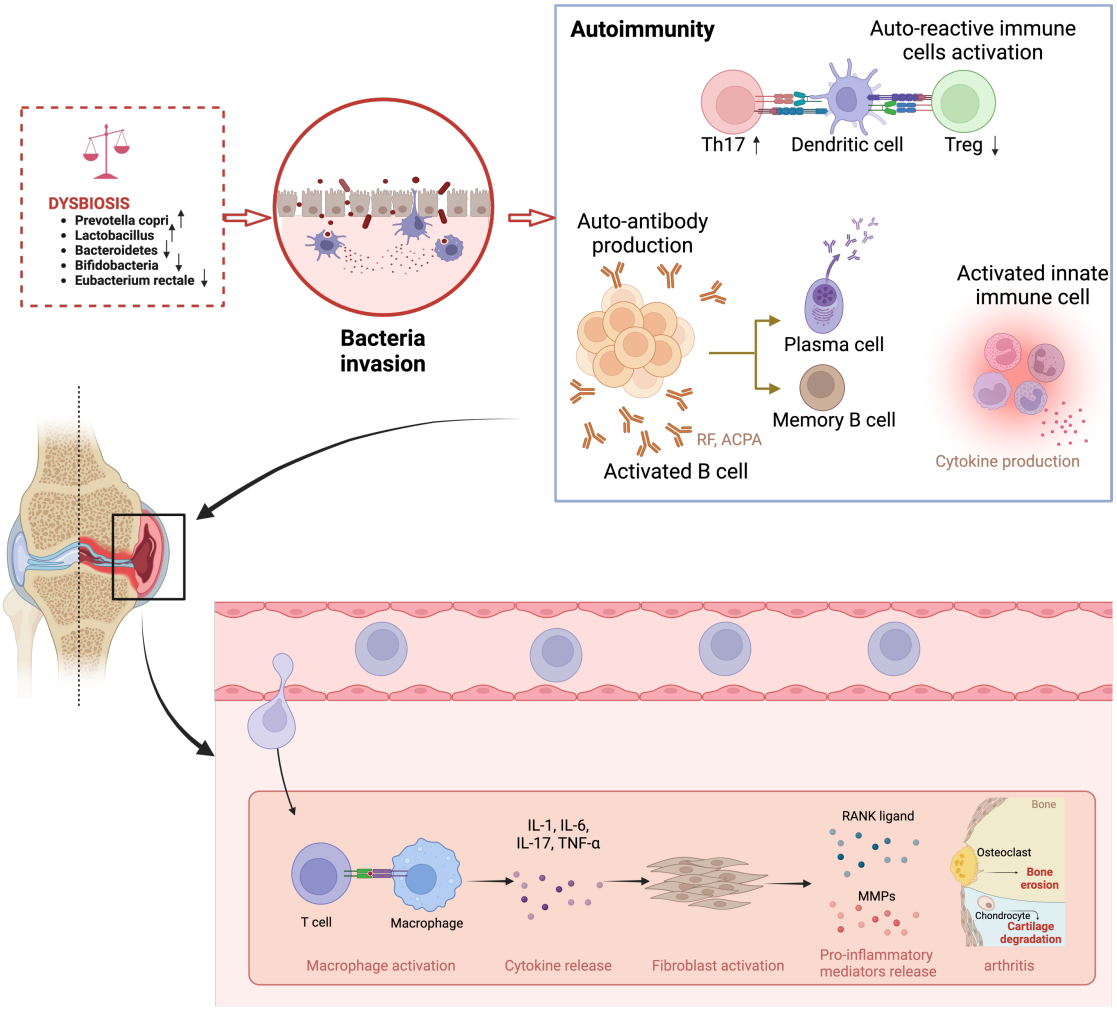

Figure 1-5 Mechanisms of gut-joint axis theory.

Changes in the composition of gut microbiota can lead to damage of the epithelium and to the opening of the paracellular pathway and can cross the epithelium and get in contact with the immune cells beneath the epithelial layer, which leads to inflammation. Furthermore, bacterial antigens promote the activation of autoreactive immune cells (B cell and T cell) in the lymphoid tissues, resulting in an imbalance between regulatory T cells (Tregs) and T helper 17 (Th17) cells, leading to expansion of inflammatory response. Activated B cells produce autoantibodies (anti-citrullinated protein antibody and rheumatoid factor). Gut microbiota imbalance can trigger the migration of autoreactive cells to the joints. Autoreactive cells activate macrophages, resulting in inflammatory cytokine production. These cytokines induce fibroblasts to produce MMPs (matrix metalloproteinases) and RANKL (receptor activator of nuclear factor kB ligand), which mediate the destruction of bone and cartilage tissue, leading to the development of RA.

Adapted from (Zhao et al., 2022), created by Biorender.

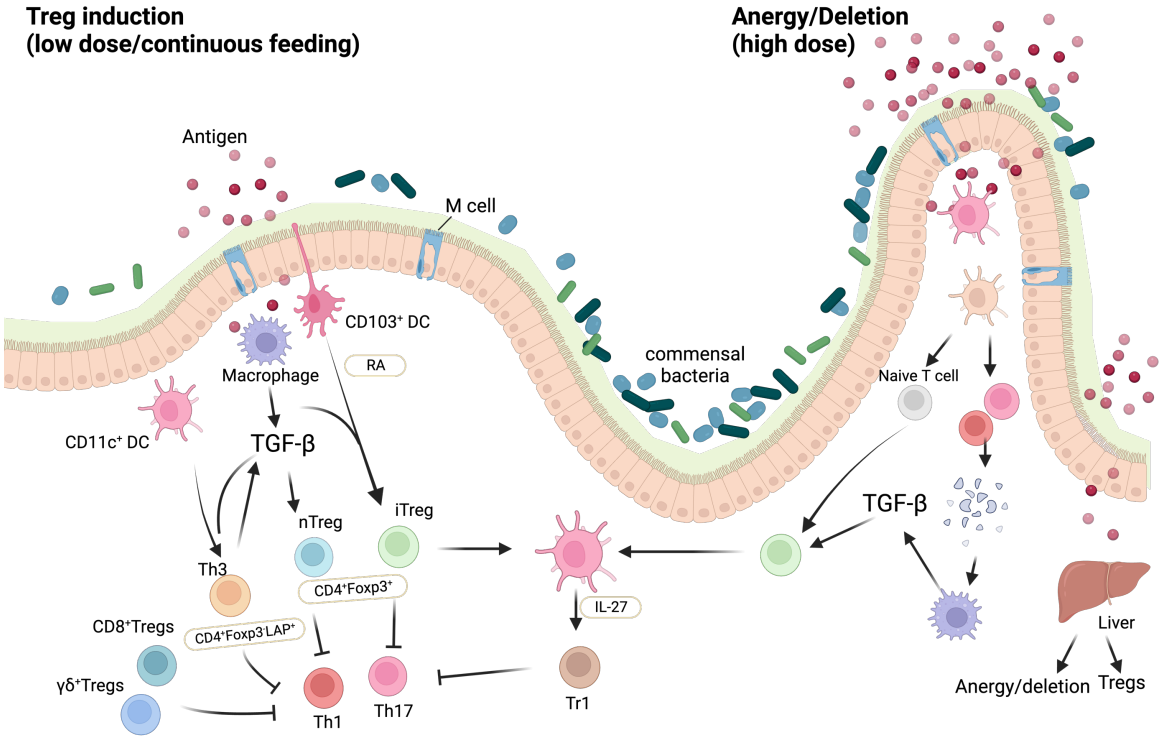

Figure 1-6 Mechanisms of oral tolerance induction.

Oral antigen crosses from the intestine into the GALT via M cells or intestinal epithelial cells. DCs in the gut are unique in that they can drive Treg differentiation from Foxp3- cells. These properties of DCs relate to their being conditioned by commensal bacteria, TGF-β and IL-10 from gut epithelial cells, and their expression of retinoic acid, which is provided in the form of vitamin A in the diet and appears to be constitutively expressed by gut DCs. CD11b monocytes may also play a role in the induction of Tregs. Macrophages are stimulated to produce TGF-β after uptaking apoptotic epithelial cells or apoptotic T cells following high-dose tolerance. Lower doses of antigen favor the induction of Tregs, whereas higher doses of antigen favor anergy/deletion as a mechanism of tolerance induction. The liver may also play a role in oral tolerance induction and antigen (high dose) may be rapidly taken up by the liver, where it is processed by plasmacytoid DCs that induce anergy/ deletion and Tregs. A number of different types of Tregs may be induced or expanded in the gut including CD4+CD25+Foxp3+ iTregs, nTregs, Tr1 cells, LAP+ Tregs (Th3 cells), CD8+ Tregs, and γδT cells. TGF, transforming growth factor; RA, retinoic acid; DC, dendritic cells; LAP, latencyassociated peptide; Foxp3, forkhead box protein; IL, interleukin; MLN, mesenteric lymph nodes.

Adapted from (Weiner et al., 2011), created by Biorender.

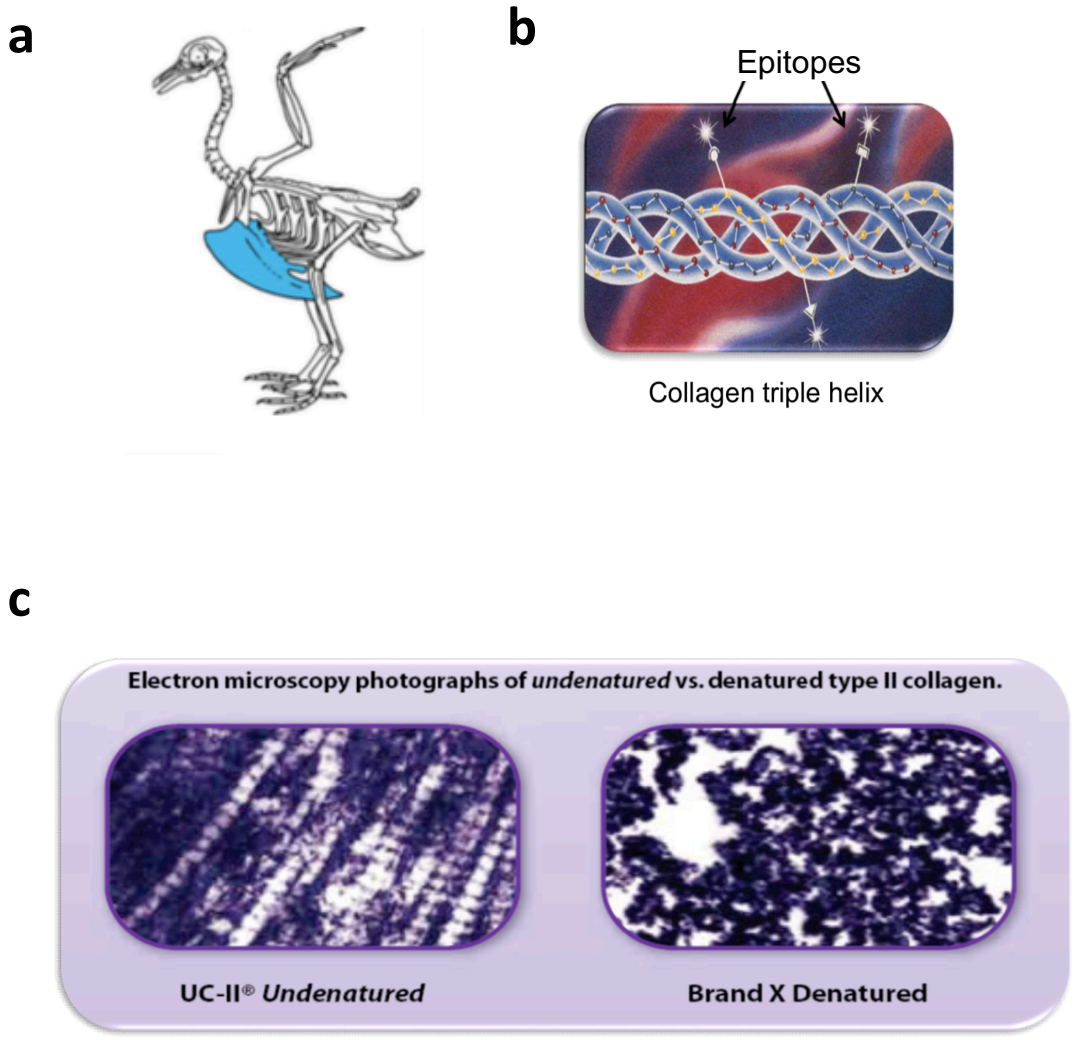

Figure 1-7 Structure of UC-II.

a) Undenatured type II collagen (UC-II®) is a patented form of collagen with undenatured (native) collagen from the cartilage of chicken sternum. **b)** Collagen triple helix of UC-II. **c)** Electron microscopy photographs of undenatured and denatured type II collagen.

Figure b) and c) cited from (Bagchid.,2002)

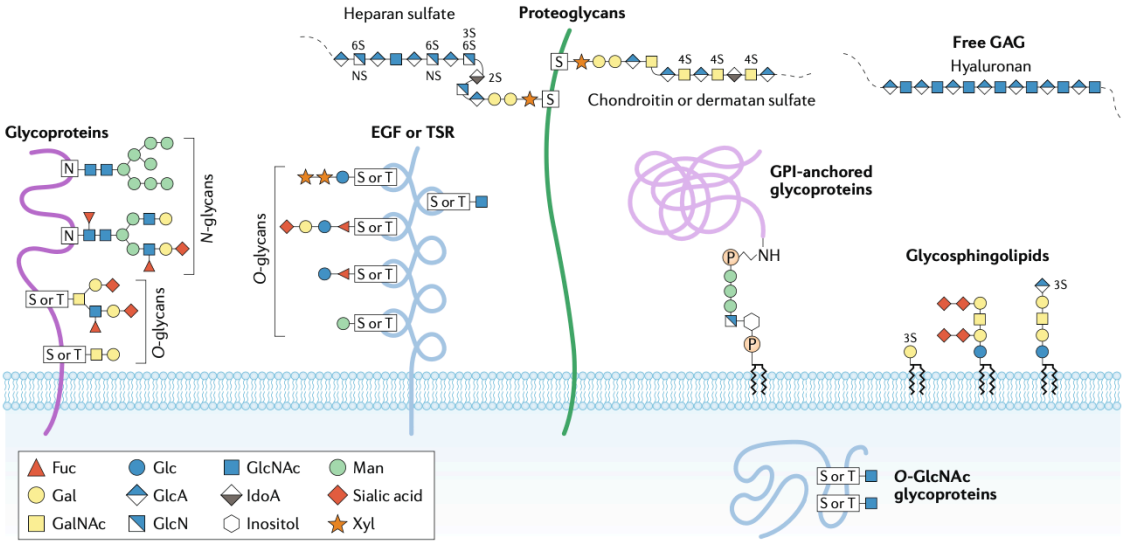

Figure 1-8 Major types of glycosylation in humans.

Glycosylation is divided into N-linked glycosylation, O-linked glycosylation, glycolipid and glycoprotein glycosylation, and glycosaminoglycan attachment. Glycoproteins consist of glycan and glycan chains linked to nitrogen and oxygen atoms of amino acid residues and are thus termed N-glycans and O-glycans, respectively. N-glycans consist of N-acetylglucosamine (GlcNAc) attached to the nitrogen atom of the amino group of Asn (N). O-glycosylation, in which glycans attach to the oxygen atom of the hydroxyl groups of Ser (S) or Thr (T) residues. O-glycans can be further subclassified mucin-type O-glycosylation and O-GlcNAc. Mucin-type glycans can be further classified on the basis of the glycans attached to the initial GalNAc. Other types of O-glycans, such as O-linked fucose (Fuc) and O-linked Man, often occur in specific proteins or protein domains, such as epidermal growth factor (EGF) repeats, thrombospondin type I repeats (TSR) or dystroglycan. O-GlcNAc occurs in the cytosol and nucleus. Proteoglycans represent a major class of glycoproteins that are defined by long glycosaminoglycan (GAG) chains. GAGs include heparan sulfate, chondroitin sulfate and dermatan sulfate. Glycosylphosphatidylinositol (GPI)-anchored glycoproteins represent another major class of glycoconjugates. These glycoproteins are linked at the carboxyl terminus through a phosphodiester linkage to phosphoethanolamine attached to a trimannosyl-nonacetylated glucosamine (Man3-GlcN) core; the GlcN residue is linked to phosphatidylinositol, which is embedded in the cell membrane. Glycosphingolipids are a class of glycoconjugate in which glycans, such as Gal or glucose (Glc), are attached to cellular membrane lipids. Another major class of glycans is represented by GAGs that are not attached to protein cores, such as hyaluronan. IdoA, iduronic acid.

Figure cited from (Reily, 2019)

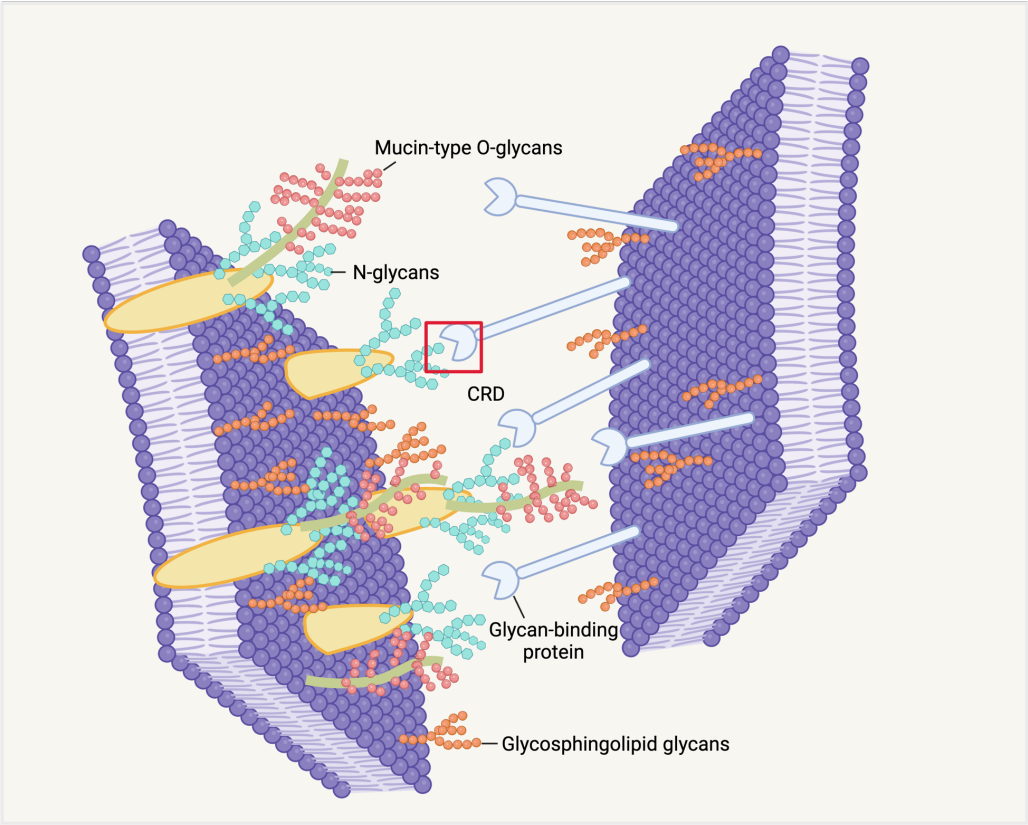

Figure 1-9 Cell-cell interactions are mediated through glycan-protein binding.

Cell interactions are mediated by glycan binding proteins (GBPs), which contains a carbohydrate recognition domain (CRD).

Adapted from (Zaia, 2011), created by Biorender.

Chapter 2 Materials and Methods

2.1 Mice

Male DBA/1 mice were purchased at 8–10 weeks of age (Envigo; Bicester, UK), housed and maintained in the Central Research Facility of the University of Glasgow. All experiments were approved by, and conducted in accordance with, the Animal Welfare and Ethical Review Board of the University of Glasgow, UK Home Office Regulations and Licences PPL P8C60C865, PPL PE1AF6E8B, PPL PP9710134, PIL I62988261, and PIL I675F0C46.

2.2 Collagen-induced arthritis (CIA) mouse model and UC-II treatment

8 to 10-week-old male DBA/1 mice received 100 µg of 2 mg/mL Chicken Bovine Type II collagen (CII; MD Biosciences) emulsified with an equal amount of complete Freund's adjuvant (CFA) on day 0 via intradermal (i.d.) injection above the tail base. On day 21, mice received 200 µg of CII in PBS via intraperitoneal (i.p.) injection. Mice were divided into five experimental groups, naïve, CFA, CIA, and CIA mice receiving undenatured collagen II (UC-II, Lonza) lower dose (0.66 mg/kg) and higher dose (7.33 mg/kg). UC-II was given to the animals by oral gavage three times a week, starting two weeks before induction of arthritis. Mice were monitored every two days for body weight, paw thickness and clinical scores. Clinical scores depend on pathological signs of joints and paws and range from 0-4 for each paw. Arthritis severity is scored as the following articular scale: 0 = no evidence of erythema or swelling, 1 = mild swelling and erythema of the ankle or tarsal joints, 2 = mild swelling and erythema of the ankle to the tarsal bone, 3 = moderate swelling and erythema of ankle to the metatarsal joints; 4 = erythema and severe swelling involving the ankle, foot, digits, or ankyloses (Pineda et al., 2012). An overall score exceeding 10; or weight loss exceeding 20%; or paw thickness exceeding 4.5 mm; or more than three paws being inflamed was considered the endpoint of the model and the mouse was immediately euthanized.

2.3 Histology

2.3.1 Paraffin blocks

Paws and gut tissue harvested from mice were fixed in 4% paraformaldehyde solution for up to 24 hours at room temperature, then transferred to 70% ethanol for storage. For joint blocks, bone decalcification, paraffin sectioning and H&E staining were completed at Histology Research Service, School of Veterinary Medicine, University of Glasgow. For gut tissue blocks, the tissue was put into the tissue processor (Lecia Asap300) followed by CRD routine program. Processed gut tissue were embedded into the paraffin blocks (Thermo scientific Histostar). The wax was left to cool and once it became solid, the paraffin blocks were removed from the mould, ready for sectioning.

For Alvetex blocks, inserts were removed and placed in to 4% paraformaldehyde fixative at 4°C for up to 24 hours. Fixative was aspirated and inserts washed with PBS three times thoroughly, and then transferred into 30% ethanol for 15 minutes, followed by 50%, 70%, 80%, 90%, 95% and then 100% ethanol for at least 30 minutes to induce dehydration. Following aspiration of ethanol, Histoclear was added for 30 minutes, and then replaced with a 50:50 solution of Histoclear and molten paraffin wax (60°C) and incubated in an oven at 60°C for 30 minutes. After this, the Histoclear: wax mix was replaced with 100 % molten wax and incubated at 60 °C for a further 60 minutes. The Alvetex inserts were then transferred to plastic embedding moulds and orientated into the required position and embedded in wax and the mould was removed once the wax hardened.

2.3.2 Haematoxylin and Eosin (H&E) staining

Paraffin-embedded sample (gut and Alvetex) sections (7 µm) were prepared by cutting the blocks using a microtome (Leica RM2125). For H&E staining, Paraffin sections/slides were heated in an oven at 60°C for at least 35 minutes to melt the wax. Sections were immersed in xylene to dewax and then in graded ethanol solutions (100%, 90% and 70%) to hydrate followed by washing in running water to remove all reagents. Sections were then stained with Harris Haematoxylin for 2-3 minutes and washed under running water to remove excess dye. The staining background was reduced by dipping sections in 1% hydrochloric acid alcohol for a few seconds, quickly rinsing in running water, immersing in Scott's Tap Water

Substitute for 30 seconds and then quickly rinsing in running water. Counterstaining was then carried out by dipping sections in 70% ethanol 9-10 times and immersing in 1% Eosin for 2-3 minutes. Sections were then dehydrated by immersion in 90% ethanol for 1 minute, 100% ethanol for 6 minutes and 100% xylene for 6 minutes. Sections were mounted with DPX and sealed with coverslips. Images were acquired on an EVOS brightfield microscope and the length of gut villi and crypt depth in the gut were determined using Image J software. Pathology of the joint tissue (cell infiltration, pannus formation, bone damage and cartilage damage) was assessed by visual evaluation according to a score system ranging from 0 (no effect) to 4 (high pathology). Assessment was conducted blindly, by two independent researchers.

2.3.3 Periodic Acid-Schiff (PAS) staining

Paraffin sections were dewaxed using the same method used for H&E staining and hydrated to water. The slides were stained with Periodic acid for 5 minutes and rinsed with water before staining with Schiff's reagent for 15 minutes. After washing with tap water for 5 minutes, the sections were counterstained with haematoxylin for 1 minute. Sections were then rinsed with tap water and dehydrated using a series of ethanol and xylene, mounted with DPX and coverslip. Images were acquired on an EVOS brightfield microscope.

2.4 Gut digestion

The gut digestion method was adapted from an established protocol (Webster et al., 2020). Basically, mouse gut samples were collected following removal of all excess fat and Peyer's patches. The gut was opened longitudinally, washed with PBS and cut into small pieces (around 1 cm) and transferred to collection buffer (HBSS with 10% FBS). Samples were then rinsed with warm HBSS and transferred. to wash buffer (HBSS no Ca^{++}, Mg^{++} and containing 2 mM EDTA) and shaken (37°C, 220 rpm) for 15 minutes. The EDTA wash step was repeated a further two times, then ileum samples were placed in digest solution (R10, 0.5 mg/mL of Collagenase IV, Cat#17104-019) and colon samples in digest solution (R10, 0.5 mg/mL of Collagenase IV containing 24 µg/mL DNase I, Cat#9003-98-9) and shaken (37°C, 220 rpm) for 15 minutes (ileum) or 20 minutes (colon). After digestion, samples were topped up with 30 mL of ice-cold RPMI and placed on ice, then filtered through a 100 µm filter then a 70 µm filter. Samples were then centrifuged for 10

minutes at 400 g, the supernatant discarded and the cells resuspended in 30 mL ice-cold R10 and centrifuged for a further 10 minutes at 400 g, prior to resuspending for antibody staining and flow cytometric analysis (Section 2.5).

2.5 Flow cytometry

For gut tissue, the samples were digested as described in section 1.4 and then resuspended at 1-10x10^6/mL in azide-free and serum/protein-free PBS and stained with viability dye for 30 minutes at 4°C. The cells were then washed with PBS twice and non-specific Fc-mediated interactions blocked by Anti-mouse CD16/CD32 (0.5-1 µg per 100 µL sample) for 15 minutes at room temperature. After washing with FACs buffer (PBS; 1% FBS; 0.4% 0.5 M EDTA), the cells were stained with antibodies according to experimental design and gating strategy. The antibodies used are listed in Table 2-1, Table 2-2, and Table 2-3. Biotinylated lectins required secondary streptavidin staining. Following washing, the cells were fixed by fixation buffer (Cat#420810, Biolegend) at room temperature for 15 minutes, avoiding light. Cells were washed with FACs buffer once and resuspended in 200-300 µL FACs buffer for analysis.

Lymph nodes were dissociated by pressing gently with 2 ml syringe on 70 µm strainer over a 50 ml falcon tube and rinsed with medium to get a single cell suspension. This process was repeated until the lymph nodes were totally dissociated and samples were stored on ice. Cells were cultured at 1x10^6/mL and stimulated with PMA (50 ng/mL; Sigma, P1585)/Ionomycin (500 ng/mL; Sigma, I0634) for 30 minutes at 37°C before adding brefeldin A (1:1000, Invitrogen, Cat#00-4506-51) and incubating for a further 3 hours. The cells were then washed with PBS twice prior to antibody staining.

For intracellular staining to check cytokine expression or nuclear staining, the cells were stained for cell surface markers as described for the gut tissue above. Samples were then permeabilised using the Foxp3/Transcription Factor Staining Buffer Set (eBioscience™, Cat#00-5523-00), according to the manufacturer's instruction. Briefly, samples were incubated with 0.5 mL Foxp3 fixation/Permeabilization working solution for 30 minutes at 4°C, avoiding light. Then 1 mL permeabilization buffer was added to each sample and cells were centrifuged (400 g, 5 minutes, room temperature). Following resuspension of the

pellet, intracellular staining antibodies (Table 2-2, Table 2-3) were added and incubated for 30 minutes at room temperature, avoiding light. Cells were then washed with permeabilization buffer and resuspended in FACs buffer and analyzed by flow cytometry. Data were acquired using an Fortessa flow cytometer (BD) and analysed using FlowJo version 10.7.1.

2.6 Epithelial cell purification by flow cytometric sorting

Gut tissue was digested as described in section 2.4. Cell suspensions were stained with antibodies and lectins (Table 2-3) following the protocol in section 2.5 and cell sorting was performed using FACS Aria III (BD) using a 100 µm nozzle into 1.5 mL tubes containing 500 µL RLT buffer provided by RNeasy Mini kit (Qiagen, Germany). After sorting, the cells were stored on ice for RNA extraction.

2.7 RNA extraction

2.7.1 RNA extraction from gut tissue

Gut tissues were dissolved in Trizol Reagent (1ml/50–100 mg of tissue) following tissue homogenization and the lysates were centrifuged for 5 minutes at 12,000 rpm at 4°C. The supernatants were transferred to a fresh tube and chloroform (0.2mL/mL of Trizol) was added to the samples for 2-3 minutes incubation then followed by centrifugation (15 minutes at 12,000 g at 4°C). Following transfer of the RNA-containing aqueous phase to a new tube, RNA was precipitated by adding 100% ethanol. Isolated RNA was cleaned using RNeasy Mini kit (Qiagen, Germany) according to the manufacturer's instructions. RNA concentrations were determined using nanodrop.

2.7.2 RNA extraction from epithelial cells freshly sorted

The epithelial cells were sorted into the tubes containing 500 µL RLT buffer provided by RNeasy Mini kit (Qiagen, Germany). The final volume was measured using a pipette with sterile tip to adjust the amount of RLT required so that there is exactly 350 µL RLT buffer to every 100 µL of sorted sample volume. 250 µL of 100% ethanol was then added for every 350 µL RLT-100 µL sample volume, mixed thoroughly and samples were applied to RNeasy mini columns, following the manufacturer's instructions. RNeasy MiniElute (74204, Qiagen, Germany) was used

for concentrating the final RNA in 14 µL. RNA concentrations were determined using nanodrop.

2.8 RT-qPCR

cDNA was synthesized before running RT-qPCR. The High-Capacity cDNA Reverse Transcriptase kit (Applied Biosystems, Life Technology, UK) was used to generate cDNA. RNA samples were diluted to the required concentration (at 10 µL) and 10 µL reaction mixes were prepared containing reverse transcriptase, dNTPs, RNase inhibitor and random primers as per manufacturer's instructions. Samples were put into Veriti 96 Well Fast Thermal Cycler (Applied Biosystems), and incubated at 25°C for 10 min, followed by 37°C for 2 h and then 95°C for 5 min to inactivate the enzyme. cDNA samples were stored at -20°C, prior to quantitative PCR.

Master mixes including Taqman probes 20x (0.5/0.25 µL), 2x reaction buffer (5/2.5 µL), cDNA (enough for 10 ng) and dH20 (enough for 10/5 µL total) were prepared in 96/384 well plates. Plates were run on Applied Biosystems StepOne PlusTM real-time PCR system (Applied Biosystems, UK) using KiCqStart® qPCR Ready Mix (Sigma-Aldrich). Cycling conditions were as follows: 20 seconds at 95°C, then 40 cycles of denaturation at 95°C for 3 seconds and annealing at 60°C for 20-30 seconds. Taqman probes (Table 2-5) were used to evaluate gene expression, including TGF-β (Mm01178820_m1, ThermoFisher Scientific), Foxp3 (Mm00475162_m1, ThermoFisher Scientific), IL-6 (Mm00446190_m1, ThermoFisher Scientific), IL-10 (Mm00439614_m1, ThermoFisher Scientific), IL-17 (Mm00434214_m1, ThermoFisher Scientific), IL-22 (Mm00444241_m1, ThermoFisher Scientific), Ahr (Mm004789312_m1, ThermoFisher Scientific), Fut1 (Mm00484518_s1, ThermoFisher Scientific), Fut2 (Mm00490152_s1, ThermoFisher Scientific), Fut4 (Mm00487448_s1, ThermoFisher Scientific), Fut7 (Mm04242850_m1, ThermoFisher Scientific), Fut8 (Mm00489789_m1, ThermoFisher Scientific), and Fut9 (Mm01717333_g1, ThermoFisher Scientific). Data were normalised to the reference gene ß-actin (NM_007393, applied biosystem, 4352663) to obtain the ΔCT values that were used to calculate the fold change or relative expression.

2.9 Serum cytokine and antibody ELISAs

Following generation of lymph node single cell suspensions (Chapter 2.5), cells were then cultured (10^6/mL) and stimulated with PMA (50 ng/mL) (Sigma, P1585)/Ionomycin (500 ng/mL) (Sigma, I0634) for 12 hours, when supernatants were collected for detection of secreted cytokines. Interleukin-17 (IL-17) (R&D systems, DuoSet, Cat#DY421-05) and interleukin-22 (IL-22) (R&D systems, DuoSet, Cat#DY582-05) were measured by ELISA kit according to the manufacturer's instructions. For determination of anti-collagen type II-specific IgG1 and IgG2a antibodies in serum, high-binding 96-well ELISA plates were coated with CII (5 µg/mL) overnight at 4°C before washing and blocking with PBS 5% BSA. The serum was diluted at appropriate concentration and incubated with HRP-conjugated goat anti-mouse IgG1 (Southern Biotech, Cat#1070-05) or IgG2a (Southern Biotech, Cat#1080-05) (1:10,000) in PBS 10% FBS prior to developing with TMB. Samples were read in a microplate reader (Sunrise) at an optical density of 450 nm.

2.10 Recall experiment

Lymph node cells were resuspended at $2x10^6$/mL (100 µL cell suspension in U-bottom 96 well plates) and stimulated with 50 µg/mL CII (MD Biosciences) or 10 µg/mL CII, collecting the supernatants at 96 hours for measurement of cytokines using Cytometric Bead Array (CBA) Mouse Th1/Th2/Th17 Cytokine kit (BD, Cat#560485) following the manufacturer's instructions and samples analysed by flow cytometry. The data was acquired at LSRII (BD) and analysed using FlowJo version 10.7.1.

2.11 IF staining

For cytokine staining, mouse joint and gut tissue sections were prepared at 7 µm thickness. Sections were deparaffinized in Xylene and dehydrated using a gradient of ethanol solutions (100%, 90%, 70%, 50% and 30%), rinsed with running water for 3 minutes and put into neutral buffered formalin (NBF) buffer for 10 minutes (NBF step not required for gut tissue). Following rinsing with water, sections were put into pre-warmed antigen retrieval buffer (Citrate buffer, Ph: 5.0) in the oven (about 70°C) for 20 minutes, then rinsed with PBS-T (0.05% Tween 20) buffer for 5 minutes twice. Sections were blocked with PBS containing 10% FBS and matching

animal serum for primary antibodies (1:200) for 30 minutes at room temperature. The slides were rinsed with PBS containing 0.5% triton for 5 minutes (x2) and incubated with primary antibodies (Table 2-4) in PBS containing 0.5% triton and 1% BSA at 4°C overnight. The slides were rinsed with PBS-T for 5 minutes (x2) and then incubated with secondary antibodies in PBS for 1 hour at room temperature. Following rinsing with PBS-T for 5 minutes (x2), streptavidin (in PBS) was applied where appropriate for 30 minutes, rinsed with PBS for 5 minutes (x3) and mounted with SlowFadeTM Diamond Antifade Mountant with DAPI (ThermoFisher Scientific, Cat#S36968) to stain nuclei and covered with glass coverslips. Staining was visualized using an EVOS^{TM} FL Auto 2 microscope (Invitrogen) and LSM880 confocal microscope (Zeiss). And the images were analysed by Image J software.

For lectin staining, the gut tissue and Alvetex sections (7 µm thickness) were dewaxed in xylene followed by treatment with 100% EtOH, 90% EtOH, 70% EtOH, 50% EtOH, and 30% EtOH (for 3 min x2), respectively. Sections were then incubated with antigen retrieval buffer (Citrate buffer, Ph: 5.0) for 20 min at 95°C (Pineda et al., 2014). To block non-specific glycoprotein binding, sections were incubated with Carbo-Free Blocking Solution (Vector labs) for 30 minutes at room temperature. The slides were washed in PBS-T for 5 minutes (x2) and Streptavidin/Biotin blocking was performed following kit instructions (Vector laboratories, SP-2002). Sections were incubated with biotinylated lectins (Table 2-4; 1:200) in PBS and incubated overnight at 4°C. Sections were washed with PBS-T at least 3 times. Streptavidin with a fluorophore (1:400 in PBS) was added at room temperature for 60 min. Slides were rinsed with PBS for 5 minutes (x3) and mounted with SlowFadeTM Diamond Antifade Mountant with DAPI. Images were acquired with EVOS^{TM} FL Auto 2 microscope and LSM880 confocal microscopy. The images were analysed by Image J software.

2.12 RNA sequencing and data analysis

Total RNA was isolated from whole gut tissue and intestinal epithelial cells, with RNA integrity checks performed using the Agilent 2100 Bioanalyzer System and nanodrop respectively, with RNA integrity numbers (RIN) > 8 for all gut tissue samples and 260/280 values of around 2 for intestinal epithelial cell samples. Library preparation was done using RNA poly A enrichment at Novogene (Cambridge, UK) and Glasgow Polyomics (Glasgow, UK). RNAseq reads were

mapped to the mouse reference genome (GRCM38) using Hisat2 version 2.1.0. Featurecounts version 1.4.6 was used to quantify read counts. Mouse ENSEMBL gene ID to gene symbol conversion was performed in R BiocManager packages. The differentially expressed (DE) genes were identified using DESeq2, and Principal component analysis (PCA) was performed using the R Bioconductor project DEbrowser (Kucukural et al., 2019). Genes passing a threshold of Padj<0.01 and |log2Foldchange| > 2 were considered as DE genes. Gene Ontology (GO) Biological Process enrichment and KEGG pathway enrichment were conducted with Metascape (Zhou et al., 2019) and PathfindR (Ulgen et al., 2019).

2.13 16s metagenomic sequencing

DNA from faecal samples were extracted using the QIAamp Fast DNA stool Mini Kit (51604, QIAGEN) following the manufacturer's instructions. DNA integrity checks were performed by nanodrop. Full-length Amplicon Metagenomics sequencing (PacBio) and library preparation were performed by Novogene (Cambridge, UK). ASV analysis and species annotation, Alpha-diversity and Beta-diversity analysis were conducted by Novogene using established bioinformatic pipelines.

2.14 Glycan isolation and permethylation from gut tissue

Glycan isolation from intestine tissue was by an adaptation of an established method (Ismail et al., 2011b) and was as shown in Figure 2-1. Briefly, gut tissues were weighed and then disrupted on ice using a Tissue Ruptor (Th-03, QIAGEN) with homogenization buffer (25 mM Tris, 150 mM NaCl, 5 mM EDTA and 1% CHAPS at pH 7.4). Glycosphingolipids were removed using methanol and chloroform, and precipitated proteins were then reduced and carboxymethylated using dithiothreitol and iodoacetic acid, followed by their digestion with trypsin. The samples were then dialyzed against 50 mM ammonium bicarbonate (Ambic, VWR CHEMICALS, UK) at 4°C overnight with buffer changes, followed by lyophilization to generate glycopeptides. Glycopeptides were subjected to tryptic digestion and purified using a C_{18} cartridge (Oasis HLB Plus Waters) prior to N-glycosidase F (Roche) treatment to release intact N-glycans. The separated N-glycans were purified and permethylated using a Sep-Pak C_{18} cartridge (Oasis HLB Plus Waters). The O-glycans were released from glycopeptides by reductive elimination using 0.1 M potassium hydroxide (KBH_4) solution, and then purified by elution from a

Dowex 50W X8 (Sigma-Aldrich) desalting column. Chemical derivatization of O-glycans was performed and followed by permethylation. Permethylated glycans were purified by using Sep-Pak C_{18} cartridge and then lyophilised.

2.15 Mass spectrometric analysis of glycans

MALDI-MS data were acquired by 4800 Plus Matrix-assisted laser desorption ionization-time of flight (MALDI-TOF) analyzer mass spectrometer (Applied Biosystems) at Department of Life Sciences at Imperial College London. MS/MS data were acquired by using the same instrument to identify specific peaks. The bioinformatic GlycoWorkBench (GWB, version 1.1) (Alessio Ceroni, 2008) tool was used to annotate mass spectra with known glycan structures.

2.16 Three-dimensional cell culture

Human gut fibroblast CCD-18Co (CRL-1459, ATCC), human epithelial cells Caco-2 (HTB-37, ATCC) and human goblet cells HT-29 (HTB-38, ATCC) cell lines were cultured using complete growth media (500 mL DMEM supplemented with 10 % heat-inactivated FCS, 0.1 mM non-essential amino acids, 2 µm L-glutamine, 100 U/mL penicillin and 100 U/mL streptomycin) in T-75 flasks, respectively. CCD-18Co cells were divided into three groups: non-treated, treated with sialyltransferase Inhibitor (3Fax-Peracetyl Neu5Ac - Calbiochem, 566224, 125 µM) and fucosyltransferase inhibitor (2F-Peracetyl-Fucose, Sigma, 344827, 100 µM). Cells were seeded on Alvetex Scaffolds at concentrations equivalent to 1×10^6 cells per well for 9 days and treated with the relevant inhibitor/vehicle for another 4 days, with one change of medium. After these 14 days, the medium was removed and 2 mg/mL rat tail collagen I solution (Gibco, Cat#A1048301) was added on the Alvetex Scaffold surface and incubated for 3 hours to set, after which fresh medium was added and culture incubated overnight. The following day, following removal of the medium, Caco-2 and HT-29 cells (9:1) were seeded on the surface of Alvetex Scaffold (0.5×10^6 cells per well). Plates were incubated for 3-4 hours to allow cells to settle on the top of the scaffold, after which the cultures were topped up with fresh medium in preparation for the following experiments.

2.17 Transepithelial Electrical Resistance (TEER) measurement

The TEER (Ω) of the insert was measured using a Millicell® ERS-2 Voltohmmeter (Sigma-Aldrich, United States). The TEER value ($\Omega \cdot cm^2$) was calculated by subtracting the resistance of the blank insert from that of the sample and multiplying it with the surface area of the insert (cm^2) (Darling et al., 2020).

2.18 Horseradish Peroxidase (HRP) Permeability Assay

The medium was completely removed from the upper chamber (only) and HRP (Sigma-Aldrich, United States) was added to the upper chamber at a concentration of 100 µg/mL. After 1 hour, the entire medium was collected from the lower chamber. To quantify the concentration of HRP in the samples, the samples were reacted with TMB solution for 5 minutes. The process was then halted using 10% H_2SO_4. A spectrophotometer was used to record the absorbance at 450 nm in order to quantify the reactant concentration in the samples (Zhu et al., 2012).

2.19 Statistical analysis

All statistical analysis was performed with Prism 8 software (GraphPad). One-way analysis of variance (ANOVA) was used for comparing differences among multiple groups. For dataset with only two groups, parametric data were analysed using Student's t-test and non-parametric data were analysed using the Mann-Whitney U test where *$p<0.05$, **$p<0.01$, ***$p<0.001$, ****$p<0.0001$, ns = not significant. For symbol key, see the the appropriate figure legend.

Table 2-1 List of antibodies used for flow cytometry (Tregs panel)

Antibody	Fluorophore	Clone	Supplier	Catalogue number	Dilution
Viability dye	eFluor 780	N/A	invitrogen	65-0865-14	1 µL/mL sample
CD3	APC	17A2	BD Biosciences	565643	1:200
CD4	BV510	GK1.5	Biolegend	100449	1:200
CD8	BV605	53-6.7	Biolegend	100744	1:200
Foxp3	BV421	MF-14	Biolegend	126419	1:200
CD25	PE	7D4	BD Biosciences	558642	1:200
CD39	PE-CY7	Duha59	Biolegend	143806	1:200
CD73	FITC	TY/11.8	Biolegend	127220	1:200

Table 2-2 List of antibodies used for flow cytometry (Cytokines panel)

Antibody	Fluorophore	Clone	Supplier	Catalogue number	Dilution
Viability dye	eFluor 780	N/A	invitrogen	65-0865-14	1 µL/mL sample
CD3	FITC	145-2C11	Biolegend	100305	1:200
CD19	BV421	6D5	Biolegend	115537	1:200
CD4	Alexa fluor700	RM4-4	Biolegend	116022	1:200
CD8	PE-Cy5	53-6.7	Biolegend	100710	1:200
IL-17	PerCO-Cy5.5	eBio17B7	eBioscience	45-7177-80	1:200
IL-22	PE	1H8PWSR	eBioscience	12-7221-80	1:200
Viability dye	eFluor 506	N/A	invitrogen	65-0866-14	1:200
CD19	BUV805	1 D3	BD Biosciences	749027	1:200
CD3	BUV395	145-2C11	BD Biosciences	563565	1:200
CD8	APC-R700	53-6.7	BD Biosciences	564983	1:200
TCR γ/δ	BV605	GL3	Biolegend	118129	1:200
CD4	Alexa fluor488	GK1.5	Biolegend	100423	1:200
RORγt	Alexa fluor647	Q31-378	BD Biosciences	562682	1:200
NKp46(CD335)	PE	29A1.4	Biolegend	137603	1:200
CD27	APC/Fire750	LG.3A10	Biolegend	124237	1:200
IL-17	BV421	TC-11-18H10.1	Biolegend	506925	1:200
IL-22	PerCP-eFlour710	1H8PWSR	eBioscience	46-7221-82	1:200

Table 2-3 List of antibodies used for flow cytometry (lectins panel)

Antibody	Fluorophore	Clone	Supplier	Catalogue number	Dilution
Viability dye	eFluor 780	N/A	invitrogen	65-0865-14	1 µL/mL sample
Viability dye	eFluor 506	N/A	invitrogen	65-0866-14	1 µL/mL sample
CD45	APC	30-F11	Biolegend	103111	1:200
EpCAM	BV421	G8.8	Biolegend	118225	1:200
CD44	PerCP	IM7	Biolegend	103036	1:200
CD31	PE	W18222B	Biolegend	160203	1:200
CD31	AF700	390	Biolegend	102444	1:200
CD45	AF700	RA3-6B2	eBioscience	56-0452-82	1:200
EpCAM	AF700	G8.8	Biolegend	118239	1:200
EpCAM	FITC	G8.8	Biolegend	118207	1:200
CD157(BP3)	BV605	BP-3	BD Biosciences	745196	1:200
PDPN	APC/Fire750	8.1.1	Biolegend	127426	1:200
PDPN	PE-Cy7	8.1.1	Biolegend	127411	1:200
CD34	PE/CY7	MEC14.7	Biolegend	119326	1:200
PDGFRA	PerCP-eFluor710	APA5	invitrogen	46-1401-82	1:200
CD90.2	PE	53-2.1	Biolegend	140307	1:200
CD81	APC	Eat-2	Biolegend	104910	1:200
Streptavidin	FITC	N/A	Biolegend	405201	1:200
UEA I	Biotinylated	N/A	Vector Laboratories	B-1065-2	1:100
AAL	Biotinylated	N/A	Vector Laboratories	B-1395-1	1:200
SNA	Biotinylated	N/A	Vector Laboratories	B-1305-2	1:200
MAA II	Biotinylated	N/A	Vector Laboratories	B-1265-1	1:50
PNA	Biotinylated	N/A	Vector Laboratories	B-1075-5	1:200

Table 2-4 List of antibodies used for Immunofluorescence

Antibody	Fluorophore	Clone	Supplier	Catalogue number	Dilution
Mouse IL-17 Biotinylated antibody	Biotinylated	N/A	R&D systems	BAF421	1:200
Mouse IL-22 antibody	N/A	140301	R&D systems	MAB582	1:200
MUC2 Polyclonal antibody	N/A	N/A	invitrogen	PA5-21329	1:200
Mouse PDGFRa antibody	N/A	N/A	R&D systems	AF1062	1:200
PDPN	N/A	eBoi8.1.1	invitrogen	14-5381-82	1:200
Streptavidin	Alexa fluor 647	N/A	invitrogen	S32357	1:400
Goat anti mouse antibody	Alexa fluor 647	N/A	invitrogen	A21236	1:400
Goat anti hamster antibody	Alexa fluor 647	N/A	abcam	ab180117	1:400
Chicken anti goat antibody	Alexa fluor 647	N/A	invitrogen	A21469	1:400
UEA I	Biotinylated	N/A	Vector Laboratories	B-1065-2	1:200
AAL	Biotinylated	N/A	Vector Laboratories	B-1395-1	1:200
SNA	Biotinylated	N/A	Vector Laboratories	B-1305-2	1:200
MAA II	Biotinylated	N/A	Vector Laboratories	B-1265-1	1:200
PNA	Biotinylated	N/A	Vector Laboratories	B-1075-5	1:200
ConA	Biotinylated	N/A	Vector Laboratories	B-1005-5	1:200
RCA I	Biotinylated	N/A	Vector Laboratories	B-1085-1	1:200

Table 2-5 List of Taqman probes used for RT-qPCR

Primer	Assay ID	Supplier	Sequence
TGF-β	Mm01178820_m1	ThermoFisher Scientific	ctc cacagagaag aactgctgtg tgcggcagct gtacattgac tttaggaagg acctgg
Foxp3	Mm00475162_m1	ThermoFisher Scientific	agcac tgccaagcag atcatctcct ggatgagaaa ggcaaggccc agtgcctcct ccagagagaa gtggtgcag
IL-6	Mm00446190_m1	ThermoFisher Scientific	tgtg caatggcaat tctgattgta tgaacaacga tgatgcactt gcagaaaaca atctgaaact tccagagata caaa
IL-10	Mm00439614_m1	ThermoFisher Scientific	tcaaacaaa ggaccagctg gacaacatac tgctaaccga ctccttaatg caggacttta agggttactt gggttgccaa
IL-17	Mm00434214_m1	ThermoFisher Scientific	ggctgagct gcagagtcaa gaatagtact tgtctggatg acagctggat ccaccccaaa aacctgaccc cgtcttcccc aaaaaacatc tatatcaa
IL-22	Mm00444241_m1	ThermoFisher Scientific	ccagcc ttgcagataa caacacagat gtccggctca tcggggagaa actgttccga ggagtcagtg ctaaggatca gtgctacct
Ahr	Mm004789312_m1	ThermoFisher Scientific	tacag gcgctgaatg gctttgtgct ggttgtcaca gcagatgcct tggtcttcta tgcttc
Fut1	Mm00484518_s1	ThermoFisher Scientific	tcgctgg caatggacag gagggtacac cggggaagga ctttgcactt ctcacacagt gtaaccacac catcatgact attggcacc
Fut2	Mm00490152_s1	ThermoFisher Scientific	attctccg ttcctcaaaa tctttaagcc agcagcagcc ttcctccccg agtggatggg catccccgca gacct
Fut4	Mm00487448_s1	ThermoFisher Scientific	tgtc tgtggacgtg tttggtcgga cgggacccgg acggccagtg ccagccatcg ggctgctgca cac
Fut7	Mm04242850_m1	ThermoFisher Scientific	caagggtac caccccacca ggaggctgcg ggcctggggc ggcctagctg gaggagcaac attcatggta atttggtttt
Fut8	Mm00489789_m1	ThermoFisher Scientific	tctccgaat accagaaggc cccattgacc aggggacagc tacaggaaga gtccgtgttt tagaagaaca gc
Fut9	Mm01717333_g1	ThermoFisher Scientific	atcgg tttttgtgaa ttctgtcttc tgcctagcgc tcggacctag gtttctccac aaagtcc

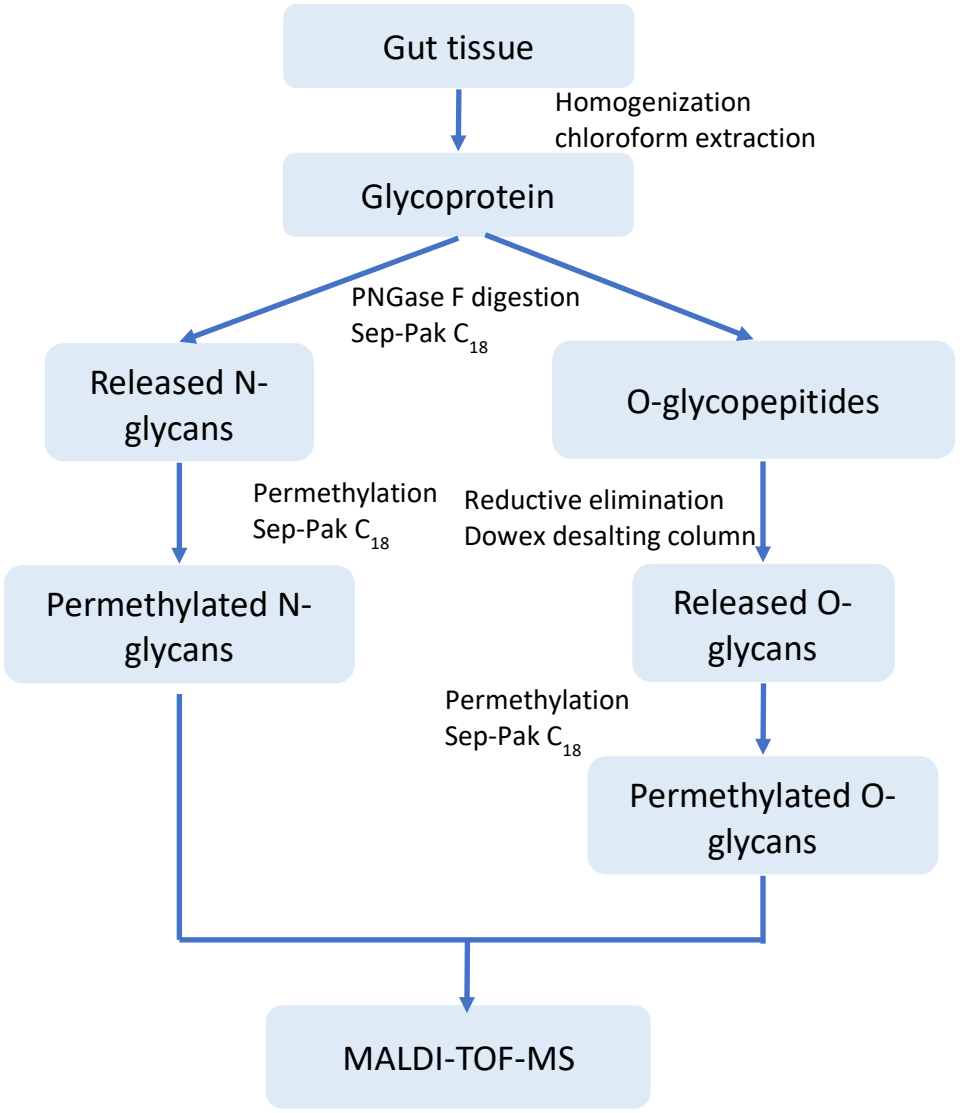

Figure 2-1 Isolation of glycans from tissue process

Gut tissue were homogenized and glycoproteins were extracted by chloroform. N-glycans were released from glycoprotein by PNGase F digest, then followed by clean up and permethylated using Sep-Pak C_{18} cartridge. O-glycopepitides were performed reductive elimination and purified by Dowex desalting column. O-glycans were released by chemical derivatization and permethylated by using Sep-Pak C_{18} cartridge.

Chapter 3 Protective effects of UC-II in experimental arthritis

3.1 Introduction

Rheumatoid arthritis is a chronic inflammatory disorder in which the most obvious affected tissue is the joint. However, it can also damage a wide variety of body systems, including the skin, eyes, lungs, heart, and blood vessels. Over the past 30 years, with the enhanced understanding of RA pathogenesis, treatment has been improved, from symptom relief strategies to biologic drugs able to interfere with and modulate immunopathological networks. However, a cure has not yet been found and some patients still do not respond to treatment.

As mentioned in the general introduction, type II collagen (CII) constitutes a potential target for clinical interventions in patients who develop anti-CII autoantibodies. For these patients, therapies are based on oral tolerance mechanisms because CII is a single well-defined molecule, opposite to ACPA antibodies. Antibodies against CII are important in the development of experimental arthritis, and CII-specific B and T-cells have been identified in human synovium and synovial fluid in RA (Toussirot, 2002, Ping Zhu, 2007). Therefore, collagen-derived products have been tested to induce oral tolerance with therapeutic goals in RA. Undenatured Type II Collagen from Lonza (UC-II®) is a modified chicken collagen that has shown an enhanced ability to induce tolerance compared to other collagen-based formulations in joint disease (Bagi et al., 2017, Lugo et al., 2016, Rui et al., 2021), although its mechanism of action has not yet been fully described. This might be because most research has focused on the immune cells directly responsible for tolerogenic responses in the gut and immune tissues, whilst very little attention has been given to the non-immune cells that support the local microenvironment.

Recent research indicates that maintenance of the local gut tissue architecture and microenvironmental cues are critical for correct immunological discrimination and homeostatic resolution of inflammation. Interestingly, loss of mucosal barrier function in the gut has been implicated in the aetiology of arthritis, providing the basis for the gut-joint axis theory (Doonan et al., 2019, Matei et al., 2021, Zaiss et al., 2021), which establishes a functional link between the gut and other

inflamed tissue and suggests that restoration of the gut barrier integrity could be exploited therapeutically. Thus, it has been postulated that RA could initiate at mucosal sites before transitioning to more distant synovial joints (Holers et al., 2018). A better understanding of the microenvironmental changes in gut mucosal sites in health and disease will allow us to understand, and ultimately utilise, the induction of oral tolerance.

In this study, we used the murine model of CIA to mimic human RA. We defined five experimental groups: i) non-treated animals (Naïve), ii) mice treated with complete Freund's adjuvant (CFA), iii) mice undergoing experimental arthritis (CIA), iv) mice undergoing arthritis with lower dose of prophylactic undenatured collagen (0.66 mg/kg) (UC-II-L) and v) mice undergoing arthritis with higher dose of prophylactic undenatured collagen (7.33 mg/kg) (UC-II-H). Regular monitoring was carried out every 2 days during the progression of the model (typically 33-35 days). The degree of arthritis was evaluated by clinical scores upon visual examination, measuring paw width and weight. We used this model to further characterise i) immune mechanisms activated upon administration of prophylactic doses of undenatured collagen in mice, and ii) functionally relevant structural changes of the gut mucosal sites associated with undenatured collagen protection against CIA. These results increase our fundamental understanding of the role(s) of the gut in autoimmunity and provide further evidence of the relevance of the gut-joint axis in arthritis. These findings show novel regulatory mechanisms linked to the therapeutic activity of undenatured collagen in joint disease and may support the development of alternative areas for clinical intervention and prevention in RA.

3.2 Results

3.2.1 UC-II ameliorates disease in experimental arthritis

To investigate the prophylactic effects of UC-II, UC-II was administrated by oral gavage two weeks (3 times/week) in advance of the model. The experimental scheme is shown in Figure 3-1a. Monitoring of disease progression showed that administration of higher dose of UC-II suppressed joint inflammation as evidenced by the significant reduction in clinical scores and paw swelling observed in UC-II-H mice compared to CIA controls. However, when mice administrated at lower

dose of UC-II, lower dose of UC-II accelerated the progression of arthritis achieving a similar level to CIA controls (Figure 3-1b-c). The healthier status of UC-II-H group was evidenced by a reduced disease incidence as well as the lack of weight loss relative to that observed in the CIA control mice. Similar results were observed in UC-II-L mice in terms of weight loss and disease incidence (Figure 3-1d-e). We also checked the proportion of mice with severe disease (articular score above 4). Higher dose of UC-II slightly reduces the percentage of mice undergoing severe disease even when the data did not reach significant differences (Figure 3-1f).

Confirming the clinical results, histopathological analysis shows high numbers of immune cells infiltrating the joints of CIA mice, causing bone damage and severe loss of cartilage. Interestingly, bone damage and loss of cartilage were ameliorated in both UC-II groups, although lower dose of UC-II showed limited effects on clinical criteria (Figure 3-2a). Consistently, disease indicators (cell infiltration, pannus formation, and cartilage and bone damage) showed that both doses of UC-II reduced tissue pathology (Figure 3.2b). The percentage of mice with no pathology, or fully protected, was higher in UC-II-L group, and was 2-3 times higher in UC-II-H group for all parameters tested, although overall histological scores did not reach statistical significance, including cell infiltration [CIA:6.3%; UC-II-H:18.8%], pannus formation [CIA:15.6%; UC-II-H:31.3%], cartilage damage [CIA:25%; UC-II-H:46.9%] and bone damage [CIA:21.9%; UC-II-H:50%] (Figure 3-2b).

3.2.2 UC-II inhibits systemic inflammatory pathways

After confirming the prophylactic effect of undenatured collagen in CIA mice, the immune mechanisms associated with protection were investigated. First, expression level of IgG2a anti-CII antibodies (Brand et al., 1996) were checked to evaluate whether UC-II regulated pathogenic humoral responses. The results show all mice undergoing CIA had elevated levels of anti-collagen antibodies in serum, but no difference was observed between CIA and UC-II groups, with respect to either IgG1 or (pathogenic) IgG2a isotypes (Figure 3-3a), indicating no suppression or repolarisation at this experimental endpoint. To evaluate cellular responses, the total number of cells in joint draining lymph nodes (DLN), i.e., axillary, brachial and popliteal were determined. A significant increase in cell number was observed in CIA mice and UC-II-L mice, whereas those in the healthy and UC-II-H groups were not significantly different (Figure 3-3b). Further analysis of distinct

immune cell populations showed that this trend was conserved for cell numbers, but not proportions of T cells, including CD4 and CD8 T cells, as the numbers of both lymphocyte groups in UC-II-H were not significantly different from the levels found in naïve and CFA mice (Figure 3-3c). Interestingly, we observed a significant change in T cell numbers between lower dose and higher dose of UC-II (Figure 3-3c). By contrast, the increase of B cell numbers was statistically significant both in CIA and both UC-II groups compared with naïve controls (Figure 3-3c), in line with the lack of effect in anti-collagen antibodies (Figure 3-3a).

Next, focusing on the most protective UC-II-H group, the numbers of regulatory T cells (Tregs), defined by their CD3+CD25+FoxP3+ expression as well as CD39 and CD73 expression, the latter two markers as evidence of their functional suppressive capacity, being regarded as immunological switches that shift ATP-driven pro-inflammatory immune cell activity towards an anti-inflammatory state mediated by adenosine (Deaglio et al., 2007) (Figure 3-4a). However, the results did not show significant differences in their number in the DLNs amongst the groups (Figure 3-4b). Likewise, there were no differences in the levels of CD39+ or CD73+ Tregs, effector cells responsible for generating functional inhibitory responses. Furthermore, a "recall" experiment was carried out to examine whether there were any changes in antigen-specific responses in the DLNs in healthy, CIA and UC-II treated groups. This showed essentially baseline responses of a variety of cytokines, with no significant differences among the groups except an apparent decrease of IL-4 when the CIA cells were exposed to lower concentration of CII, indicating potential suppression of Th2 response in UC-II-H mice (Figure 3-5). Collectively, these data suggested that Treg-mediated mechanisms were not responsible for the observed UC-II protection against CIA.

Thus, it was hypothesised that protection in UC-II-H mice was associated with a reduction in pro-inflammatory cytokines, rather than an increase of regulatory responses. Specifically, expression of IL-17 and IL-22 was measured in DLNs and joints, as both cytokines have been reported to promote joint inflammation in arthritis (Pineda et al., 2012, Kim et al., 2012, Geboes et al., 2009). The results suggest that IL-17 was significantly up-regulated in the DLNs cells from CIA mice upon TPA/Ionomycin stimulation in vitro, but not in UC-II-H mice (Figure 3-6a). IL-22 was under the ELISA detection limit so we could not confirm IL-22 expression

in the DLNs. The increase of both IL-17 and IL-22 were observed in the joints in CIA mice, but not in UC-II-H mice (Figure 3-6b-c). Furthermore, flow cytometric analysis of intracellular cytokine expression by DLN cells supported the idea that higher dose of UC-II inhibited the up-regulation of both IL-17 and IL-22 systemic responses under arthritic conditions (Figure 3-7). We also observed a significant difference of frequency of IL-17 positive lymphocytes in the DLNs between CFA and CIA mice, and also between the UC-II groups (Figure 3.7b). Cell number data show no differences. Next, the cell types affected were investigated, analysing CD4+ and CD8+ T cells, and CD19+ B cells by flow cytometry (Figure 3-7a). Visualisation of cell frequency and numbers in radar charts (Figure 3-8) revealed changes in IL-17 and IL-22 producers in UC-II groups, especially the UC-II-H group. Thus, whilst IL-17+ and IL-22+ CD4 and CD8 T cells were significantly reduced compared to CIA mice, B cell-dependent production of IL-17 and, to a lesser extent, IL-22 was less affected or even increased. We also observed a significant reduction in IL-22 CD4+ T cell numbers in the higher dose of UC-II compared to the lower dose, providing an interpretation for the observed significant increase in T cell numbers (Figure 3-3c). Supporting the pathogenic roles of IL-17 and IL-22 in CIA, the numbers of cytokine producers in T cells in DLN significantly correlated with disease scores (Figure 3-9), with less correlation of B cell-derived cytokines with disease.

3.2.3 Oral administration of UC-II protects against damage to gut tissue in CIA

Although inflammatory cytokines and cellular responses were reduced in the joint and DLN tissue of higher dose UC-II treated animals, other complementary mechanisms could work simultaneously. As described in the general introduction, establishment of oral tolerance by feeding of antigens is a direct consequence of specific immune responses triggered in the gastrointestinal tract and gut-associated lymphoid tissue (GALT), which can lead to loss of mucosal barrier function in RA, suggesting that gut tissue architecture can modulate gut immunity and host-microbiome interactions (Matei et al., 2021). Our previous studies showed that gut pathology precedes and perpetuates chronic systemic inflammation driving autoimmunity and joint damage in CIA (Doonan et al., 2019). To further investigate whether this is targeted in the protective effect of UC-II, the integrity of the gastrointestinal tract (duodenum, jejunum, ileum, and colon)

was evaluated in our experimental model (Figure 3-10a). CIA mice showed substantial damage in all gut areas, such as disruption of the epithelial layer, cell infiltration and thickening of the muscular layer and reduced villi length/crypt depth ratio, pathological signs that were weakened in both UC-II groups (Figure 3-10b). Likewise, PAS staining showed that colon from UC-II mice lacked attachment/effacement lesions (Figure 3-10c) that we and others have previously associated with arthritis (Doonan et al., 2019, Matei et al., 2021).

To evaluate how this gut tissue protection was reflected in terms of regulatory responses in the gut, the expression of tolerogenic genes including TGF-β, Foxp3 and IL-10, and pro-inflammatory cytokines were determined in the ileum and colon by RT-qPCR (Figure 3-11). Collectively, the data showed limited regulatory response in the UC-II treated mice regarding cytokine and transcription factor expression but suggested that expression of pro-inflammatory factors were down-regulated in UC-II groups compared to CIA mice in the colon but not in the ileum. Moreover, a significant increase of TGF-β in UC-II-H group compared to UC-II-L group was observed in the colon.

Further to this, total cell numbers in the MLNs did not change significantly between healthy mice and collagen induced mice (Figure 3-12a). Analysis of B cells and CD4+ and CD8+ T cells in the MLNs showed that the UC-II-H group mice had a significant expansion of B cells in MLNs compared not only with the CIA group, but also with the naïve controls (Figure 3-12b). By contrast, the number of $CD4^+$ and $CD8^+$ T cells in MLNs was not altered. A significant increase in CD8+ T cell frequency in UC-II-H group compared to UC-II-L group was also noted (Figure 3-12b).

Next, IL-17 and IL-22 expression was measured by flow cytometry (Figure 3-13), with the goal of assessing correlations between gut cellular networks and distant responses within the joint. However, first, IL-17 expression in the supernatants of MLNs was measured by ELISA. No differences among these groups were observed, although there was a slight reduction in the UC-II-H group (Figure 3-14a). Contrary to the DLN data (Figure 3-6, Figure 3-7), the levels of IL-17 producers in total MLNs, ileum and colon were not significantly elevated in CIA mice although, perhaps surprisingly, there was a trend for UC-II-H mice to show a higher

percentage of IL-17+ cells than in CIA animals (Figure 3-14b-d). However, analysis of the specific cell types revealed a distinct rewiring of pathogenic cellular networks in the UC-II-H group, in MLNs (Figure 3-14e), ileum (Figure 3-14f) and colon (Figure 3-14g). Overall, a broad analysis indicates that in healthy conditions, IL-17 is generally produced by innate cells (NKT, ILC3 and γδ T cells), whilst in CIA this predominantly switches to adaptive CD4/CD8 cell responses, with UC-II-H group showing a mixed pattern distinct to both health and CIA networks. Intriguingly, higher dose UC-II protection tended to correlate with increased IL-17 in ileum, albeit the results did not achieve statistical significance.

A similar evaluation of IL-22 expression in MLNs and gut tissue was performed (Figure 3-15), bearing in mind that in contrast to its inflammatory effect in the joint, IL-22 exerts key mucosal healing mechanisms, promoting epithelial regeneration and integrity, mucus production and synthesis of antimicrobial peptides(Lindemans et al., 2015, Zhang et al., 2019b, Patnaude et al., 2021). We also included NKT cells, as key producers of IL-22 in the gut. Although there was a trend pointing at increased total IL-22 production in the MLNs of UC-II-H mice (Figure 3-15a), no significant differences in ileum (Figure 3-15b) or colon (Figure 3-15c) were observed. Nevertheless, and in line with the previous results shown for IL-17, flow cytometric analysis of distinct populations suggests that IL-22 networks are actively rewired in UC-II-H mice compared to CIA and naïve controls. Thus, the production of IL-22 in naïve MLNs comes from innate ILC3 and B cells, whilst in CIA mice it expands to CD4+ T cells, NKTs and γδ T cells, the latter being the only enhanced population in UC-II-H (Figure 3-15e). All innate populations increased the expression of IL-22 in UC-II-H mice, as measured by mean fluorescence intensity (MFI) (Figure 3-15d). Although on the basis of these data it is not possible to define intestinal IL-22 as a protective or pathogenic factor in the various groups, the results in the ileum (Figure 3-15d) and colon (Figure 3-15f) highlight that distinct rewiring of the IL-22+ cells is associated with inflammatory or homeostatic conditions, with a general expansion of IL-22+ innate populations and significant increase in IL-22 production by NKT cells in UC-II-H mice. Finally, IL-22 staining in gut tissue showed an increased IL-22 secretion/deposition in the tissue epithelium in UC-II mice, especially in the colon (Figure 3-16).

3.2.4 Orally administered UC-II reshapes gut glycosylation and microbiome composition

In healthy gut, IL-22 supports homeostatic expression of mucins in epithelial cells (Sugimoto et al., 2008), as well as physical levels of fucosylation (Pham et al., 2014). As described in the general introduction, tissue and cell glycosylation play an important role in interactions between microbiota and host tissue, affecting cell signalling (Paulson et al., 2006, Ilarregui et al., 2009). Moreover, mucus in the gut can prevent inflammation by shielding the underlying epithelium from bacteria and antigens (Shan et al., 2013). Mucus is primarily composed of glycoproteins called mucins, and these mucins are heavily glycosylated (Corfield, 2000). Therefore, because our results revealed that UC-II protected gut integrity and enhanced IL-22 expression, we hypothesised that UC-II was associated with changes in glycosylation in the gut, which would in turn prevent gut damage during inflammation.

To investigate this, gut tissue was first stained with a broad range of lectins that recognise specific glycans in the gut tissue of naïve and CIA mice (Figure 3-17). A diagram showing lectin specificity is shown in Figure 3-17a and Figure 3-17b. An initial experiment, showing glycan changes along gastrointestinal tract in mice undergoing arthritis (Figure 3-17c), in line with our hypothesis. Five lectins, including *Ulex european* Agglutinin *I* (UEA I), *Auleria aureate* lectin (AAL), *Sambuccus nigra* agglutinin (SNA), *Maackia aurensis II* lectin (MAA II) and Peanut agglutinin (PNA), which can recognise fucose, sialic acid and galactose, these glycans are the most variable and common structures in the gut, were then selected for deeper analysis (Garber et al., 2021, Meimei Shan, 2013, Yao et al., 2022).

The fucosylation profile, including terminal (UEA I) and core fucose (AAL) along the gut tissue (Figure 3-18, Figure 3-19) show different patterns of staining in the small intestine and colon. Terminal fucose was mostly expressed on the villi and crypt, while core fucose has more binding sites including villi and their surface, endothelial cells, and crypt (Figure 3-18a, Figure 3-19a). In terms of fluorescence intensity of lectin staining, a down-regulation was observed along the gastrointestinal tract in terms of terminal fucose expression in the CIA mice, especially in the jejunum, while those from UC-II-H mice resembled healthy tissue

(Figure 3-18b). The core fucose expression shows an opposite trend to the terminal fucose expression (Figure 3-19b), but no significant was seen amongst experimental groups. However, an interesting finding is the expression of fucose was more reduced with a higher articular score (Figure 3-18c, Figure 3-19c).

Next, with respect to sialyation of the gut, SNA binds more endothelial cells and fewer epithelial cells than MAA II staining in the jejunum (Figure 3-20a, Figure 3-21a). Also, MAA II binds very little in the colon compared to other lectins (Figure 3-21a). Nevertheless, CIA mice exhibited a less sialylated gut tissue in general, while UC-II treated mice recovered to some extent (Figure 3-20, Figure 3-21). However, there was no clear correlationship between sialylation level and articular score.

Finally, PNA staining in the gut tissue to see galactose expression was performed, and it was found to bind more in the small intestine than in the colon, possibly due to lack of villi (Figure 3-22a) as PNA binding was similar amongst all experimental groups in the small intestine sections. No significant changes were seen in the colon sections, although CFA and UC-II groups trended to have lower levels when compared with Naïve mice (Figure 3-22b). However, the mice have higher articular scores tend to have low expression of PNA binding in the jejunum and ileum, when we checked the correlationship between PNA binding and severity of disease (Figure 3-22c).

Collectively, these data suggest that orally administrated UC-II restored the reduction in terminal fucose in mice undergoing arthritis, and reshaped sialylation and galactose expression.

Since fucosylation is associated with differential levels of chronic inflammation, to further investigate the cause of fucosylation changes, mRNA expression of fucosyltransferases (FUTs), enzymes responsible for fucosylated glycan biosynthesis was evaluated throughout the whole gut. Fut2, which is responsible for adding fucose in an α1,2-linkage to terminal galactose residues, was significantly reduced in CIA mice in the duodenum, and in UC-II-H mice in the jejunum when compared to the levels in the naïve control group. Also, Fut8 catalyzing the transfer of fucose to the core N-acetylglucosamine of N-glycans in an α1,6-linkage was significantly reduced in UC-II-H mice in the ileum. All these

data are in opposition to the observed maintenance of fucosylation in UC-II-H mice (Figure 3-23). Besides, a significant upregulation of Fut4, responsible for the addition of fucose to glycoproteins and glycolipids in an α1,3-linkage, was observed in CFA mice in duodenum and jejunum. Thus, collectively, these results suggest that fucosylation in the gut was not critically regulated at the transcriptome level, but that some other factors are participating in the reduction and rescue of fucosylation in the gut during arthritis and prophylactic treatment with UC-II-H.

Gut epithelial fucosylation is indeed strongly dependent on environmental factors, such as microbiome composition via IL-22-dependent mechanisms (Nagao-Kitamoto et al., 2020). Therefore, an alternative hypothesis is that the rewiring of IL-17/IL22 immune networks upon undenatured collagen administration modifies the composition of the gut microbiome, which in turn, can affect mucin fucosylation, consolidating dysregulation of the microbiome and inflammatory responses. To investigate support for this hypothesis, 16s sequencing of the microbiome DNA from the ileum and colon in naïve, CIA and UC-II-H groups was performed. We found the composition of microbiome was changed from that of naïve mice, both in ileum and colon in CIA and UC-II-H mice (Figure 3-24, Figure 3-26). To be specific, in the ileum, the proportion of *Firmicutes* was increased and Bacteroidota was decreased in the CIA mice, which is consistent with previous findings (Doonan et al., 2019), while these changes were rewired in the UC-II-H group (Figure 3-24a-b). Interestingly, we also found *Campilobacterota* and *Proteobacteria* were increased only in the UC-II-H group. Since the ratio between the Firmicutes and Bacteroidetes (F/B ratio) has been associated with maintaining homeostasis, changes in this ratio can lead to various pathologies (Stojanov et al., 2020) including IBD with decreased F/B ratio. In our model, no significant changes were observed although a slight increase in CIA mice (Figure 3-24c). The ratio of the UC-II-H group was similar to Naïve group. To see the microbial changes in more detail, the top 35 abundance genera in each condition group were selected. This showed that specific types of *Firmicutes* and *Bacteroidota* increased only in CIA group such as *Lachnospiraceae_UCG-001, Alistipes, and Roseburia* (Figure 3-25). In addition, some genera including *Romboutsia, Helicobacter, Allobaculum, Dubosiella, and Mycoplasma* were increased only in UC-II-H mice. To investigate the bacteria diversity in the gut, alpha diversity analysis was performed, but no

significant changes in all indices were observed during arthritis (Figure 3-26, Table S 1).

Analysis of the colon samples showed as before (Martins Dos Santos et al., 2010) that the microbial composition was different from the ileum sample, with more *Bacteroidota* and fewer *Firmicutes* in the colon than ileum (Figure 3-27). The proportion of *Bacteroidata* was increased in CIA and UC-II-H groups compared to healthy control. While UC-II rewired the decrease of *Deferribacterota* and increase of *Patescibacteria* in CIA group (Figure 3-27a-b), surprisingly, *Actinobacteriota* existed in CIA mice but not the other two groups, and *Desulfobacterota* only in UC-II-H mice (Figure 3-27b). The F/B ratio was significantly reduced in the CIA mice and slightly increased in the UC-II-H group, suggesting inflammatory colon tissue in CIA mice partially rescued by UC-II-H. The heatmap of most highly expressed bacteria data shows Lactobacillus, *Alistipes, RF39, Lachnospiraceae_NK4A136_group,* and *Candidatus Saccharimonas* to be increased and *UCG-009, Incertae_Sedis, Colidextribacter,* and *Mucispirillum,* to be decreased only in the CIA group (Figure 3-28). No significant changes in alpha diversity indices were found amongst the groups in the colon (Figure 3-29, Table S 2), although the values were higher in the colon than in the ileum, which was consistent with previous reports of more abundant bacteria in the colon.

3.3 Discussion

Mice treated with higher dose of undenatured collagen present a significant reduction in disease incidence and severity, which is associated with regulation of IL-17 and IL-22 cytokines in the joint and rewiring of associated $\gamma\delta$ T cell and ILC cytokine networks in the gut. Specifically, these effects of UC-II-H were associated with the protection of gut villi and crypt structure and the maintenance of local levels of fucosylation. In describing the local gut responses by which UC-II-H acts to suppress inflammatory responses, these findings increase our fundamental understanding of the role(s) of the gut in autoimmunity and will support the development of alternative areas for clinical intervention and prevention in RA.

Oral tolerance mechanisms have been the subject of investigation since the beginning of the 20th century but translation of these findings into a clinical setting has not always been successful, indicating that key pathways are still unknown.

Our results support the previously described protective role of undenatured collagen (Schon et al., 2022, Bagchi et al., 2002, Lerman et al., 2015), indicating a preservation of both bone and cartilage health in joint disease. Additionally, the protective effect of undenatured collagen occurs at least in part, through protection of targeted organs distal to the joint such as the gut, where it acts broadly to rewire cytokine networks and regulate the gut dysbiosis observed in arthritic mice. These results not only provide further support for the existence of a pathogenic gut-joint axis, but also describe new networks that can modulate induction of anti-inflammatory responses upon exposure to fed antigens such as undenatured collagen.

The lower dose of UC-II has a less protective effect in terms of clinical score than the higher dose, although the histology results showed protection of cartilage and bone damage in both conditions (Figure 3-2). Thus, the lower dose of UC-II protected mice against bone and cartilage damage but not swelling or inflammation of the joint. However, it is crucial to consider the experimental conditions under which the models were conducted. Experiments comparing lower and higher UC-II doses took place amid the COVID-19 pandemic, during a period of severely restricted access to animal facilities. These constraints necessitated the involvement of different staff performing the oral administration of UC-II to the mice, potentially influencing the experimental outcomes and compromising standardised handling of the mice and oral gavage. Another factor that could have been affected by these conditions is the actual amount of UC-II given to the mice, that could not be totally standardised due to the insolubility of UC-II in water. Manipulation of UC-II suspensions by different technicians could add some additional errors in the experiments. Moreover, the skin ulcers and injuries caused by intra-cage fighting could have potentially impacted immunoregulatory networks (Dokoshi et al., 2021), behavioural changes that could have been affected by animal handling. Thus, a limitation of our first models including two UC-II doses was our limited capacity to control these factors due to restricted access to our facilities. Subsequent experiments did not face such externally imposed handicaps, allowing us to clearly demonstrated the protective effect of UC-II at the established higher dose, but a future comparative study involving different UC-II doses should be repeated to yield significant conclusions about the protective efficacy of UC-II at different doses in inflammatory arthritis.

Our results show that the establishment of oral tolerance in the gut is spread out systemically to the joint tissue, downregulating the expression of pro-inflammatory Th17 cytokines and lymphocyte responses. This can explain why UC-II feeding reduces disease incidence, but it does not explain the differences observed at the histological level and some of the apparently contradictory data observed in the UC-II-L groups, where bone and cartilage were protected despite having high disease scores. Previous studies suggest that synovial fibroblasts are responsible for mediating inflammation or tissue damage in the arthritic joint by secreting inflammatory cytokines and chemokines, invading and degrading cartilage, and stimulating osteoclastogenesis to cause bone erosion (Turner et al., 2015). Interestingly, not all fibroblasts have the same roles in the synovium. Deletion of FAPα+ fibroblasts suppressed both inflammation and bone erosions in murine models of resolving and persistent arthritis (Croft et al., 2019). Two distinct fibroblast subsets within the FAPα+ population were identified by single cell transcriptional analysis. FAPα+ THY1+ immune effector fibroblasts, located in the synovial sub-lining, result in more severe and persistent inflammatory arthritis. FAPα+ THY1- destructive fibroblasts, restricted to the synovial lining layer, selectively mediate bone and cartilage damage with little effect on inflammation (Croft et al., 2019). Thus an explanation for the UC-II-L groups exhibiting higher clinical scores despite reduction of bone damage, could be related to UC-II-L targeting FAPα+ THY1- fibroblasts to prevent bone damage but not swelling of the joint.

In addition, a significant increase in TGF-β expression was observed in the colon but not the ileum tissue in UC-II-H mice compared to UC-II-L group and this could reflect their different composition of microbiota since the colon is the main location enriched with microbiome and TGF-β regulates gut microbiota (Bauche et al., 2017). Multiple environmental factors contribute to the microbiota composition, which could impact on the function of UC-II.

Despite these pitfalls, the data clearly show that UC-II ameliorates joint inflammation and bone damage during arthritis, and this is associated with the downregulation of pro-inflammatory IL-17 in the joint and draining lymph nodes. Some other tolerogenic mechanisms were not affected, including suppression of anti-collagen antibodies or increases in regulatory T cells (Treg) in the gut and

draining lymph nodes, although it has been reported that oral type II collagen increased levels of Treg and TGF-ß, in addition to the reduction of IL-17 (Tong et al., 2010). This study focused on the established stages of joint disease, and we cannot rule out that Tregs are involved prior to the induction of IL-17-mediated pathways. Likewise, we did not evaluate the numbers of regulatory B cells (Bregs), but there is experimental evidence showing that aberrant regulation of this cell type modulates arthritis progression via gut-dependent mechanisms (Doonan et al., 2019, Matei et al., 2021). In fact, we observed a significant increase in the number of B cells in the gut in response to undenatured collagen treatment, but no effects in the production of anti-collagen antibodies, perhaps indicating a role for Bregs, something that will be included in follow-up studies. Because regulatory cells are generated in the gut during the induction phase of disease (Cosovanu et al., 2020), additional studies including pre-clinical disease stages are required to provide a full understanding of undenatured collagen-dependent regulatory responses.

Moreover, in recall experiments, the results show potential UC-II-H restraint of the Th2 response by reducing expression of IL-4, which can be beneficial to suppression of inflammatory response by interacting with other immune cells and cytokines involved in RA pathogenesis (Schulze-Koops et al., 2001). However, the specific role of Th2 cells and their modulation in RA treatment is an area of ongoing research, which could be helpful to the following research.

Reduction of IL-17 can be directly related to bone protection, as IL-17 increases RANKL and osteoclastogenesis (Kotake et al., 1999). Interestingly, IL-22 expression was increased in CIA mice and decreased in the UC-II-H group in draining lymph nodes and joints (both IL-17+/IL-22+ CD4 T cell levels show positive correlations with increasing articular score), contrary to the observations in the gut, where IL-22 was generally up-regulated in UC-II-H mice. This provides further support for the dual role described by this group for IL-22 during arthritis (Pineda et al., 2014), perhaps related to the ability of this cytokine to promote gut epithelial cell regeneration(Pickert et al., 2009). This effect can be a critical part of disease pathology and protective responses, as the newly defined gut-joint axis theory(Zaiss et al., 2021) proposes that the gut mucosa is the first site of disease initiation. Consistent with this, CIA mice displayed significant gut pathology and

structural damage that was absent in UC-II-H mice. Interestingly, tolerogenic genes were up-regulated in the CIA mice but less in UC-II-H group, which could be the CIA mice were trying to produce more tolerogenic signals to counteract inflammation/damage in the gut. IL-17 acts to regulate mucosal host defence against many invading pathogens in the gut but unresolved IL-17-associated inflammation may cause gut pathology (O'connor et al., 2010). In addition, IL-22 has been proposed to play both pathologic and protective roles in gut integrity and homeostasis. Thus, to identify pathological mechanisms, the cells producing IL-17 and IL-22 in MLNs, ileum, and colon, as sites of Th17/22 induction and tolerance were investigated. Interestingly, whilst the results show upregulation of IL-17 in the gut tissue from CIA but not UC-II-H mice, the most striking changes appear to reflect UC-II-H-induced switches in the cellular networks of IL-17+ and IL-22+ cells in the gut, with these cytokines being predominantly produced by innate effector cells like NKT and ILCs, rather than the CD4+ helper and $\gamma\delta$ T cells driving systemic autoimmunity in CIA (Pineda et al., 2012). IL-22 was increased in all cell types isolated from the ileum in response to undenatured collagen administration, expanding IL-22+ $\gamma\delta$T cells, NKT cells and CD4 T cells. Overall, our data potentially shows that the protective role of gut IL-17/IL-22 depends on the relative contribution coming from innate and adaptive immune cells, although we have not investigated all the molecular mechanisms underlying these protective cytokine and cellular networks.

Future studies may focus on the ability of UC-II to harness protective IL-22 actions in the mucosal epithelium (Pickert et al., 2009, Parks et al., 2015). IL-22 promotes epithelial glycosylation, which is crucial to maintaining barrier integrity and immunity (Zheng et al., 2008, Goto et al., 2014). Certainly, the data suggest CIA mice exhibited lower fucosylation compared to healthy mice. Indeed, perhaps linking the gut-joint axis, fucose can play a protective role in both local gut and systemic inflammation (Pickard et al., 2015). Interestingly, UC-II-H reshaped the glycosylation profile in the gut, especially restoring the reduced gut fucosylation observed in CIA mice. The mechanism controlling these changes in tissue fucosylation were not defined, but since this was not associated with changes in the mRNA expression of fucosyltransferases, environmental factors could be controlling local fucose content. To address this, 16s DNA sequencing to examine microbial composition of the ileum and colon was performed. *Lachnospirales,*

which belongs to the *Clostridia* class increased in CIA gut tissue both in the ileum and colon samples, which is consistent with previous findings in RA patients (Liu et al., 2013). Mice treated with UC-II can restore the increase of this type of bacteria, but the mechanism behind this is still unclear.

Interestingly, *Parasutterella,* which has been defined as characteristic of healthy microbiome (Ju et al., 2019), was increased only in the ileum tissue of UC-II-H mice. Moreover, the genus *Parasutterella* is likely to rely on amino acids such as asparagine, aspartate and serine, where N-glycan and O-glycan bind, to support its metabolic activities and physiological functions. Importantly, they produce succinate as a fermentative end-product, which is correlated with the relative abundance of genera including *Bacteroides* and *Lactobacillus* in a dextran sulfate sodium(DSS)-induced colitis mouse model (Osaka et al., 2017). In addition, succinate acting as an intermediate metabolite, is important for cross-feeding metabolic pathways (Fernandez-Veledo et al., 2019, Connors et al., 2018). However, in the colon, we found a decrease in *Mucispirllum* in the CIA mice, which is relatively enriched in the colonic mucus. Dysregulation of this bacteria is associated with intestinal inflammation (Herp et al., 2021). In addition, we found an upregulated abundance of *Candidatus Saccharimonas,* which is involved in the mucin degradation process in the gut (Gryaznova et al., 2022). When the balance of mucin production and degradation is disrupted, it can affect the mucus layer and gut barrier. Moreover, these bacteria can cleave glycans in the mucus layer as a nutrient source, which might alter the glycosylation profile as well. Therefore, our data provided evidence that changes in glycosylation are associated with changes in the microbiome in the gut, although the causality between changes in glycosylation and microbial composition is still unknown.

Collectively, our study demonstrates the importance of differential IL-17 and IL-22 producing cell networks in the joint-gut inflammatory axis and the therapeutic potential of undenatured collagen. We identified molecular and cellular parameters in the gastrointestinal tract correlating with low inflammatory conditions, including regulation of cytokines, cellular networks, tissue glycosylation and microbial profiles. These findings could offer new opportunities to treat arthritis and other chronic inflammatory disorders affected by changes in mucosal tissues.

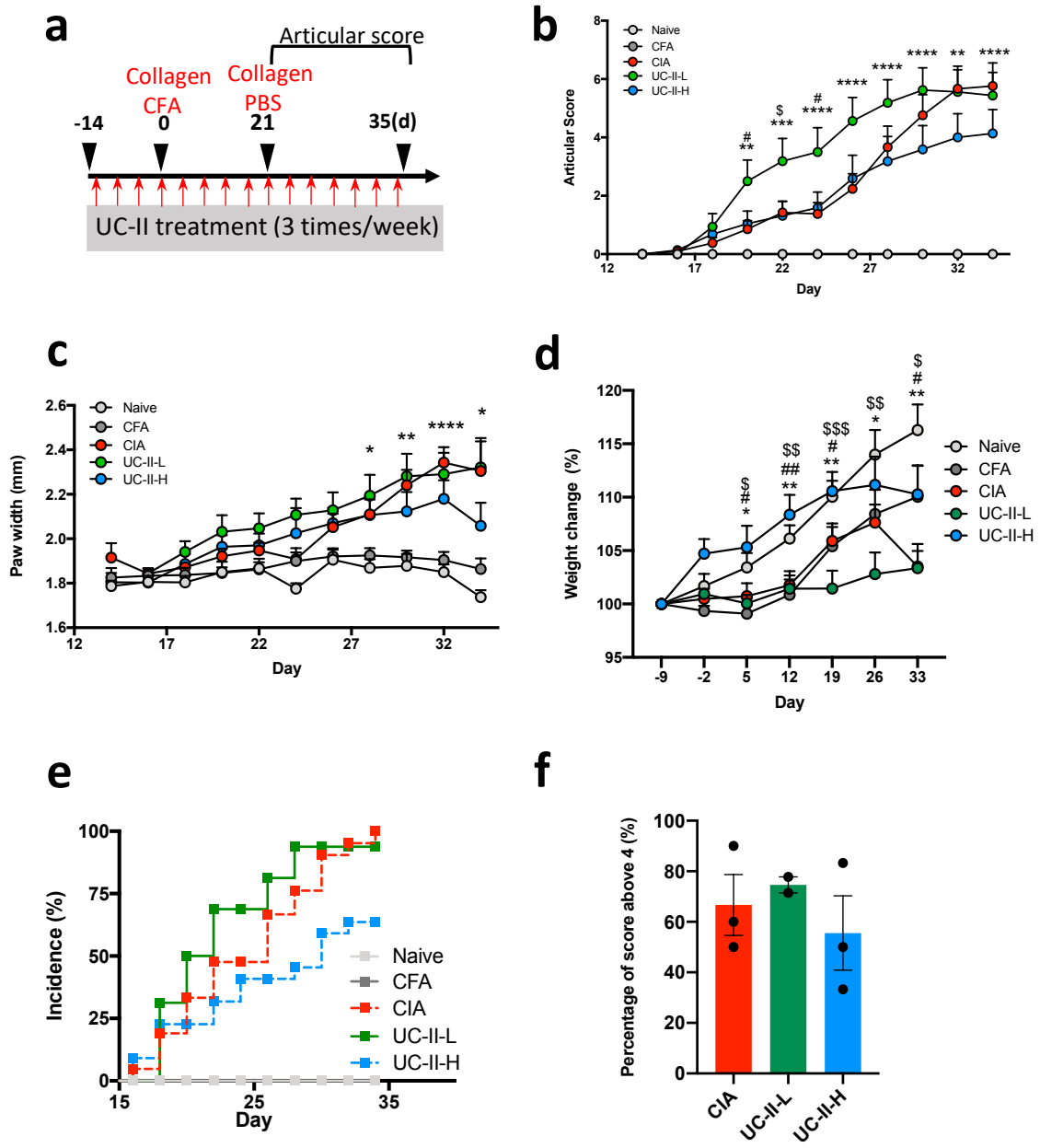

Figure 3-1 UC-II can reduce inflammation in experimental arthritis.

a) Experimental scheme. Articular score was assessed after day 21, being 0 to 4 upon visual examination. **b)** Mean articular scores of four paws. **c)** Mean paw width measured by calliper. **d)** Percentage of weight change of original weight. **e)** Incidence of disease. **f)** Percentage of high score (above 4) of sick mice. Data were pooled from at least two individual models (Naïve,n=13; CFA, n=13; CIA, n=21; UC-II-L=16; UC-II-H, n=22). Data was presented as mean ± SEM. Statistical significance was determined using Ordinary one-way ANOVA (b-d). Significance indicated by asterisks, *p < 0.05, **p < 0.01 and ***p < 0.001. Significance indicated by hash, $^{\#}$p < 0.05, $^{\#\#}$p < 0.01 (CIA vs UC-II-H). Significance indicated by dollar, $^{\$}$ p < 0.05, $^{\$\$}$ p < 0.01 and $^{\$\$\$}$ p < 0.001 (UC-II-L vs UC-II-H). CFA, Complete Freund's Adjuvant. CIA, collagen induced arthritis. UC-II-L, UC-II lower dose. UC-II-H, UC-II higher dose.

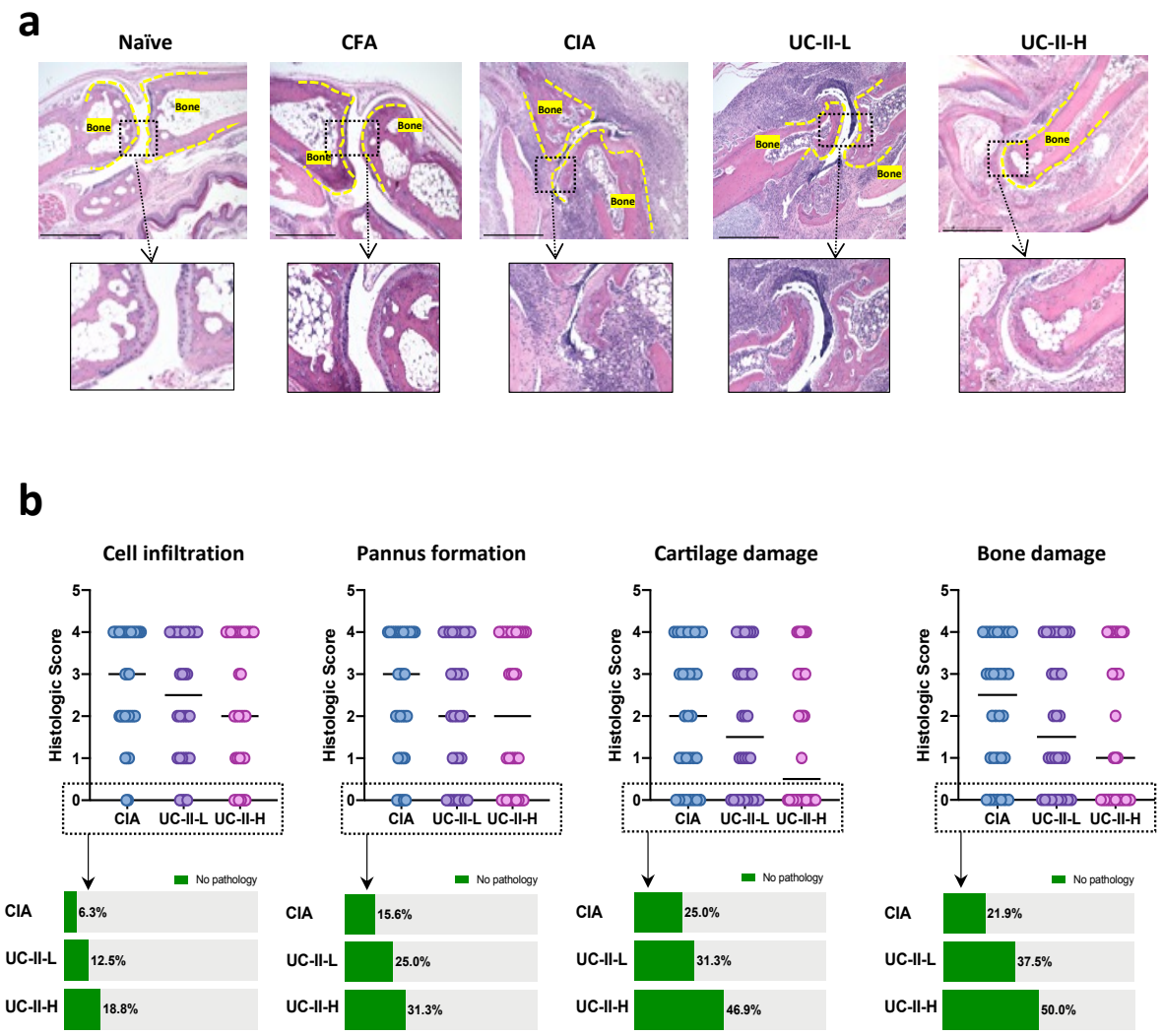

Figure 3-2 UC-II protects bones and cartilage in the joints during arthritis.

a) H&E staining images of paws in each group. Scale bar = 500 um. **b)** Histological score of paws in mice induced with arthritis. Four parameters (inflammation, pannus formation, cartilage damage and bone damage) were assessed by giving a score from 0 to 4. The paws with score=0 were regarded as having no pathology. Each dot represents an individual paw. Data was presented by median. Data was pooled from two individual experiments (CIA, n=32; UC-II-L, n=32; UC-II-H, n=32). Statistical analysis was determined using Kruskal-Wallis test. CFA, Complete Freund's Adjuvant. CIA, collagen induced arthritis. UC-II-L, UC-II lower dose. UC-II-H, UC-II higher dose.

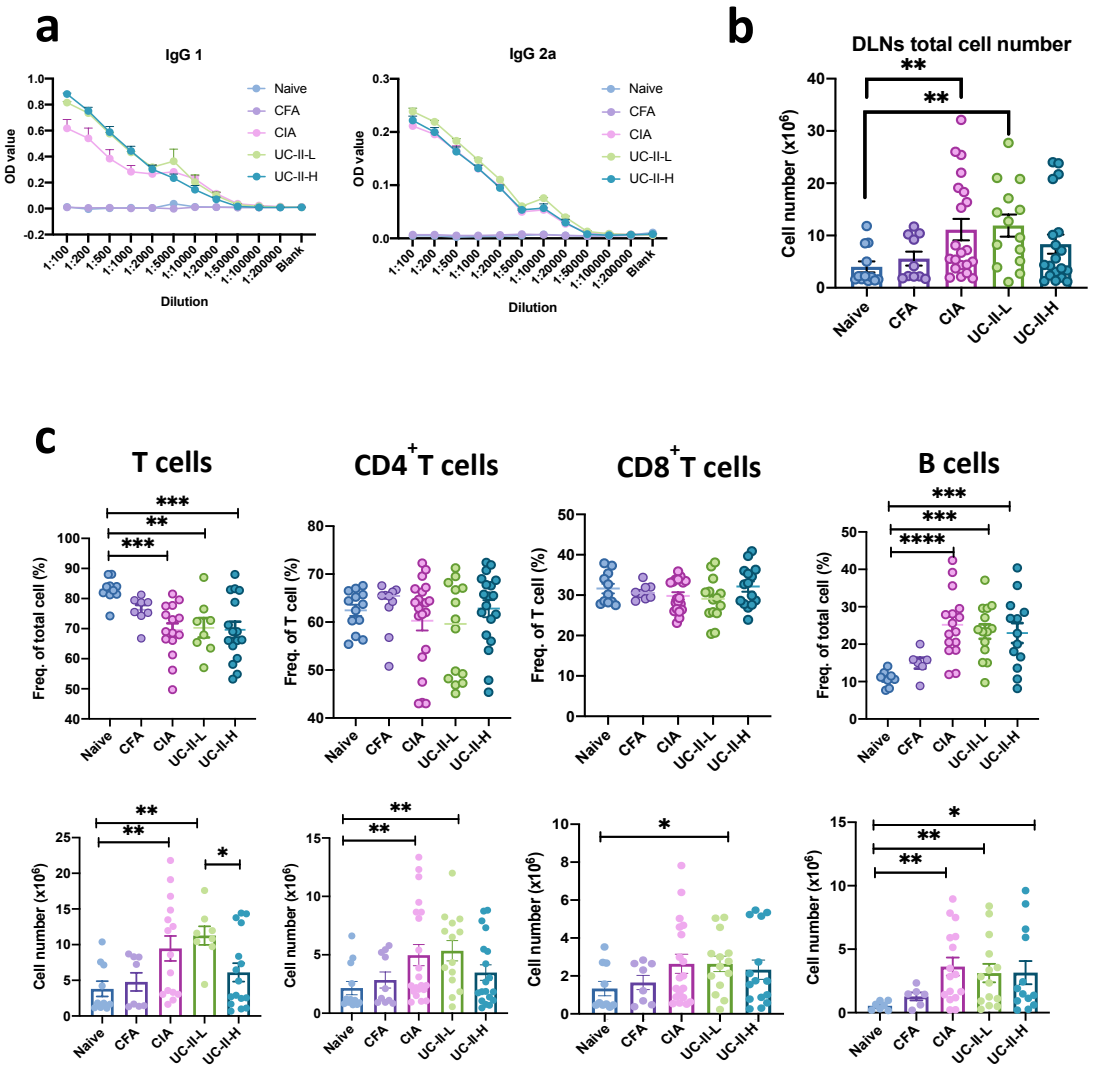

Figure 3-3 Cellular and humoral responses in response to UC-II.

a) Anti-CII antibody expression in the serum with different dilutions examined by Elisa. **b)** Total cell number in the joint draining lymph node in each group **c)** Frequency and cell number of T cells ($CD4^+$T cell and $CD8^+$T cell) and B cell in the joint draining lymph node. Data were pooled from at least two individual models (b-c). Data was presented as mean ± SEM. Each dot represents one individual mouse. Statistical significance was determined using Ordinary one-way ANOVA. Significance indicated by asterisks, *$p < 0.05$, **$p < 0.01$, ***$p < 0.001$ and ****$p < 0.0001$. DLNs, draining lymph nodes; CFA, Complete Freund's Adjuvant; CIA, collagen induced arthritis; UC-II-L, UC-II lower dose; UC-II-H, UC-II higher dose.

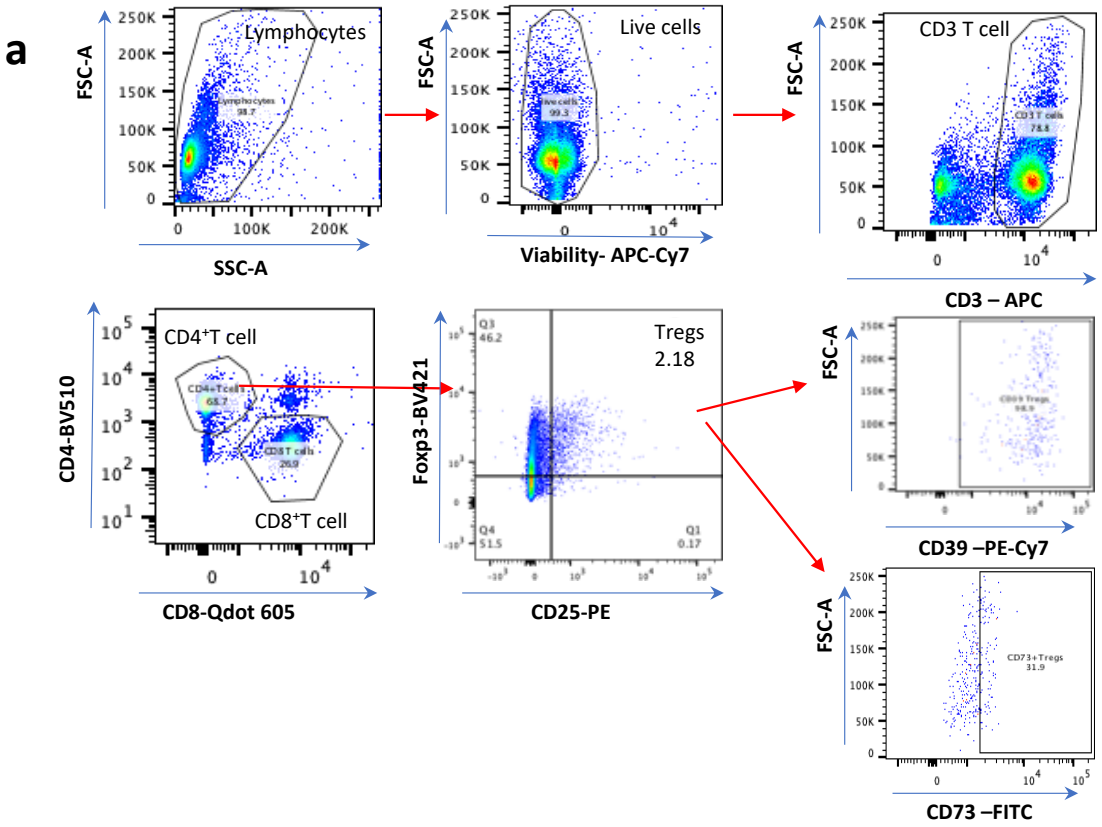

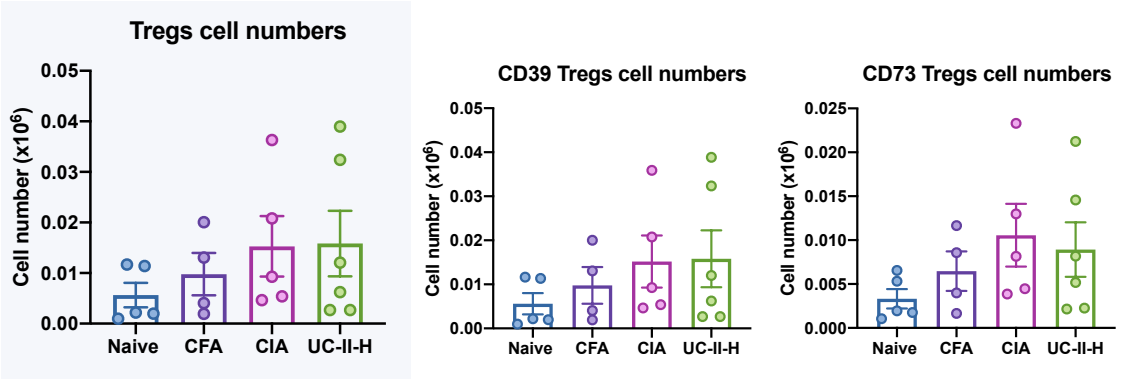

Figure 3-4 Treg-mediated immune response in CIA model upon UC-II administration.

Joint draining lymph nodes were collected and smashed into single cell suspension. **a)** Gating strategy of Tregs and CD39 and CD73 Treg subsets. **b)** Total cell number of Tregs and Treg subsets gated in a. Data was presented as mean ± SEM. Each dot represents one individual mouse. CFA, Complete Freund's Adjuvant; CIA, collagen induced arthritis; UC-II-H, UC-II higher dose.

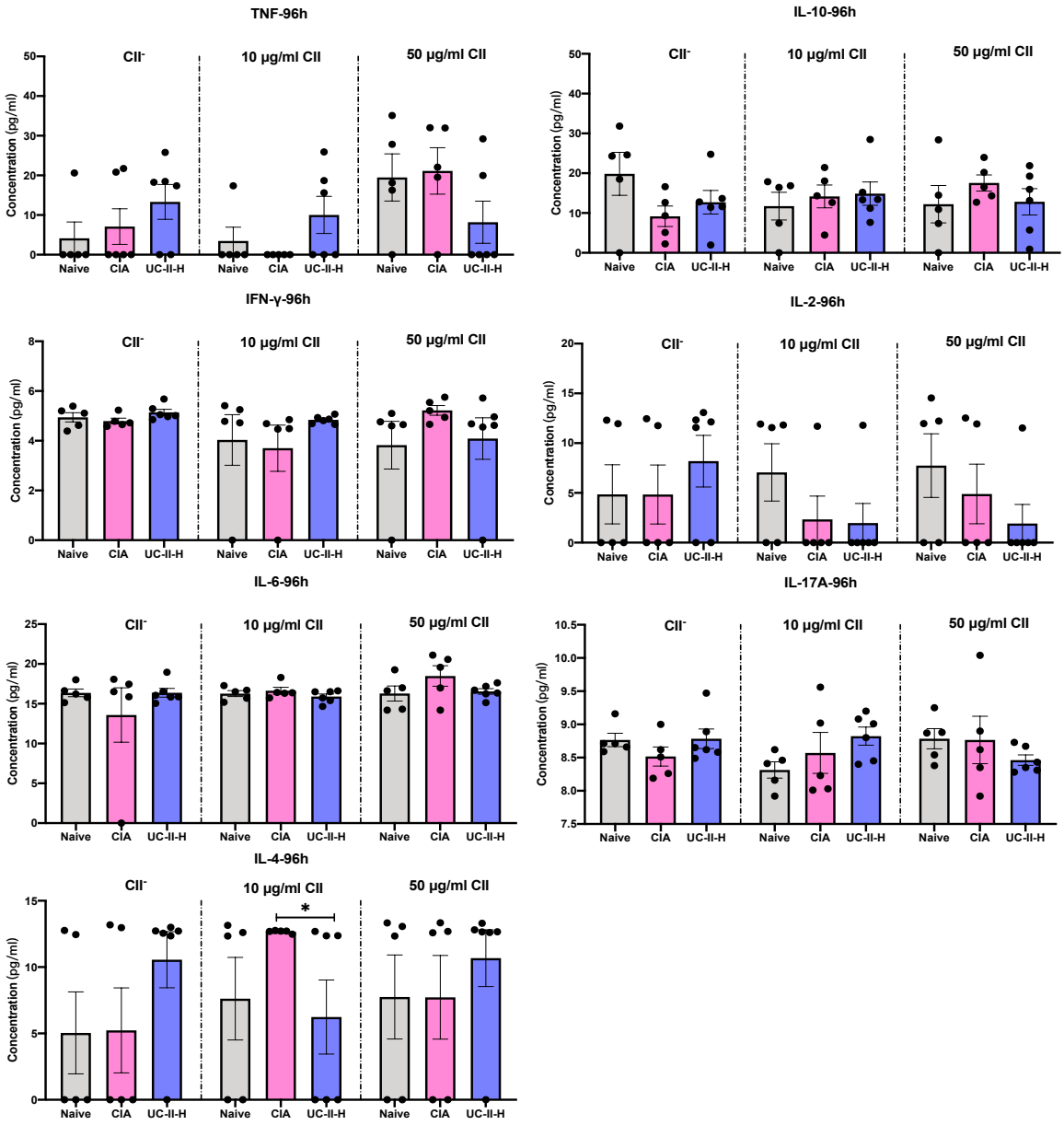

Figure 3-5 Recall experiment in CIA model upon UC-II administration.

Lymph nodes were harvested from mouse and smashed into single cell suspension, cultured in the plate with lower concentration (10 µg/ml), higher concentration (50 µg/ml) or without CII activation. The supernatant was collected after 96 hours and examined by CBA Mouse Th1/Th2/Th17 cytokine kit. Data was presented as mean ± SEM. Each dot represents one individual mouse. Statistical significance was determined using Ordinary one-way ANOVA. Significance indicated by asterisks, *p < 0.05. CII, type II collagen; CFA, Complete Freund's Adjuvant; CIA, collagen induced arthritis; UC-II-H, UC-II higher dose.

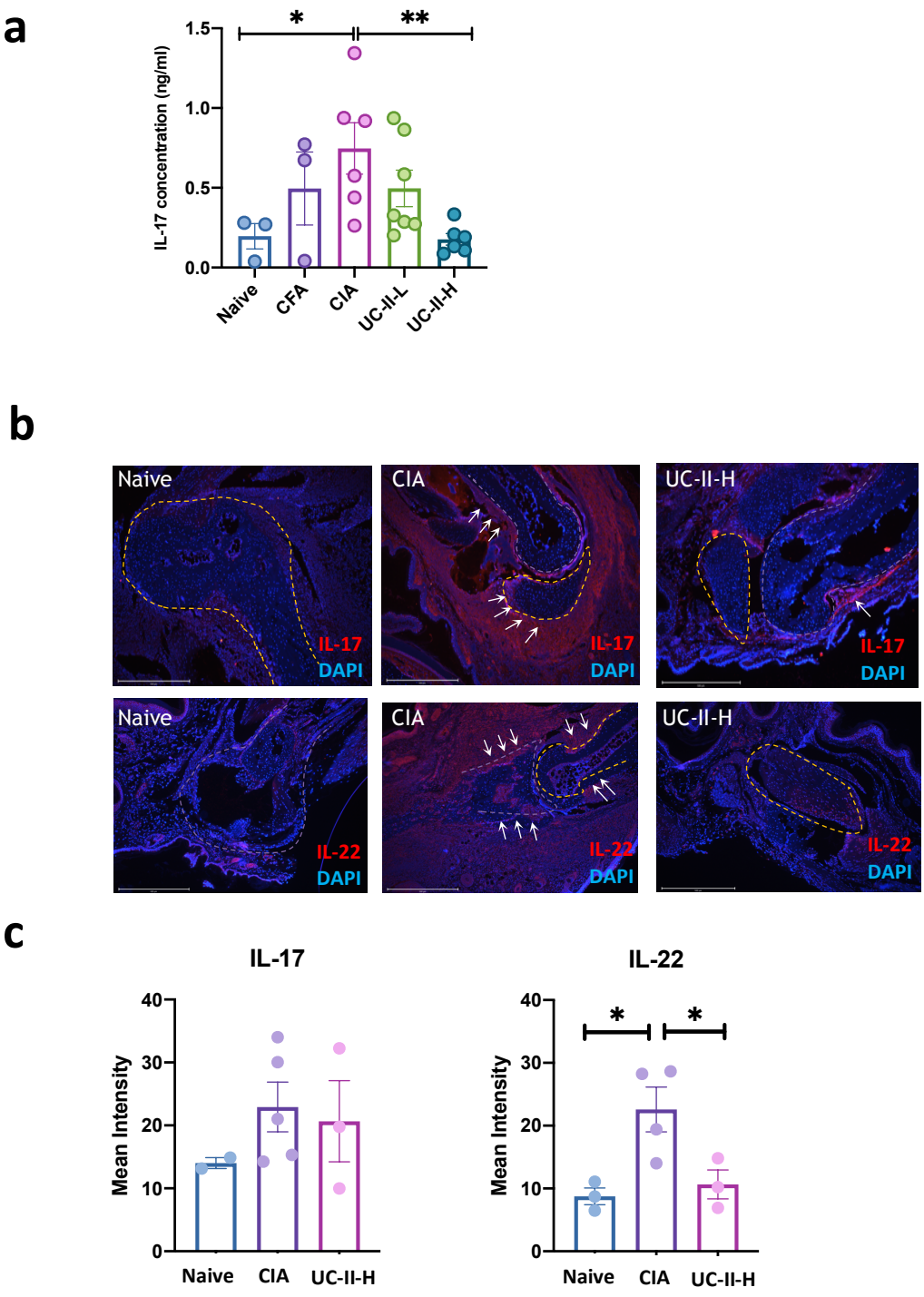

Figure 3-6 High dose of UC-II reduces the pathogenic upregulation of IL-17 and IL-22 in the joint.

a) IL-17 concentration was evaluated by ELISA in the supernatants of draining lymph node cells upon PMA (50 ng/ml)/Ionomycin (500 ng/ml) stimulation for 12 hours. **b)** Expression of IL-17 and IL-22 (red) was evaluated in the joint tissue by immunofluorescence. DAPI (Blue) was used to satin nuclei as counterstaining. Superimposed dotted lines show bone tissue, areas of cell infiltration are indicated by white arrows. Scale bars= 500 μm. **c)** Quantification of IL-17 and IL-22 expression in the joint. Data was presented as mean ± SEM. Each dot represents one individual mouse. Statistical significance was determined using Ordinary one-way ANOVA. Significance indicated by asterisks, *$p < 0.05$ and **$p < 0.01$. CFA, Complete Freund's Adjuvant; CIA, collagen induced arthritis; UC-II-L, UC-II lower dose; UC-II-H, UC-II higher dose.

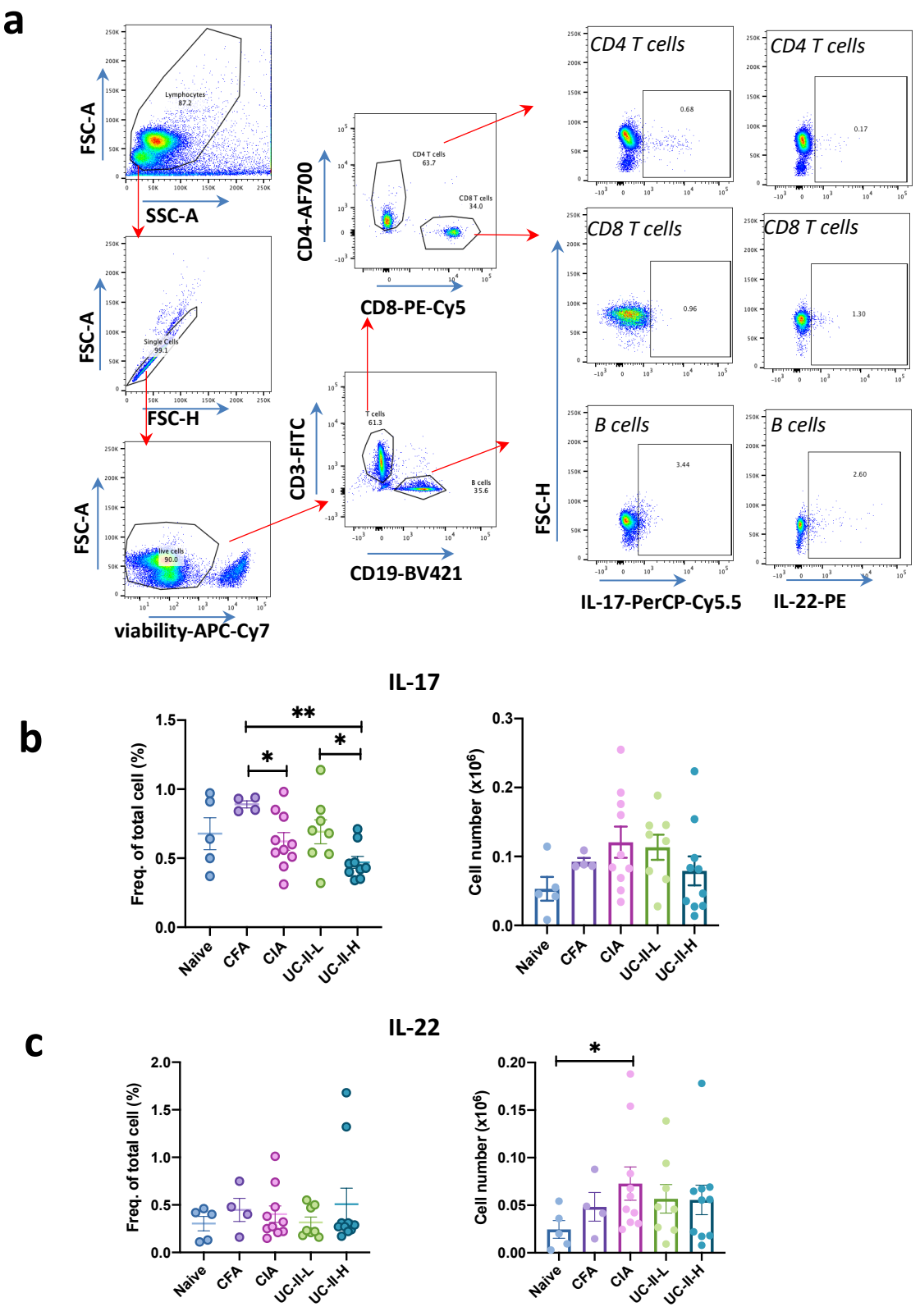

Figure 3-7 High dose of UC-II reduces the pathogenic upregulation of IL-17 and IL-22 in DLNs.

a) Gating strategy for IL-17+ and IL-22+ CD4 T cells, CD8 T cells and B cells in DLNs. **b-c)** Relative frequency and total cell number of IL-17+ and IL-22+ DLN cells were evaluated by flow cytometry. Data was presented as mean ± SEM. Each dot represents one individual mouse. Statistical significance was determined using Ordinary one-way ANOVA. Significance indicated by asterisks, *p < 0.05 and **p < 0.01. CFA, Complete Freund's Adjuvant; CIA, collagen induced arthritis; UC-II-L, UC-II lower dose; UC-II-H, UC-II higher dose.

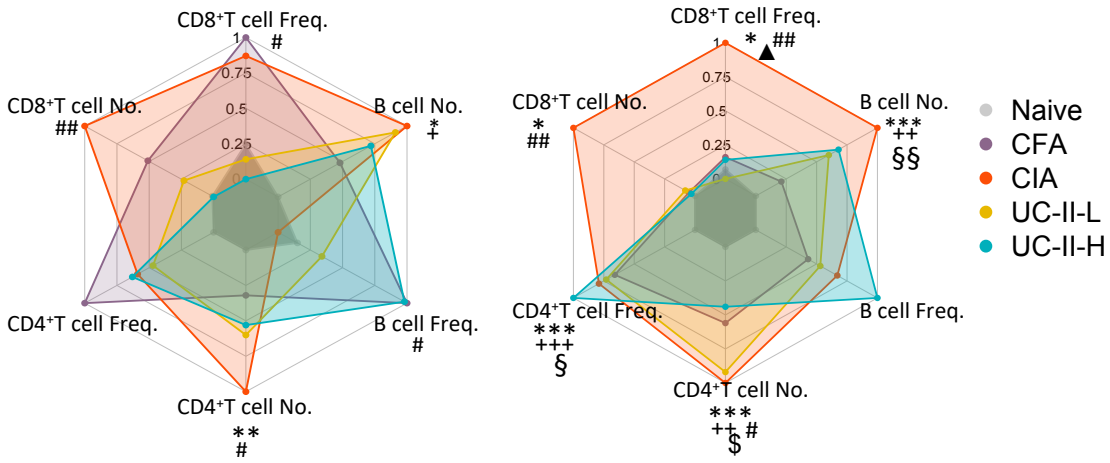

Figure 3-8 Regulation of IL-17 and IL-22 producer in the draining lymph nodes upon UC-II administration.

Cell frequency and total cell numbers of IL-17+ and IL-22+ CD4 T cells, CD8 T cells and B cells in DLNs, represented at the corners of radar charts: Naïve (grey), CFA (purple), CIA (red), UC-II-L (yellow), UC-II-H (blue); data were normalized to maximum expression in each group. Significance on the raw data among groups was evaluated by ordinary one-way ANOVA, where

*p < 0.05, **p < 0.01 and ***p < 0.001 in CIA vs naive,

# p < 0.05 and ##p < 0.01 in CIA vs UC-II-H;

+p < 0.05, ++p < 0.01 and +++p < 0.001 in UC-II-L vs naïve;

§p < 0.05 and §§p < 0.01 in Naïve vs UC-II-H;

$p < 0.05 in UC-II-L vs UC-II-H;

▲ p < 0.05 in UC-II-L vs CIA.

CFA, Complete Freund's Adjuvant; CIA, collagen induced arthritis; UC-II-L, UC-II lower dose; UC-II-H, UC-II higher dose.

All raw data for the radar chart was attached in Appendix Figure S1.

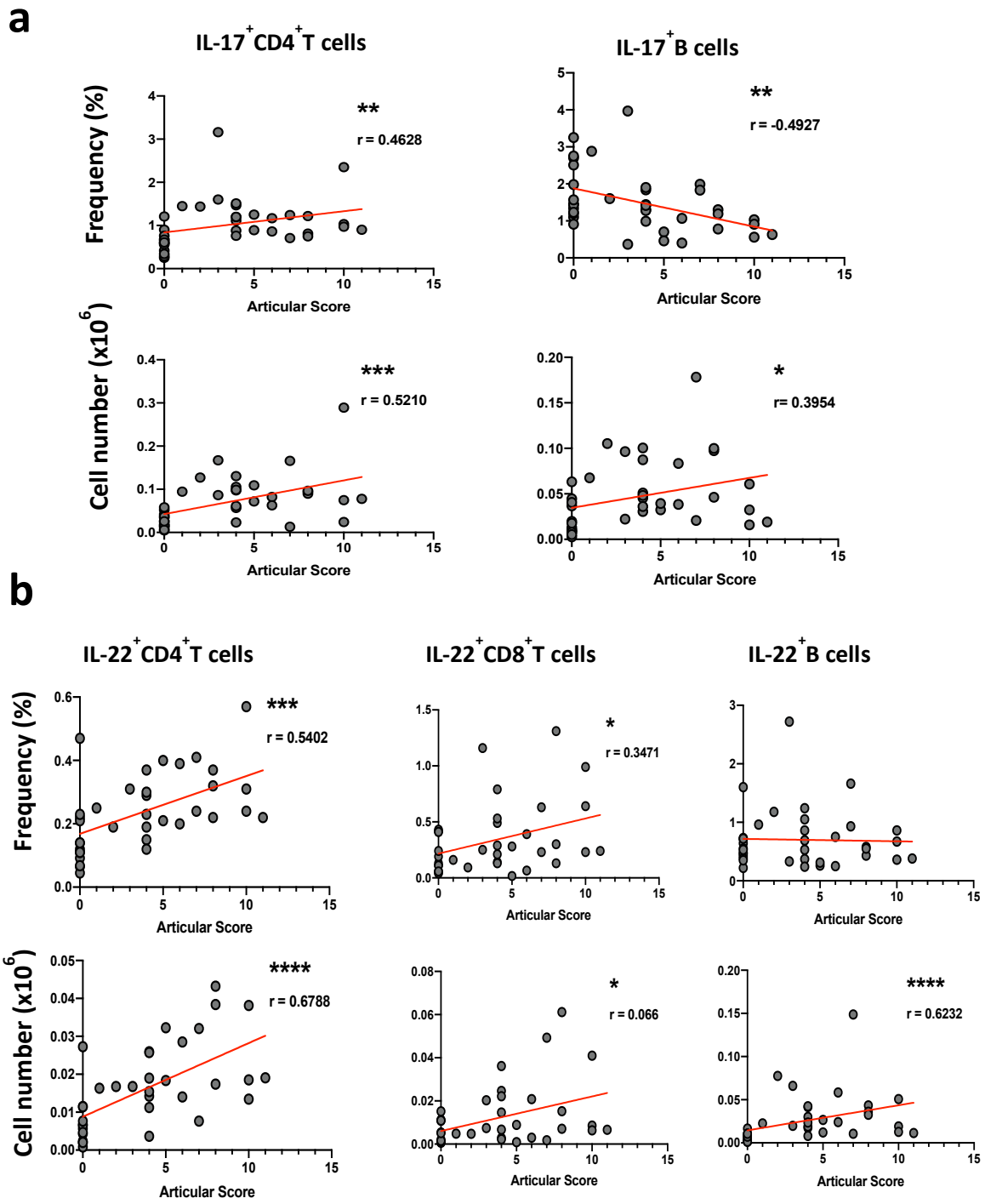

Figure 3-9 Correlation between of IL-17+ and IL-22+ lymph node cells and articular scores in DLNs.

a-b) Correlation between numbers of IL-17 (a) and IL-22 (b) positive lymph node cells and articular scores in draining lymph nodes (DLNs). Every dot represents cells from individual mice. r: Pearson's coefficient. Statistical significance was determined using Spearman correlation. Significance indicated by asterisks, *p < 0.05, **p < 0.01, ***p < 0.001 and ****p < 0.0001.CFA, Complete Freund's Adjuvant; CIA, collagen induced arthritis; UC-II-L, UC-II lower dose; UC-II-H, UC-II higher dose.

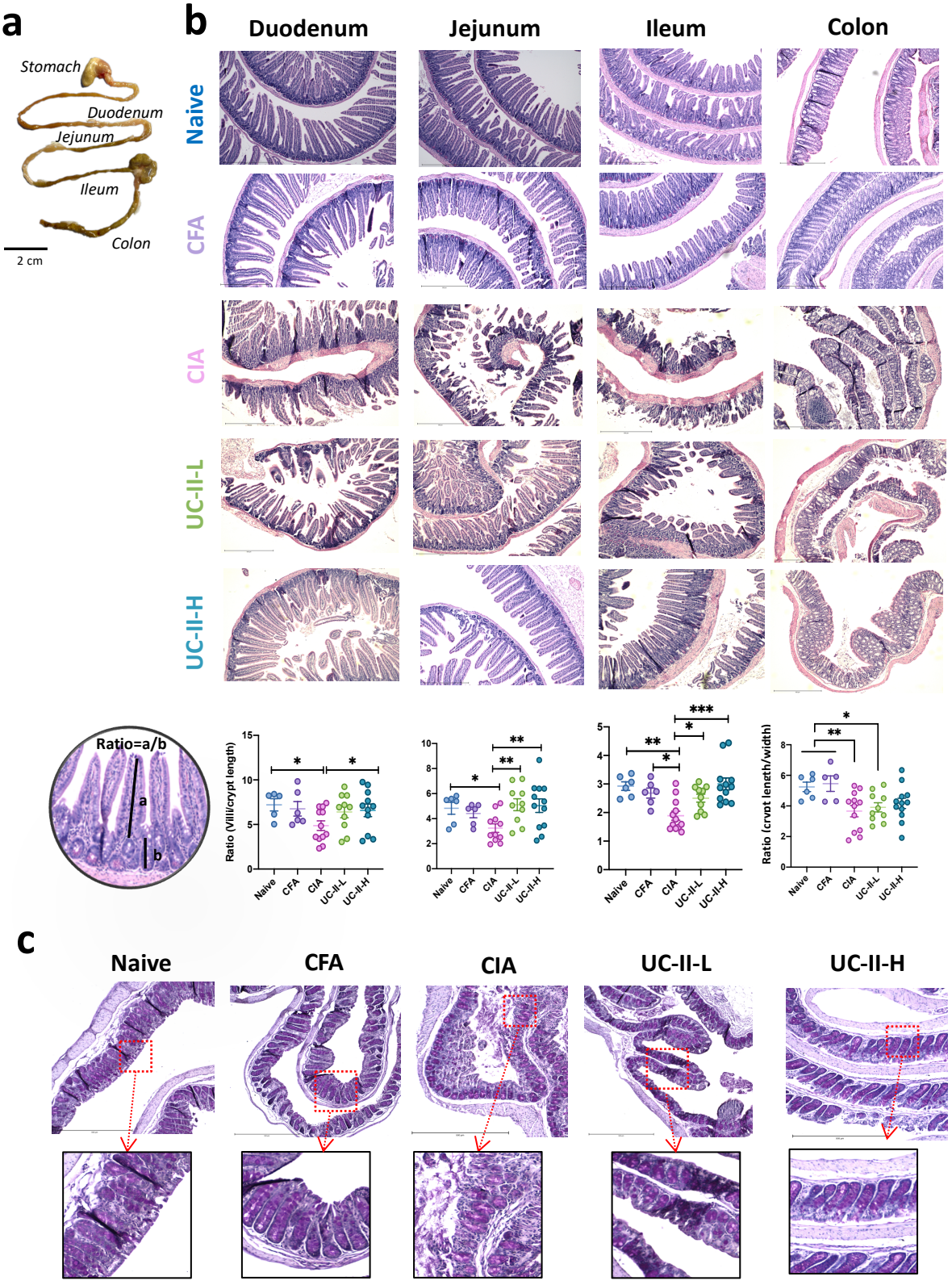

Figure 3-10 UC-II protects against gastrointestinal damage to inflammatory arthritis.

a) Isolated gastrointestinal tract showing the four anatomical areas used for further study. **b)** Areas of duodenum, jejunum, ileum, and colon were fixed, and tissue sections were subjected to hematoxilin and eosin staining. Length of villi and crypts was measured using Image J software, and the ratio of villi/crypt (small intestine) and ratio of crypt length/width (colon) were quantified. Data were pooled from two individual models. Data was presented as mean ± SEM. Each dot represents one individual mouse. Statistical significance was evaluated by ordinary one-way ANOVA, where *p < 0.05, **p < 0.01 and ***p < 0.001. **c)** Colon tissue sections were stained with PAS to detect changes in mucus layer and associated pathology. Scale bars = 500 µm. CFA, Complete Freund's Adjuvant; CIA, collagen induced arthritis; UC-II-L, UC-II lower dose; UC-II-H, UC-II higher dose.

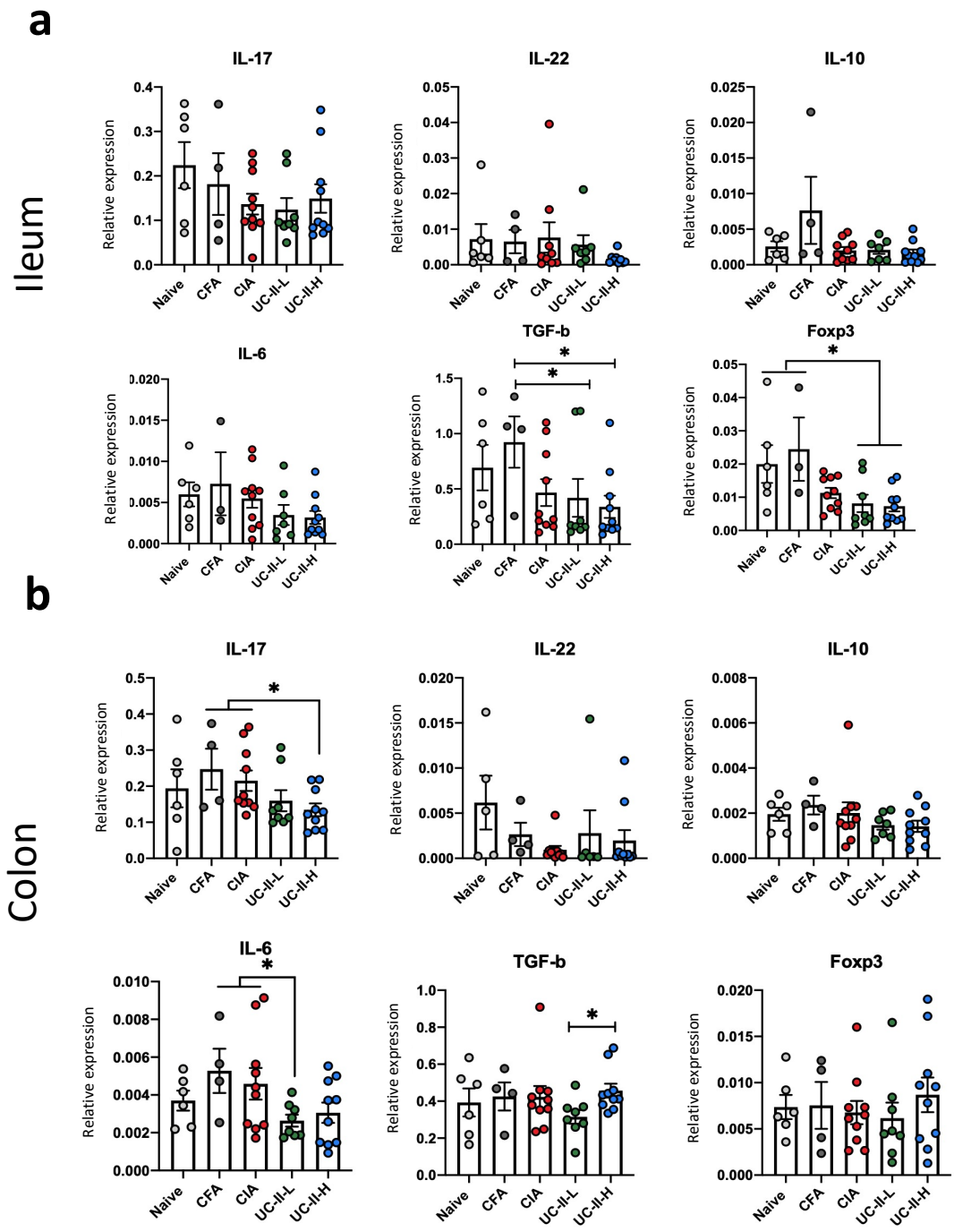

Figure 3-11 Pro-inflammatory cytokines and tolerogenic genes expression in the ileum and colon.

a-b) Pro-inflammatory cytokines and tolerogenic genes expression in the ileum (a) and colon (b) examined by RT-qPCR. Data was presented as mean ± SEM. Each dot represents one individual mouse. Statistical significance was evaluated by ordinary one-way ANOVA, where *p < 0.05. TGF-β, Transforming growth factor beta; Foxp3, forkhead box P3; CFA, Complete Freund's Adjuvant; CIA, collagen induced arthritis; UC-II-L, UC-II lower dose; UC-II-H, UC-II higher dose.

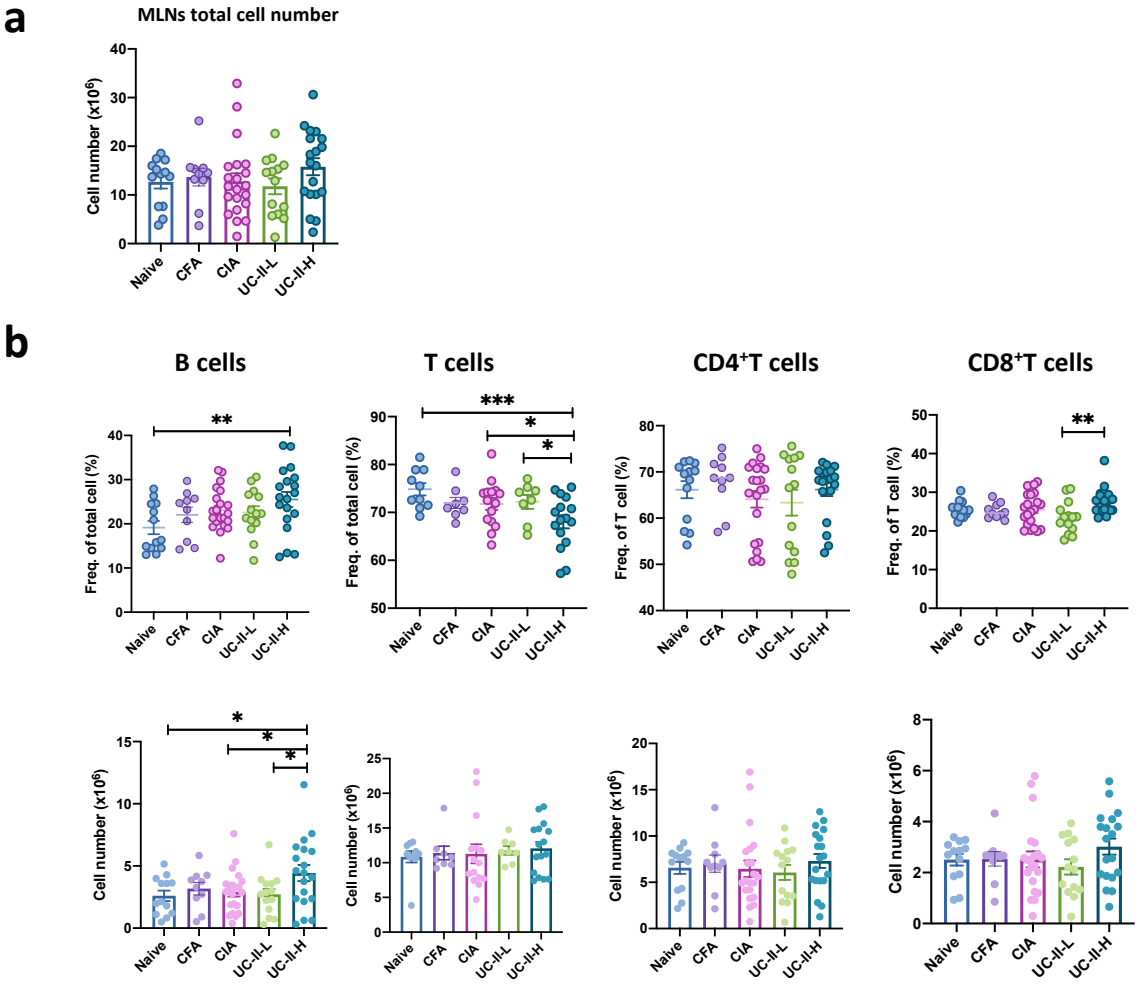

Figure 3-12 Cellular and humoral responses in response to UC-II in MLNs.

a) Total cell number in mesenteric lymph nodes (MLNs) in each group. **b)** Frequency and cell number of T cells ($CD4^+$T cell and $CD8^+$T cell) and B cell in MLNs. Data were pooled from two individual models. Data was presented as mean ± SEM. Each dot represents one individual mouse. Statistical significance was determined using Ordinary one-way ANOVA. Significance indicated by asterisks, *$p < 0.05$, **$p < 0.01$, and ***$p < 0.001$. CFA, Complete Freund's Adjuvant; CIA, collagen induced arthritis; UC-II-L, UC-II lower dose; UC-II-H, UC-II higher dose.

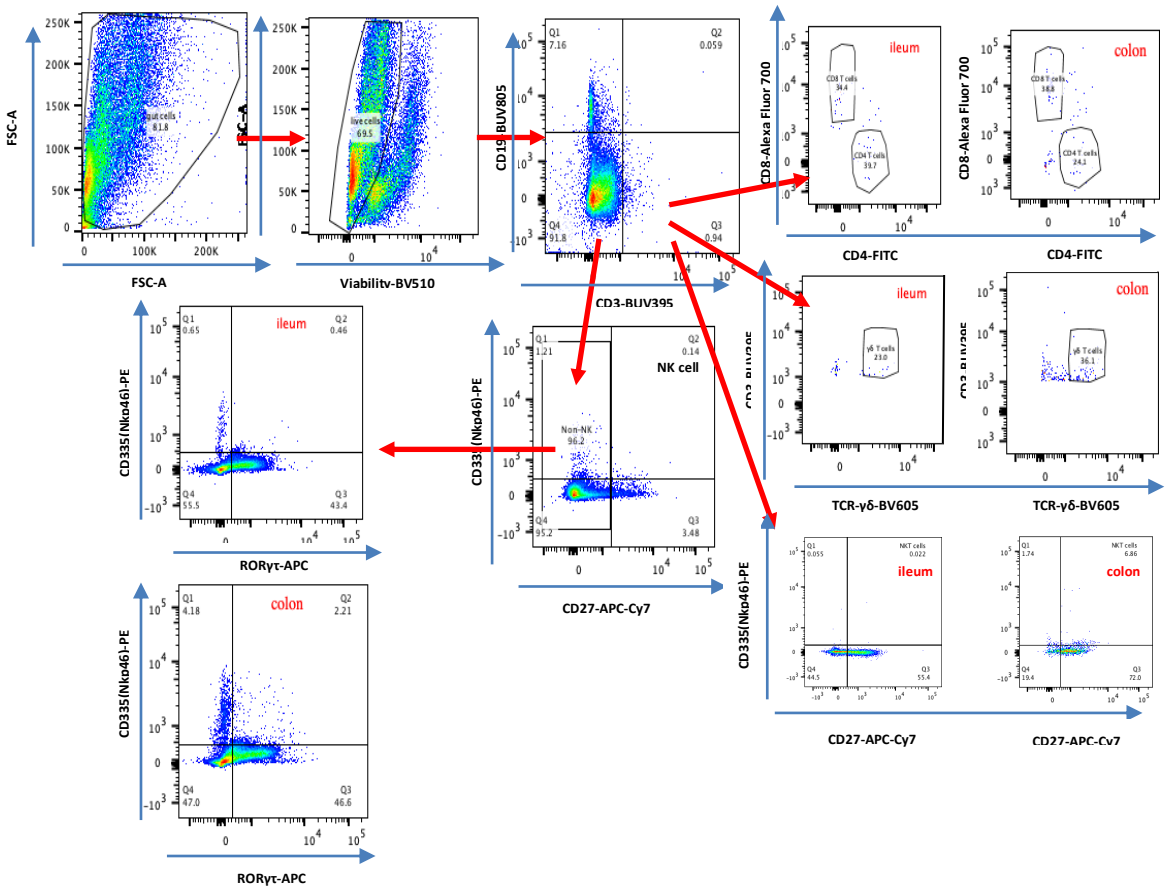

Figure 3-13 Gating strategy for immune cells in the gut tissue.

Gut tissue were digested by collagenase and stained with antibodies. Relevant cell populations were first gated on the basis of FSC/SSC analysis and singlet and live-dead cell discrimination using Viability dye (BV510). T cells and B cells were identified by markers CD3 (BUV395) and CD19 (BUV805), respectively. T cells (CD3+) were further identified: CD8 Tcell (CD8, Alexa Fluor 700), CD4 T cell (CD4, FITC), γδ Tcell (TCR- γδ, BV605), and NKT cell (CD335+ (PE) CD27+ (APC-Cy7)). Other cells (CD3-CD19-) can be further identified NK cells by marker CD335 (PE) and CD27 (APC-Cy7).CD27- cells can be identified ILC3 by marker CD335 (PE) and RORγt (APC). IL-17 was stained in BV421 fluorophore, and IL-22 was stained in PerCP-eFlour 710 fluorophore.

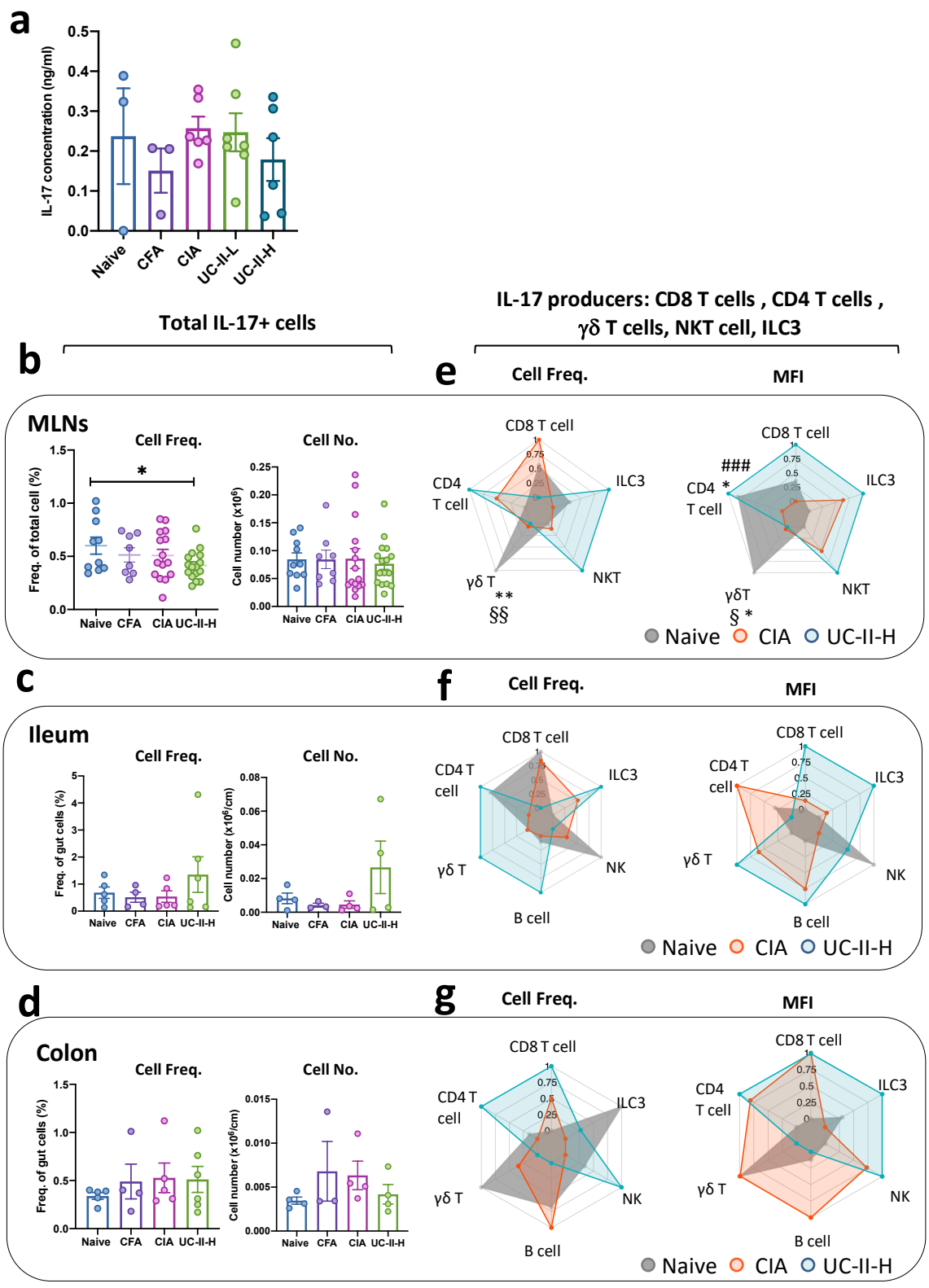
a
IL-17 concentration (ng/ml)
0.5
0.4
0.3
0.2
0.1
0.0
Naive
CFA
CIA
UC-II-L
UC-II-H
Total IL-17+ cells
IL-17 producers: CD8 T cells , CD4 T cells , γδ T cells, NKT cell, ILC3
b
MLNs
Cell Freq.
Cell No.
Freq. of total cell (%)
Cell number (x10⁶)
*
Naive CFA CIA UC-II-H
e
Cell Freq.
MFI
CD8 T cell
CD4 T cell
ILC3
NKT
γδ T
**
§§
###
*
§ *
Naive
CIA
UC-II-H
c
Ileum
Freq. of gut cells (%)
Cell number (x10⁶/cm)
f
CD4 T cell
NK
B cell
d
Colon
g

Figure 3-14 Expression of IL-17 in mesenteric lymph nodes and gastrointestinal tract.

Mesenteric lymph nodes (MLNs), ileum and colon samples were collected to detect IL-17 expression by flow cytometry. a) IL-17 concentration was evaluated by ELISA in the supernatants of MLNs upon PMA (50 ng/ml)/Ionomycin (500 ng/ml) stimulation for 12 hours. b-d) Frequency and number of total IL-17+ cells were quantified in MLNs (b), ileum (c) and colon (d). e-g) Frequency of IL-17+ cells, and IL-17 mean fluorescence (MFI) intensity of CD4 T cells, CD8 T cells, group 3 innate lymphoid cells (ILC3) and γδ T cells were quantified by flow cytometry in MLNs (e), ileum (f) and colon (g). Each corner of the radar chart represents the indicated normalized parameter for naïve (grey), CIA (red) and UC-II-H (blue) mice. Statistical significance was determined using raw data and ordinary one-way ANOVA, where *$p < 0.05$, **$p < 0.01$ in CIA versus Naïve, ###$p < 0.001$ in CIA vs UC-II-H; § $p < 0.05$ in UC-II-H vs naïve. Data was presented as mean ± SEM. For all dot plot graphs, each dot represents one individual mouse. Statistical significance was determined using Ordinary one-way ANOVA. Significance indicated by asterisks, *$p < 0.05$, **$p < 0.01$, and ***$p < 0.001$. CFA, Complete Freund's Adjuvant; CIA, collagen induced arthritis; UC-II-L, UC-II lower dose; UC-II-H, UC-II higher dose.

All the raw data for radar chart was attached in the Appendix Figure S2.

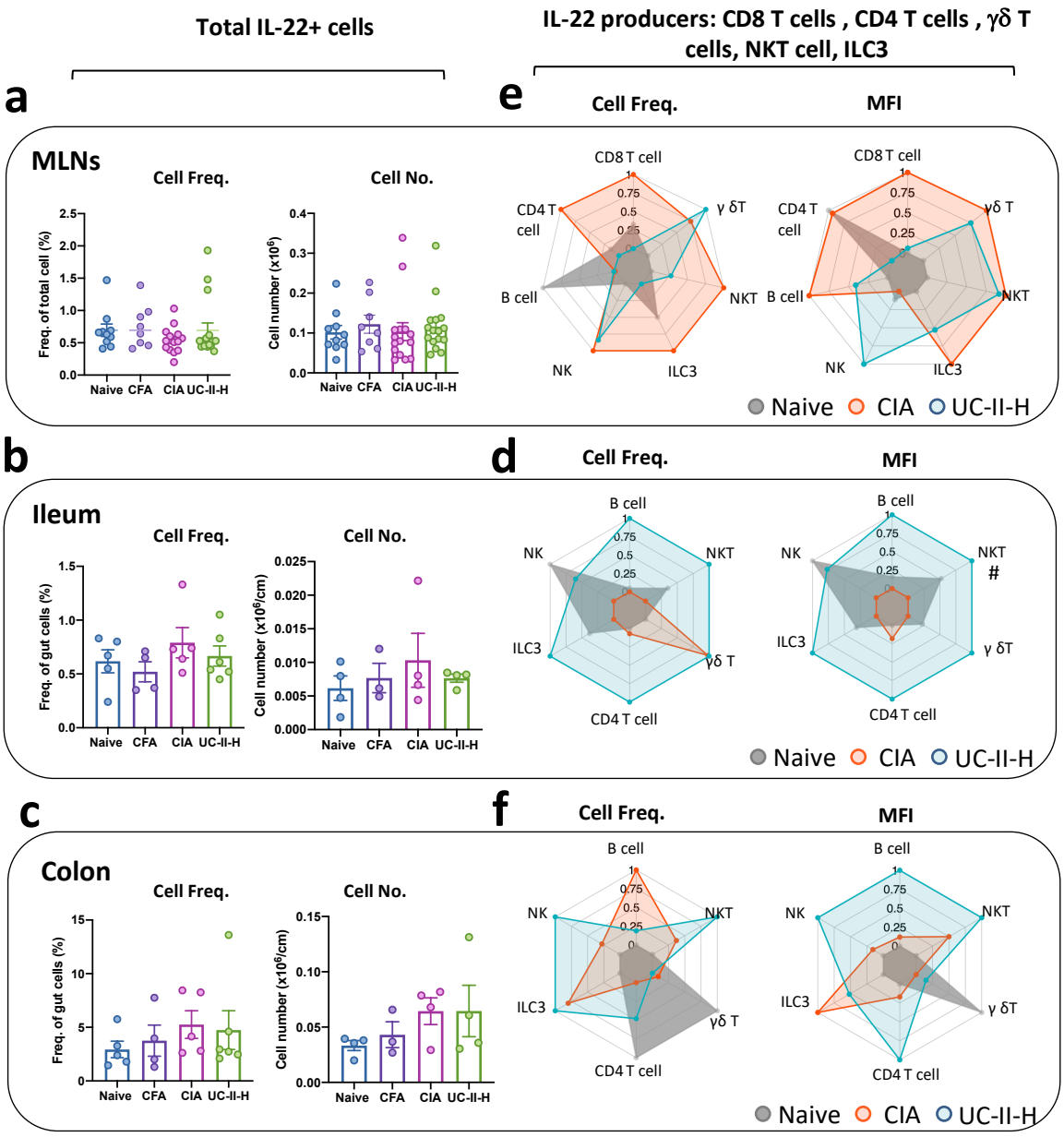

Figure 3-15 Expression of IL-22 in mesenteric lymph nodes and gastrointestinal tract.

Mesenteric lymph nodes (MLNs), ileum and colon samples were collected to detect IL-22 expression by flow cytometry. a-c) Frequency and number of total IL-22+ cells were quantified in MLNs (a), ileum (b) and colon (c). d-f) Frequency of IL-22+ cells, and IL-22 mean fluorescence (MFI) intensity of CD4 T cells, CD8 T cells, group 3 innate lymphoid cells (ILC3), γδ T cells and NKT cells was quantified by flow cytometry in MLNs (d), ileum (e) and colon (f). Each corner of the radar chart represents the indicated normalized parameter for naïve (grey), CIA (red) and UC-II-H (blue) mice. Statistical significance was determined using raw data and ordinary one-way ANOVA, where #$p < 0.05$ in CIA vs UC-II-H. Data was presented as mean ± SEM. For all dot plot graphs, each dot represents one individual mouse. Statistical significance was determined using Ordinary one-way ANOVA. Significance indicated by asterisks, *$p < 0.05$, **$p < 0.01$, and ***$p < 0.001$. CFA, Complete Freund's Adjuvant; CIA, collagen induced arthritis; UC-II-L, UC-II lower dose; UC-II-H, UC-II higher dose.

All the raw data for radar chart was attached in the Appendix Figure S3.

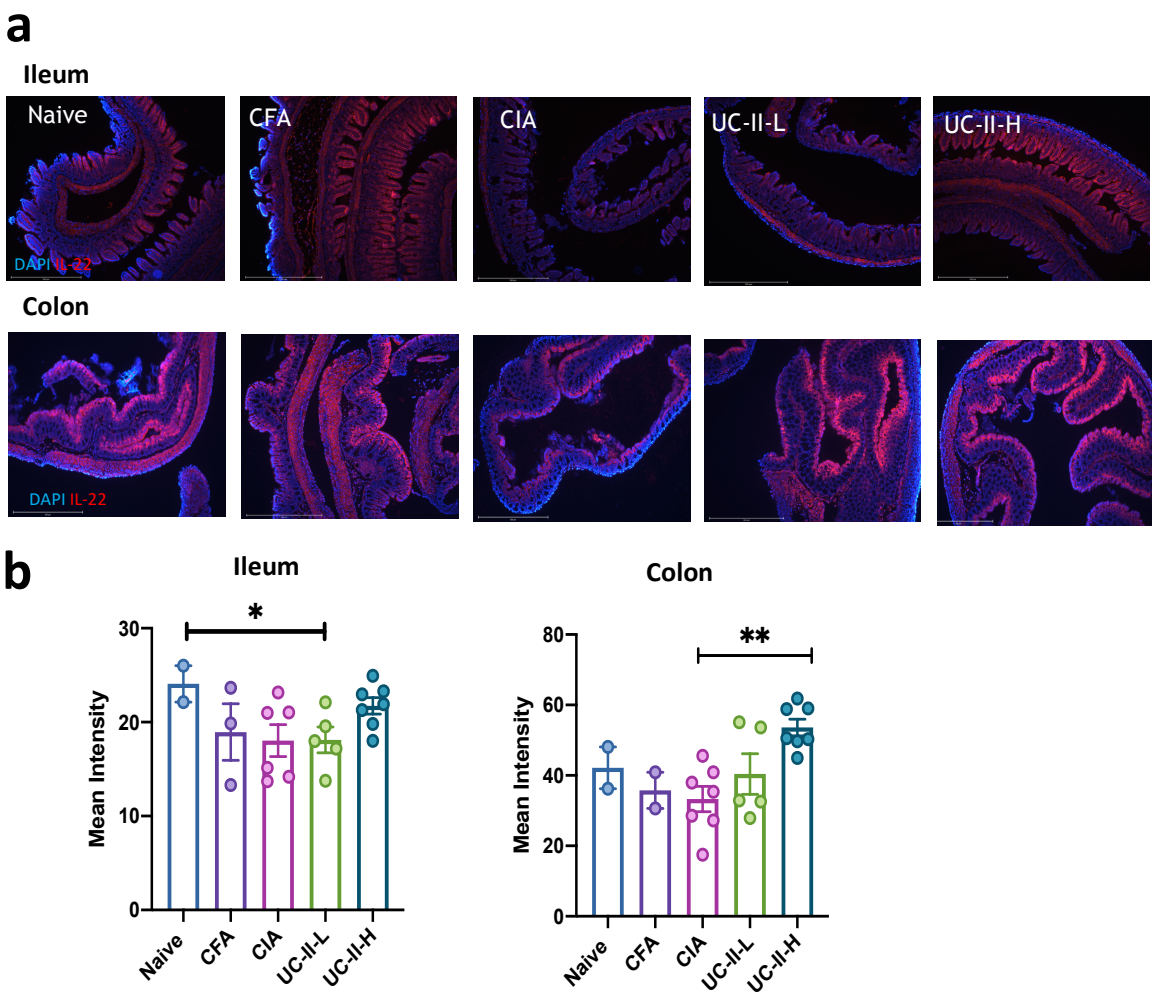

Figure 3-16 Expression of IL-22 in ileum and colon under UC-II administration.

a) Ileum and colon sections were stained with anti-IL-22 antibodies (Red) and DAPI (Blue) as counterstaining. **b)** Pixel intensity for IL-22 staining in a was quantified using ImageJ, each dots shows one individual mouse. Data was presented as mean ± SEM. Statistical significance was determined using raw data and ordinary one-way ANOVA, where *p < 0.05, **p < 0.01. CFA, Complete Freund's Adjuvant; CIA, collagen induced arthritis; UC-II-L, UC-II lower dose; UC-II-H, UC-II higher dose.

a

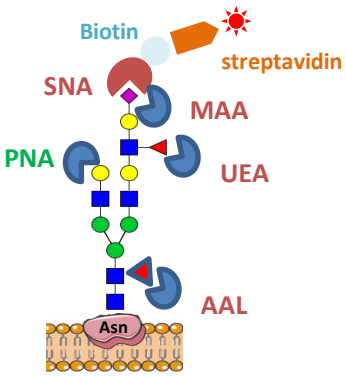

b

Lectin	Sugar Specificity
UEA I	Fucose(α-1,2), Arabinose
PHA	Galactose, Complex Structures
AAL	Fucose(α-1,6), Arabinose
SNA	Sialic Acid
ConA	Mannose
RCA I	Galactose, Lactose
PNA	Galactose

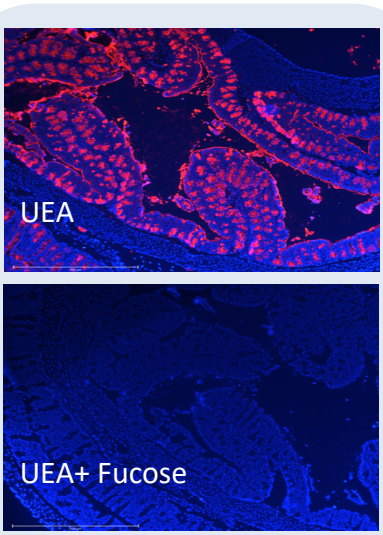

c

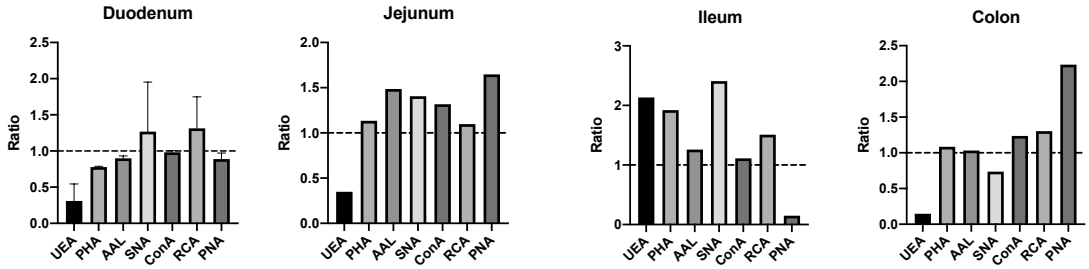

Figure 3-17 Multiple glycosylation staining in the gut tissue.

a) Diagram of immunofluorescence staining of lectin. SNA, Sambuccus nigra agglutinin; PNA, Peanut agglutinin; UEA I, Ulex Europaeus Agglutinin I; AAL, Aleuria aurantia lectin. PHA, Phytohaemagglutinin; ConA, Concanavalin A; RCA I, Ricinus Communis Agglutiniin I. **b)** Sugar specificity of each lectin (left) and example of lectin staining with UEA I and UEA I preincubated with fucose for 30 minutes in healthy colon tissue (right). UEA I staining (Red) and DAPI (Blue) as counterstaining **c)** General glycosylation changes along the gastrointestinal tract in arthritic mice. Ratio = mean fluorescence intensity of arthritic mouse gut/healthy gut. Plot in duodenum of UEA, SNA and RCA were presented as mean± SEM.

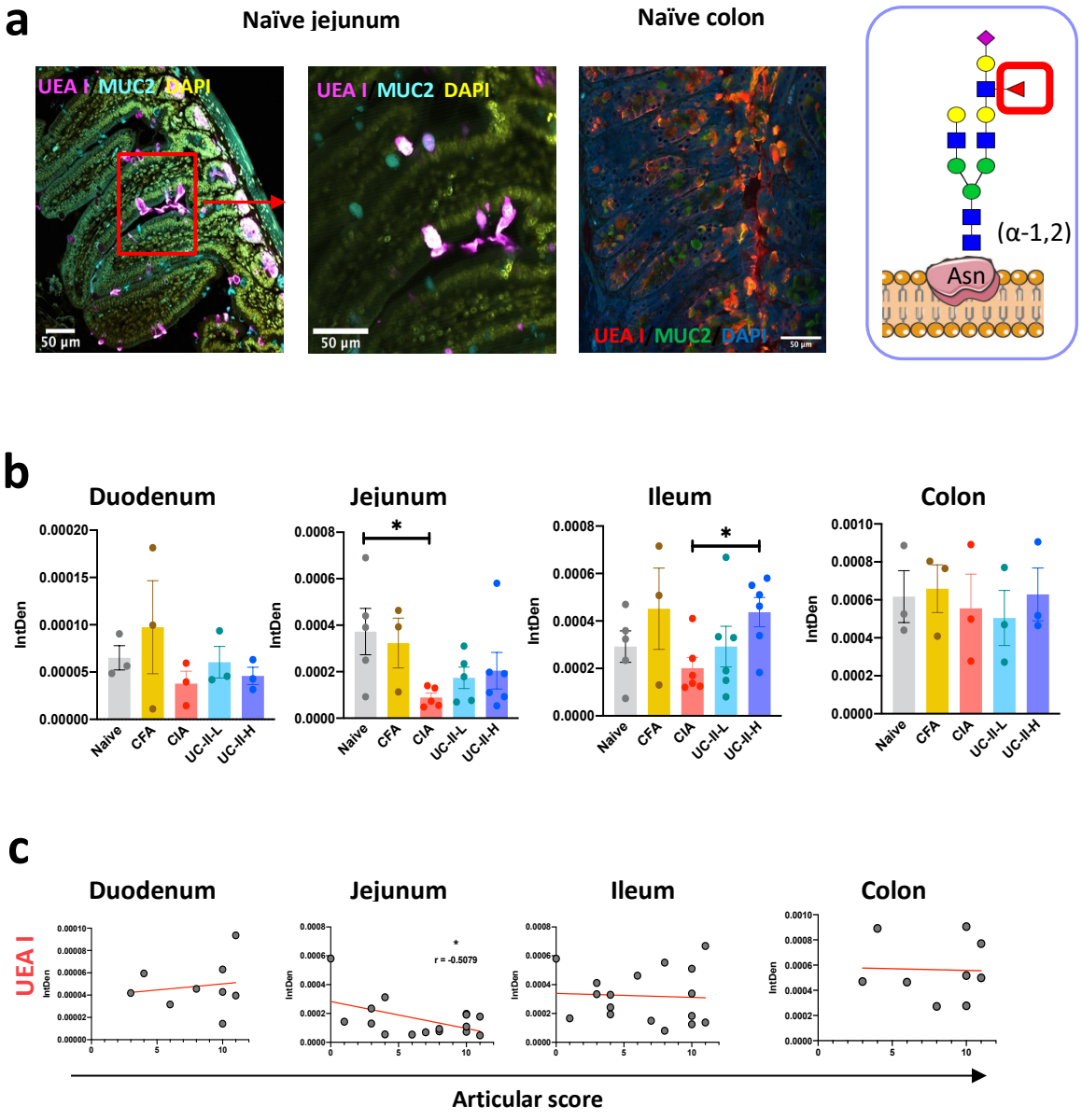

Figure 3-18 Terminal fucose expression along gastrointestinal tract.

a) Representative images of Immunofluorescence staining of UEA I, MUC2 and DAPI in the naïve jejunum and colon. Specific glycan structure is attached in the box. Scale bar= 50 µm. **b)** Immunofluorescence intensity of UEA staining images along the gastrointestinal tract measured by Image J of each group. Data was presented as mean ± SEM. Each dot is represented as one individual mouse sample. Statistical significance was determined using raw data and ordinary one-way ANOVA, where *p < 0.05. **c)** Correlations between UEA I binding immunofluorescence intensity and articular score. r: Pearson's coefficient. Statistical significance was determined using Spearman correlation. Significance indicated by asterisks, *p < 0.05. UEA, Ulex Europaeus Agglutinin I; CFA, Complete Freund's Adjuvant; CIA, collagen induced arthritis; UC-II-L, UC-II lower dose; UC-II-H, UC-II higher dose.

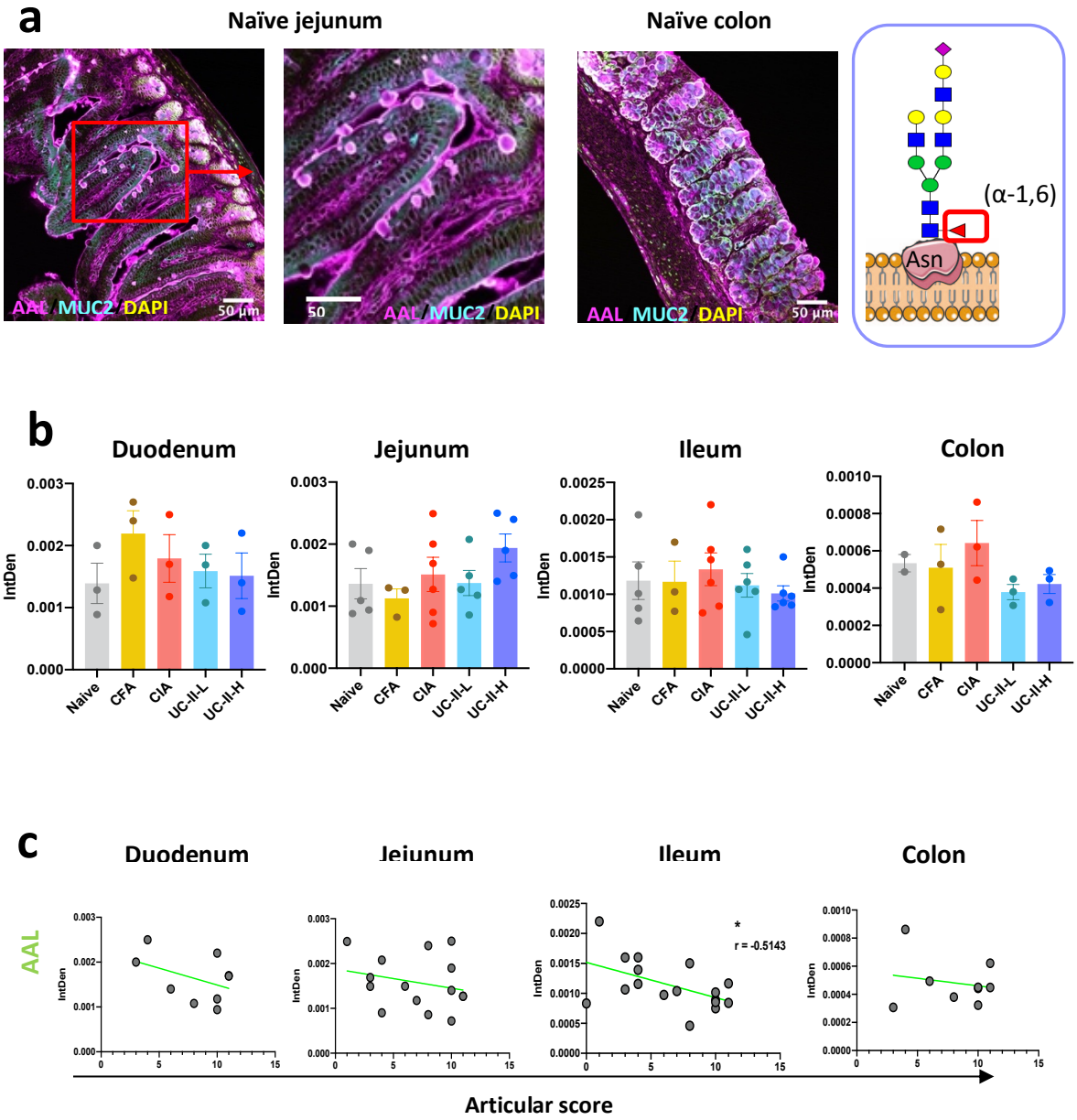

Figure 3-19 Core fucose expression along gastrointestinal tract.

a) Representative images of Immunofluorescence staining of AAL, MUC2 and DAPI in the naïve jejunum and colon. Specific glycan structure is attached in the box. Scale bar= 50 µm. **b)** Immunofluorescence intensity of AAL staining images along gastrointestinal tract measured by Image J of each group. Data was presented as mean ± SEM. Each dot is represented as one individual mouse sample. Statistical significance was determined using raw data and ordinary one-way ANOVA. **c)** Correlations between AAL binding immunofluorescence intensity and articular score. r: Pearson's coefficient. Statistical significance was determined using Spearman correlation. Significance indicated by asterisks, *p < 0.05. AAL, Aleuria aurantia lectin; CFA, Complete Freund's Adjuvant; CIA, collagen induced arthritis; UC-II-L, UC-II lower dose; UC-II-H, UC-II higher dose.

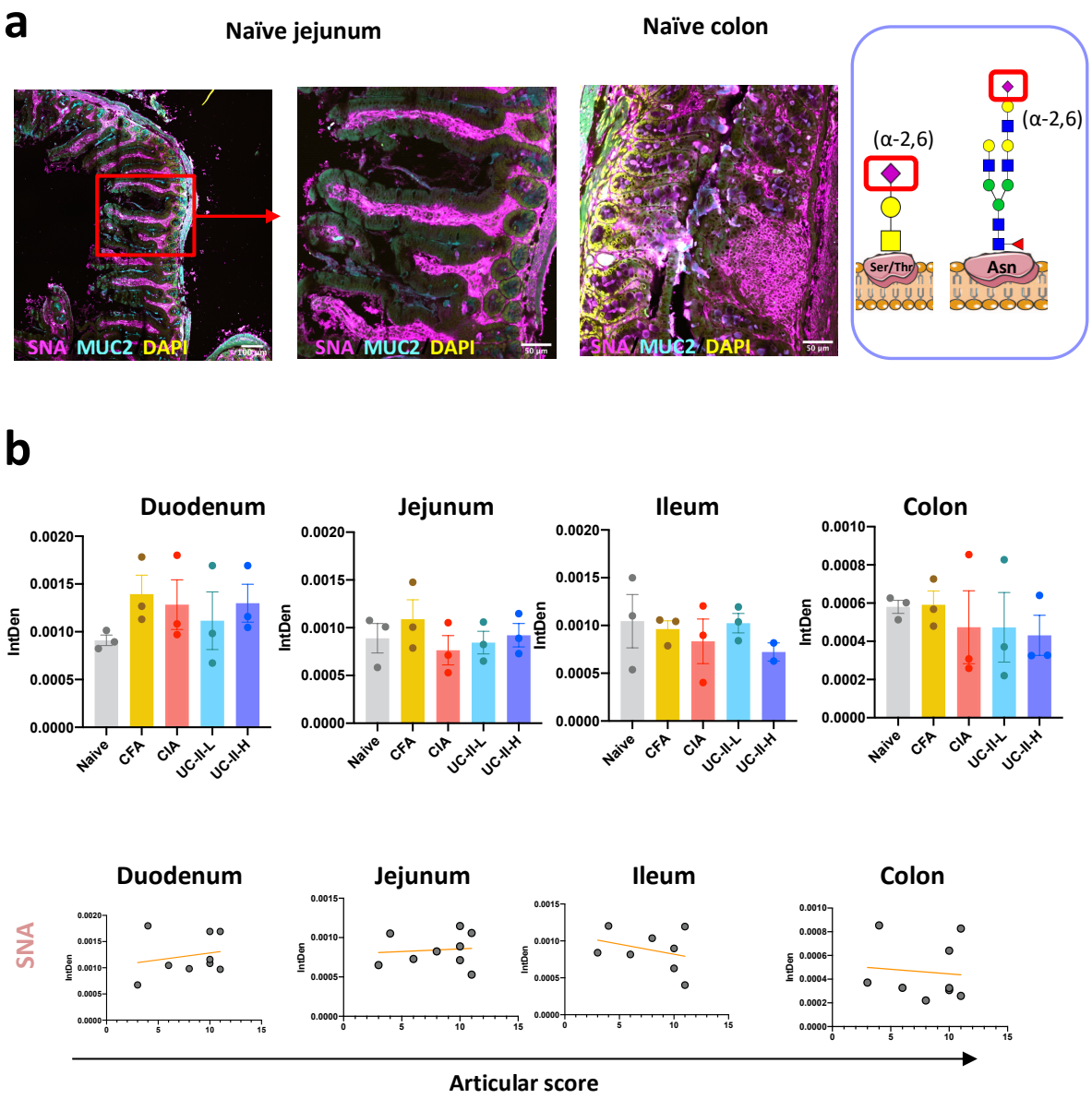

Figure 3-20 α-2,6 sialic acid expression along the gastrointestinal tract.

a) Representative images of Immunofluorescence staining of SNA, MUC2 and DAPI in the naïve jejunum and colon. Specific glycan structure is attached in the box. Scale bar= 50 μm. **b)** Immunofluorescence intensity of SNA staining images along the gastrointestinal tract measured by Image J of each group. Data was presented as mean ± SEM. Each dot is represented as one individual mouse sample. Statistical significance was determined using raw data and ordinary one-way ANOVA. **c)** Correlations between SNA binding immunofluorescence intensity and articular score. SNA, Sambuccus nigra agglutinin; CFA, Complete Freund's Adjuvant; CIA, collagen induced arthritis; UC-II-L, UC-II lower dose; UC-II-H, UC-II higher dose.

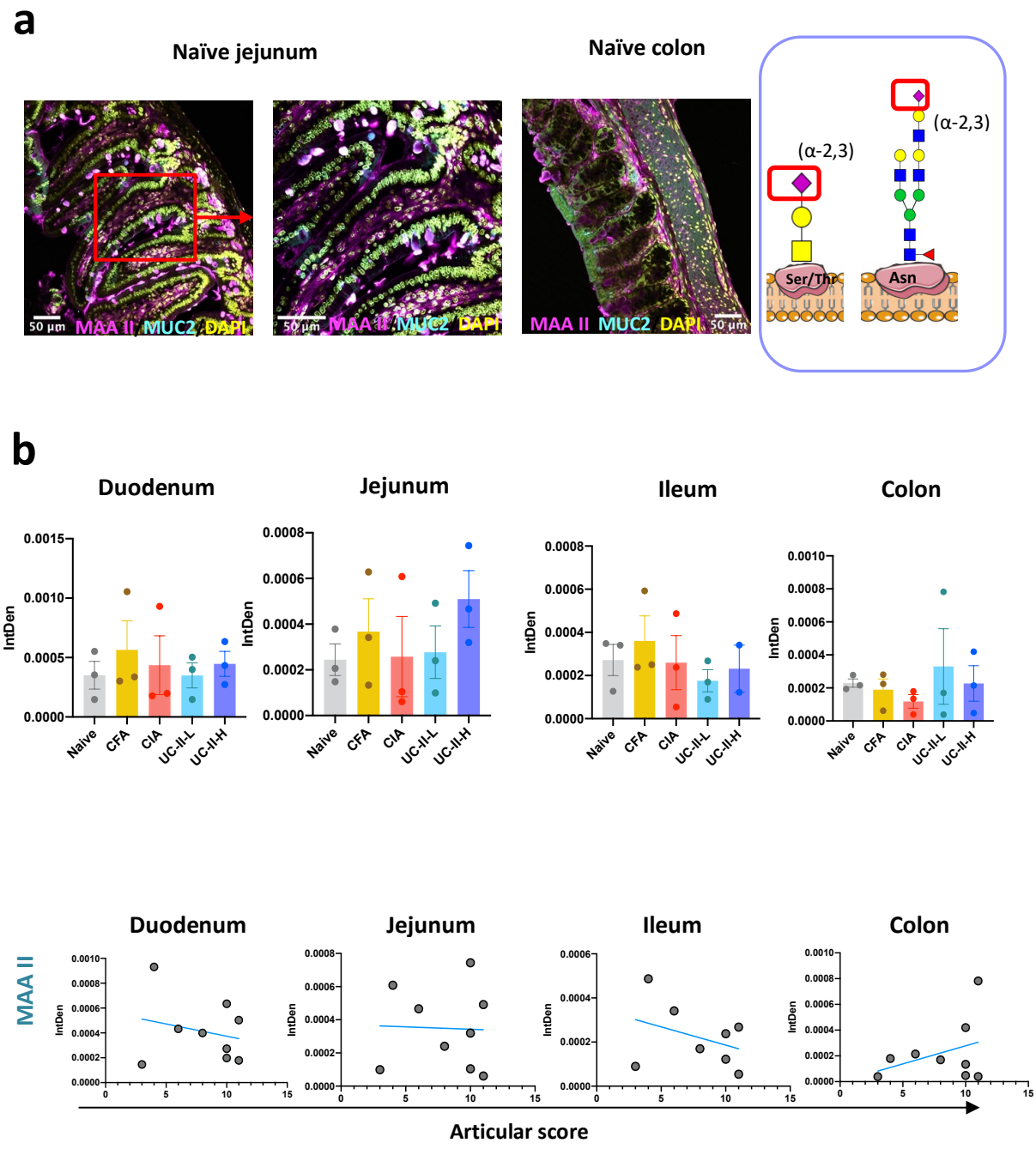

Figure 3-21 α-2,3 sialic acid expression along the gastrointestinal tract.

a) Representative images of Immunofluorescence staining of MAA II, MUC2 and DAPI in the naïve jejunum and colon. Specific glycan structure is attached in the box. Scale bar= 50 µm. **b)** Immunofluorescence intensity of MAA II staining images along the gastrointestinal tract measured by Image J of each group. Data was presented as mean ± SEM. Each dot is represented as one individual mouse sample. Statistical significance was determined using raw data and ordinary one-way ANOVA. **c)** Correlations between MAA II binding immunofluorescence intensity and articular score. MAA II, Maackia aurensis lectin II; CFA, Complete Freund's Adjuvant; CIA, collagen induced arthritis; UC-II-L, UC-II lower dose; UC-II-H, UC-II higher dose.

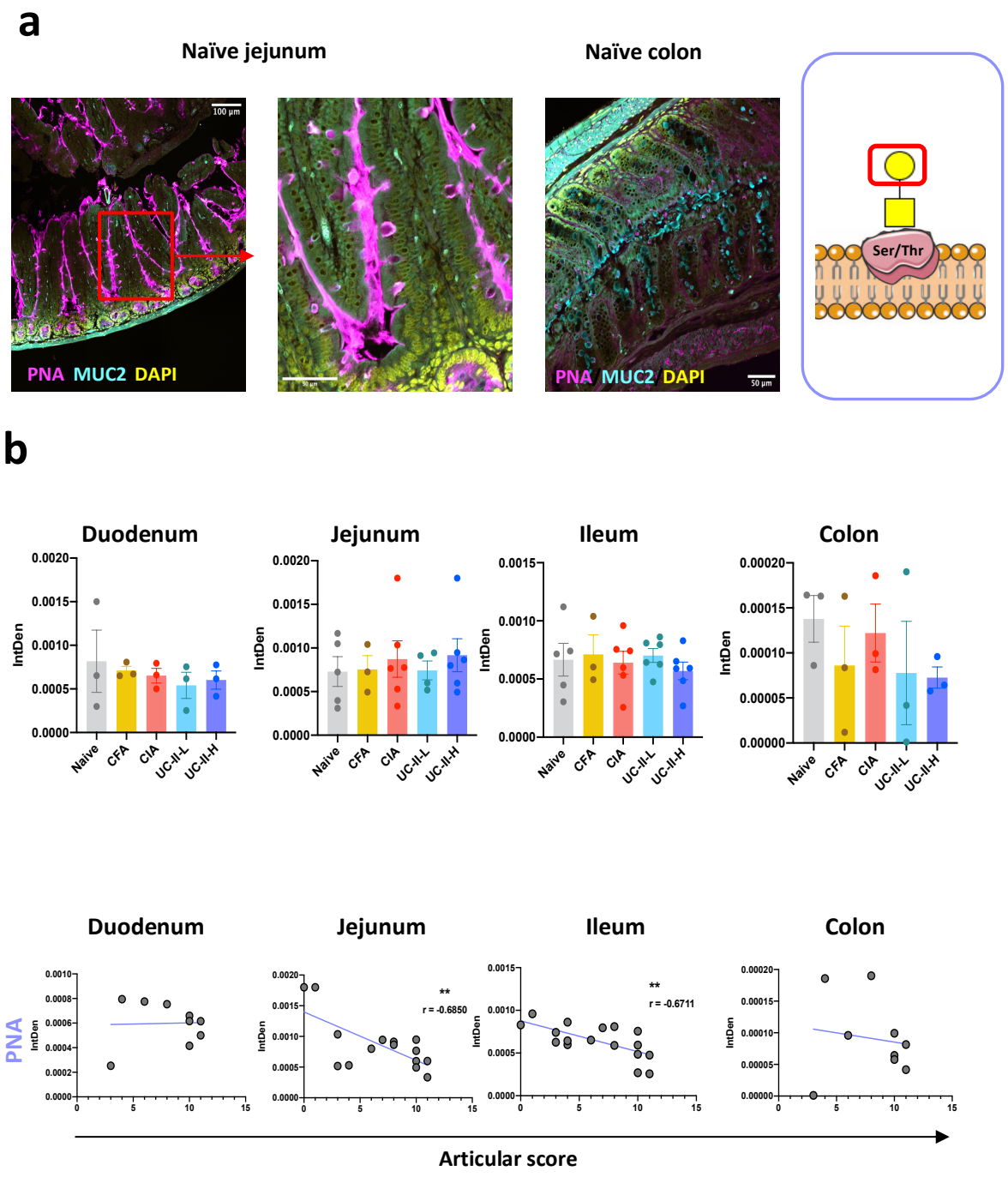

Figure 3-22 Galactose expression along the gastrointestinal tract.

a) Representative images of Immunofluorescence staining of PNA, MUC2 and DAPI in the naïve jejunum and colon. Specific glycan structure is attached in the box. Scale bar= 50 µm. **b)** Immunofluorescence intensity of PNA staining images along the gastrointestinal tract measured by Image J of each group. Data was presented as mean ± SEM. Each dot is represented as one individual mouse sample. Statistical significance was determined using raw data and ordinary one-way ANOVA. **c)** Correlations between PNA binding immunofluorescence intensity and articular score. r: Pearson's coefficient. Statistical significance was determined using Spearman correlation. Significance indicated by asterisks, **p < 0.01. PNA, Peanut agglutinin; CFA, Complete Freund's Adjuvant; CIA, collagen induced arthritis; UC-II-L, UC-II lower dose; UC-II-H, UC-II higher dose.

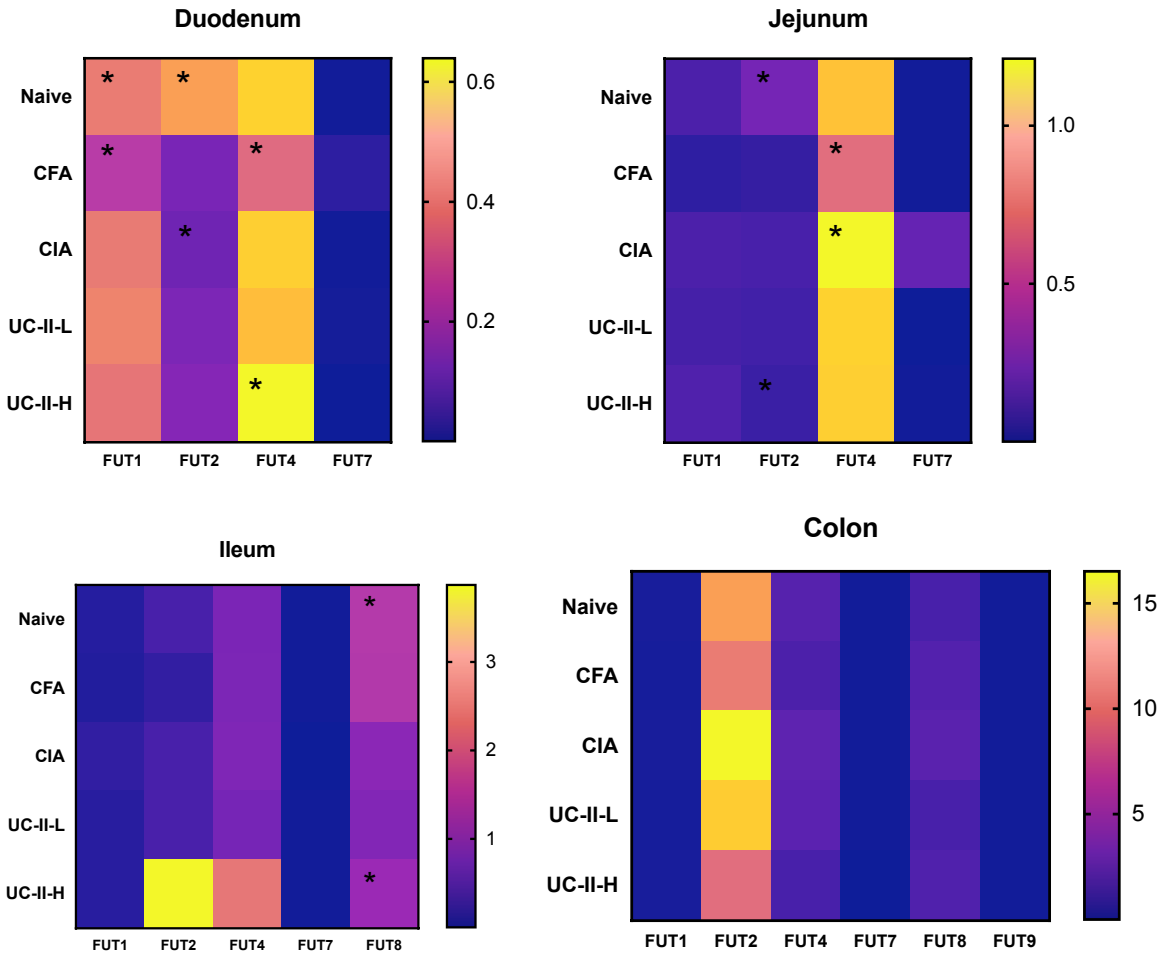

Figure 3-23 mRNA expression of fucosyltransferases in the whole gut tissue.

Mice gut tissue were collected when culled. RNA was extracted using QIAGEN mini RNA extraction kit, and transfected using HiPerFect Transfection reagent according to the manufacturer's instructions. mRNA expression of fucosyltransferases was evaluated by RT-qPCR. Heatmap was made by the mean value of the relative expression to Actin in each experimental group. Statistical significance was determined by ordinary one-way ANOVA. Significance indicated by asterisks, *p < 0.05. FUT, fucosyltransferases; CFA, Complete Freund's Adjuvant; CIA, collagen induced arthritis; UC-II-L, UC-II lower dose; UC-II-H, UC-II higher dose.

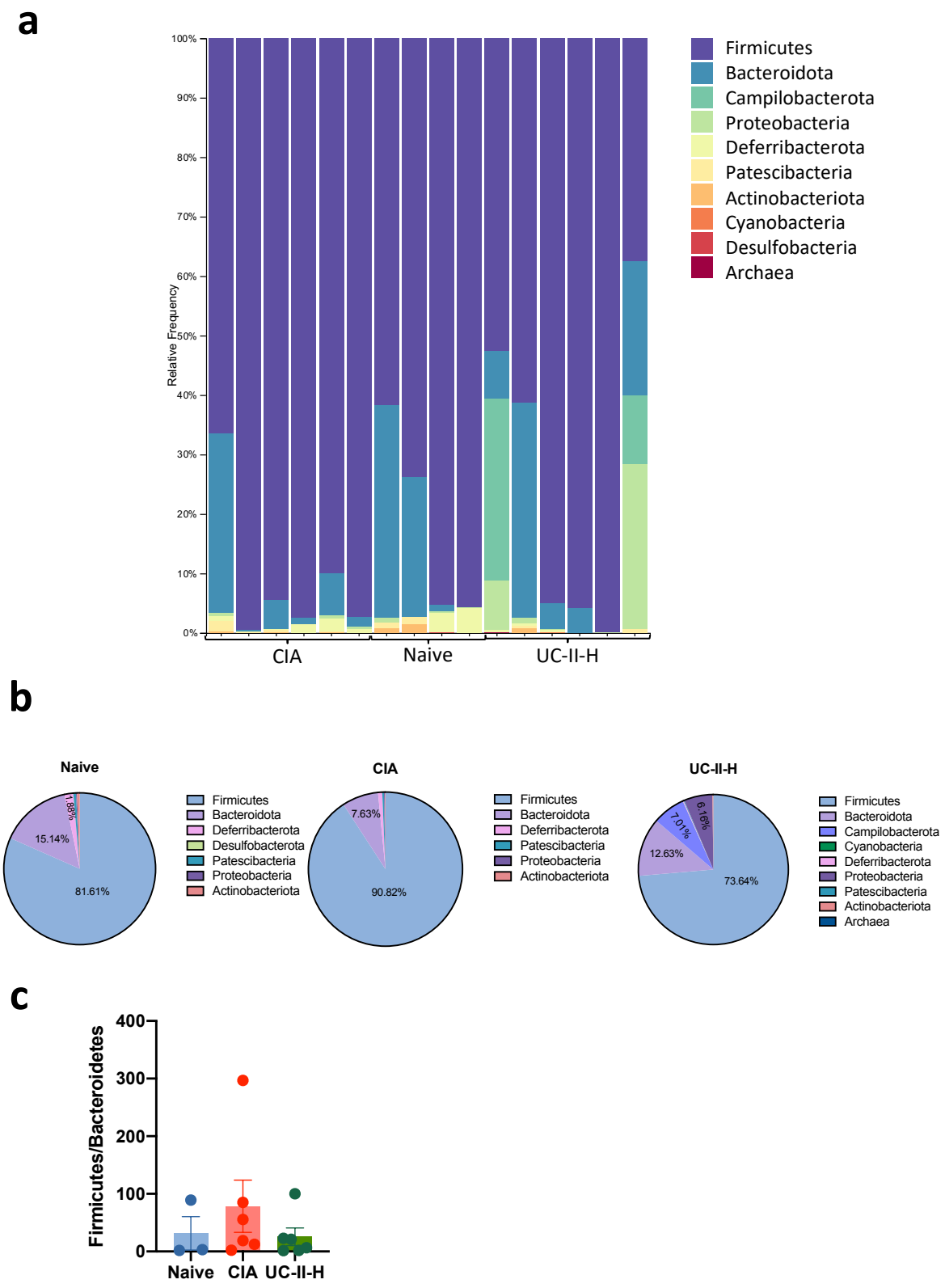

Figure 3-24 Microbial composition in the ileum during experimental arthritis.

Faeces were collected when mice were culled (Score: Naïve =0, n =4; CIA = 6.5±3.4, n =6; UC-II-H = 2.83±2.6, n = 6). DNA were extracted by QIAGEN DNA stool extraction kit, and followed by 16s sequencing. a) Relative abundance of different phyla in the ileum stool sample in each sample. b) Pie chart of the microbial composition of each condition. Pooled samples from at least four mice in each condition. c) Ratio of Firmicutes/Bactrioidetes in each condition during experimental arthritis. Data was presented as mean ± SEM. CIA, collagen induced arthritis; UC-II-H, UC-II higher dose.

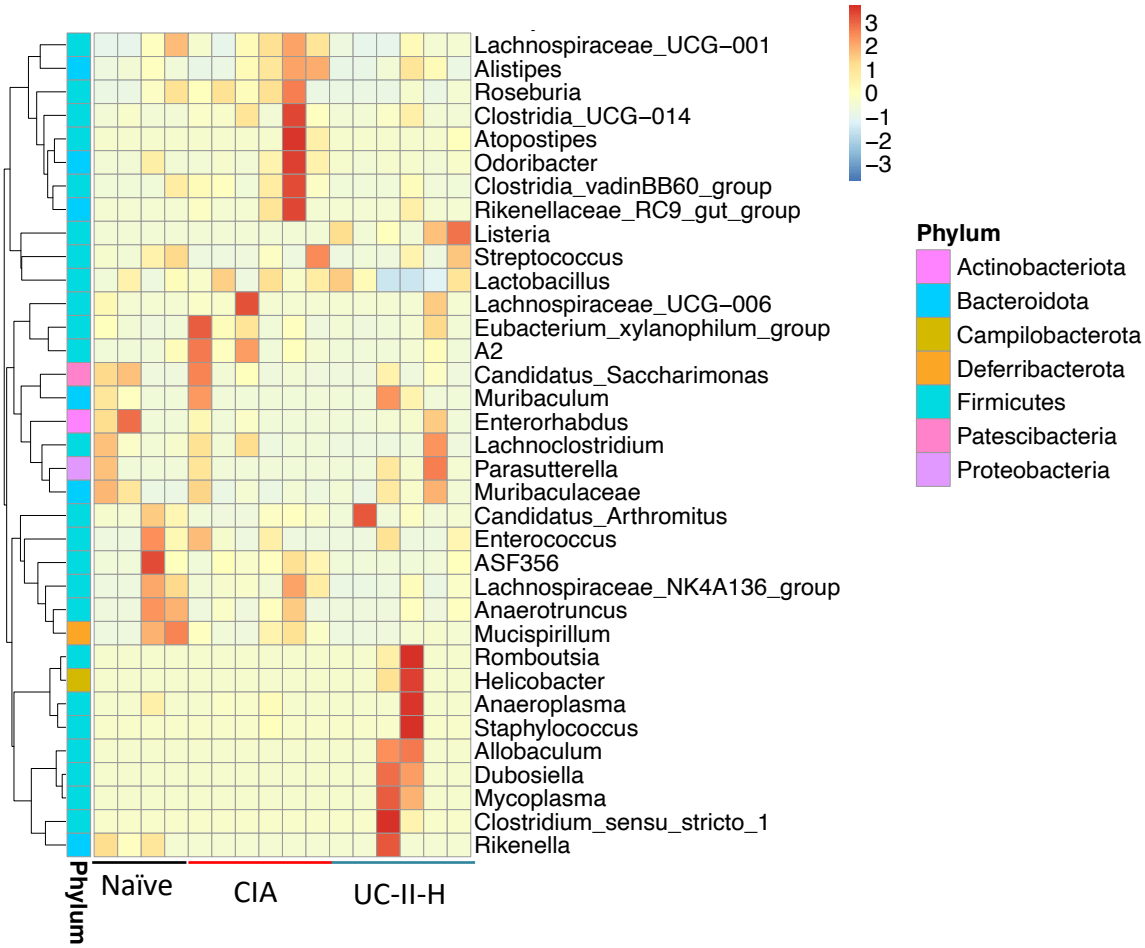

Figure 3-25 Heatmap of clustering of genus abundance in ileum.

According to the species annotations and abundance information of all samples at the genus level, select the top 35 genera in abundance in each condition group. CIA, collagen induced arthritis; UC-II-H, UC-II higher dose (Score: Naïve =0, n =4; CIA = 6.5±3.4, n =6; UC-II-H = 2.83±2.6, n = 6).

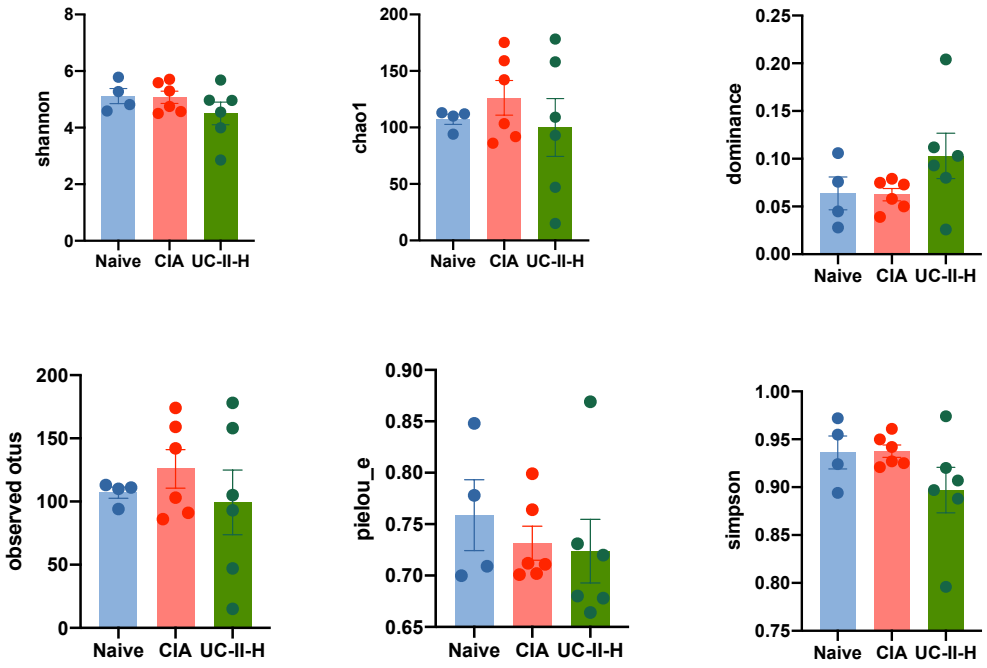

Figure 3-26 Statistics of Alpha diversity indices in ileum.

Alpha diversity indices including shannon, chao1, dominance, observed otus, pielou_e and Simpson are plotted in each group. Each dot represent each individual mouse. Data was presented as mean ± SEM. CIA, collagen induced arthritis; UC-II-H, UC-II higher dose. (Score: Naïve =0, n =4; CIA = 6.5±3.4, n =6; UC-II-H = 2.83±2.6, n = 6).

Note: chao1: Estimate the total number of species contained in the community sample. The more low-abundance species in the community, the greater the chao1 index; dominance: the probability when randomly select two sequences from the same sample, the better the community species uniformity, the larger the index; observed_otus: the number of species observed directly, the larger the index, the more species are observed; pielou_e: the evenness index, the more even the species, the larger the pielou_e; Shannon: the total number of categories in the sample and their proportions. The higher the community diversity, the more uniform species distribution, and the greater the shannon index; simpson: characterizes the diversity and uniformity of species distribution in the community. The better the species uniformity, the greater the simpson index.

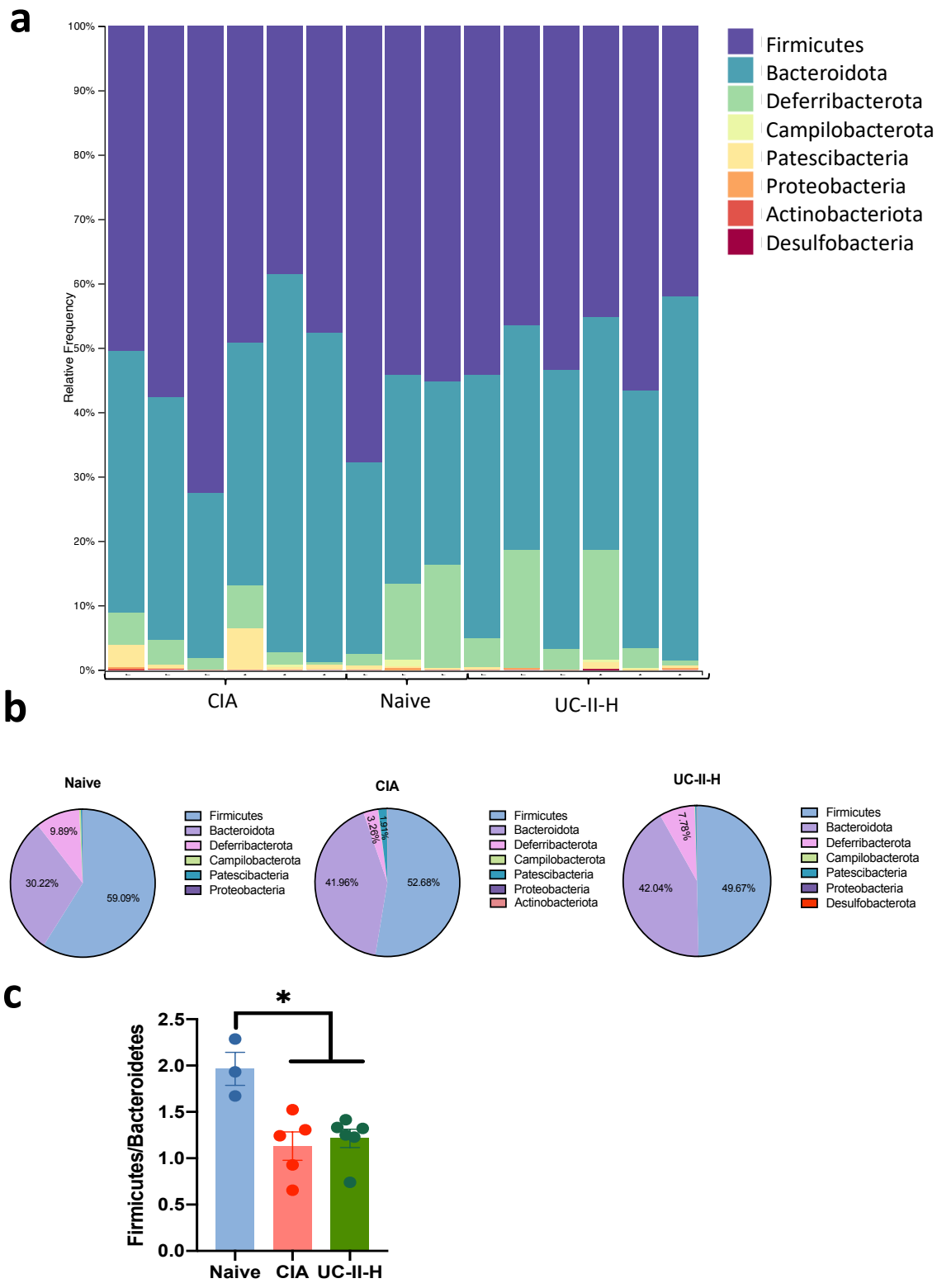

Figure 3-27 Microbial composition in the colon during experimental arthritis.

Faeces were collected when mice were culled (Score: Naïve =0, n =3; CIA = 6.5±3.4, n =6; UC-II-H = 2.83±2.6, n = 6). DNA were extracted by QIAGEN DNA stool extraction kit, and followed by 16s sequencing. a) Relative abundance of different phyla in the colon stool sample in each sample. b) Pie chart of the microbial composition of each condition. Pooled samples from at least three mice in each condition. c) Ratio of Firmicutes/Bactrioidetes in each condition during experimental arthritis. Statistical significance was determined using one-way ANOVA. Significance indicated by asterisks, *p < 0.05. Data was presented as mean ± SEM. CIA, collagen induced arthritis; UC-II-H, UC-II higher dose.

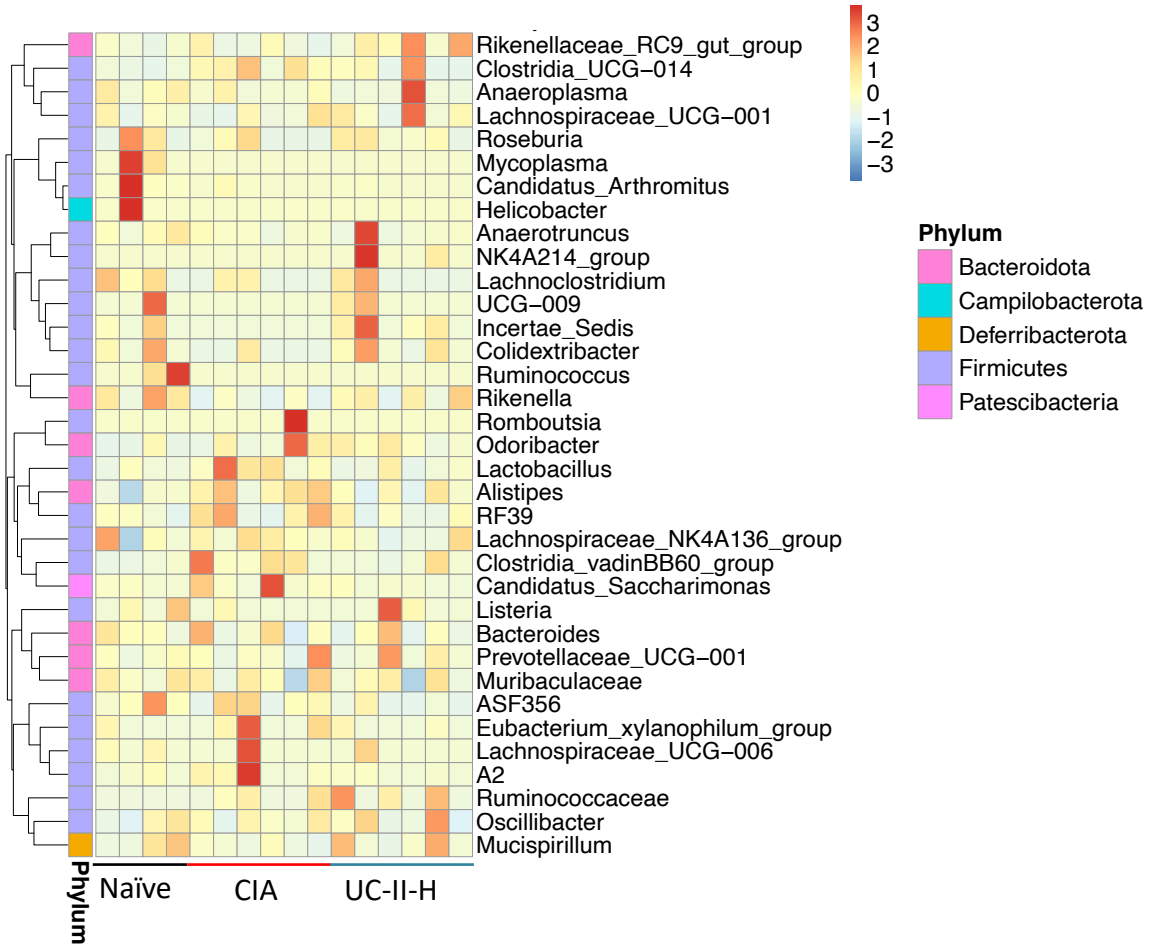

Figure 3-28 Heatmap of clustering of genus abundance in the colon.

According to the species annotations and abundance information of all samples at the genus level, select the top 35 genera in abundance in each condition group. CIA, collagen induced arthritis; UC-II-H, UC-II higher dose (Score: Naïve =0, n =4; CIA = 6.5±3.4, n =6; UC-II-H = 2.83±2.6, n = 6).

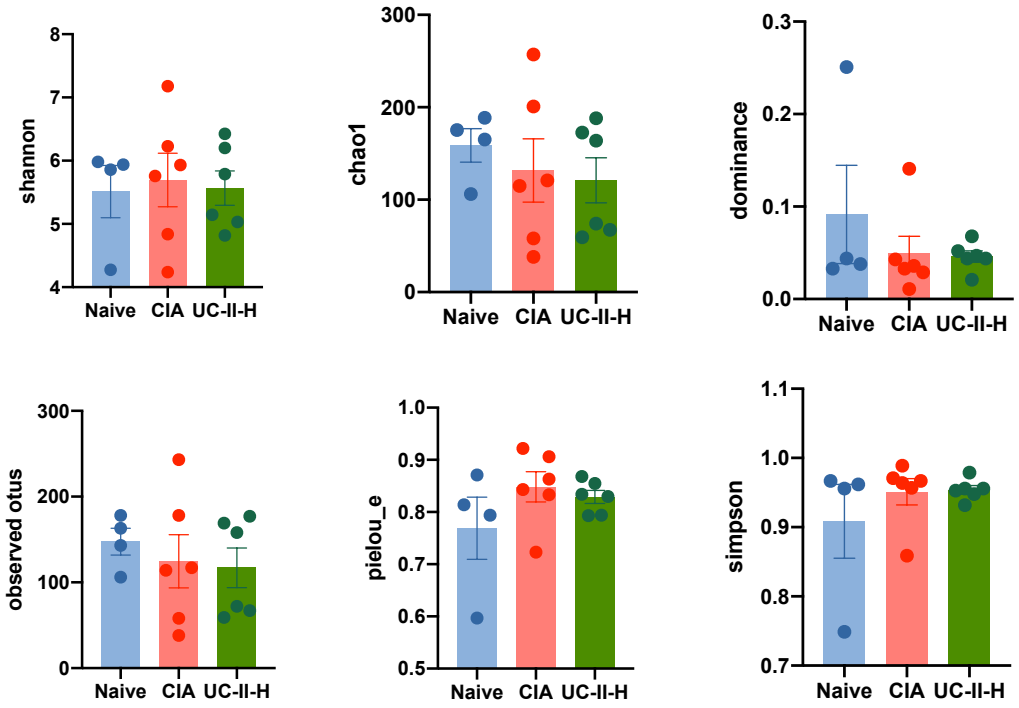

Figure 3-29 Statistics of Alpha diversity indices in colon.

Alpha diversity indices including shannon, chao1, dominance, observed otus, pielou_e and Simpson are plotted in each group. Each dot represent each individual mouse. Data was presented as mean ± SEM. CIA, collagen induced arthritis; UC-II-H, UC-II high dose. (Score: Naïve =0, n =4; CIA = 6.5±3.4, n =6; UC-II-H = 2.83±2.6, n = 6).

Note: chao1: Estimate the total number of species contained in the community sample. The more low-abundance species in the community, the greater the chao1 index; dominance: the probability when randomly select two sequences from the same sample, the better the community species uniformity, the larger the index; observed_otus: the number of species observed directly, the larger the index, the more species are observed; pielou_e: the evenness index, the more even the species, the larger the pielou_e; Shannon: the total number of categories in the sample and their proportions. The higher the community diversity, the more uniform species distribution, and the greater the shannon index; simpson: characterizes the diversity and uniformity of species distribution in the community. The better the species uniformity, the greater the simpson index.

Chapter 4 Transcriptomic profile of the gut in health

4.1 Introduction

The gut, also known as the gastrointestinal tract (GI tract), plays a pivotal role in maintaining overall health and well-being. Its significance extends far beyond simply digesting food; it acts as an immune system organ in the body, containing haematopoietic tissue and cells and maintaining immune homeostasis, making it one of the most important immunological interfaces in the body (Katie Lynn Mason, 2008). The gastrointestinal associated lymphoid tissue (GALT) includes structures such as Peyer's patches (PPs), mesenteric lymph nodes (MLNs) and immune system cells, whilst the immunological interactions of the intestine are the mostly mucosal epithelium and underlying lamina propria (LP). Here there are activated T cells, plasma cells, mast cells, dendritic cells (DCs) and macrophages even under normal conditions, which are responsible for gut homeostasis in our body (Wershil et al., 2008).

A breakdown in intestinal homeostasis can result in chronic inflammatory diseases of the gut including inflammatory bowel disease, coeliac disease and allergy (Coombes et al., 2008). Various factors can disrupt this delicate balance, potentially leading to gastrointestinal issues, immune dysregulation, and other health problems. Apart from eating habits and lifestyles like diet, exercise, obesity and stress (Valdes-Ramos et al., 2010), the microbiome plays an important role in intestinal homeostasis (Shi et al., 2017). However, few studies have investigated glycan changes in the intestine during the RA progression, despite reports on the importance of glycosylation in gut inflammation (Dias et al., 2018, Goto et al., 2016, Kudelka et al., 2020) and gut microbial composition (Kononova et al., 2021). This places glycans at the centre of local gut immunity, since the microbiome can regulate gut function by producing byproducts and active immunomodulatory metabolites.

Therefore, given the distinct functions of the gut and the variety of anatomical locations within the tissue, we hypothesised that the glycosylation profile of different gut regions will contribute to their specific functions and will therefore vary among them. To test these hypotheses, we will analyse the expression profile

of enzymes and proteins involved in glycan biosynthesis and glycan recognition in two RNASeq datasets provided by Prof. Robert Nibbs's lab and Prof. Simon Milling's lab:

1- Whole gut tissue from different areas, including duodenum, jejunum, ileum and colon (provided by Prof. Robert Nibbs's lab).

2- DCs isolated from different anatomic locations(provided by Prof. Simon Milling's lab).

Collectively, these studies aim to investigate whether differential transcriptomic expression related to glycans is found in different anatomical areas of the healthy gut and their associated DC populations, to provide a cornerstone for our hypothesis and future studies.

Because of the importance of DCs in the induction of oral tolerance and gut homeostasis, knowing the transcriptomic expression related to glycans of different subsets of DCs in relation to the local glycome can uncover novel homeostatic networks, as the pattern of glycans and GBPs expressed by DCs can influence the behaviour and subsequent immune and tolerogenic responses. For example, Ilarregui's group found that galectin-1 alters DCs function, promoting IL-10-mediated T-cell tolerance and suppressing autoimmune neuroinflammation (Ilarregui et al., 2009).

4.2 Results

4.2.1 Biological functions of the gut

To test the hypothesis that different gut regions show a distinctly functional glycosylation, it is necessary to understand both the functions of the different anatomical areas and their glycosylation profile under healthy conditions. Unfortunately, this project started in April 2020, right at the beginning of the COVID-19 pandemic, when lab work and animal services were very limited due to lockdown and access to the lab was cancelled. Given these circumstances, it was decided to establish the functional and glycosylation pathways of the GI tract by analysing existing transcriptomic datasets, which were available at the time. To achieve this, an analysis of an intestinal RNA-sequencing dataset from C57BL/6J

mice (9 weeks old) was supplied by Prof. Robert Nibbs's lab was performed jointly with Nawshin Nazia (a MSc student in the Pineda group that I co-supervised).

To confirm the functional specialization of different anatomical areas in the gut at the transcriptomic level, the differential genes that were significantly expressed in specific areas (compared to the rest of the gut) were assessed. The resulting heatmap showed a clear distinction in gene expression between the small intestine and the large intestine (Figure 4-1), with the genes that are upregulated in the small intestine being almost the same genes that are downregulated in the colon samples. Closer inspection, however, shows that the expression pattern of genes in the ileum is somewhat different to that of the duodenum and jejunum samples (Figure 4-1), with a distinctive pattern of its own relative to the rest of the small intestine.

For functional analysis, we next used Gene Ontology (GO) and Kyoto Encyclopedia of Genes and Genomes (KEGG) pathway enrichment (https://biit.cs.ut.ee/gprofiler/gost) for both the small intestine (Figure 4-2) and colon (Figure 4-3). Interestingly, this revealed different biological activities in the individual gut locations. For example, more metabolic processes involving nutrition absorption and digestion of fat and carbohydrates were implicated in the duodenum and jejunum, while genes associated with homeostasis of cellular metabolism were differentially regulated in the ileum (Figure 4-2a). Likewise, the immunological pathways in the duodenum and jejunum show more similarities than those associated with the ileum. Nevertheless, they all exhibited pathways involved in both innate and adaptive immune responses associated with cell activation, proliferation, and differentiation of T cells and B cells, along with the production of cytokines such as IL-10 and IL-12 (Figure 4-2b). Reflecting this, they identify signalling pathways like NF-kappa B and JAK-STAT signalling pathways. Specific antigen receptor-mediated and Toll-like receptor 9 signalling pathways were found in the ileum (Figure 4-2a).

In the large intestine, metabolism appears to be shifted towards glycoprotein and glycolipid and G protein-coupled receptor signalling pathways. Interestingly, pathways involved in the generation of neurons were found in the colon, supporting the gut-brain axis theory (Johannes A. Romijn, 2008). The colon also appears to be the site responsible for glycosphingolipid biosynthesis and responses

to chemical, stimulus and organic cyclic compounds (Figure 4-3). Interestingly, the O-linked glycosylation of mucins stands out in the colon in terms of immunological pathways (Figure 4-3), which points to the importance of glycosylation in its function.

4.2.2 Distinct transcriptomic expression related to glycans in anatomical areas

Collectively, these data indicated the biological functions of the small intestine and colon to be distinct, likely reflecting their different microenvironments such as microbial composition. As glycans can affect the microenvironment of the intestine, it was hypothesised that glycans define tissue function and that dysregulation of glycosylation leads to tissue dysfunction.

To address testing this hypothesis, we first identified glycan signatures associated with different anatomical locations in the healthy gut. Specifically, transcriptomic analysis of genes encoding glycosyltransferases and sulfotransferases were analysed, as glycosyltransferases are important enzymes in the process of glycosylation and sulfotransferases act as modifiers of glycans (Schnaar, 2016). Corroborating our hypothesis, similarly to the results we got for whole gene expression, analysis of the differential expression of glycosyltransferase genes revealed a different, almost inverse, overall pattern between the small and large intestine (Figure 4-4). However, significantly expressed genes related to glycosyltransferases and sulfotransferases specific to each anatomical area in the gut were identified, but again clustering the duodenum and jejunum together, consistent with the previous similar functions proposed for these two locations. Interestingly, the genes associated with the synthesis of O-linked glycans were upregulated in duodenum and jejunum in the small intestine (Figure 4-5, Figure 4-6). Furthermore, genes involved in the non-specific branching and elongation of N-linked and O-linked glycans and glycolipids (B4galt1, B4galt6, B4galt5, B4galt3, B4galnt4) were consistently upregulated in the duodenal and jejunal samples (Figure 4-5). Additionally, the duodenum and jejunum samples express the terminal fucosylation gene Fut7, which was absent in the ileum. By contrast, in the ileum, the significantly expressed genes were involved in antennae branching and sialylation (Figure 4-6). However, a number of genes involved in N-glycan branching/termination, O-linked glycoprotein (mucin, mannose, and fucose) and

glycolipid were up-regulated throughout the large intestine, which makes colon are enriched in complex glycans.

Overall, the distinct transcriptomic expression related to glycans was identified in different anatomical regions in the gut, which was consistent with a distributed function in the intestine.

4.2.3 Glycan-related pathways and DC migration in the gut

As described in the general introduction, GALT is the main location where oral tolerance is generated, and DCs are key to the activation of Tregs. Different subsets of DCs have been identified in the intestine on the basis of their unique functional properties and anatomical localizations (Coombes et al., 2008, Persson et al., 2013a). Hence, DCs play an essential role in tolerance and homeostasis in the gut, making it an important site for investigation of the gut-joint axis theory in RA.

Dendritic cells are versatile antigen-presenting cells, being key for both priming and tolerogenic immune responses (Figure 1-6). Conventional DCs (cDCs) were divided into cDC1s and cDC2s. cDC1s are characterized by the surface markers XCR1 and CD103 whilst cDC2s are a group expressing the surface marker CD11b (but not XCR1) (Worbs et al., 2017). cDC1s take up antigens and present them to CD8+T cells, while cDC2s play a role in activating CD4+T cells and promoting antibody responses (Figure 4-8) (Liu et al., 2021). In the lamina propria, intestinal cDC1s are characterized by expression of CD103 and lack of CD11b, while cDC2s were found to be CD103+CD11b+ (Persson et al., 2013b). Interaction between DCs and immune system cells through glycan-related pathways has been reported (Ilarregui et al., 2009). Therefore, since we found distinct glycosylation signature in the different anatomical area in the gut, it is important to evaluate how these subsets of DCs may interact with glycans in the local environment to induce tolerance and intestinal homeostasis.

To investigate this, three subsets of DCs were selected based on the populations found in the lamina propria, namely CD11b+DCs, CD103+DCs and CD103+CD11b+ double positive DCs (DP DCs). We evaluated the expression of GBPs of these DCs during the migration route from lamina propria, thoracic duct (the lymph), to

mesenteric lymph nodes in the intestine to understand the ability of DCs to interact with glycans expressed by cells and tissues within the particular environment. Moreover, the genes related to glycosyltransferases were also evaluated, to define the glycosylation profile of the DCs themselves. Unsupervised clustering of the GBP genes alone demonstrated the three subsets DCs to express quite different sets from each other during migration (Figure 4-9a-c). For example, as represented in Figure 4-9, generally cDC2s showed changes in GBP expression during migration. For example, double positive DCs (cDC2s) increased the expression of GBPs while they travelled from the lamina propria to the lymph node. On the contrary, CD11b+DCs (cDC2s) exhibited a decreased expression of GBP. However, cDC1s (CD103+DCs) exhibited the same level of GBP expression during migration. In terms of their own glycan expression, CD11b+DCs show a down-regulation of glycosyltransferases in the duct that is upregulated when they arrive at the lymph node, while CD103+DCs behave oppositely, upregulating glycosyltransferases in the duct and downregulating the when they have finished their journey. Double-positive DCs gradually decreased expression of glycosyltransferases along the migration route (Figure 4-9). Overall, distinct profiles of glycan binding proteins and glycosyltransferases are expressed by these three subsets throughout the migration, suggesting that glycans may have the ability to regulate the behaviour of DCs, and further, affect oral tolerance.

To further investigate their distinct transcriptomic glycan expression, the expression of genes involved in different steps of glycosylation biosynthesis, such as the glycosyltransferases and glycosidases responsible for mannosylation, fucosylation, sialylation and glycan degradation. No significant changes were observed in the results (data not shown), however the expression of galectins and siglecs show distinct patterns in DC subsets during migration (Figure 4-10). Galectins recognize galactose on branched glycans whilst Siglecs are cell-surface proteins that can recognize glycans containing sialic acid. Both are involved in the regulation of inflammation and cell migration (Schnaar, 2016). The results suggest that CD11b+DCs highly expressed galectins and siglecs in the lamina propria, compared to the duct and mLNs (Figure 4-10). By contrast, CD103+DCs exhibited high expression of galectins in the lamina propria and duct, but few when they arrived in mLNs whilst double-positive DCs only expressed galectins in lamina propria (Figure 4-10). Collectively, the results pointed towards differential

modulation of glycan-related pathways or networks of the DC subsets during their migration from the lamina propria to mLNs, although the detailed mechanisms and functional implications behind this needs further investigation.

4.3 Discussion

A healthy intestine is fundamental to health and well-being. Therefore, the understanding of how the intestine works and its surroundings under healthy conditions is pivotal. In this chapter, in order to address the role of glycans in these processes, the potential biological functions as well as glycan-related expression identified by transcriptomics were evaluated along the GI.

These results suggested that the small intestine expresses more genes involved in digestive and immunoregulatory functions than the colon, which exhibited more involvement in metabolic functions, especially O-linked glycosylation pathways (Figure 4-1, Figure 4-2, and Figure 4-3). Mucin O-linked glycans are the main components of the intestinal mucus and are essential for the maintenance of the barrier function of intestine, preventing microbiota from entering the colonic mucosa (Johansson et al., 2011). Interestingly, evaluation of the distribution of genes encoding glycan biosynthetic enzymes in the distinct intestinal regions showed a similar type of compartmentalization to the functional pathways in the intestine, suggesting the role of glycans is not just as a structural component but also constitutes a functional and immunological component in the gut. For example, whilst the ileum samples showed distinct glycosyltransferase and sulfotransferase gene profiles compared to duodenum and jejunum, even they all are part of the small intestine, they show distinct immune pathways, being the ileum the most different (Figure 4-4, Figure 4-6). These data indicated the correlationship between glycans and the functional pathways of intestine, immunologically and metabolically.

The glycosylation profile of DC subsets was also evaluated as they have an important role in the gut regarding activating Tregs and inducing oral tolerance (Coombes et al., 2008). Interestingly, therefore, CD103+DCs showed a different GBP profile from CD11b+DCs and CD103+CD11b+DCs during their migration route from LP to MLN. Compared to CD103+DCs (cDC1s), CD11b+DCs and CD103+CD11b+DCs (cDC2s) have more active ‘glycan-communications’ when they

travel from lamina propria to mLNs (Figure 4-9). Functionally, cDC1s potently cross-prime CD8+T cells for viral clearance and activation of Th1/Th17 response to protect against bacteria; while cDC2s normally migrate to mLNs to initiate a Th2 cell-dependent responses (Liu et al., 2021). Moreover, cDC2s generate responses against extracellular pathogens and play an important role in the maintenance of the Treg population (Murphy et al., 2022, Reparaz et al., 2022), which makes sense in healthy mice (Figure 4-8).

Further investigation of the galectins and siglecs of DC subsets during migration, revealed similar active communication of CD11b+DCs (Figure 4-10). Many studies have been reported the importance of galectin and siglecs in migration and immunoregulatory function (Ilarregui et al., 2009, Fermin Lee et al., 2013, Querol Cano et al., 2019, Jennifer A. Fulcher, 2006, Wang et al., 2022). CD11b+ DCs have upregulation of both galectins and siglects only in the lamina propria, perhaps suggesting these lectins provide ‘signals’ to move. Collectively, our results provided evidence that the glycosylation profile of DCs may affect their function and behaviour in the intestine.

In this chapter, we defined glycan expression by transcriptomics in distinct intestinal regions and the glycan-related pathways of DC subsets during migration in healthy animals, although there were certain limitations. As glycosylation is a dynamic process that is also regulated by environmental factors, this transcriptomic data cannot fully draw a picture of the glycome precisely. However, these data provide a glycosylation map of the intestine and DCs trafficking between the LP and MLNs. In order to fully understand whether the alteration of glycans in the gut could regulate inflammation and immune responses, and hence affect the development of diseases like RA, further studies are needed.

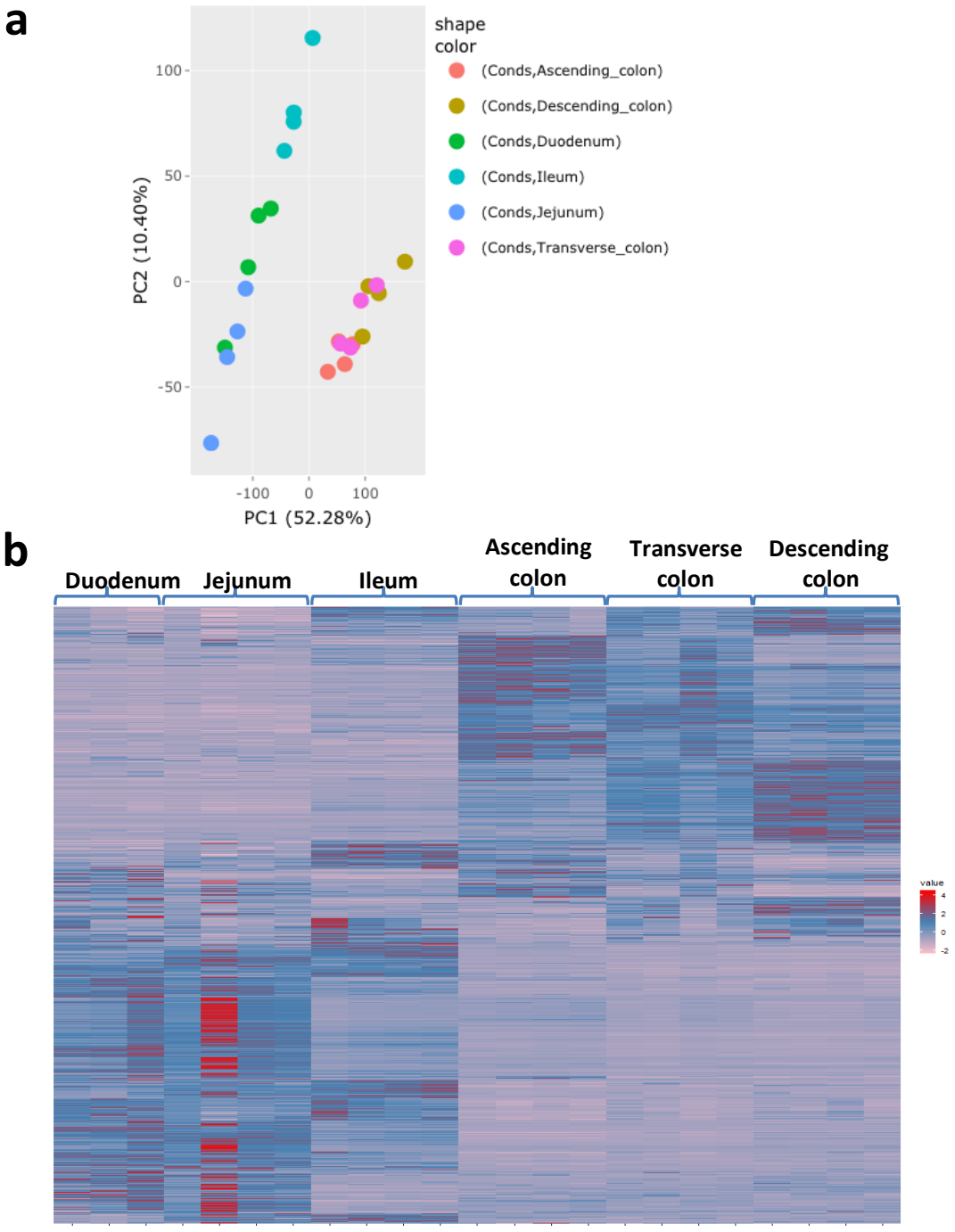

Figure 4-1 All the significantly expressed genes in both small and large intestine of healthy mice.

Intestinal RNA-sequencing dataset supplied by Prof. Robert Nibbs's lab C57BL/6J mice harvested for 9 weeks. Significant genes along gastrointestinal tract were selected based on Reshape2 and ggplot2 with the genes that passed the threshold of p adj < 0.01 and log2FoldChange > 1.5 in DE analysis. **a)** Principal component analysis (PCA) shows that the plots are clustered by anatomical location in the gut. **b)** Heatmap of significantly expressed genes in the small intestine and large intestine of healthy mice.

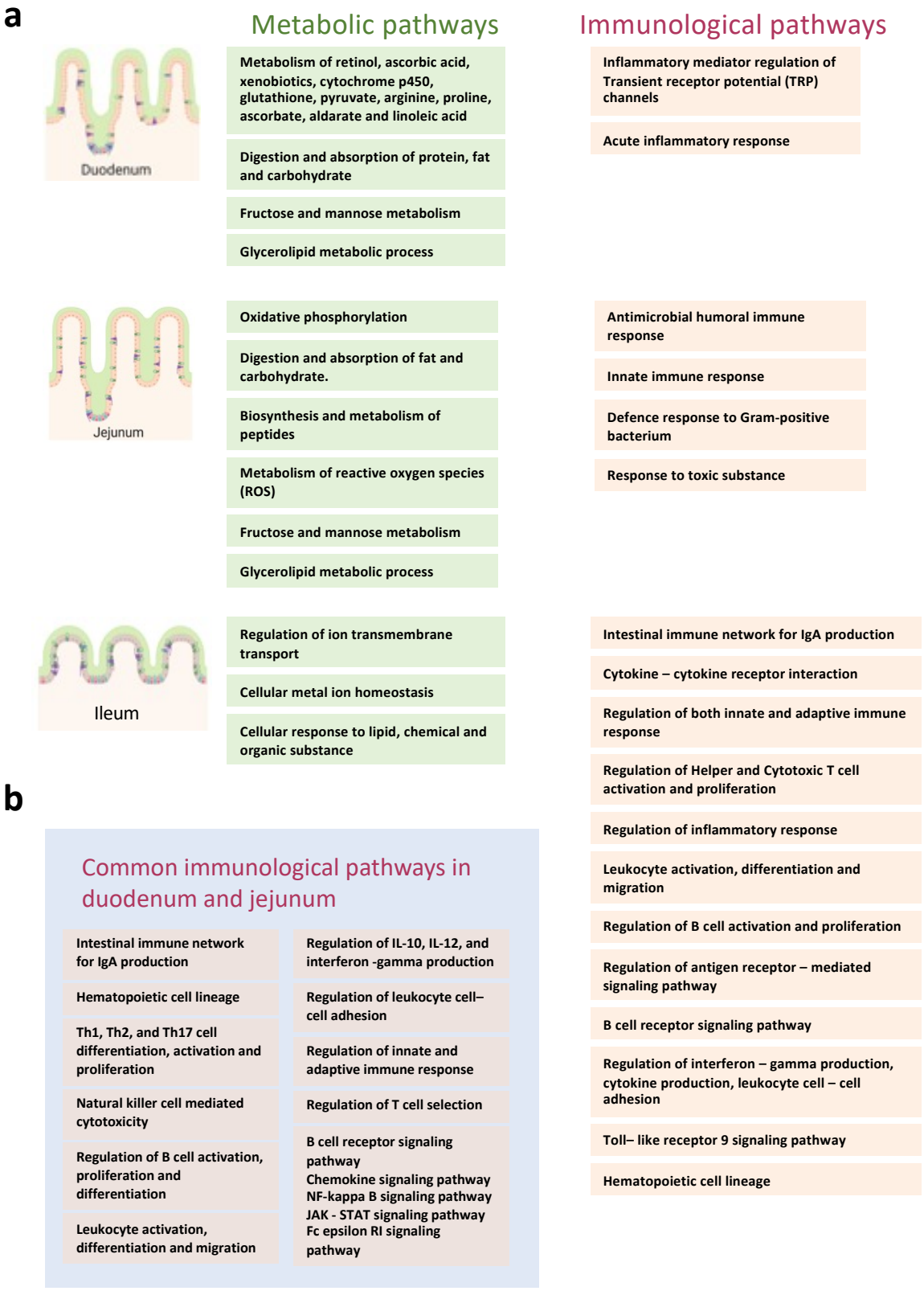

Figure 4-2 Functional pathways of small intestine

Significant genes (Figure 4.1b) were analyzed the Gene Ontology (GO) enrichment and Kyoto Encyclopedia of Genes and Genomes (KEGG) pathway enrichment using g: Profiler version e104_eg51_p15_3922dba (https://biit.cs.ut.ee/gprofiler/gost) a) metabolic (green box) and immunological pathways (yellow box) of duodenum, jejunum, and ileum. b) common immunological pathways in duodenum and jejunum.

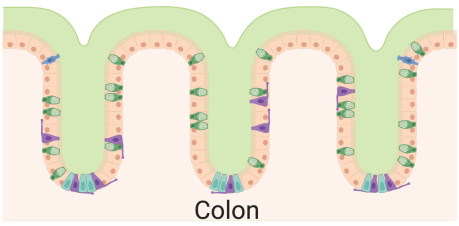

Metabolic pathways Immunological pathways

Ascending colon

- G protein-coupled receptor signaling pathway
- Cell surface receptor signaling pathway involved in cell – cell signaling
- Sulfur metabolism
- O – linked glycosylation of mucins
- Neuroactive ligand - receptor interaction
- Regulation of cell differentiation, ion transport, hormone secretion and membrane potential
- Generation of neurons

Transverse colon

- Ion transmembrane transport
- Glycosphingolipid biosynthesis – lacto, ganglio and neolacto series
- Transport of calcium ion and carboxylic acid
- Response to chemical, stimulus and organic cyclic compound
- Glycoprotein and glycolipid metabolism
- O – linked glycosylation of mucins
- G protein – coupled receptor signaling pathway
- Neuroactive ligand – receptor interaction
- Regulation of cell differentiation, ion transport, hormone secretion and membrane potential
- Generation of neurons

Descending colon

- Ion transmembrane transport
- Glycosphingolipid biosynthesis – lacto, ganglio and neolacto series
- Transport of calcium ion and carboxylic acid
- Response to chemical, stimulus and organic cyclic compound
- Glycoprotein and glycolipid metabolism

Figure 4-3 Functional pathways of large intestine.

Significant genes (Figure 4.1b) were analyzed the Gene Ontology (GO) enrichment and Kyoto Encyclopedia of Genes and Genomes (KEGG) pathway enrichment using g:Profiler version e104_eg51_p15_3922dba (https://biit.cs.ut.ee/gprofiler/gost). Metabolic (green box) and immunological pathways (yellow box) in ascending, transverse, and descending colon.

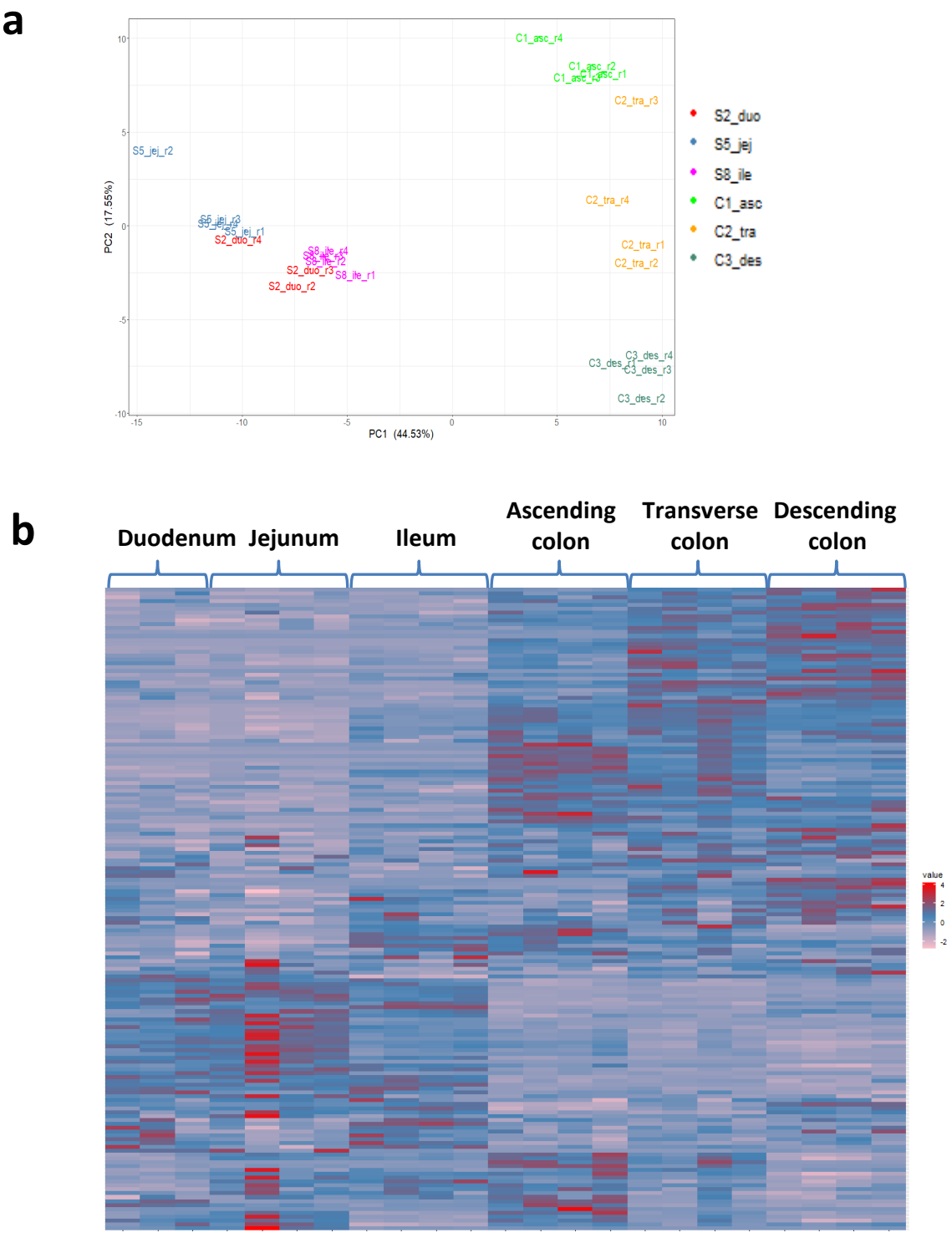

Figure 4-4 Transcriptomic expression related to glycans of healthy gut.

Transcriptomic analysis of genes encoding glycosyltransferases and sulfotransferases were analysed in the small intestine and large intestine. **a)** PCA plot of genes encoding glycosyltransferases and sulfotransferases in healthy gut. **b)** heatmap of genes encoding glycosyltransferases and sulfotransferases.

a

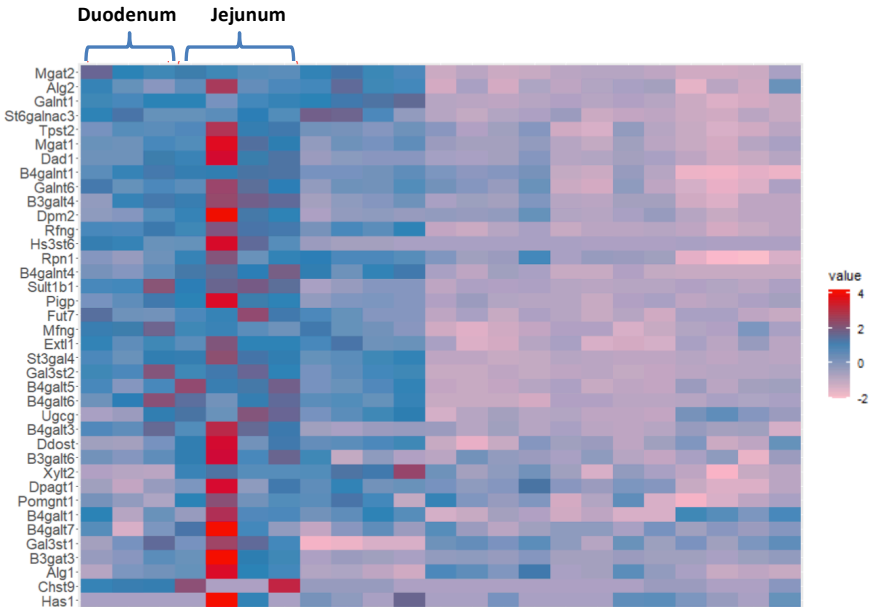

b

	N-linked glycoprotein	O-linked glycoprotein: Mucin	O-linked glycoprotein: Mannose	O-linked glycoprotein: Fucose	Glycosaminoglycan	Glycosphingolipid	GPI-anchor
	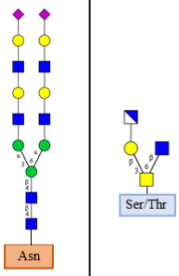		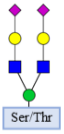	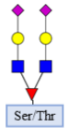	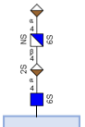	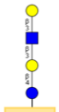	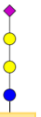
Initiation	Alg1 Alg2 Dpagt1 Ddost Dad1	Galnt1 Galnt6			Xylt2	Ugcg	
Core extension	Mgat1		Pomgnt1	Rfng Mfng	B3gat3 B3galt6 B4galt7 Extl1 Chst9		Dpm2 Pigp
Pathway specific branching and/or elongation and/or modification of antennae	Mgat2					B4galnt1 B3galt4	
Pathway non-specific branching and/or elongation and/or modification of antennae	B4galt1 B4galt6 B4galt5 B4galt3 B4galnt4					B4galt1 B4galt6 B4galt5 B4galt3 B4galnt4	
Terminatial Sialylation/ Fucosylation	St3gal4 St6galnac3 Fut7					St3gal4 St6galnac 3 Fut7	

Figure 4-5 Significantly upregulated genes encoding glycosyltransferases and sulfotransferases in duodenum and jejunum.

a) heatmaps of significantly upregulated genes in duodenum and jejunum. **b)** Involvement of the same genes in glycosylation pathway. Predicable structures were shown in the table.

a

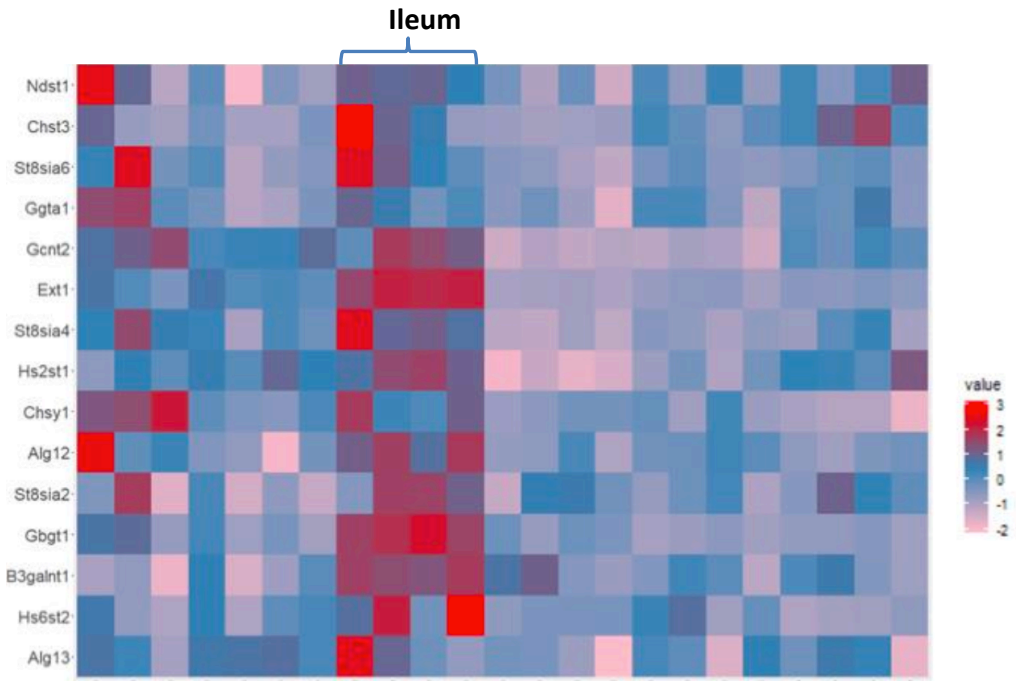

b

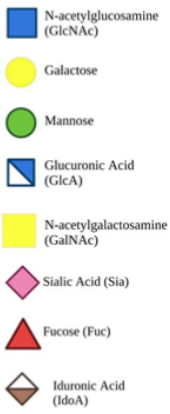	N-linked glycoprotein	Glycosaminoglycan	Glycosphingolipid
	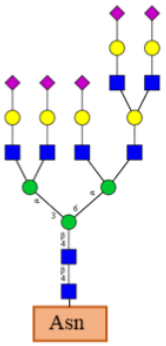	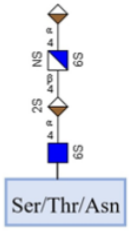	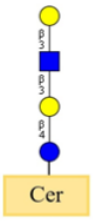
Initiation	Alg13 Alg12		
Core extension		Ext1 Chsy1 Hs2st1 Hs6st2	Gbgt1 Ggta1
Branching and/or elongation and/or modification of antennae	Gcnt2	Chst3 Ndst1 Hs2st1 Hs6st2	B3galnt1 Gcnt2
Terminatial Sialylation/ Fucosylation	St8sia6 St8sia2 St8sia4		St8sia6 St8sia2 St8sia4

Figure 4-6 Significantly upregulated genes encoding glycosyltransferases and sulfotransferases in ileum

a) heatmaps of significantly upregulated genes in ileum. b) Involvement of the same genes in glycosylation pathway. Predicable structures were shown in the table.

a

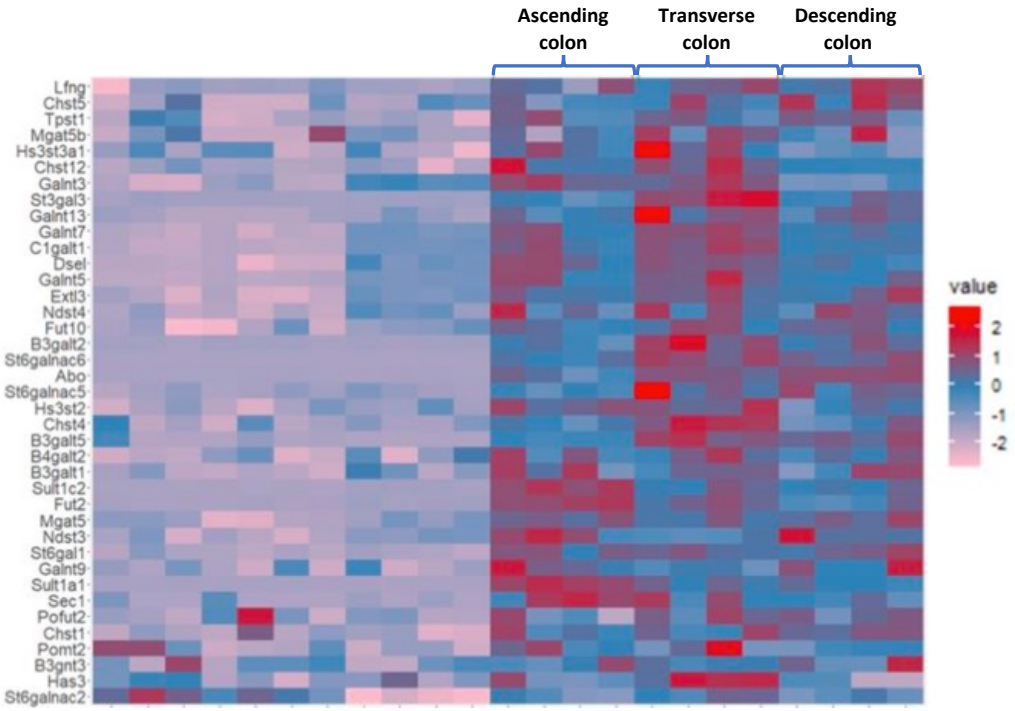

b

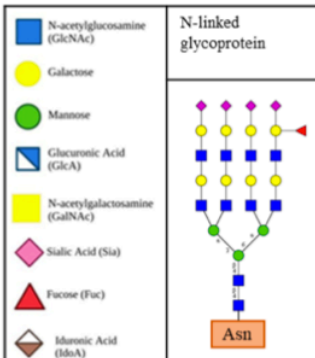

	N-linked glycoprotein	O-linked glycoprotein: Mucin	O-linked glycoprotein: Mannose	O-linked glycoprotein: Fucose	Glycosaminoglycan	Glycosphingolipid
Initiation		Galnt13 Galnt3 Galnt5 Galnt7 Galnt9	Pomt2	Pofut2	Has3	
Core extension		C1galt1			Extl3	
Pathway specific branching and/or elongation and/or modification of antennae	Mgat5 Mgat5b					
Pathway non-specific branching and/or elongation and/or modification of antennae	B3galt1 B3galt2 B3galt5 B3gnt3 B4galt2	B3galt1 B3galt2 B3galt5 B3gnt3 B4galt2	B3galt1 B3galt2 B3galt5 B3gnt3 B4galt2	B3galt1 B3galt2 B3galt5 B3gnt3 B4galt2	Hs3st2 Hs3st3a1 Ndst3 Ndst4 Chst1 Chst12 Chst4 Chst5	B3galt1 B3galt2 B3galt5 B3gnt3 B4galt2
Terminatial Sialylation/ Fucosylation	St3gal3 St6gal1 St6galnac2 St6galnac5 St6galnac6 Fut10 Fut2 Abo	St3gal3 St6gal1 St6galnac2 St6galnac5 St6galnac6 Fut10 Fut2 Abo	St3gal3 St6gal1 St6galnac2 St6galnac5 St6galnac6 Fut10 Fut2 Abo	St3gal3 St6gal1 St6galnac2 St6galnac5 St6galnac6 Fut10 Fut2		St3gal3 St6gal1 St6galnac2 St6galnac5 St6galnac6 Fut10 Fut2 Abo

Figure 4-7 Significantly upregulated genes encoding glycosyltransferases and sulfotransferases in colon.

a) heatmaps of significantly upregulated genes in colon. **b)** Involvement of the same genes in glycosylation pathway. Predicable structures were shown in the table.

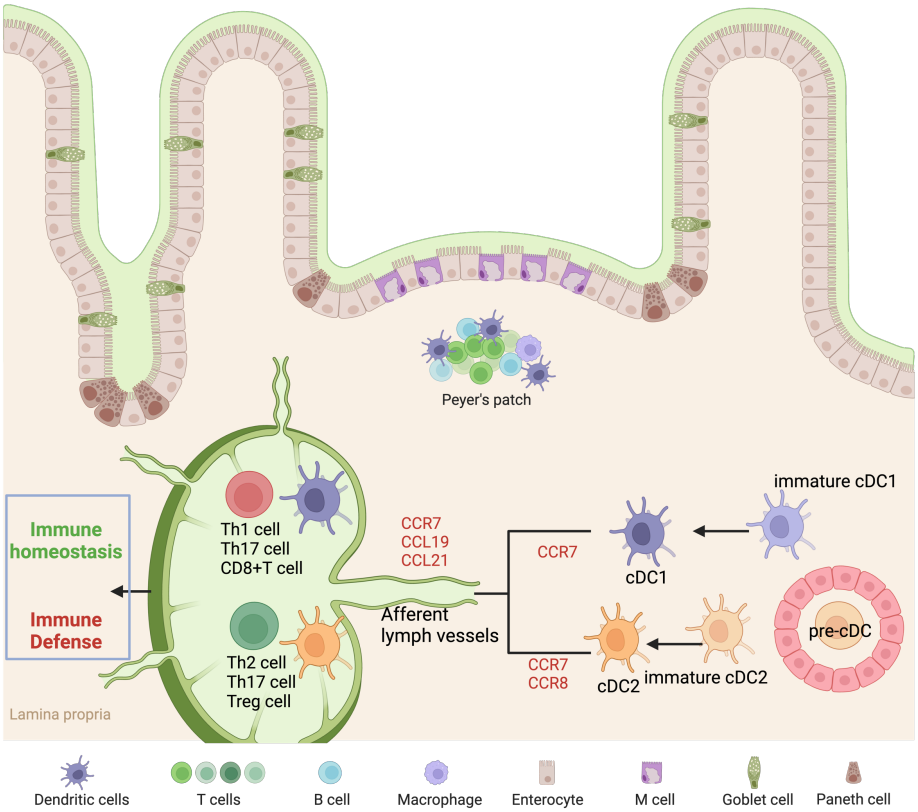

Figure 4-8 DC migration in the regulation of immune defense and homeostasis.

Preconventional dendritic cells (pre-cDCs) give rise to immature cDCs (cDC1s and cDC2s), which undergo maturation and express high levels of CCR7 upon stimulation by pathogenic or inflammatory signals. CCR7 interacts with its ligands CCL19 and CCL21 to guide mature cDC trafficking toward lymph nodes via afferent lymphatics to regulate T-cell immunity. cDC1s potently cross-prime CD8+ T cells for viral clearance and activation of the Th1/Th17 response to protect against bacteria. CCR7 and CCR8 mediate cDC2 trafficking to the lymph node parenchyma to initiate a Th2 cell-dependent allergic immune response.

Adapted from (Liu et al, 2021)

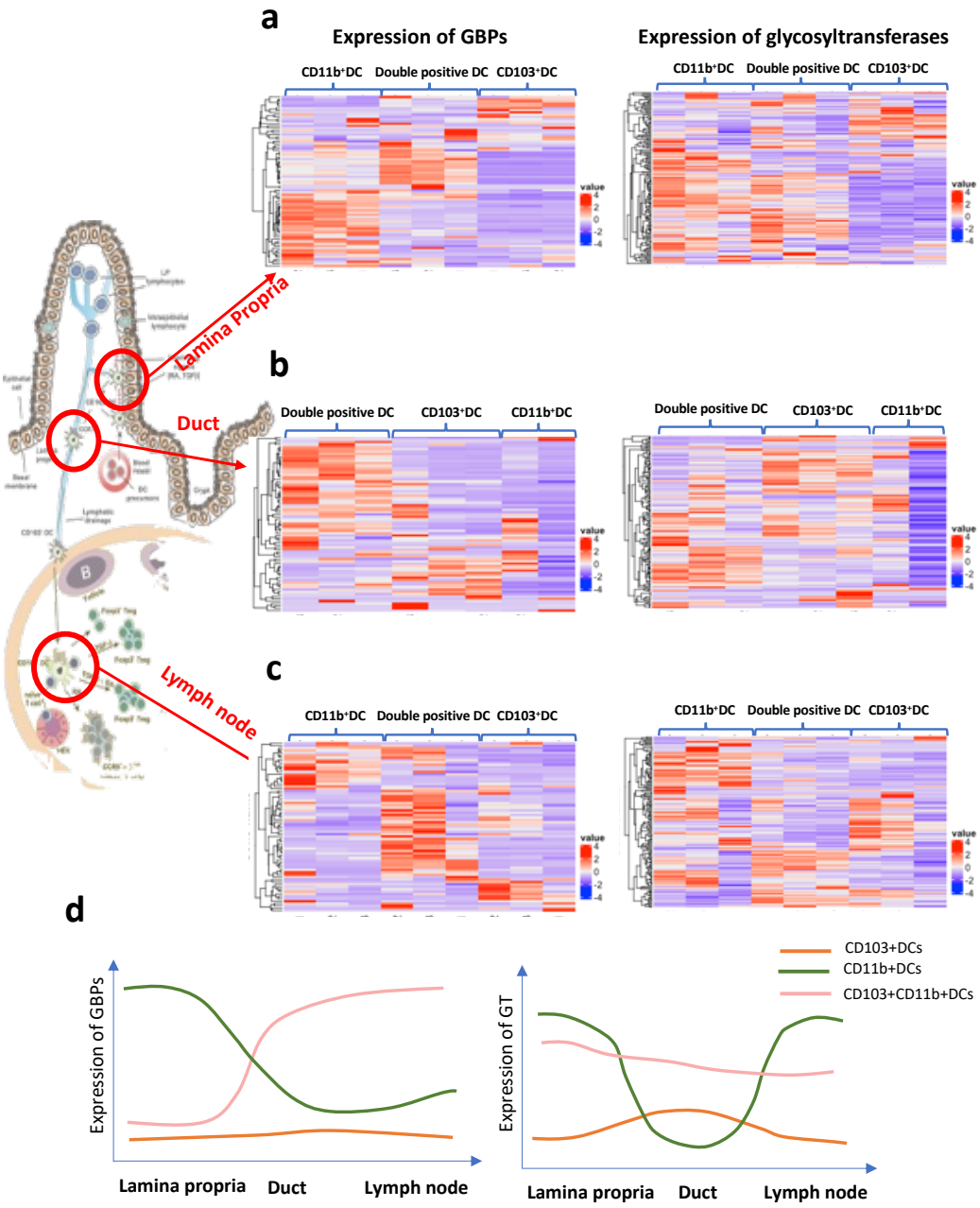

Figure 4-9 Expressions of GBPs and glycosyltransferases (GT) of DCs in different locations.

a-c) Expression of GBPs and GT of CD11b+DCs, CD103+DCs and double positive DCs in lamina propria (a), duct (b) and lymph node (c). **d)** Tendency changes in GBP and GT expression of three DC subsets during migration from lamina propria to lymph node.

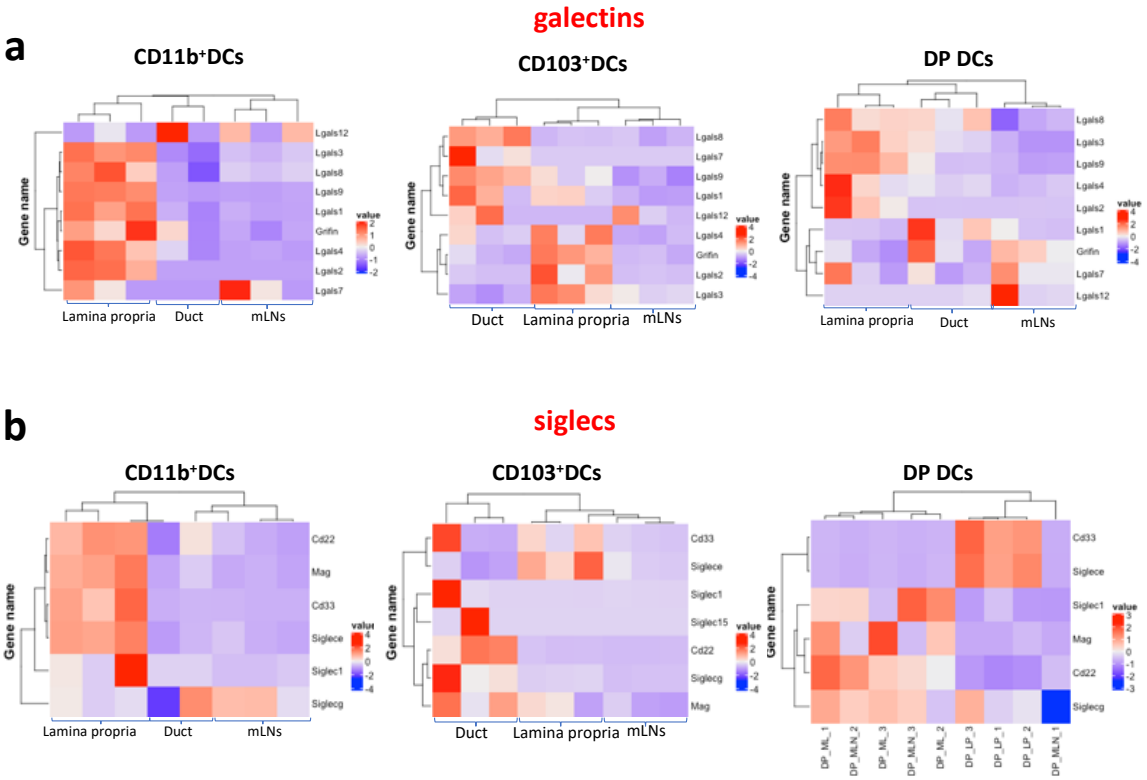

Figure 4-10 Expressions of galectins and siglecs of DCs during migration in the gut.

a-b) Expressions of galectins (a) and siglecs (b) of CD11b+DCs, CD103+DCs and double positive DCs during migration from lamina propria to mesenteric lymph nodes in the gut.

Chapter 5 Alterations of glycosylation in the gut during CIA

5.1 Introduction

Glycans are important in maintaining gut integrity and homeostasis (Brazil et al., 2021) and reflecting this, alterations of glycosylation were observed in many intestinal inflammatory diseases (Reily et al., 2019). The general glycosylation profile of a healthy gut was described in Chapter 4, and downregulation of terminal fucosylation in the gut was identified as a hallmark of CIA mice, as described in Chapter 3. However, further details of glycosylation changes in the distinct intestine areas and associated resident cells during RA remain unclear.

Therefore, in this chapter, the aim is to investigate the glycosylation profile at molecular and cellular level in the intestine, both in health and during experimental arthritis.

To identify the glycosylation profile at the mRNA and molecular level, RNASeq transcriptomics of ileum and colon in healthy and arthritic mice using RNA-sequencing were conducted. Results in Chapter 4 highlighted the relevance of ileum and colon, justifying the choice of tissue. To complement the RNASeq experiments, glycan structures were defined by Mass spectrometry, a technique that has been widely used for analysis of complex biomolecules (Jianjun Li, 2010), in collaboration with Professor Stuart Haslam at Imperial College London. Finally, fluorescently labelled lectin binding combined with flow cytometry was used to delineate the glycosylation of different cell types in the healthy and arthritic gut, including IECs, endothelial cells, fibroblasts, and immune system cells. Collectively, these data provide a broader and more detailed glycomic analysis of the gut tissue to identify glycosylation changes associated with arthritis.

5.2 Results

5.2.1 Transcriptomic changes in the gut during CIA

To further understand how changes in the ileum and colon could affect gut function and tissue glycosylation, we used bulk RNA-sequencing of whole gut tissue from healthy and arthritic mice. We first identified genes that significantly

changed (2 fold increase, adj $p < 0.01$) in the ileum and colon of arthritic mice compared to healthy controls (Figure 5-1). PCA and unsupervised hierarchical clustering of transcriptomic data show that our experimental samples were clustered by condition, suggesting that arthritis is associated with specific gene induction both in ileum and colon (Figure 5-1a-b). Specifically, in the ileum, genes related to the generation of antibody diversity, such as immunoglobulin kappa variable (IgKV) gene family were downregulated in the CIA mice. In addition, genes associated with tissue repair like Mcpt9 and serpina3g and apoptosis related genes such as Gzma and Gzmb were also downregulated in such mice (Figure 5-1c). While Bcan (related to neural development) and Fras1 (related to mutations) were upregulated in the ileum of arthritic mice. Surprisingly, the inflammatory chemokine and chemokines receptor (Cxcl9 and Ccr3) showed higher expression in healthy mice, perhaps reflecting a homeostatic role to preserve the immune cell population and structure required for normal gut function (Wei et al., 2022, Wang et al., 2018, Ignacio et al., 2022). Similarly, in the colon sample, genes belonging to IgKV gene family and immunoglobulin heavy variable (IGHV) gene family were downregulated in the CIA mice (Figure 5-1d). Also, CIA mice exhibited reduced expression of the genes associated with modulating immune responses and homeostasis (Cd209b, Cd209f, Cd163, Cd300lb, and Spn) and tissue repair (Clca3b, Il1rl1, Mmp9, Pf4, and Retnla). Moreover, we noticed the gene Clca3b, which is involved in promoting mucus production, was significantly downregulated in CIA colon. Importantly, we found Cmah and Siglec-1 to be downregulated in CIA mice, genes that are involved in sialic acid biosynthesis and recognition. These results suggest that not only mucus production may be impaired in CIA, by virtue of Clca3b regulation, but also mucin glycosylation, since reduction of Cmah expression could change the overall expression of sialylated O-glycans (Figure 5-1d). Because sialylation is a protective factor promoting intestinal mucus integrity and tissue homeostasis (Yao et al., 2022), a reduction of sialic acid content could explain the functional dysregulation of the gut tissue described in arthritis, a hypothesis that we will test. Finally, we also see genes involved in membrane transport (Best2, Ces2b) among the significantly upregulated group in CIA mice.

Subsequent functional enrichment analysis of differentially expressed genes reveals that immunological responses involved in many signalling pathways

including the chemokine signalling pathway and C-type lectin receptor signalling pathway are modulated in arthritis (Figure 5-2a-b). GO biological process pathway results show that interspecies interaction between organisms and cellular and immune system processes were affected in the ileum (Figure 5-2c). In the colon, the process related to immunoglobulin production was remarkably downregulated in the arthritic mice, as well as the negative regulation of the adaptive immune response and cell surface interaction at the vascular wall (Figure 5-2c). By contrast, regulation of membrane potential and response to hormones was upregulated in the CIA colon. Overall, this analysis confirms the impact of inflammatory arthritis in the gut tissue, providing specific pathways involved in disease pathophysiology.

Following our first unsupervised analysis, we decided to use this RNASeq dataset to investigate the regulation of glycan biosynthetic pathways in the ileum and colon. To do this, we examined the expression of glycosyltransferases and glycosidases, compartmentalising this process into mannosylation, poly LacNAc/Branching, fucosylation, sialylation and glycan degradation (Figure 5-3a). Results in ileum indicate high expression of mannosylation and LacNAc branching related genes, as well as glycan degradation in naïve mice, which are reduced in CIA tissue. Generally, sialyltransferases are up-regulated in CIA, with the exception of St6gal1 and St6galnac1 (Figure 5-3b), making it difficult at this stage to predict the effect on the actual expression of sialsides. On the contrary, the colon of arthritic mice exhibited upregulation of LacNAc branching and downregulation of sialylation compared to the healthy mice (Figure 5-4a). The expression of enzymes involved in glycan degradation clustered healthy and arthritic mice in the colon. Specifically, downregulation of galactosidase (Gla), Glucronidases (Gusb), Hexosaminidases (Hexa) and mannosidases (Man2a1, Man2a2) was observed during arthritis, while upregulation of some miscellaneous genes (Naga) and sulfatases (Galns, Id) were observed. No significant differences were observed regarding fucosylation, neither in ileum, nor in colon. Interestingly, downregulation of siglec expression was observed in the colon of CIA mice (Figure 5-4b), suggesting a dysregulation of local immune responses, since siglecs play an important role in suppressing immune responses to self-antigens to prevent autoimmunity (Macauley et al., 2014). Furthermore, we examined pathways regulating the integrity of the gut barrier, such as mucins production and tight

junction formation (Figure 5-5). Interestingly, mucin production in ileum and colon of arthritic mice was down-regulated, whilst modest up-regulation of tight-junction-related genes were observed in ileum and colon from arthritic mice. (Figure 5-5b).

Collectively, our findings identified changes in the transcriptomic profile of both ileum and colon tissue during experimental arthritis, suggesting that immune pathways and glycan biosynthesis are modulated during disease. Notably, such regulation is specific in different anatomical locations, such as ileum and colon, reflecting the distinct function and homeostatic mechanisms found in these locations. However, transcriptomic changes should generally be taken with caution, as they might not reflect changes and the translation and/or stability levels. This is particularly relevant when extrapolating changes in glycan biosynthetic pathways because glycans are synthesised in a non-template manner (unlike proteins) and are far more dynamic and susceptible to environmental (diet, enzymes produced by local microbiota, smoking, etc) changes (Moran et al., 2011). Therefore, to unambiguously define the glycomic profile of murine gut tissue, we next conducted a mass spectrometry analysis of glycans directly isolated from ileum and colon.

5.2.2 Glycosylation altered in the ileum and colon in CIA

To obtain the exact glycan structures found in the gut, mass spectrometry (MS) was applied. Although sample preparation and analysis are complex, MS is a powerful technique that can identify glycan structure at the molecular level (Jianjun Li, 2010), providing us with a valuable dataset to evaluate the regulation of distinct glycan structures in the gut associated with inflammatory arthritis.

We first evaluated the N-linked glycans in the ileum and colon in both healthy and arthritic mice, upon release of N-Glycans using recombinant PNGase F digest. Higher mass to charge ratio (m/z) glycans, corresponding with elongated LacNAc structure, were up-regulated in the ileum of CIA mice (Figure 5-6), whilst the colon showed the opposite trend (Figure 5-7). Moreover, glycans containing the Sd^a epitope, a specific blood group antigen found on the surface of red blood cells, are enriched in the ileum, while Lewis X and Sialyl Lewis X are abundant in the

colon, indicating the glycosylation profile is area-specific, perhaps in line with their specific function.

For global analysis of the MS-based data, peaks were annotated with specific structures based on the observed m/z values and known biosynthetic pathways. Additionally, individual structures were grouped based on common structural motifs, such as fucosylation, sialylation, LacNAc elongation or high mannose content, as indicated in Figure 5-8a. The intensity of each peak was used to evaluate the relative expression of individual structures (Figure 5-8b-c) and groups (Figure 5-9). Interestingly, a significant upregulation of sialylation in the colon of CIA mice was observed (Figure 5-4), providing some conclusive data to describe the effect of arthritis in gut sialylation, since the ambiguous transcriptomic results showed both down-regulation and up-regulation of sialyltransferase expression.

We conducted a similar analysis to the O-linked glycans in the ileum and colon of Naïve and CIA mice, in this case releasing the O-glycans chemically as there is no enzyme that cleaves O-glycans (Figure 5-10, Figure 5-11). We found the O-linked glycosylation profile in the colon is more susceptible to changes than profiles in the ileum during arthritis. (Figure 5-10). Consistent with the results in the N-glycan pool, an increase of sialylation in the colon was observed ($p = 0.0502$).

In addition, we also noticed the downregulation of fucosylation in the ileum (N-glycan) (Figure 5-9) and colon (O-glycan) (Figure 5-11), which is consistent with data we got in Chapter 3 in the CIA mice immunofluorescence staining data (Figure 3-18).

5.2.3 Distinct glycosylation profile of intestinal cells during CIA

We have depicted the glycosylation profile of the whole ileum and colon tissue, however, the exact glycosylation profile of different compartments and cell types in the gut is required to understand specific functions of glycans on gut immunity and their role in arthritis pathogenesis. To address this, we stained gut tissue with different lectins (Figure 3-17b) and quantified the fluorescence intensity in a range of gut anatomical areas, such as the epithelial layer and lamina propria layer. This approach will allow us to see differences between cells that are communicating with luminal content and stromal cells resident in deeper layers.

In the ileum, we did not observe any significant differences in the epithelial layer and lamina propria layer between naïve and CIA mice with any of the tested lectins (Figure 5-12). However, a significant decrease of α-2,3 sialylation (MAA II binding) was observed in colon of CIA mice compared to healthy mice (Figure 5-13).

These results show a clear modulation of sialic acid in the tissue, but we still cannot be sure that we are seeing individual cell types in IF data, which can mask, or alter some of the results. Given the variability that we predict here, we used Flow cytometry to identify events in individual cells. We digested the gut tissue by collagenase with two fractions (EDTA fraction and collagenase-digested fraction) to get a single-cell suspension. We stained the cells with distinct markers and different lectins to gate the cells including epithelial cells, immune system cells, fibroblasts, endothelial cells, and crypt cells (Figure 5-14). In this case, we can see whether glycosylation changes in the whole gut tissue are caused by changes in different cell populations. In the FACs data, we noticed a decrease in frequency of lymphatic cells (CD45-CD31+PDPN+), and blood endothelial (CD45-CD31+PDPN-) cells in CIA mice along the gastrointestinal tract (Figure 5-15). On the contrary, an increase of immune system cells in the CIA mice along the intestine compared to healthy mice, perhaps consistent with the potential inflammation and immune responses happening in the intestine when mice undergo arthritis.

An initial screen, pooling mice, was performed to identify potential cells of interest, focusing on endothelial cells, epithelial cells and fibroblasts. Fucosylation profile was obtained by UEA I and AAL lectin staining (Figure 5-16). The alteration of fucosylation was indicated by colour code compared to healthy mice. Interestingly, terminal fucose (UEA I) expression was decreased in the duodenum and jejunum; while increased in the ileum and colon compared to healthy control (Figure 5-16). On the other hand, core fucose (AAL) was increased in epithelial cells in EDTA layer along the gut, while decreased in the lamina propria layer except jejunum along the gut in the CIA mice (Figure 5-16).

Importantly, we observed an interesting phenomenon that is the glycosylation profile of fibroblast, endothelial cells and epithelial cells almost keep the same fucosylation shift in the same local area (Figure 5-16).

We next examined the sialylation profile along the intestine by staining SNA and MAA II lectins, we observed a global downregulation of sialylation along the intestine except in the middle small intestine (Figure 5-17). Similarly, the cells in the same local microenvironment tend to have the same changes of sialylation profile.

We also examined the galactose expression along the intestine by PNA staining (Figure 5-18). Interestingly, the changes of galactose expression exhibit two similar compartments with EDTA layer and lamina propria layer. In EDTA layer, the epithelial cells exhibited an increase of galactose expression in CIA mice, and almost other cells kept the same changes. While in the lamina propria layer, the galactose expression was downregulated in most areas of different cell types except epithelial cells in jejunum and ileum. In fact, galactose and sialic acid share the same epitope, binding with sialic acid will result in less binding with galactose and vice versa. The increase of expression of galactose in the EDTA layer can further indicate the decrease of sialylation in epithelial layer in CIA mice.

5.3 Discussion

The mucosal site in the gut is pivotal in maintaining general homeostasis, not only because it is where tolerance is defined, but also where commensal microbiome reside and interact with the host to preserve general health. Understanding how changes in gut tissue affect immunity and tissue integrity during RA could therefore provide novel insights into RA pathology.

In the RNA-sequencing analysis, the differences among Naïve mice are bigger than CIA mice, which may be because of the less diversity of microbiome in CIA mice. Lack of diversity in the microbiome could result in inflammation in the gut including IBD and colitis (Rohani et al., 2015, Human Microbiome Project, 2012). Interestingly, gut glycans in mucins can regulate the microbial composition and further, cause inflammation and intestinal disorders (Moran et al., 2011, Dias et al., 2018), especially fucosylation and sialylation (Goto et al., 2016, Wang et al., 2017b, Yao et al., 2022, Giron et al., 2020). Consistently, our findings suggest the main alteration is of sialylation and fucosylation in the ileum and colon samples of CIA mice compared to healthy mice (Figure 5-3, Figure 5-4, Figure 5-9, Figure 5-11, Figure 5-16, and Figure 5-17). For example, downregulation of siglec

expression was observed in the colon of CIA mice (Figure 5-4b). Supporting this, siglec-G deficiency mice showed increased severity and earlier onset of disease in the CIA model (Bokers et al., 2014). We found another member of the Siglec family to be downregulated in the gut of CIA mice, Siglec-1 (Figure 5-1d). The significantly downregulated gene siglec-1, which is expressed on macrophages, binds to sialylated LPS on bacteria, lack of siglec-1 in the colon could reduce their phagocytosis by macrophages (Jones et al., 2003). Siglec-1 also contributes to bacteria phagocytosis, via binding of sialylated LPS (Jones et al., 2003), perhaps indicating that the reduced expression of siglec-1 in the colon could affect the phagocytic activity of local macrophages and subsequent immune responses. Furthermore, we examined pathways regulating integrity of the gut barrier, such as mucins production and tight junction formation (Figure 5-5). Interestingly, mucin production in ileum and colon of arthritic mice was down-regulated, whilst modest up-regulation of tight-junction-related genes were observed in ileum and colon from arthritic mice. (Figure 5-5b). Additionaly, we also found distinct glycosylation profile between ileum and colon at molecular level. For example, Sd^a epitope is enriched in the ileum, while Lewis X and Sialyl Lewis X are abundant in the colon. In fact, Sd^a antigen synthesis relies on the activity of ß1,4 N-acetylgalactosaminyl transferase 2 (B4GALNT2). B4GALNT2 is able to inhibit cancer progression (Duca et al., 2023). B4GALNT2 is also involved in controlling the growth of intestinal microbiome such as *Escherichia coli* (E. coli) bacteria and *Salmonella typhimurium (Duca et al., 2023, Suwandi et al., 2022)*. Lewis X and Sialyl Lewis X play an important role in immune responses as they are involved in the recruitment of immune cells to the site of inflammation (Schnaar, 2016).

Although the changes of sialylation and fucosylation were observed in CIA mice, however the ileum and colon samples did not exhibit the same sialylation and fucosylation shift at the transcriptomic level, molecular level and protein level. These data show the classic features of the glycan synthesis pathway which is not a one-way template. It can be affected by many environmental factors. Glycosyltransferase expression at the transcriptomic level may be different from the translation level. The final actual glycan expression (MS data) can also be modulated by the environment like microbiota in the gut, which can in turn affect the transcriptomic expression. For example, in the ileum, sialyltransferases were upregulated while the mass spectrum data shows the downregulation of sialylation

in CIA mice. Similarly, the downregulation of sialyltransferase gene expression in the colon and a significant increase of sialylation in the mass spectrum results in arthritic mice. In addition, a decrease of sialic acid expression was observed in the ileum and colon in immunofluorescence and flow cytometry results in CIA. These data together suggested a dynamic process of final sialic acid expression in the gut. In fact, the microbiome in the gut could affect the sialylation in the gut. For example, pathogenic infections are usually initiated by sugar recognition, pathogens like bacteria and viruses would like to synthesize or obtain sialic acid from host cells such as IECs to escape from immune surveillance and survive (Severi et al., 2007, Khatua et al., 2010), which could explain sialylation expression inconsistency of our results. In addition, loss of sialic acid will result in damage to mucus integrity and increase the sensitivity of cells to microenvironmental stimuli, which makes the bacteria easier to access into the intestine (Yao et al., 2022, Zhao et al., 2023). An increase of sialylated glycans in mucus correlated with a higher diversity of microbiome and lower inflammation and microbial translocation (Giron et al., 2020).

Recent studies found fucosylation of intestinal epithelium plays an important role in commensal bacteria composition and homeostasis (Goto et al., 2016). Loss of fucosylation resulted in intestinal inflammation and disorders like colitis and IBD (Wang et al., 2017b, Kudelka et al., 2020). Lack of fucosylation alters the diversity and composition of faecal microbiota (Rausch et al., 2011). In our study, a general downregulation of fucosylation was observed in ileum and colon in our mass spectrum results (Figure 5-9, Figure 5-11), especially in O-linked glycans in colon, where mucus and bacteria enriched. Although no significant changes in expression of fucosyltransferases were observed, a downregulation of several fucosyltransferases such as Fut1, Fut4 and Fut8 were noticed in colon compared to healthy mice (Figure 5-3, Figure 5-4). Interestingly, Fut1 and Fut2 are responsible for the intestinal epithelial fucosylation in the gut, to be specific, α-1,2-fucose on enterocytes and goblet cells is regulated by Fut2, while Fut1 regulates α-1,2-fucose on M cells located in the dome epithelium of Peyer's patches (Goto et al., 2014, Terahara et al., 2011).

To further investigate the differences in fucosylation between the epithelial layer facing luminal content and lamina propria layer where more immune responses happened, we digested the ileum and colon tissue and separated them into two

fractions and stained them with lectins and evaluated by flow cytometry. In addition, we also stained the tissue with the same lectins by immunofluorescence and quantified the mean fluorescence intensity in two layers. Interestingly, immunofluorescence results and flow cytometry results show opposite trends despite there were no statistical differences. The UEA I binding fucose, regulated by Fut1 and Fut2, is downregulated in the whole epithelial layer, but upregulated in epithelial cells in EDTA fractions in ileum. No major changes were found in colon in immunofluorescence data but increase in flow cytometry results. On the contrary, the AAL binding fucose, regulated by Fut8, is upregulated in both layers of ileum and colon in immunofluorescence data, while only upregulated in EDTA fraction but downregulated in lamina propria layer in ileum and colon of CIA mice. This could be the mucus layer residue in the gut tissue and be stained in IF results, while mucus was properly washed off in FACs data. Overall, these results collectively indicated the fucosylation of the epithelial layer in the gut is not a one-way-regulation governed by fucosyltransferases. Additionally, the bacteria in the intestine could produce fucosidase which cleaves fucose from host cells and use it as energy and therefore affecting epithelial fucosylation (Comstock et al., 2006, Goto et al., 2016).

Therefore, the regulation of fucosylation and sialylation of intestinal epithelial layer is complex and mixed with the influence of bacteria in the intestine. The mechanisms underlying the alteration of glycosylation still need further investigation. However, in our flow cytometry results, we found very interesting data that most cells in the same local area including epithelial cells, endothelial cells and fibroblasts share the same shift of glycosylation, which drove us to think about whether stromal cells which surround all effector cells could be the initial driving force for alteration of glycosylation? In fact, similar findings have been reported in the joint where loss of sialylation activated synovial fibroblasts into a proinflammatory phenotype, and created a proinflammatory microenvironment in the synovium (Wang et al., 2021). In the gut, intestinal fibroblasts play a key role in tissue homeostasis and disease, a role which has been appreciated only in recent years (Brugger et al., 2023, Wong et al., 2023). Functional heterogeneity of intestinal fibroblasts could regulate epithelial cell fate determination (Brugger et al., 2023). Whether dysregulation of glycosylation of intestinal fibroblast could

affect the behaviour of epithelial cells and therefore determine the functional changes in the gut needs more exploration.

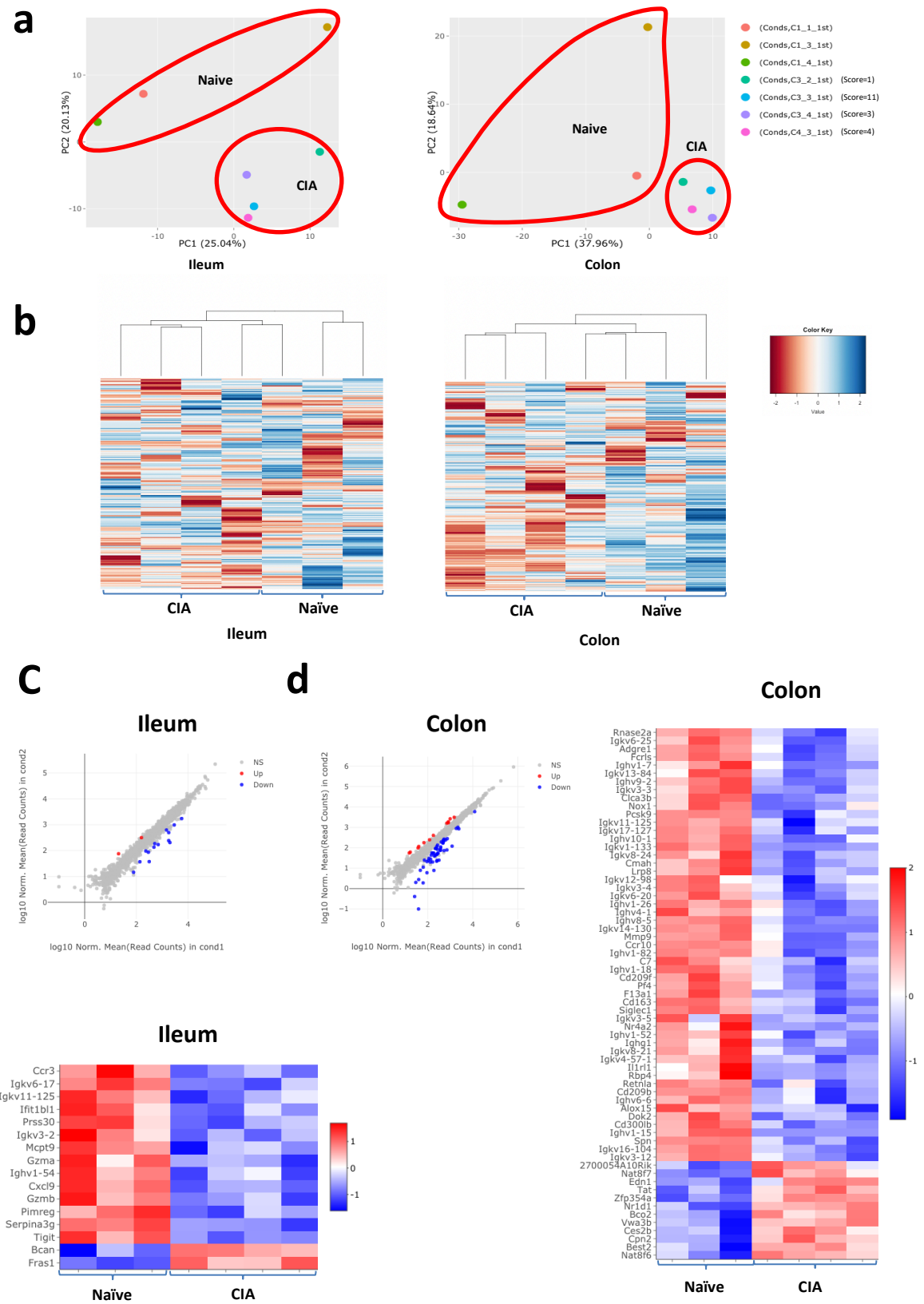

Figure 5-1 Significant genes analysis in ileum and colon of naïve and arthritic mice.

RNA was extracted from whole ileum and colon tissue from naïve and CIA mice, and subjected to bulk RNAseq (75 bp paired-end, 30 M reads). **a)** Principal component analysis (PCA) is shown that the plots circled represent CIA and the rest represent Naïve (cond: condition). **b)** Heatmap of all detected genes. **c-d)** All detected genes were plotted in a scatter plot in ileum and colon, genes that pass the threshold of padj < 0.01 and |log2Foldchange| > 1 were considered as differentially expressed genes. In CIA samples, upregulated genes are coloured in red and downregulated genes are coloured in blue. Heatmap shows the differentially expressed genes detected in scatter plot.

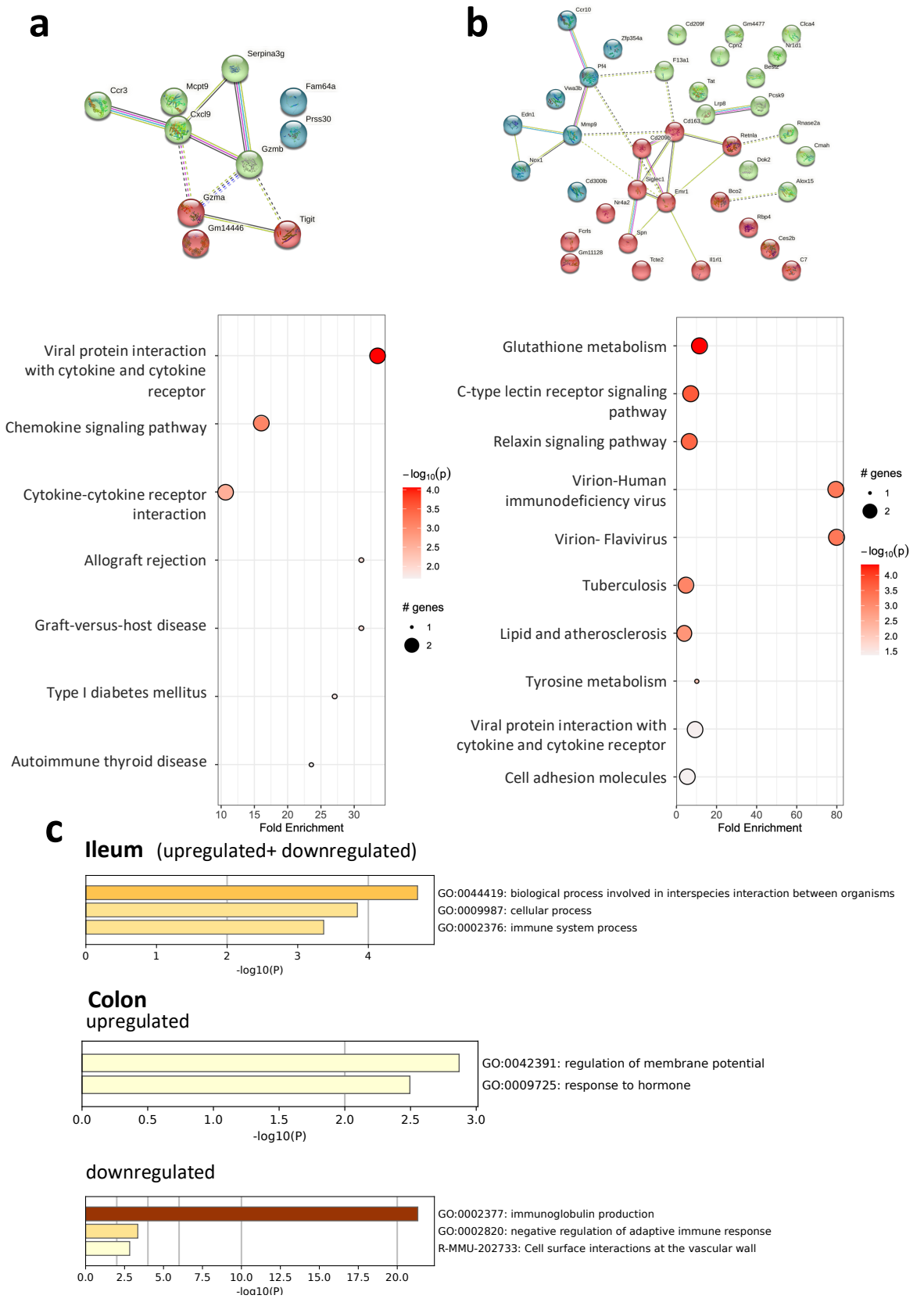

Figure 5-2 Functional enrichment and network analysis in ileum and colon of naïve and arthritic mice.

a-b) Differentially expressed genes identified in Figure 5.1c-d were for pathway enrichment analysis of the KEGG pathway in ileum (a) and colon (b). KEGG pathways were plotted in bubble charts using the PathfindR package, with fold change on the X-axis and -log10 p-value on the coloured scale. The size of the bubble is proportional to the number of differentially expressed genes. **c)** GO biological process pathways of genes identified in Figure 5.1c-d. GO-biological process pathways were plotted in bar charts using Metascape (https://metascape.org).

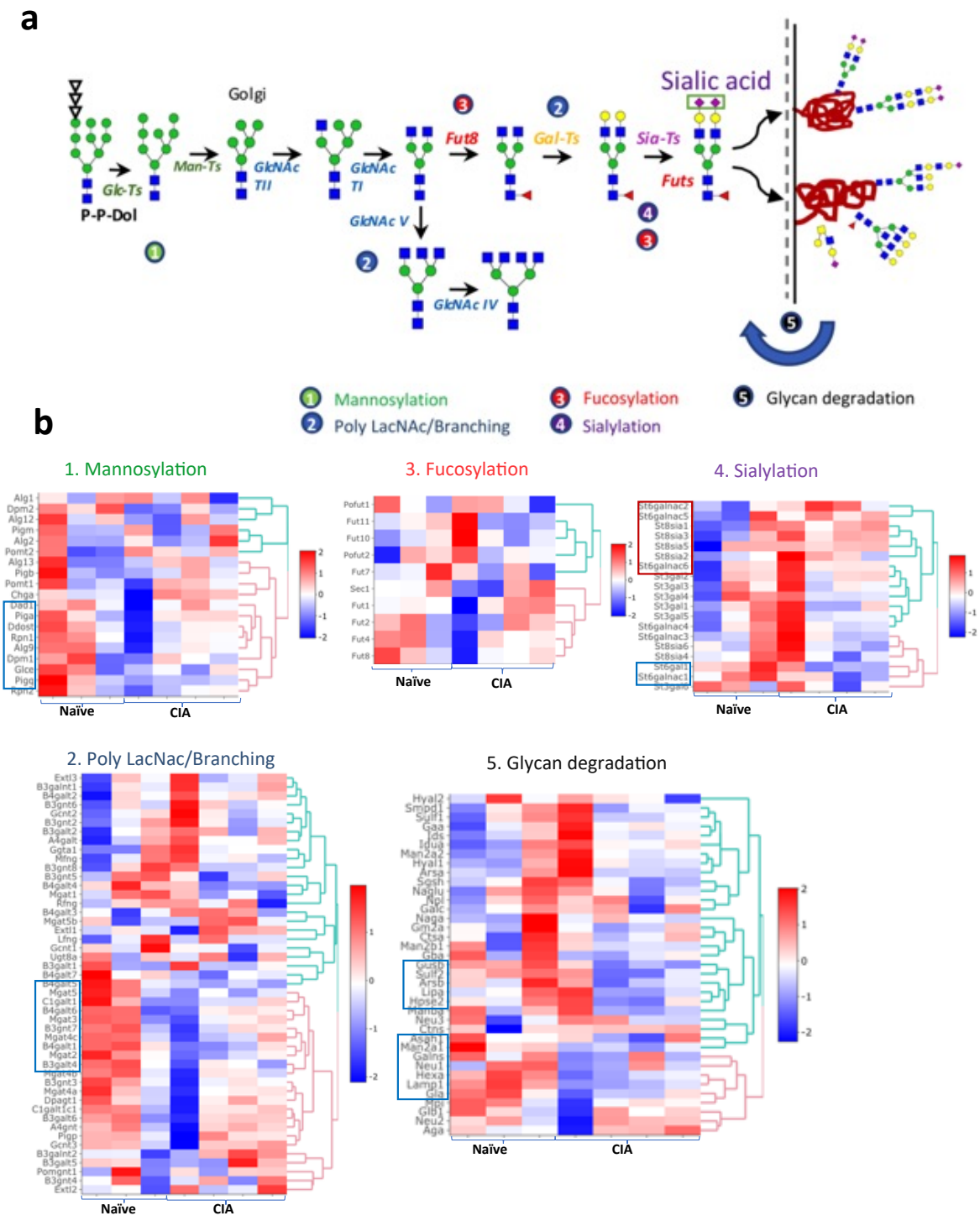

Figure 5-3 Heatmap of expression of genes involved in glycosylation pathways in the ileum.

a) Illustration of N-glycan synthesis pathway. **b)** Heatmap of expression of genes involved in glycosylation pathways in the ileum. Upregulated genes (red box) and downregulated genes (blue box) in the CIA sample compared to Naïve sample.

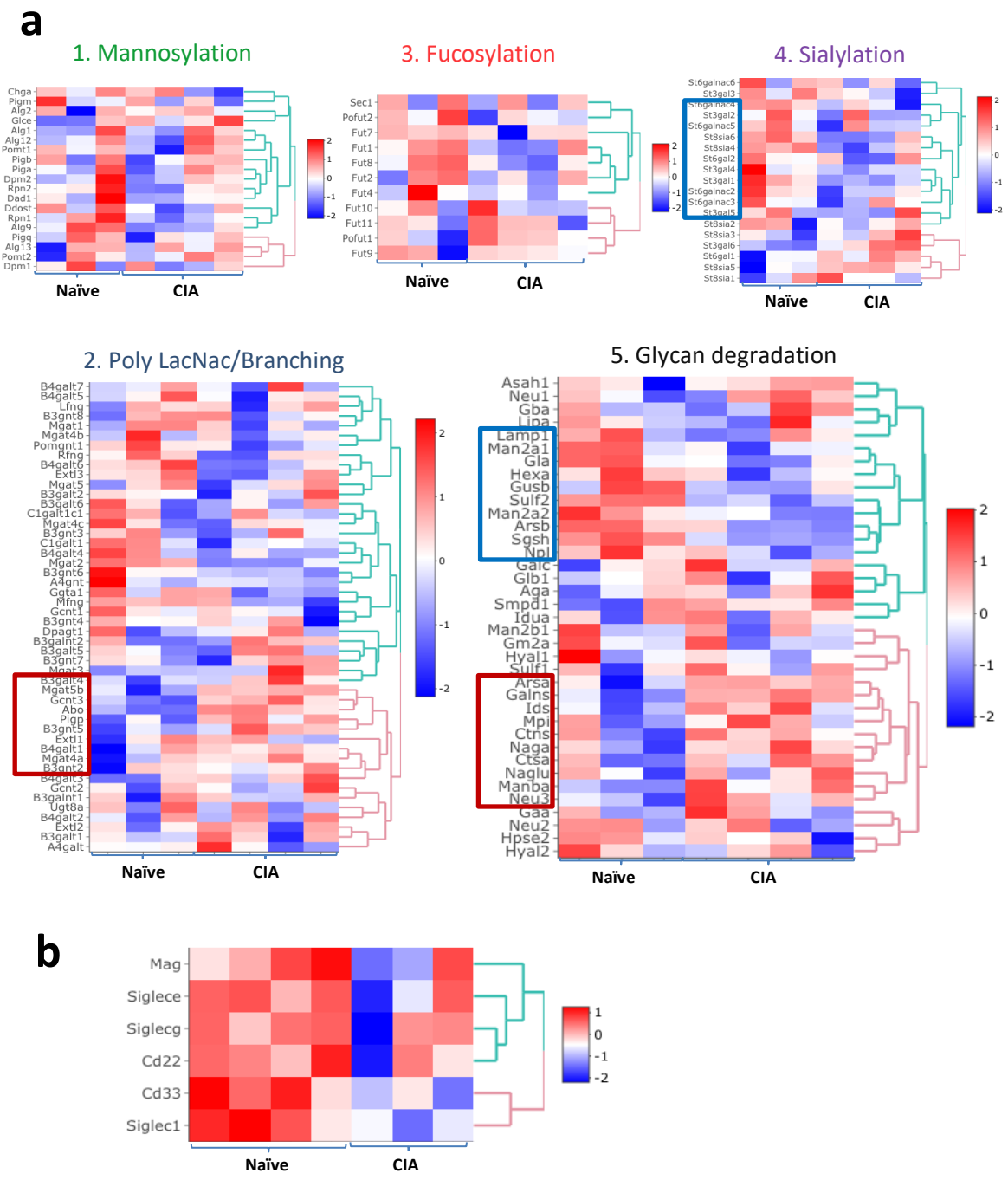

Figure 5-4 Heatmap of expression of genes involved in glycosylation pathways in the colon.

a) Heatmap of expression of genes involved in glycosylation pathways in the colon. **b)** Heatmap of expression of genes involved siglec. Upregulated genes (red box) and downregulated genes (blue box) in the CIA sample compared to Naïve sample.

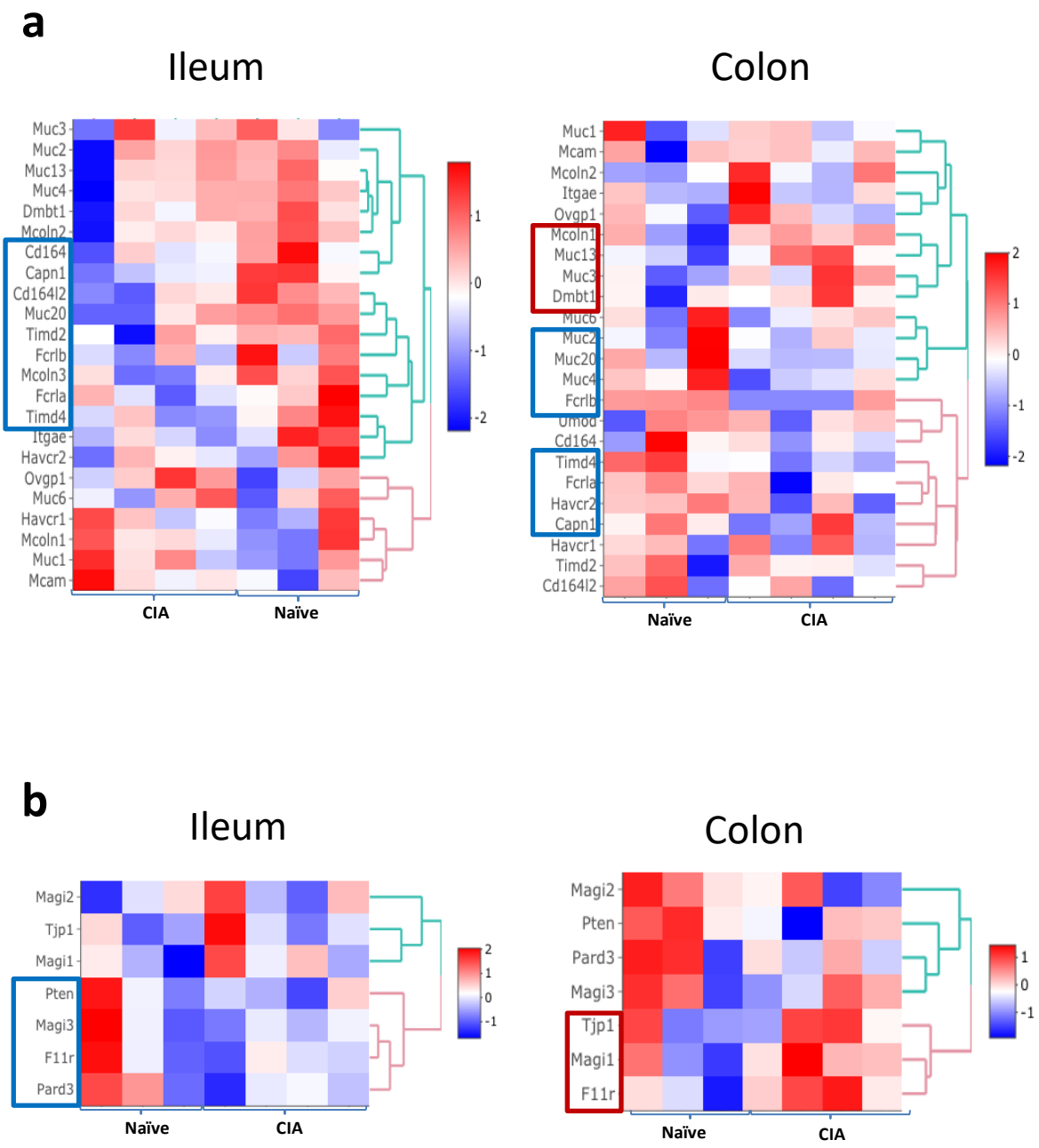

Figure 5-5 Heatmap of expression of genes involved in gut barrier in the ileum and colon.

a) Heatmap of expression of genes involved in mucins production. **b)** Heatmap of expression of genes involved tight junction. Upregulated genes (red box) and downregulated genes (blue box) in the CIA sample compared to Naïve sample.

a

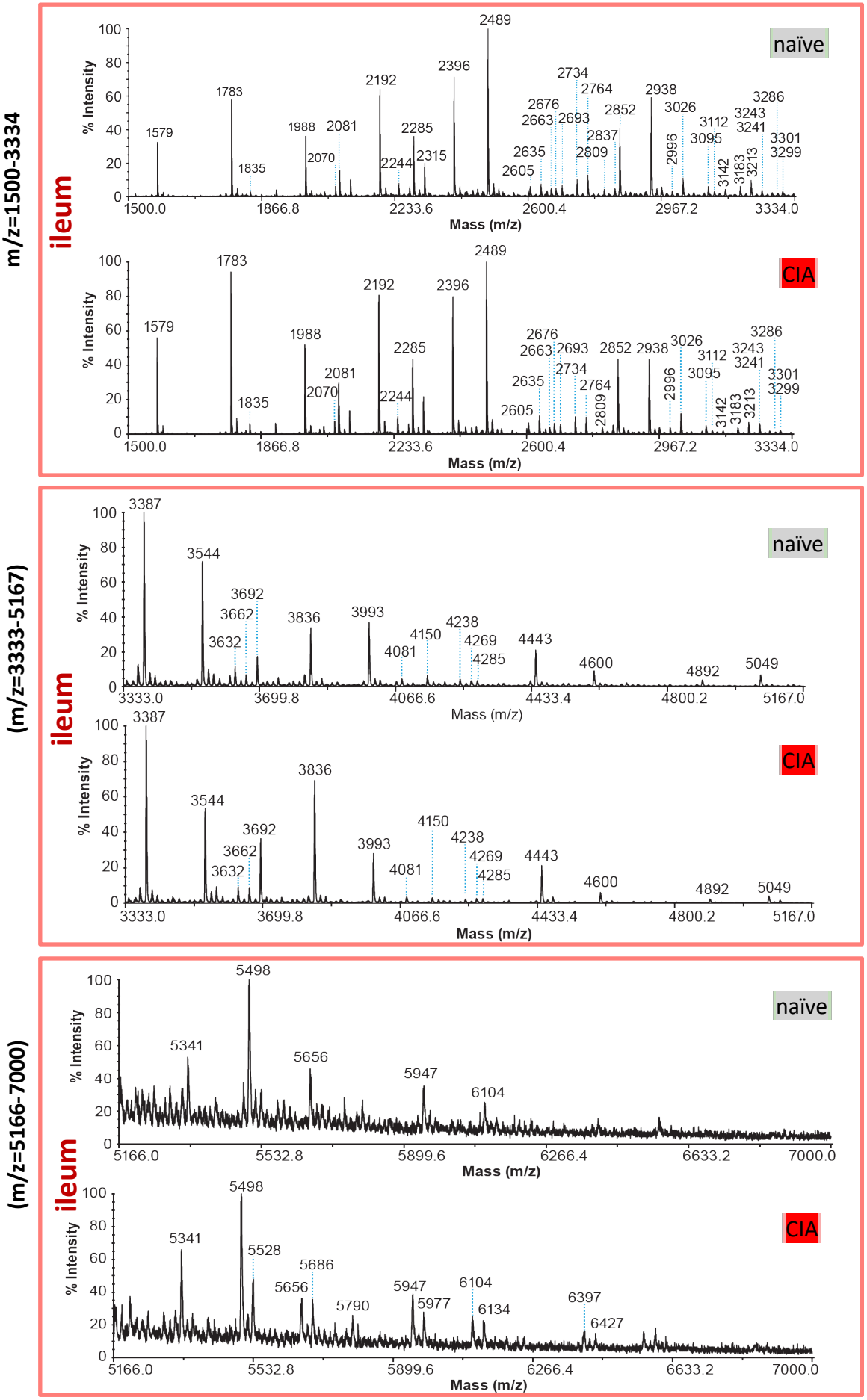
m/z=1500-3334
ileum
naïve
CIA
% Intensity
Mass (m/z)
(m/z=3333-5167)
(m/z=5166-7000)

b

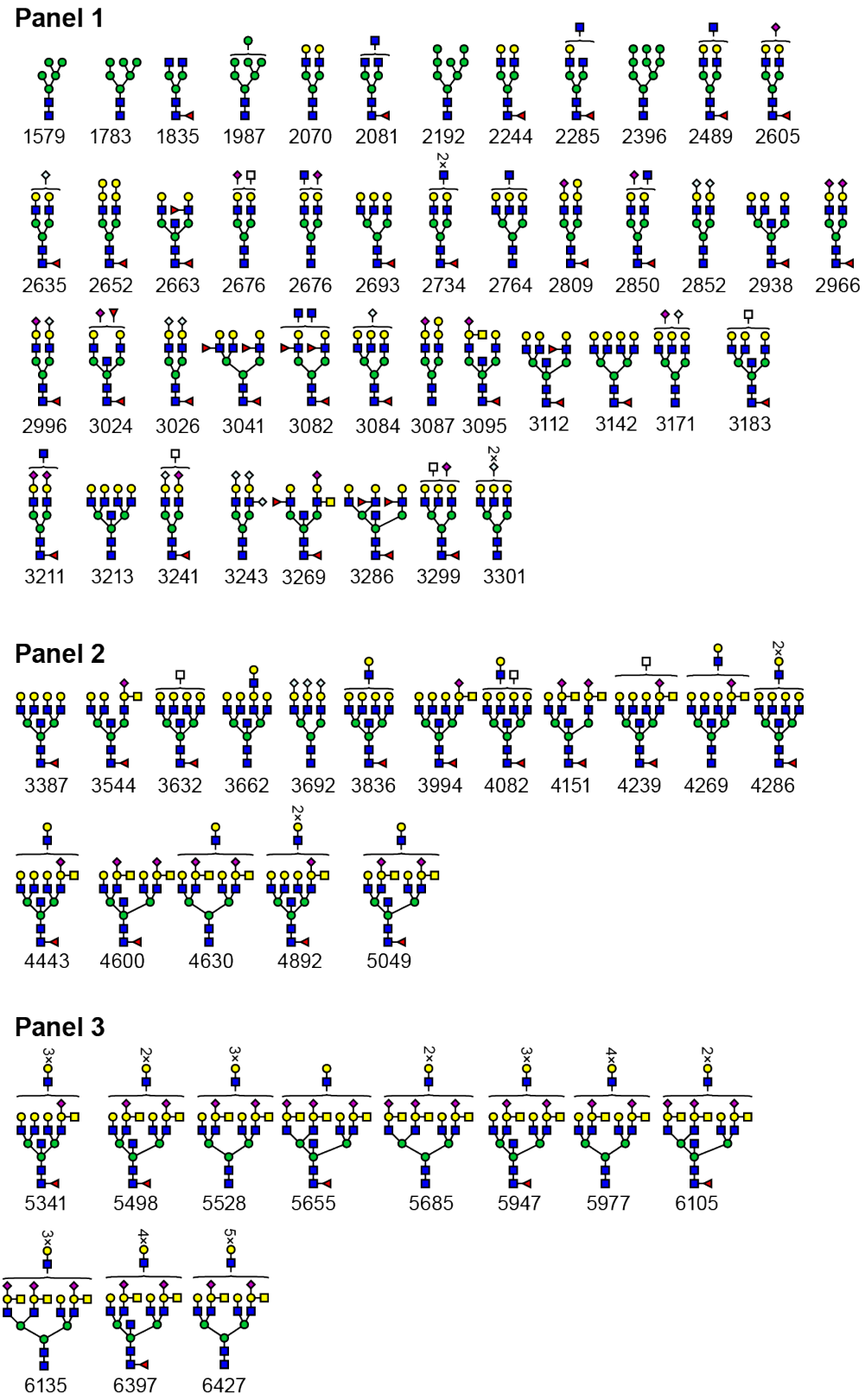

Figure 5-6 N-linked glycan profile in ileum.

Glycans were extracted from whole gut tissue when mice were culled. a) N-linked glycan profile from mass to charge (m/z) 1500 to 7000 measured by mass spectrum of ileum compared to arthritic mice (up green, naïve; down red, CIA). b) N-linked glycan structure annotated in (a)

a

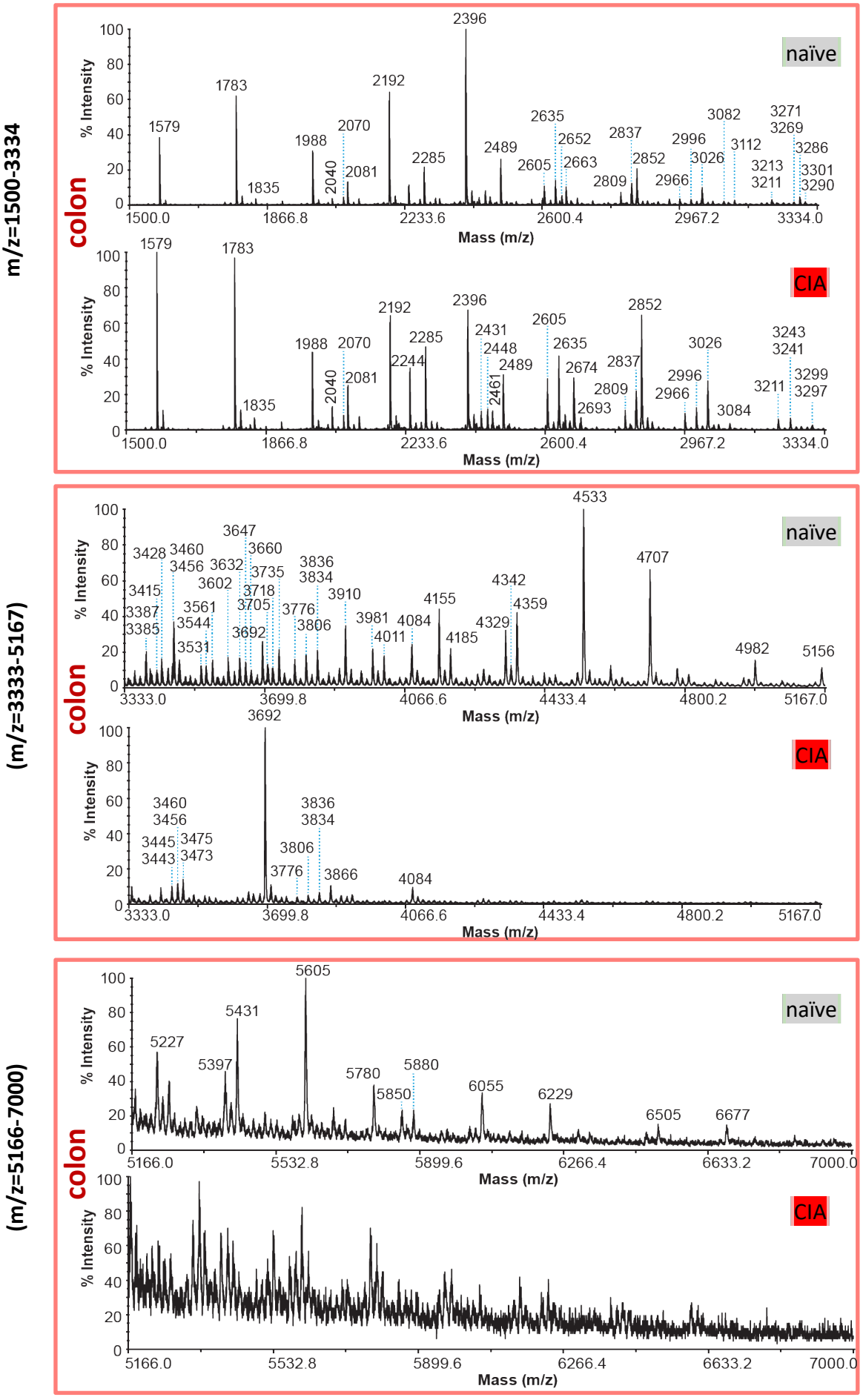
m/z=1500-3334
(m/z=3333-5167)
(m/z=5166-7000)
colon
CIA
naïve
% Intensity
Mass (m/z)

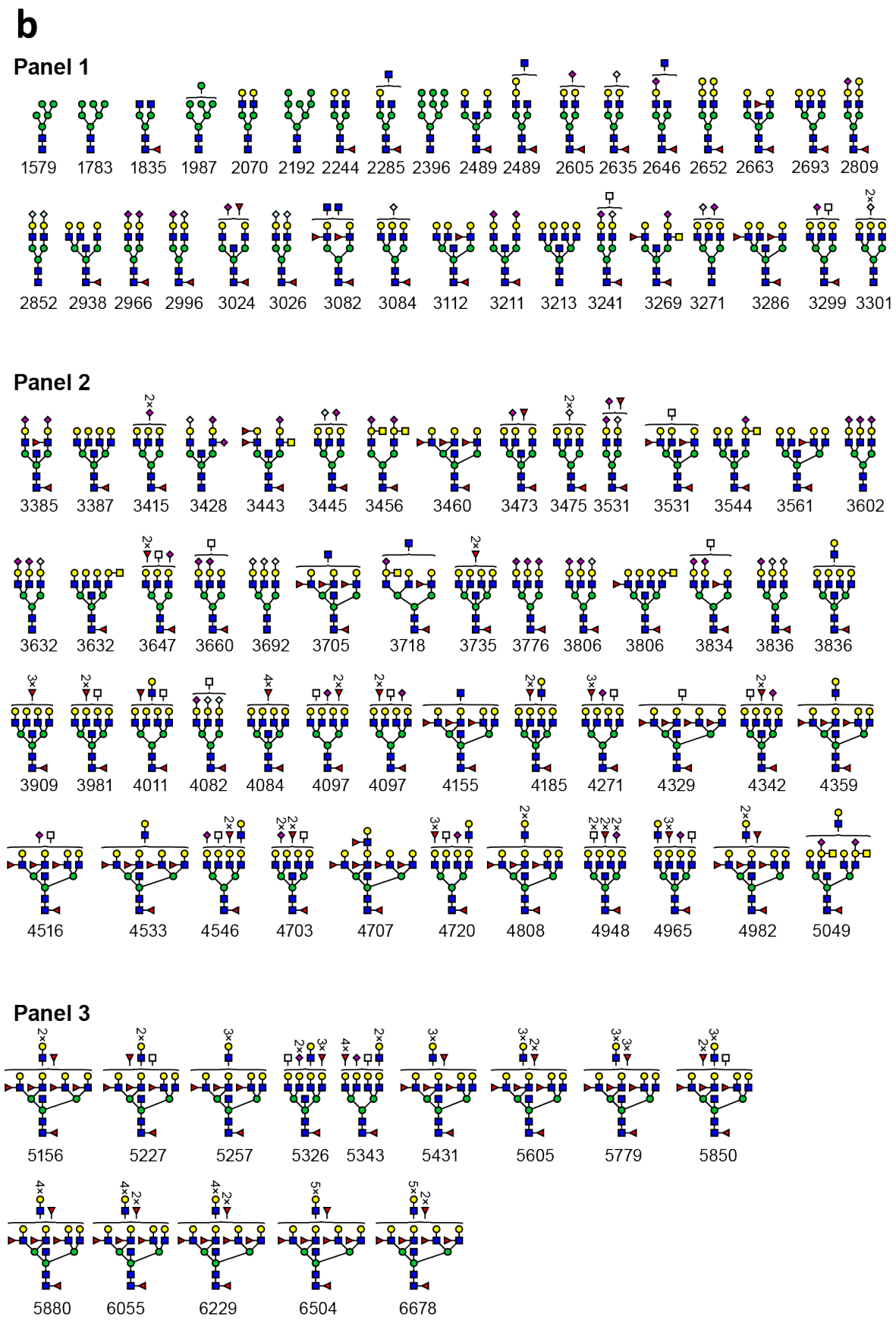

Figure 5-7 N-linked glycan profile in colon.

Glycans were extracted from whole gut tissue when mice were culled. N-linked glycan profile from mass to charge (m/z) 1500 to 7000 measured by mass spectrum of colon compared to arthritic mice (up green, naïve; down red, CIA). b) N-linked glycan structure annotated in (a).

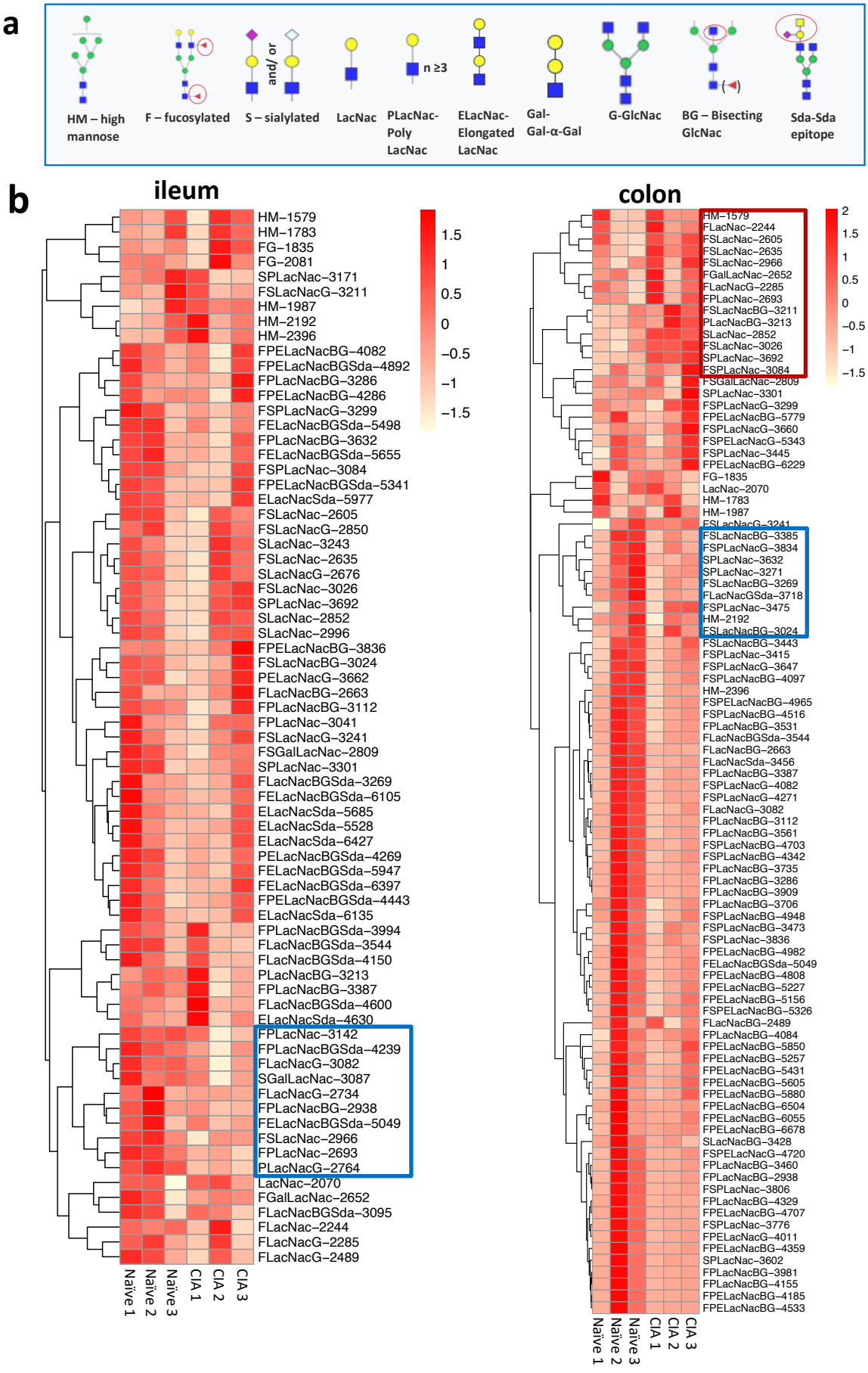
a
HM – high mannose
F – fucosylated
S – sialylated
and/ or
LacNac
PLacNac- Poly LacNac
n ≥3
ELacNac- Elongated LacNac
Gal- Gal-α-Gal
G-GlcNac
BG – Bisecting GlcNac
Sda-Sda epitope
b
ileum
HM–1579
HM–1783
FG–1835
FG–2081
SPLacNac–3171
FSLacNacG–3211
HM–1987
HM–2192
HM–2396
FPELacNacBG–4082
FPELacNacBGSda–4892
FPLacNacBG–3286
FPELacNacBG–4286
FSPLacNacG–3299
FELacNacBGSda–5498
FPLacNacBG–3632
FELacNacBGSda–5655
FSPLacNac–3084
FPELacNacBGSda–5341
ELacNacSda–5977
FSLacNac–2605
FSLacNacG–2850
SLacNac–3243
FSLacNac–2635
SLacNacG–2676
FSLacNac–3026
SPLacNac–3692
SLacNac–2852
SLacNac–2996
FPELacNacBG–3836
FSLacNacBG–3024
PELacNacG–3662
FLacNacBG–2663
FPLacNacBG–3112
FPLacNac–3041
FSLacNacG–3241
FSGalLacNac–2809
SPLacNac–3301
FLacNacBGSda–3269
FELacNacBGSda–6105
ELacNacSda–5685
ELacNacSda–5528
ELacNacSda–6427
PELacNacBGSda–4269
FELacNacBGSda–5947
FELacNacBGSda–6397
FPELacNacBGSda–4443
ELacNacSda–6135
FPLacNacBGSda–3994
FLacNacBGSda–3544
FLacNacBGSda–4150
PLacNacBG–3213
FPLacNacBG–3387
FLacNacBGSda–4600
ELacNacSda–4630
FPLacNac–3142
FPLacNacBGSda–4239
FLacNacG–3082
SGalLacNac–3087
FLacNacG–2734
FPLacNacBG–2938
FELacNacBGSda–5049
FSLacNac–2966
FPLacNac–2693
PLacNacG–2764
LacNac–2070
FGalLacNac–2652
FLacNacBGSda–3095
FLacNac–2244
FLacNacG–2285
FLacNacG–2489
1.5
1
0.5
0
–0.5
–1
–1.5
Naïve 1
Naïve 2
Naïve 3
CIA 1
CIA 2
CIA 3
colon
HM–1579
FLacNac–2244
FSLacNac–2605
FSLacNac–2635
FSLacNac–2966
FGalLacNac–2652
FLacNacG–2285
FPLacNac–2693
FSLacNacBG–3211
PLacNacBG–3213
SLacNac–2852
FSLacNac–3026
SPLacNac–3692
FSPLacNac–3084
FSGalLacNac–2809
SPLacNac–3301
FSPLacNacG–3299
FPELacNacBG–5779
FSPLacNacG–3660
FSPELacNacG–5343
FSPLacNac–3445
FPELacNacBG–6229
FG–1835
LacNac–2070
HM–1783
HM–1987
FSLacNacG–3241
FSLacNacBG–3385
FSPLacNacG–3834
SPLacNac–3632
SPLacNac–3271
FSLacNacBG–3269
FLacNacGSda–3718
FSPLacNac–3475
HM–2192
FSLacNacBG–3024
FSLacNacBG–3443
FSPLacNac–3415
FSPLacNacG–3647
FSPLacNacBG–4097
HM–2396
FSPELacNacBG–4965
FSPLacNacBG–4516
FPLacNacBG–3531
FLacNacBGSda–3544
FLacNacBG–2663
FLacNacSda–3456
FPLacNacBG–3387
FSPLacNacG–4082
FSPLacNacG–4271
FLacNacG–3082
FPLacNacBG–3112
FPLacNacBG–3561
FSPLacNacBG–4703
FSPLacNacBG–4342
FPLacNacBG–3735
FPLacNacBG–3286
FPLacNacBG–3909
FPLacNacBG–3706
FSPLacNacBG–4948
FSPLacNacBG–3473
FSPLacNac–3836
FPELacNacBG–4982
FELacNacBGSda–5049
FPELacNacBG–4808
FPELacNacBG–5227
FPELacNacBG–5156
FSPELacNacBG–5326
FLacNacBG–2489
FPLacNacBG–4084
FPELacNacBG–5850
FPELacNacBG–5257
FPELacNacBG–5431
FPELacNacBG–5605
FPELacNacBG–5880
FPELacNacBG–6504
FPELacNacBG–6055
FPELacNacBG–6678
SLacNacBG–3428
FSPELacNacG–4720
FPLacNacBG–3460
FPLacNacBG–2938
FSPLacNac–3806
FPLacNacBG–4329
FPELacNacBG–4707
FSPLacNac–3776
FPELacNacG–4011
FPELacNacBG–4359
SPLacNac–3602
FPLacNacBG–3981
FPLacNacBG–4155
FPELacNacBG–4185
FPELacNacBG–4533
2
1.5
1
0.5
0
–0.5
–1
–1.5
Naïve 1
Naïve 2
Naïve 3
CIA 1
CIA 2
CIA 3

Figure 5-8 Relative intensity of peaks in N– linked glycan profile of ileum and colon during the arthritis.

a) Abbreviation of distinct type glycan structure **b)** Heatmap of all annotated peaks in the ileum and colon of naïve and CIA mice. Lower expression (blue box) and higher expression (red box) glycan structures in the CIA mice compared to healthy mice are indicated in the box.

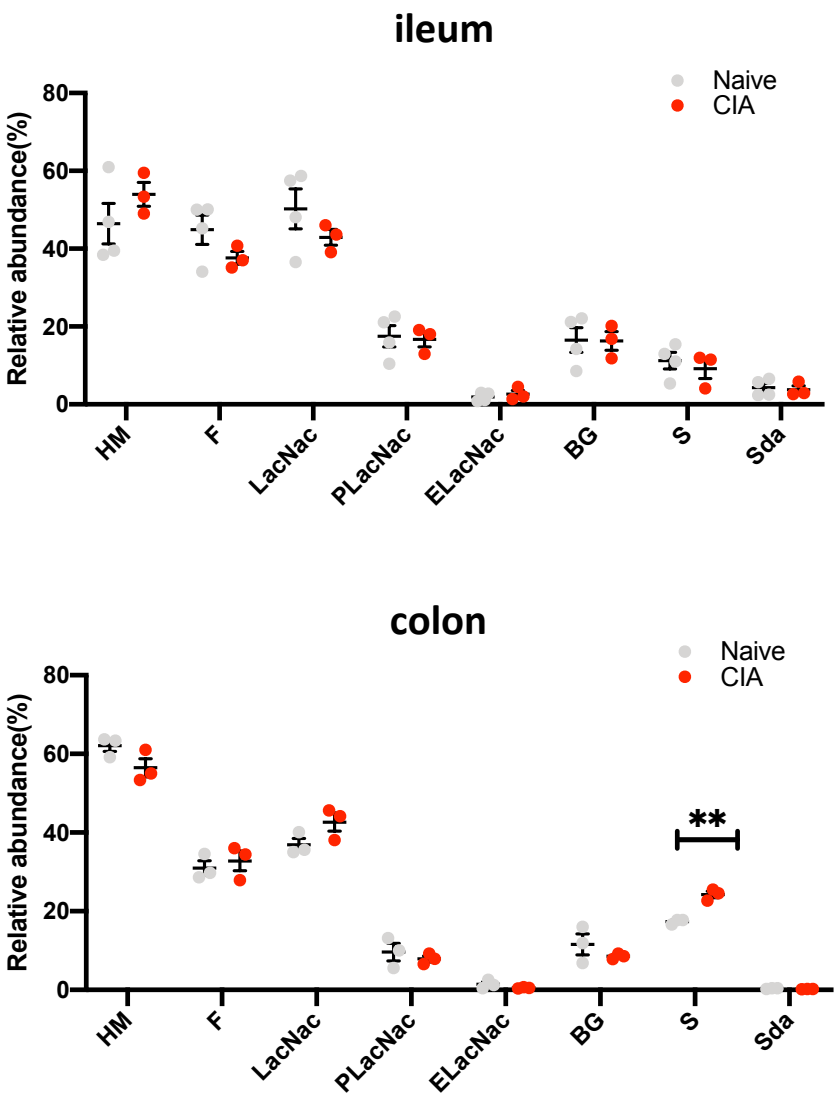

Figure 5-9 Relative abundance of types of glycan structure compared to the CIA mice.

Relative abundance of different types of glycan structure in ileum and colon of healthy mice compared to CIA mice. Statistical significance was determined using Unpaired t-test. Significance is indicated by asterisks, **p < 0.01. HM, high mannose; F, fucosylated; PLacNac, poly LacNac; ELacNac, elongated LacNac; BG, bisecting GlcNac; S, sialylated; Sda, Sda epitope.

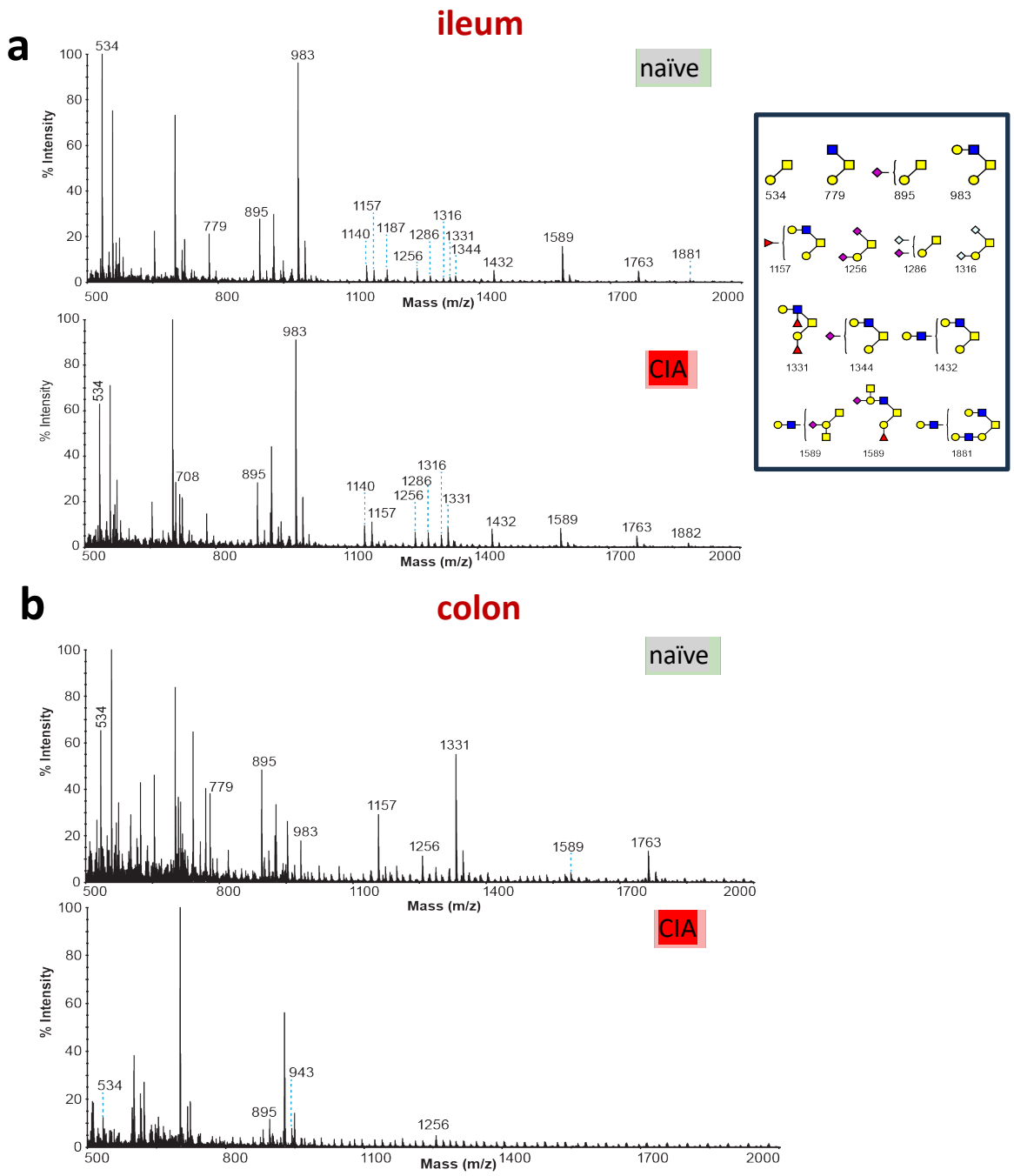

Figure 5-10 O-linked glycan profile in ileum and colon.

a-b) Glycans were extracted from whole gut tissue when mice were culled. O-linked glycan profile from mass to charge (m/z) 500 to 2000 measured by mass spectrum of ileum (a) and colon (b) compared to arthritic mice (up green, naïve; down red, CIA).

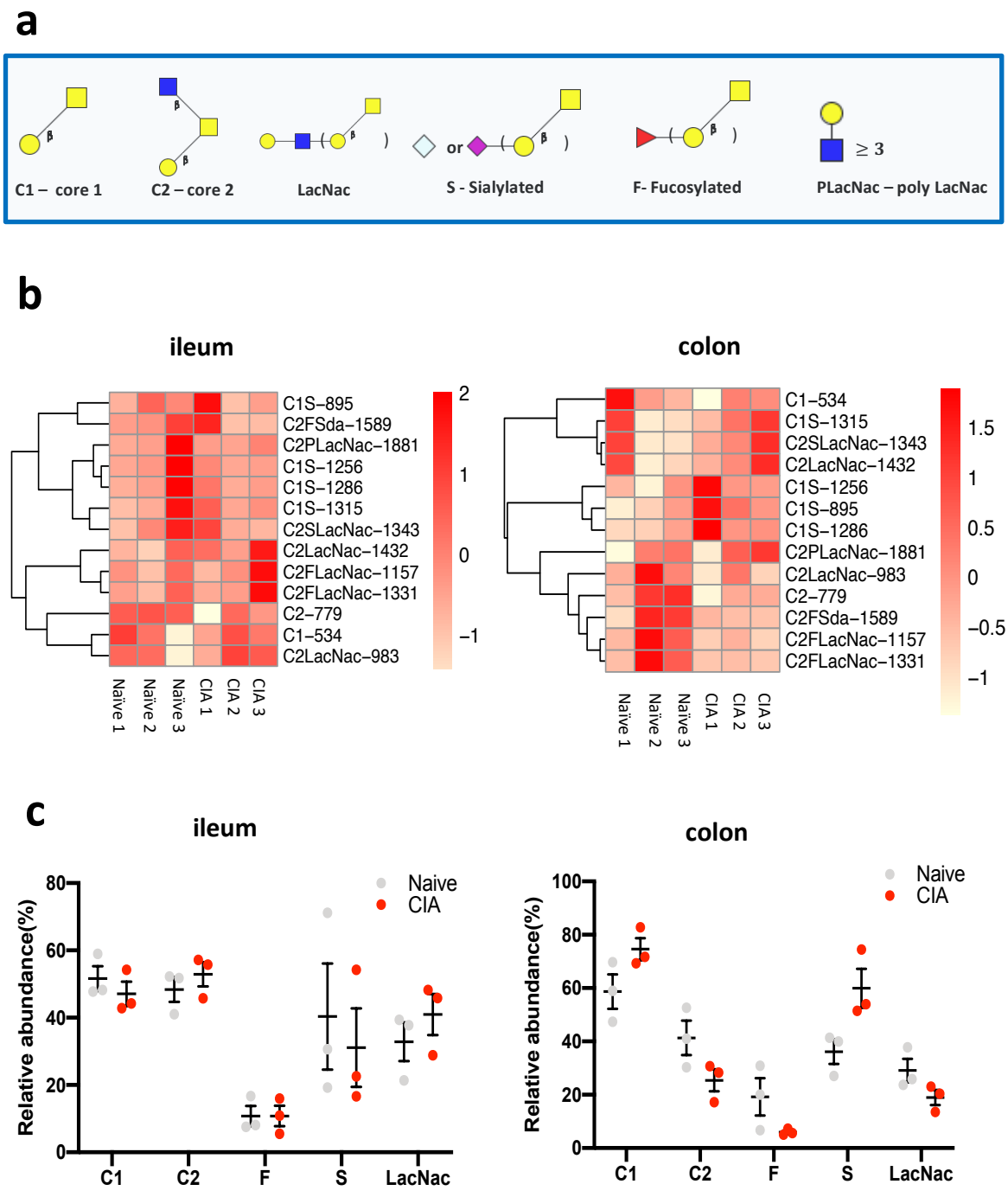

Figure 5-11 Relative abundance of O-linked glycans in ileum and colon.

a) Abbreviation of distinct structure. **b)** Heatmap of all annotated O-linked glycan peaks in the ileum and colon of naïve and CIA mice. **c)** Relative abundance of different types of glycan structure in ileum and colon of healthy mice compared to CIA mice. C1, core 1 structure; C2, core 2 structure; F, fucosylated; PLacNac, poly LacNac; S, sialylated.

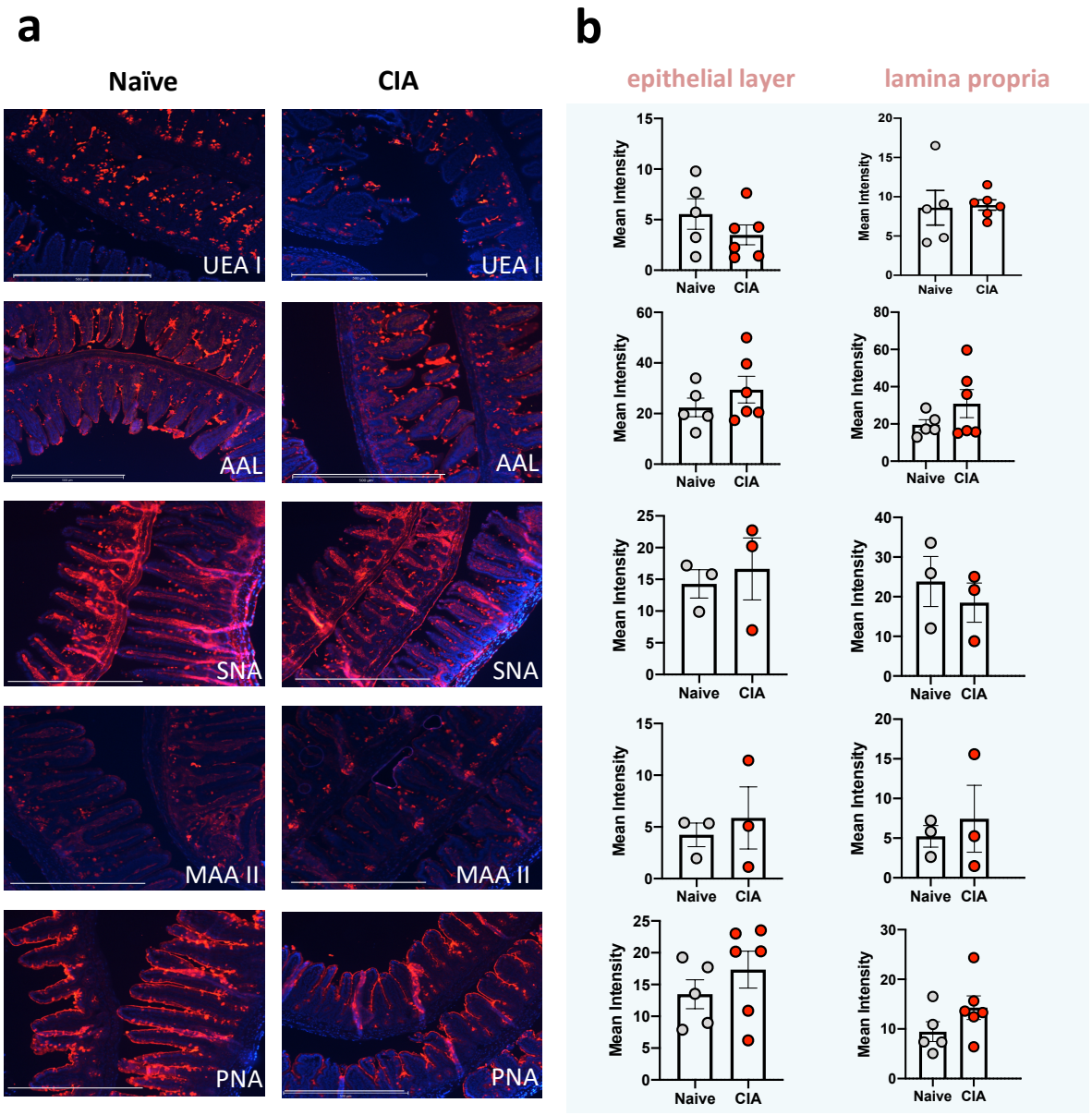

Figure 5-12 Immunofluorescence intensity quantification of lectins in ileum.

a) Representative images of UEA I, AAL, SNA, MAA II, and PNA immunofluorescence staining in ileum. DAPI (blue), lectin (red). scale bar = 500 μm. **b)** Immunofluorescence intensity quantification of lectins in epithelial layer and lamina propria layer in ileum. UEA, *Ulex Europaeus Agglutinin I*; AAL, *Aleuria aurantia lectin;* SNA, *Sambuccus nigra agglutinin*; MAA II, *Maackia aurensis lectin II*; PNA, *Peanut agglutinin.*

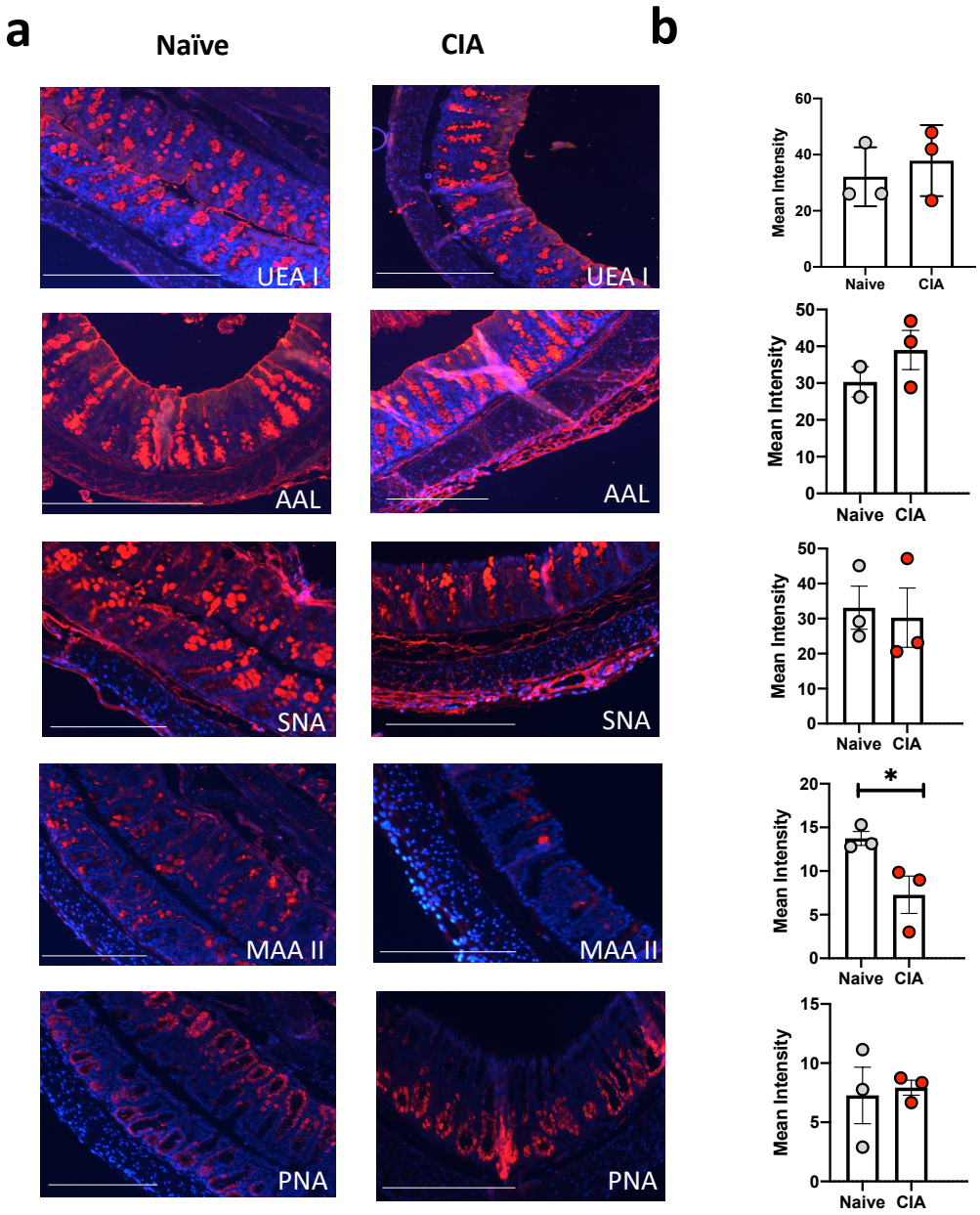

Figure 5-13 Immunofluorescence intensity quantification of lectins in colon.

a) Representative images of UEA I, AAL, SNA, MAA II, and PNA immunofluorescence staining in colon. DAPI (blue), lectin (red). scale bar = 250 µm. **b)** Immunofluorescence intensity quantification of lectins in colon. Statistical significance was determined using Unpaired t-test. Significance is indicated by asterisks, *p < 0.05. UEA I, *Ulex Europaeus Agglutinin I*; AAL, *Aleuria aurantia lectin;* SNA, *Sambuccus nigra agglutinin*; MAA II, *Maackia aurensis lectin II*; PNA, *Peanut agglutinin.*

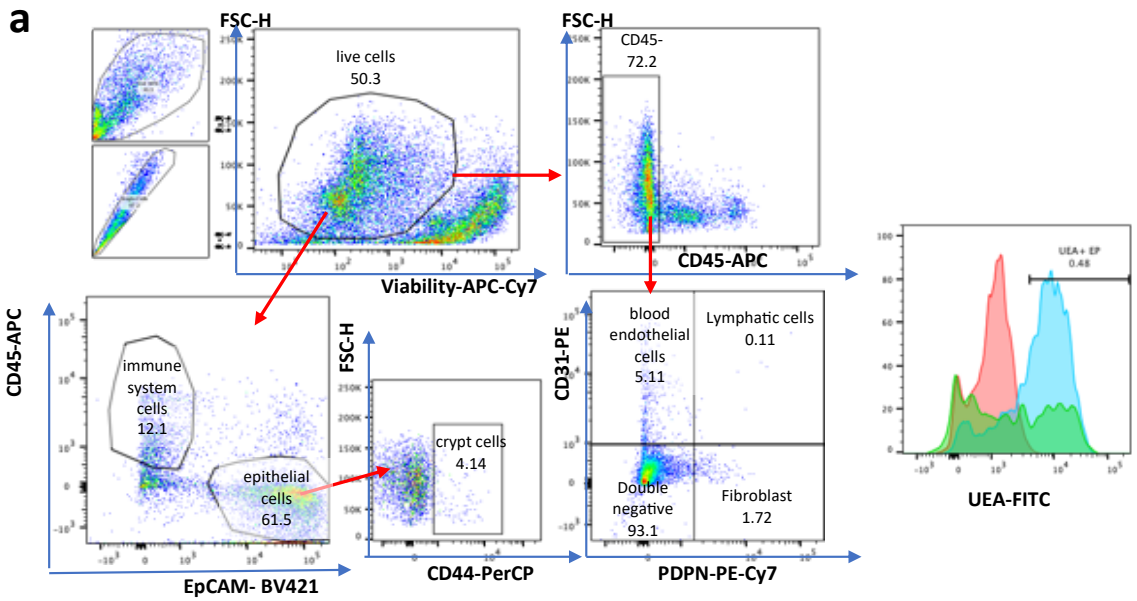

Figure 5-14 Gating strategy of different cell types in the gut.

Gut tissue were digested by collagenase and stained with antibodies. Relevant cell populations were first gated on the basis of FSC/SSC analysis and singlet and live-dead cell discrimination using Viability dye (APC-Cy7). immune system cells and epithelial cells were identified by markers CD45 (APC) and EpCAM (BV421), respectively. Non-immune cells (CD45-) were further identified: blood endothelial cells (CD31+PDPN-), lymphatic cells (CD31+PDPN+), and fibroblasts (CD31-PDPN+) . Epithelial cells can be further identified crypt cells by marker CD44 (PerCP). Lectins were stained in FITC fluorophore.

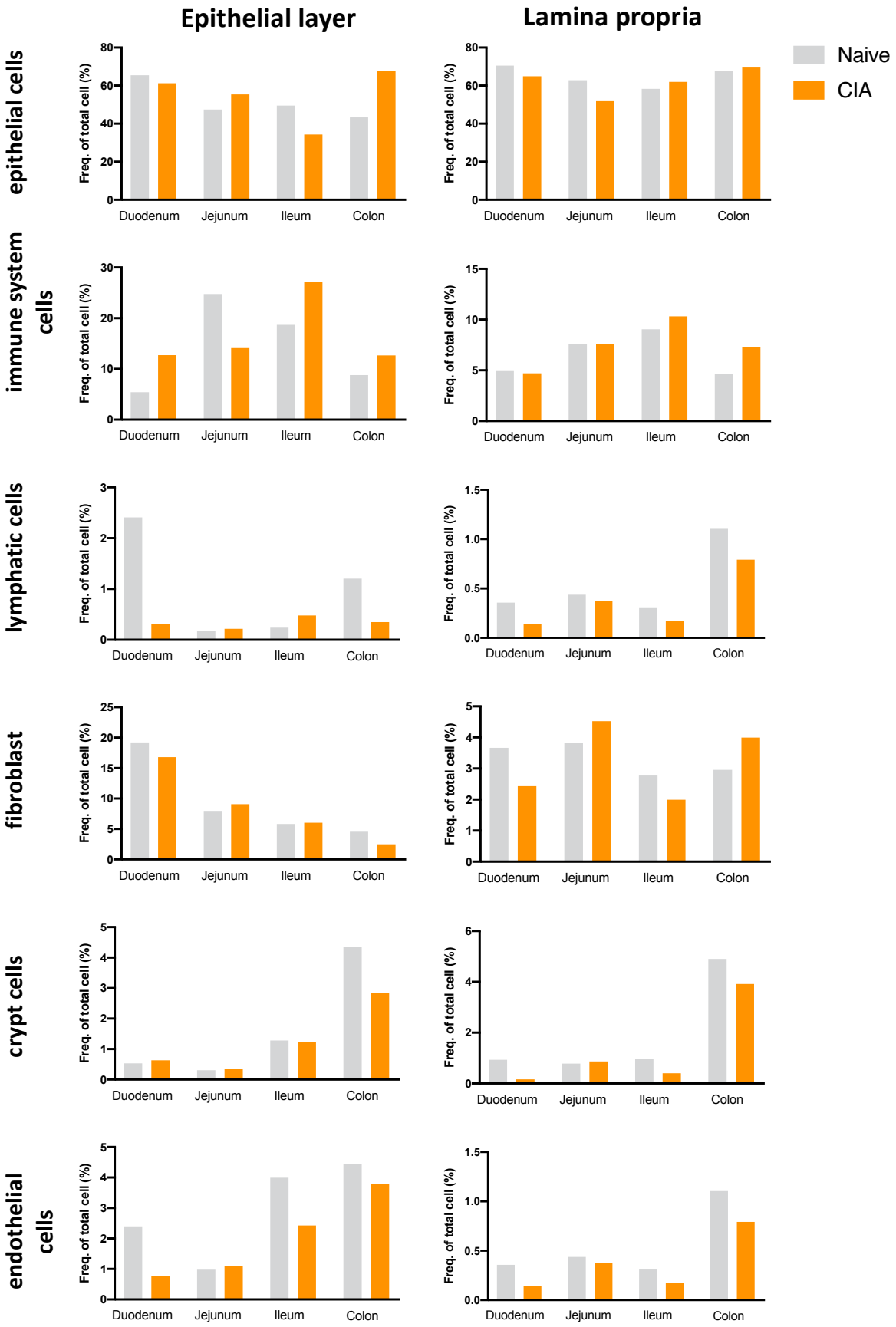

Figure 5-15 Frequency of different cell types in epithelial layer and lamina propria.

Gut tissue were digested by collagenase and stained with antibodies. Different cell types were gated by flow cytometry. Each sample were pooled from three individual mouse.

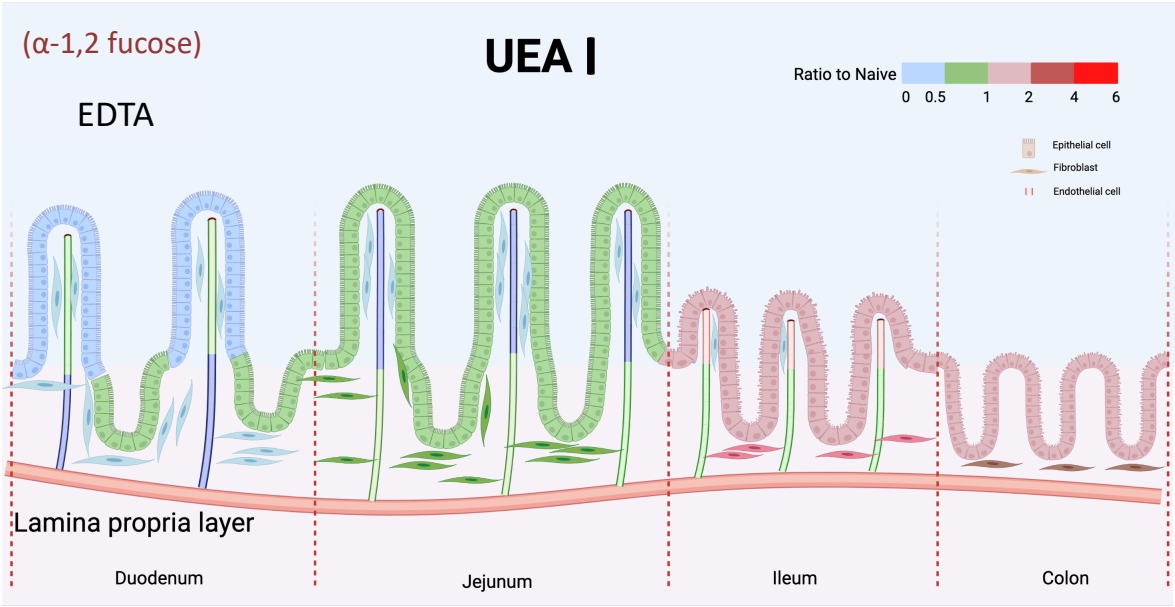

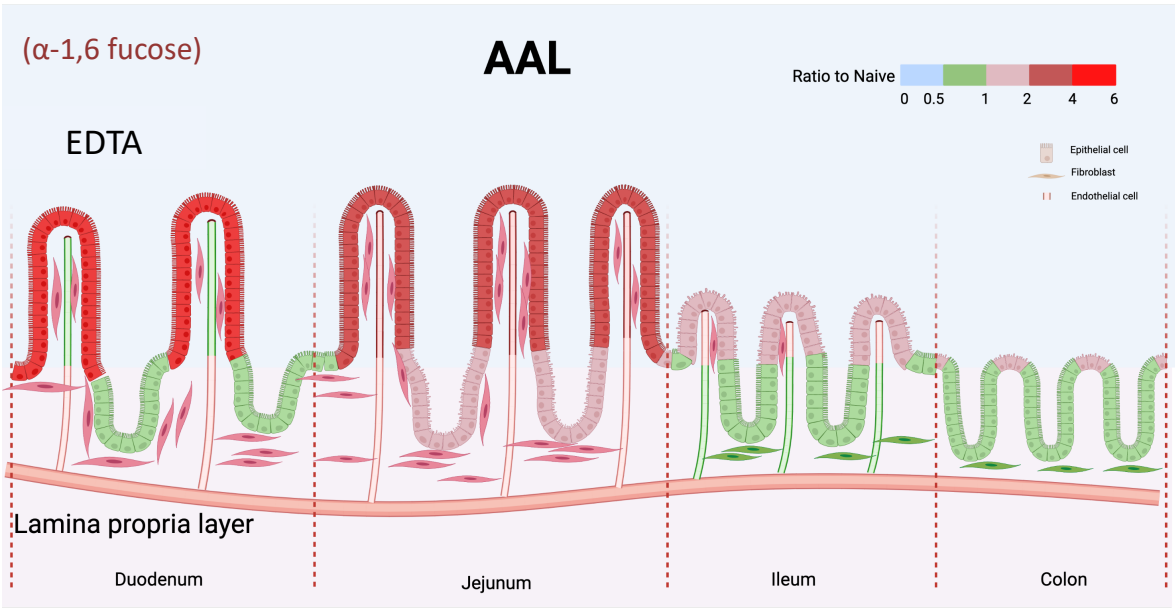

Figure 5-16 Fucosylation profile of different cell types along the intestine.

Terminal fucosylation (top) and core fucosylation (bottom) profiles of different cell types along the intestine were depicted by flow cytometry. Figure was divided into EDTA layer and lamina propria layer. downregulation of fucose expression were in blue and green; upregulation of fucose expression were in different shades of red according to ratio compared to Naïve sample. UEA, *Ulex Europaeus Agglutinin I*; AAL, *Aleuria aurantia lectin.*

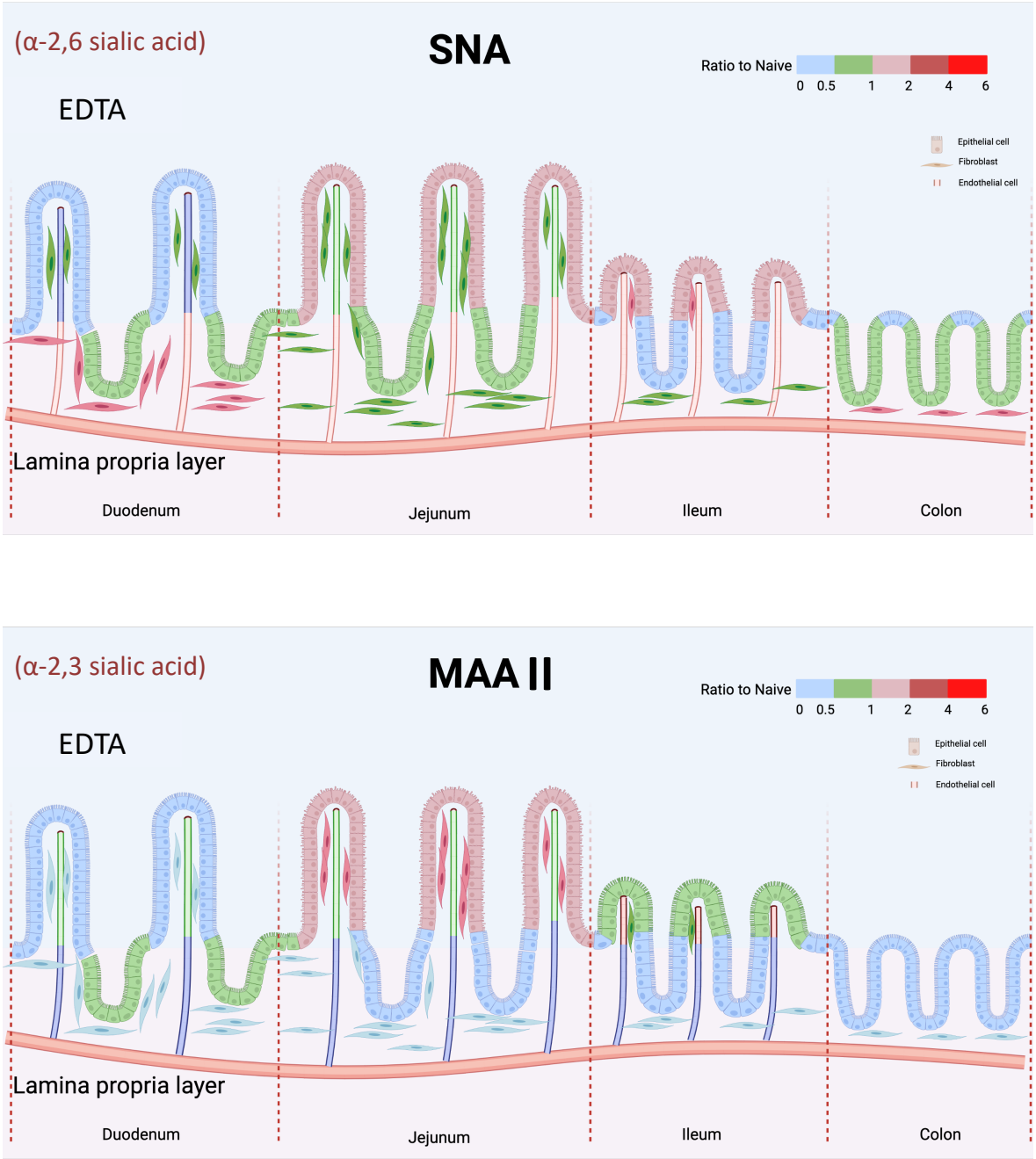

Figure 5-17 Sialylation profile of different cell types along the intestine.

α-2,6 sialylation (top) and α-2,3 sialylation (bottom) profiles of different cell types along the intestine were depicted by flow cytometry. Figure was divided into EDTA layer and lamina propria layer. downregulation of fucose expression were in blue and green; upregulation of fucose expression were in different shades of red according to ratio compared to Naïve sample. SNA, *Sambuccus nigra agglutinin*; MAA II, *Maackia aurensis lectin II*.

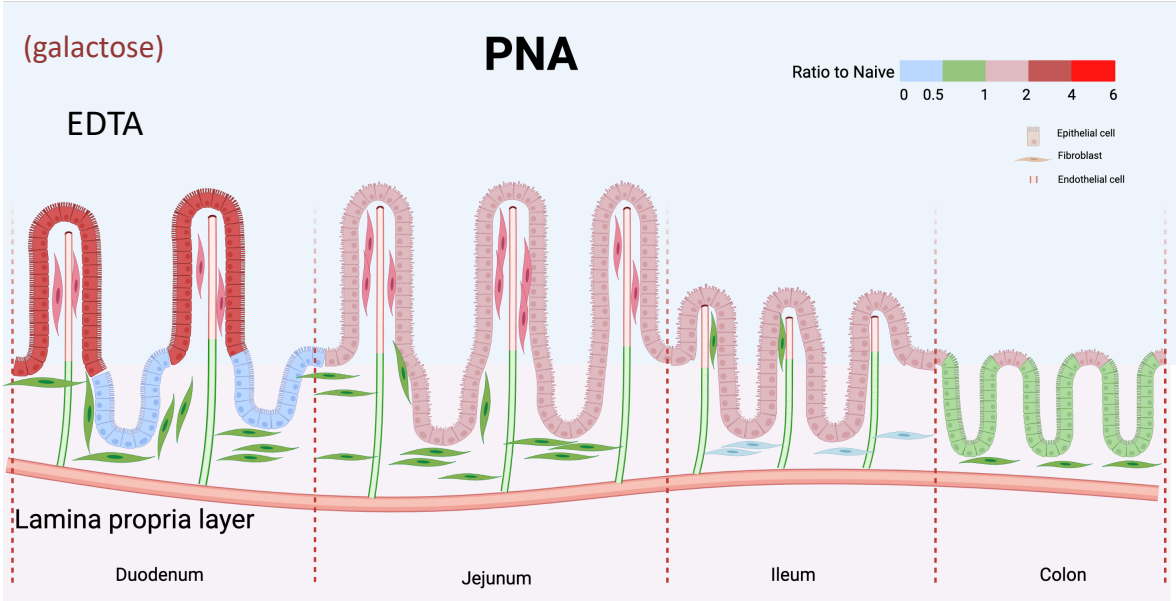

Figure 5-18 Galactose expression of different cell types along the intestine.

Galactose expression of different cell types along the intestine were depicted by flow cytometry. Figure was divided into EDTA layer and lamina propria layer. downregulation of fucose expression were in blue and green; upregulation of fucose expression were in different shades of red according to ratio compared to Naïve sample. PNA, *Peanut agglutinin.*

Chapter 6 Crosstalk between intestinal fibroblast and epithelial layer

6.1 Introduction

Intestinal fibroblasts (FB) are a cellular network of cells existing under the basal lamina of the epithelium. The importance of Intestinal fibroblasts in maintaining epithelial and immune homeostasis in the intestine has been widely recognised in recent years (Chalkidi et al., 2022, Brugger et al., 2023). FBs are major producers of extracellular matrix proteins like collagen, fibronectin, and proteoglycans that provide structure to the mucosa (Furuya et al., 2007, Roulis et al., 2016). They also play an important role in epithelial and endothelial homeostasis (Degirmenci et al., 2018, Wu et al., 2021, Thomson et al., 2018, Fawkner-Corbett et al., 2021, Stzepourginski et al., 2017). In addition, FBs could affect immune cell localization and function (Powell et al., 2011, Beswick et al., 2014).

Several functional subsets of intestinal fibroblasts have been recently identified, characterised by distinct expression of PDGFRa, (PDGFRα^{hi} FB and PDGFRα^{lo}CD34^{hi} FB) that could be further separated by expression of CD81, CD90 and CD34 and PDGFRα^{lo}CD34^{lo} FB (Pærregaard et al., 2021). They are located in different anatomical areas and they show distinct functions. CD34+ FB were located around crypts and in the submucosa but excluded from the villus core. They are producers of Wnt2b, Gremlin1, and R-spondin1 and play an important role in response to intestinal injury by upregulating Gremlin1 and R-spondin1 (Stzepourginski et al., 2017). They are also involved in gut immunity and tissue repair by secreting IL-7, Ccl2, Ptgs2, and Amphiregulin (Stzepourginski et al., 2017). CD81+FB, also called trophocytes (Mccarthy et al., 2020a), are located around the vessels, close to and within the submucosa, with some located close to crypts (Figure 6-1a) (Pærregaard et al., 2021). They are responsible for secreting WNTs (Wnt2 and Wnt2b), and BMP antagonist Gremlin1(Mccarthy et al., 2020b, Hong et al., 2020). In addition, they also express the atypical chemokine receptor Ackr4, which can regulate endothelial cell function (Thomson et al., 2018). PDGFRα+CD34-FB are located directly underlying the epithelium and within the villus core (Pærregaard et al., 2021). They are the main producer of BMPs, especially Bmp3 and Bmp7, which are uniquely expressed by PDGFRα^{hi} FB (Mccarthy et al., 2020b). They play an important role in epithelial cell differentiation due to their location and BMPs

expression (Kosinski et al., 2007, Beumer et al., 2022). However, there is still some controversy on the number, classification, terminology, and functional properties of these subsets. Dysfunction of intestinal fibroblast could result in dysbiosis of the intestine, causing many diseases like IBD and intestinal fibrosis (Roulis et al., 2016, Furuya et al., 2007).

Despite recent progress in recognizing the importance of fibroblasts in intestinal homeostasis, how individual fibroblast subsets can regulate intestinal homeostasis and the molecular mechanisms controlling the crosstalk between fibroblasts and the associated epithelial layer remain elusive. Moreover, the understanding of the role of distinct intestinal fibroblast subsets during RA is very limited. In Chapter 5, it was found that the changes in glycosylation of cells surrounding the fibroblasts have a similar profile to fibroblasts Suggesting that intestinal fibroblasts send signals to the epithelial layer via changes of glycans on their surface. In fact, similar findings in the joint have been reported (Wang et al., 2021). This has led to the hypothesis that the changes in FB glycosylation during RA affect the communication with IECs, ultimately disrupting intestinal integrity and homeostasis.

Therefore, in this chapter, FB subsets and their responses were investigated during experimental arthritis, analysing numbers, inflammatory responses and glycosylation profile. In addition, the transcriptome of intestinal fibroblasts and epithelial cells was analysed in naïve and CIA mice to check the crosstalk between these two cell types during pathogenesis. Finally, to verify the hypothesis, in vitro three-dimensional (3D) gut culture systems were developed to validate the in vivo findings regarding fibroblast function and immunity in the gut.

6.2 Results

6.2.1 PDGFRα^{hi} intestinal fibroblasts are expanded in arthritis.

To understand the role of intestinal fibroblasts during arthritis progression, the cell numbers of each subset of intestinal fibroblasts in healthy and arthritic mice were assessed by flow cytometry. Four main subsets were selected in this study, including PDGFRα^{hi} FB, PDGFRα^{lo}CD34^{hi} FB, that were subsetted into more specialised groups by their expression of CD81 and CD90 (CD81+CD90+ FB), and

PDGFRα^{lo}CD34^{lo} FB, based on the research done by Pærregaard's team (Figure 6-1) (Pærregaard et al., 2021). Podoplanin (PDPN) was used to stain general stromal cells. The data show more PDPN+ cells in the colon compared to the ileum and these are mainly PDGFRα^{lo}CD34^{hi} FB, with more CD90+FB found in the colon compared to ileum (Figure 6-1b). This result is consistent with previous findings that colonic CD90+ crypt fibroblasts are enriched in the colon, to support epithelial cell growth (Karpus et al., 2019). Looking at the composition of all PDPN+ cells in the ileum and colon, similar findings were noticed in that CD90+ FB were enriched in the colon (Figure 6-2a).

Interestingly, a significant expansion of PDGFRα^{hi} FB in both ileum and colon was noticed during CIA (Figure 6-2b). The proportion of other subsets of intestinal fibroblast was at a similar level between naïve and CIA group. Next, the fucosylation, sialylation and galactose expression was examined (similarly to the previous chapter) of each intestinal fibroblast subset. Surprisingly, the terminal fucose which UEA I binds to was significantly downregulated of PDGFRα^{hi} FB subset in the ileum (Figure 6-3b), which might correlate with the variable downregulation of UEA I staining in the ileum of individual CIA mice (Figure 3-18, Figure 5-12). By contrast, no significant differences in core fucosylation among each subset were observed in CIA mice. In addition, galactose expression was decreased in PDGFRα^{hi} FB and PDGFRα^{lo} CD34^{lo} FB, although the data did not reach statistical significance (Figure 6-3b). The intestinal fibroblast subsets exhibited a similar level of sialylation (both SNA and MAA II binding) in CIA mice compared to Naïve control. Overall, an expansion of PDGFRα^{hi} intestinal fibroblast was noticed in both ileum and colon during RA, and a reduction of terminal fucose expression of this subset was observed at the meanwhile.

6.2.2 Epithelial cell sequencing results during CIA

Because PDGFRα^{hi} intestinal fibroblasts were specifically expanded in arthritis, it was decided to further explore their functional role during arthritis. It was hypothesised that this FB subset could be responsible for the damage in the epithelial layer observed in the gut of arthritic mice. Therefore, PDGFRα^{hi} intestinal fibroblast and epithelial cells (EpCAM+CD45-) in the ileum and colon of healthy and arthritic mice were isolated by FACS, with the goal of performing bulk RNA sequencing of these two populations. Unfortunately, the RNA samples of the

PDGFRα^{hi} intestinal fibroblast subset did not pass the quality control due to the limited cell numbers obtained. However, the experiment was successful regarding the epithelial cells.

Firstly, a functional analysis of the epithelial cells during CIA was addressed by identifying genes that were significantly changed (fold change >2, adj p < 0.01) in the ileum and colon of arthritic mice. PCA plot shows that only the colon samples clustered by condition, suggesting that the colon epithelium is more susceptible to changes resulting from the induction of arthritis than its counterparts in the small intestine. However, Unsupervised hierarchical clustering of transcriptomic data did not exhibit a clear pattern of condition in either location (Figure 6-4a-b), perhaps reflecting the effects of environmental factors in this tissue among individual mice. Due to this heterogeneity, in the ileum, only two genes Per2 and Hsph1 were significantly downregulated in CIA mice compared to healthy mice. Interestingly, Per2 plays a crucial role in the regulation of circadian rhythms and Hsph1 encodes a protein known as heat shock protein family H member 1 (HSPH1), which is involved in cellular stress responses, protein folding and maintenance of cellular homeostasis (Figure 6-4c-d). In the colon, more genes were significantly changed in arthritic mice. Among the upregulated genes, genes associated with oxygen transport and metabolism of substances such as drugs and xenobiotics were found (Figure 6-4d). Similarly to the ileum, Hsph1 was downregulated, and additional genes involved in membrane and cellular transportation (Rab37, Slco3a1, Cacna2d4) and cellular interactions (Ccn3, sdk2, Ffar4, Lamb1) were also downregulated in the arthritic mice, suggesting their dysregulation might happen in inflammatory colon of CIA mice. Expression of Tff2, which is involved in protecting and repairing the mucous lining of the gastrointestinal tract was reduced in CIA mice, consistent with the mucus barrier in the colon of arthritic mice being impaired. Interstingly, Cmah, which is involved in the biosynthesis of sialic acid (Neu5Gc) was downregulated in the colonic epithelial cells, as in the whole colon tissue (Figure 5-1d). Interestingly, downregulation of genes associated with cilia and flagella (Cfap45 and Dnah10) was observed in the colon. Cilia and flagella are more commonly found in tissues and cells where they serve specific motility and sensory functions like respiratory cilia, inner ear cilia, and sperm flagellum. Cilia is important for regulation in terms of cell signalling and signal transduction (Wheway et al., 2018, Wachten et al., 2021).

The transcriptomic data shows colonic epithelial cells are more susceptible during arthritis, so we performed subsequent functional enrichment analysis of differentially expressed genes in the colonic epithelial cells. Data reveals the immunological responses involved in protein processing in the endoplasmic reticulum, antigen processing and presentation, and IL-17 signalling pathways are modulated in colonic epithelial cells of arthritic mice (Figure 6-5a-b). GO biological process pathways results show negative regulation of biological process, cellular process, localization and response to stimulus are changed in colonic epithelial cells during CIA (Figure 6-5c).

Overall, the transcriptomic analysis confirms the dysregulation of epithelial cells during arthritis, especially in the colon, this dysregulation could related to dysbiosis and impaired integrity in the gut, ultimately resulting in inflammation and onset of CIA. However, the DE genes and fold enrichment were limited, whilst the damage in the gut during CIA was dramatic. There might be other pathways involving the dysregulation of the epithelial cells. As described in the general introduction and results in previous chapters, glycans in the epithelium could be involved in the damage and changes, because even if the expression of glycosyltransferases is not (much) modulated, a lot of small changes could have a very big impact on the glycan expression, and these molecules are important in mucus barrier integrity (Goto et al., 2016).

In line with this, following the unsupervised analysis, we performed expression of glycosyltransferases and glycosidases to investigate the regulation of glycan biosynthetic pathways in ileal and colonic epithelial cells of healthy and arthritic mice. Results in ileal epithelial cells show no significant differences between healthy mice and CIA mice (Figure 6-6). By contrast, colonic epithelial cells exhibited distinct changes during inflammatory arthritis, including downregulation of mannosylation, poly LacNac/branching, fucosylation (except Fut7) and glycan degradation (except Ctns and Neu3) and upregulation of sialylation and some genes (Fut7, Ctns and Neu3) (Figure 6-7a). Galectins are important in tissue repair and regeneration processes. They can promote cell proliferation and tissue remodelling, which is vital for wound healing and tissue regeneration after injury. Since colonic epithelial cells are more susceptible, their galectin expression was checked and increased expression of Lgals8 and Lgals7 and decreased expression of Lgals9 in colonic epithelial cells regarding of galectin expression, was noted

(Figure 6-7b). Furthermore, in terms of pathways involved in regulation of gut barrier integrity, genes like Muc2 and Muc4 were downregulated in both ileal and colonic epithelial cells in inflammatory arthritis, while Muc5b, Mcoln3, and Ovgp1 were upregulated in epithelial cells in both locations during CIA (Figure 6-8a). No significant changes were observed in tight junction-related genes in ileal and colonic epithelial cells during disease (Figure 6-8b).

Collectively, these approaches attempted to investigate the correlation between expansion of PDGFRα^{hi} FB and impaired epithelium in the gut during arthritis. The transcriptomic results of epithelial cells revealed functional changes in epithelial cells during experimental arthritis, despite modulation being limited. Glycan biosynthesis was also shown to be regulated in the epithelial cells, especially in the colon. However, whether these changes in epithelial cells are induced by the glycan changes in intestinal fibroblast remains unknown, not least due to their unsuccessful RNA-sequencing analysis. Therefore, to further define the crosstalk between intestinal fibroblast and epithelial cells, three-dimensional model organoid cultures were developed to investigate the functional interactions between these two cells.

6.2.3 3D model culture

A decrease in fucosylation of intestinal fibroblast subset (Figure 6-3) as determined by flow cytometry and functional and glycomic changes in epithelial cells as evidenced by transcriptomic analysis was reported above. However, whether this downregulation of fucosylation is related to the dysfunction of epithelial cells is unclear. To investigate this, a three-dimensional (3D) organoid culture was developed by seeding the intestinal fibroblast cell line (CCD-18Co) into Alvetex Scaffold culture inserts, treating the fibroblasts with/without the fucosyltransferase inhibitor (2FF) to mimic the postulated conditions in the gut during experimental arthritis. A sialyltransferases inhibitor(3 Fax) was used as an internal control to compare with fucose changes. Moreover, as a previous study from this group found that loss of sialic acid in synovial fibroblasts could imitate responses resulting from the inflammation in the joint (Wang et al., 2021), it was hypothesised that this could happen in the gut as well. Epithelial (Caco-2 cell line) and goblet (HT-29 cell lines) cells were then seeded on the surface of the Scaffold compartmented from the fibroblasts by a layer of collagen (Figure 6-9a).

Immunofluorescence images of staining with UEA I (binds with fucose) and SNA (binds with sialic acid) show the success of inhibition of expression of fucose and sialic acid in fibroblasts (Figure 6-9b).

To check whether fibroblast glycans affect the formation of the monolayer, the thickness of the epithelial layer was measured. Interestingly, the results indicate the loss of fucose or sialic acid resulted in thinner epithelial layers (Figure 6-10). In addition, it was noticed that the control cells tend to aggregate and form surface structures when compared to the samples treated with the glycosyltransferase inhibitors (Figure 6-10). Next, the integrity and permeability of the monolayer were evaluated by Transepithelial Electrical Resistance (TEER) potential measurement. Interestingly, samples treated with/without 2FF exhibited an increased TEER potential along the experiment from day 3 to day 9. A significant increase in TEER value was observed in the 2FF-inhibited group at day 9 (Figure 6-11), suggesting a better integrity and reduced permeability of monolayer although there were no significant changes in HRP permeability experiment. By contrast, no significant differences were noticed between samples treated with/without 3 Fax, indicating the changes in sialic acid expression have less impact on properties of monolayer.

6.3 Discussion

The intestinal barrier between the host and external environment is important for protection against pathogen invasion. The intestinal fibroblast acts as a signalling hub, thereby regulating epithelial and immune homeostasis in the gut and maintaining intestinal health. Therefore, to further understand the processes involved, the intestinal fibroblast subset populations, and their glycosylation profiles were examined during the course of inflammatory arthritis.

Interestingly, only the PDGFRα^{hi} FB subset expanded, and its terminal fucosylation profile was modulated in arthritic mice. PDGFRα^{hi} FBs are directly located under the epithelial layer and concentrated at the top of crypts and villi. They are the main producers of BMP such as Bmp3, Bmp5 and Bmp7, which are largely restricted to PDGFRα^{hi} FB. They are hence pivotal to epithelial differentiation and homeostasis (Hong et al., 2020, Mccarthy et al., 2020b, Kosinski et al., 2007, Beumer et al., 2022). Reflecting this, the genetic blockage of PDGFRα decreased

both epithelial and immune system cell maturation (Jacob et al., 2022). In addition, PDGFRα was required to respond to intestinal injury and inflammation for repair and recovery (Jacob et al., 2022). Therefore, in these results, the expansion of PDGFRα^{hi} FB in CIA mice perhaps reflected the inflammation in the gut, and an attempt to recover the intestinal integrity and homeostasis of mice undergoing RA. Despite recent progress in recognising the importance of fibroblasts in intestinal homeostasis, the molecular mechanisms controlling the crosstalk between fibroblasts and the associated epithelial layer remain elusive. Here, the downregulation of terminal fucosylation of PDGFRα^{hi} FB, which could be related to the loss of fucose in epithelial cells in inflammation disorders in the gut was observed. Nevertheless, more studies on the fucose of these two cells need to be done in the future to understand the relationship between them.

To address whether changes in this special intestinal fibroblast subset during CIA could regulate the inflammatory pathways and glycomic profile of epithelial cells, PDGFRα^{hi} FB and epithelial cells were sorted for bulk RNA-sequencing. Unfortunately, it did not prove possible to get the PDGFRα^{hi} FB results due to the shortage of cell numbers. However, reduced expression of genes involved in cellular interactions and mucus protection and repair were observed in colonic epithelial cells. Interestingly, Fut2, which is the main fucosyltransferase responsible for epithelial fucosylation was downregulated in arthritic colonic epithelial cells when the glycan synthesis pathways were examined, suggesting dysfunction of the gut barrier (Wang et al., 2017b, Kudelka et al., 2020, Goto et al., 2014). However, an increase of fucosylation in the colon epithelial layer in flow cytometry data (Figure 5-16), suggests the factors in the luminal were affecting the fucose expression. In addition, a reduction in expression of mannosylation and poly LacNAc were observed in arthritic colonic epithelial cells. Interestingly, mannosylation and poly LacNAc are two main contributors to the glycocalyx, a layer of carbohydrate chains on the cell surface, which plays an important role in in the maintenance of the epithelial barrier by preventing pathogens and harmful substances from easily crossing the epithelial layer (Varki A, 2022, Varki, 2011).

Furthermore, galectin-9 expression was also reduced in arthritic mice, which was mainly expressed by gastrointestinal epithelial cells (Liu et al., 2023). Galectin-9 is associated with B cell activation, the galectin-9 knock-out mice exhibited

reduced IgA production following oral antigen exposure (Liang et al., 2018, Liu et al., 2023). The increase of galectin-7 and galectin-8 in CIA mice may indicate bacterial infections as these two galectins recognize some bacteria and result in the destruction of the bacteria (Liu et al., 2023, Thurston et al., 2012, Lin et al., 2020).

In addition, consistent increases of Muc5b and decreases of Muc2 and Muc4 expression were found in both ileal and colonic epithelial cells of arthritic mice. In fact, mucins are classified into secreted mucin (providing lubrication and forming gel) and membrane mucin (maintaining structural integrity of epithelial surface) (Kim et al., 2010, Corfield, 2000, Bansil et al., 2018). Interestingly, Muc4 belongs to membrane mucin, secreted by goblet cells and enterocytes, downregulation of this type of mucin in arthritic mice will affect the integrity of the epithelial layer and allow pathogens to invade the barrier more easily. By contrast, Muc2 and Muc5b belong to secreted mucins, secreted by goblet cells located in villi and deep crypts, respectively the results indicate that the low expression of Muc2 could result in higher expression of Muc5b secreted in deeper goblet cells to provide a secondary protection line.

A 3D cell line culture model was developed to investigate the crosstalk between intestinal fibroblast and epithelial cells. As there is downregulation of terminal fucose in PDGFRα^{hi} FB during experimental arthritis, the intestinal fibroblast cell line was treated with 2FF to inhibit its fucose synthesis. Meanwhile, 3Fax was used to inhibit sialic acid synthesis in intestinal fibroblasts as well because the loss of synovial fibroblasts initiated a proinflammatory microenvironment in the joint (Wang et al., 2021). The results indicated that the change of fucosylation and sialylation in intestinal fibroblast reduced the thickness of the monolayer. However, the TEER measurement suggested loss of terminal fucose could provide a better epithelial barrier. Actually, the TEER value of the human small intestine is usually between 50 and 100 Ω·cm^2 (Srinivasan et al., 2015). Here, the TEER of the Fuc – samples reached more than 150 Ω·cm^2, which perhaps suggested the abnormal formation of an epithelial layer. Moreover, the traditional Caco-2 monolayer cell model requires 17–21 days of culture to differentiate and demonstrate the desired complete characteristics of small intestinal enterocytes (Natoli et al., 2012). This experiment stopped on day 9 because of the large expansion of enterocytes and goblet cells overflowing the Alvetex Scaffold.

Therefore, the property of a stable monolayer after day 9 is still unknown. Hence, more studies need to be repeated and parameters like cell seeding concentration and measurement period need to be adjusted in future research to characterise the monolayer.

Although the 3D model is a good approach to mimic gut *in vivo*, there is still a limitation. For example, the PDGFRα^{hi} FB expanded in arthritic mice, but the general intestinal fibroblast cell line was used in 3D experiment, and this can not exactly represent the real situation in the gut *in vivo*. In fact, it was not possible to culture specific intestinal fibroblast subsets *in vitro* due to the loss of their phenotype after isolation. Indeed, it is challenging to recreate the complex microenvironment with multiple cell types and extracellular matrix components required to keep intestinal fibroblast subset phenotypes. The interaction with other cell types in the tissue like immune system cells and endothelial cells is crucial for maintaining intestinal fibroblast subset, and these interactions may be disrupted or difficult to replicate *in vitro*. Therefore, more research could be investigated here, for example, knocking out the PDGFRα gene in intestinal fibroblasts prior to seeding the Alvetex Scaffold to mimic the situation in arthritic mice. The use of PDGFRα-deficient mice could be another option as well. Despite not entirely mimicking the findings observed *in vivo*, collectively they provide the preliminary results to show crosstalk between intestinal fibroblast and associated epithelial cells, and the impact on intestinal fibroblast fucosylation and sialylation in the regulation of epithelial layer formation.

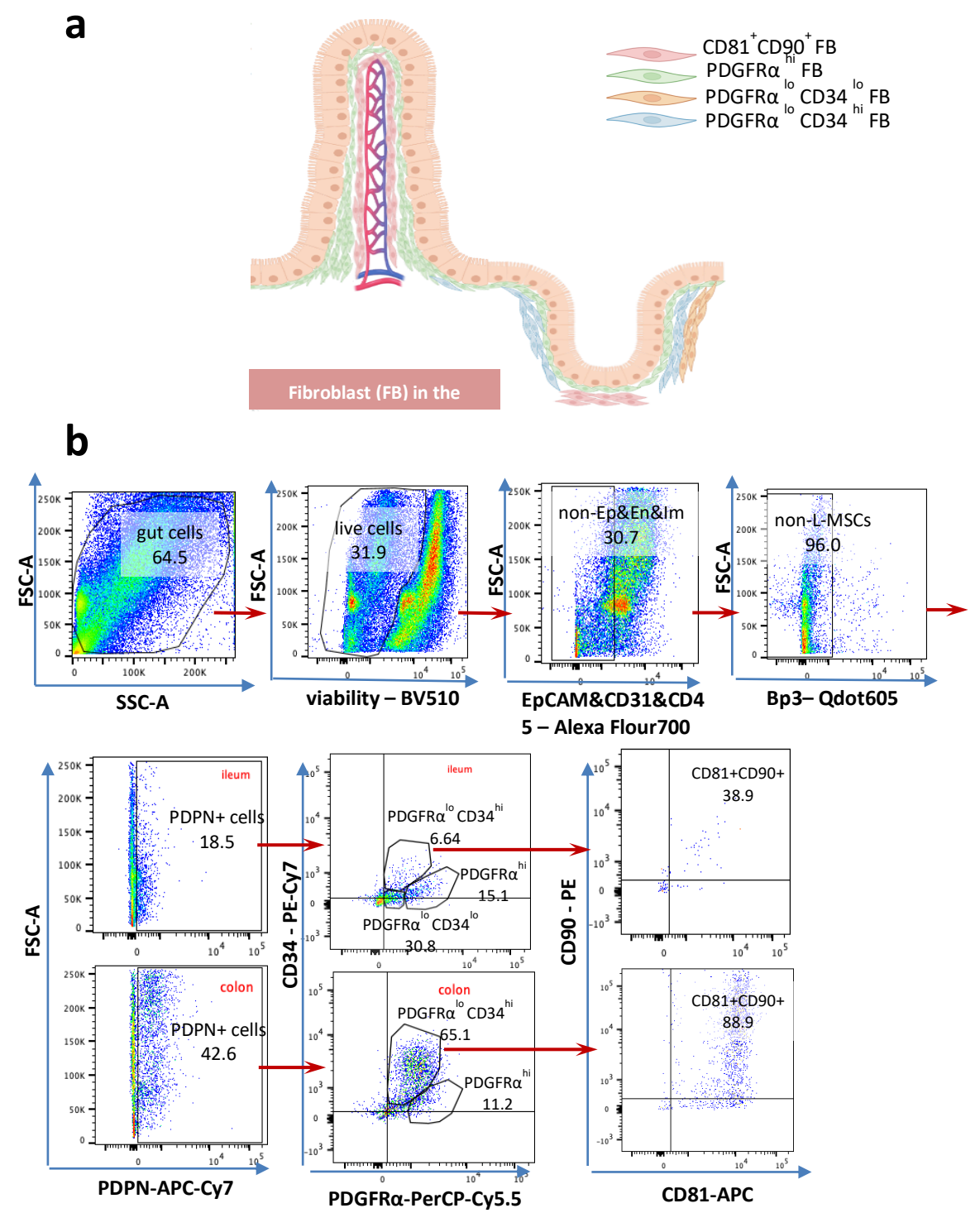

Figure 6-1 Gating strategy of intestinal fibroblast subset.

a) Diagram of location of intestinal fibroblast subset. **b)** Gut tissue were digested by collagenase and stained with antibodies. Relevant cell populations were first gated on the basis of FSC/SSC analysis and singlet and live-dead cell discrimination using Viability dye (BV510). Immune system cells, epithelial cells, and endothelial cells were in dump channel (Alexa Flour700), and non-Ep&En&Im cells were futher identified as non-L-MSCs (lymphoid tissue-associated MSCs) by expression of BP3. Non-L-MSCs were further identified as PDPN+ cells. PDPN+ cells were divided into three subsets of intestinal fibroblasts: PDGFRα^{lo} CD34^{hi} FB, PDGFRα^{hi} FB, and PDGFRα^{lo} CD34^{lo} FB. PDGFRα^{lo} CD34^{lo} FB can be further identified by marker CD81 and CD90. Lectins were stained in FITC fluorophore. Ep, epithelial cells; En, endothelial cells; Im, immune cells; MSCs, mesenchymal stromal cells; PDPN, Podoplanin; FB, fibroblast.

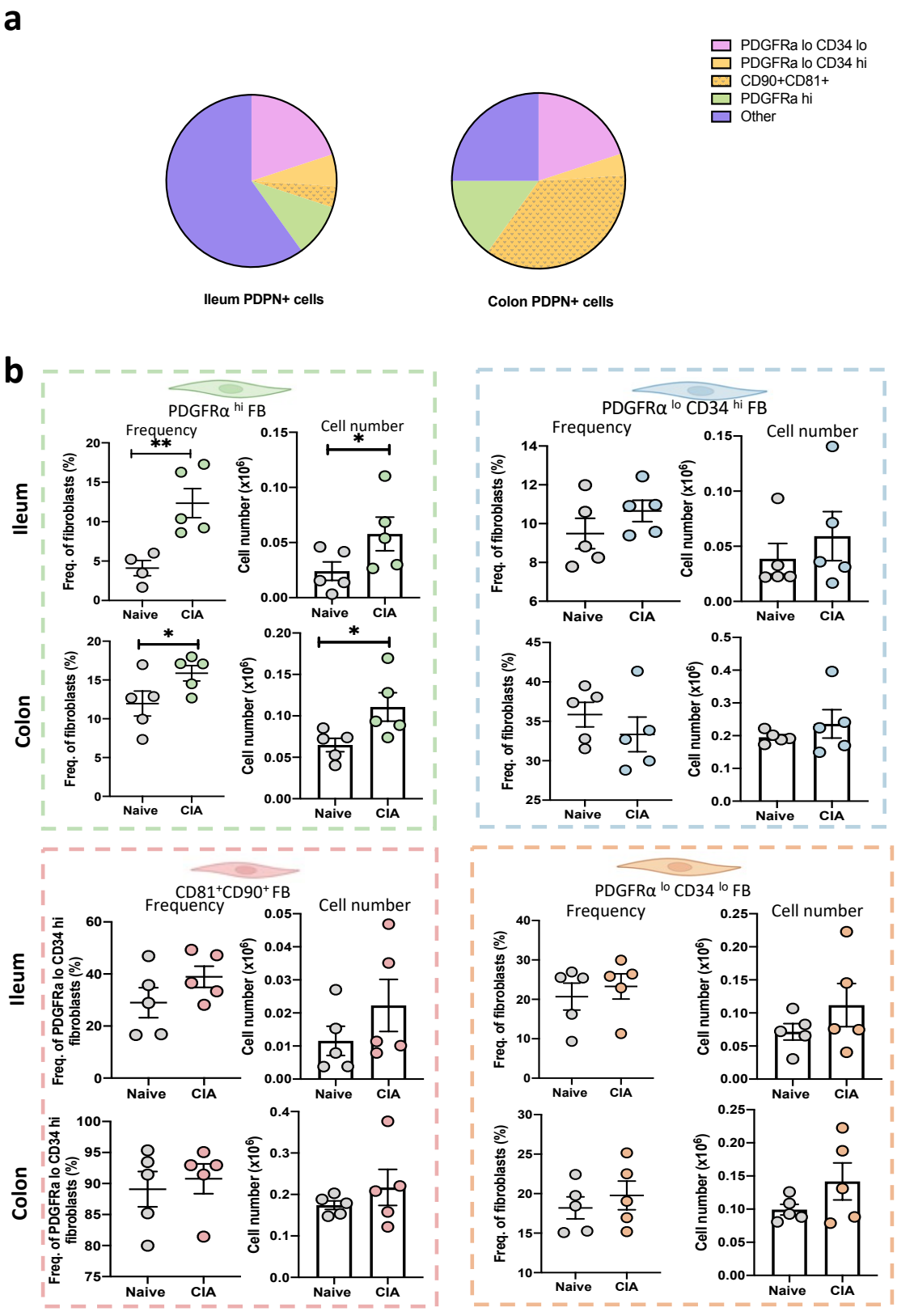

Figure 6-2 PDGFRαhi fibroblasts are increased in the gut of arthritic mice.

a) Fibroblast subsets (all Podoplanin+) proportions in ileum and colon. **b)** Frequency and cell number of different fibroblast subsets in PDPN^{+} fibroblast in the ileum and colon. Each dot represents individual mouse. Statistical significance was determined using Unpaired t-test. Significance is indicated by asterisks, *p < 0.05.

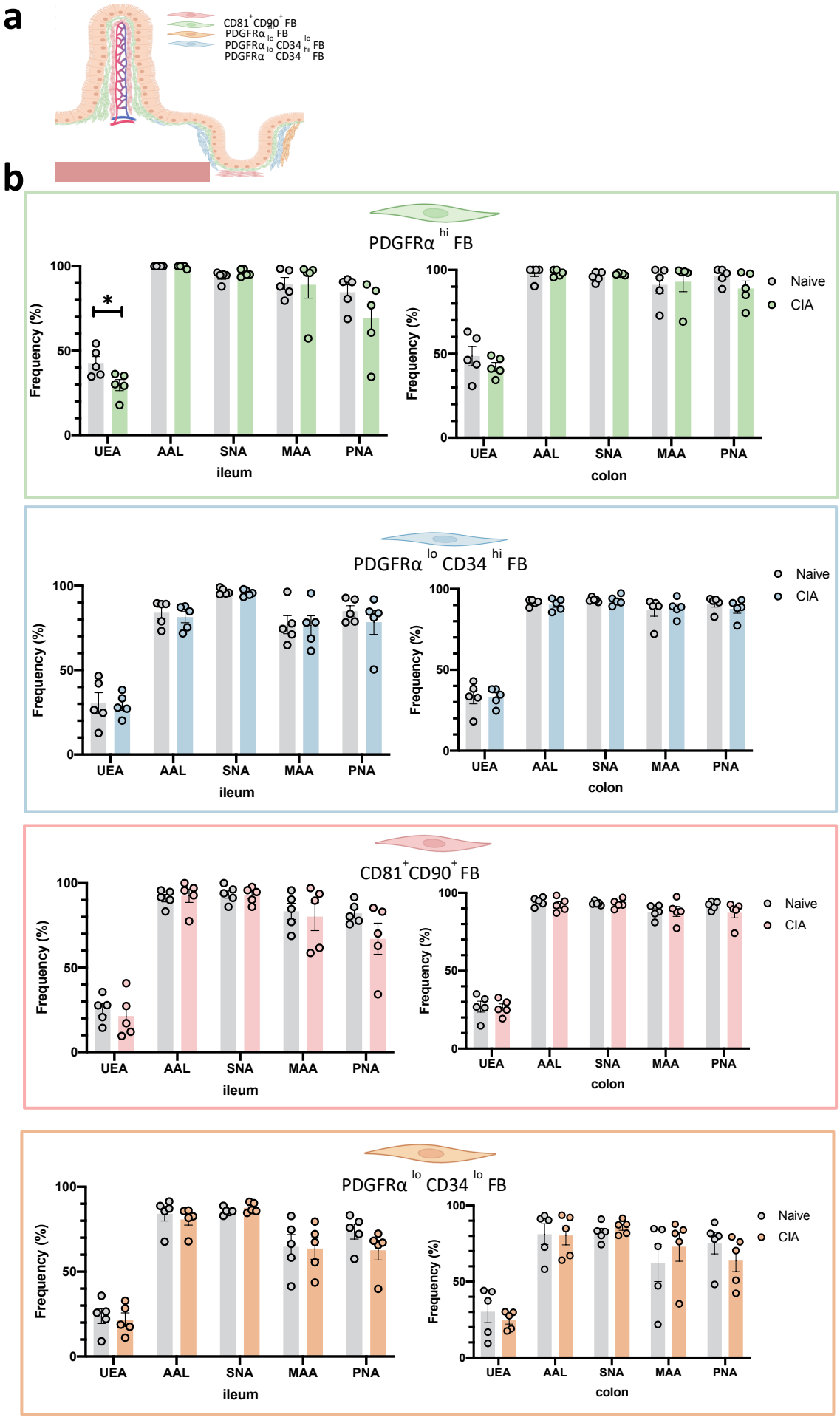
a
CD81+CD90+ FB
PDGFRα lo FB
PDGFRα lo CD34 hi FB
PDGFRα - CD34 lo FB
b
PDGFRα hi FB
PDGFRα lo CD34 hi FB
CD81+CD90+ FB
PDGFRα lo CD34 lo FB
Frequency (%)
100
50
0
*
UEA
AAL
SNA
MAA
PNA
ileum
colon
Naive
CIA

Figure 6-3 Alteration of lectin binding expression of intestinal fibroblast subsets during RA.

a) Diagram of location of intestinal fibroblast subset. **b)** Frequency of lectin+ cells of each intestinal fibroblast subset in the ileum and colon. Each dot represents individual mouse. Statistical significance was determined using Unpaired t-test. Significance is indicated by asterisks, *p < 0.05. UEA, *Ulex Europaeus Agglutinin I*; AAL, *Aleuria aurantia lectin;* SNA, *Sambuccus nigra agglutinin*; MAA, *Maackia aurensis lectin II*; PNA, *Peanut agglutinin.*

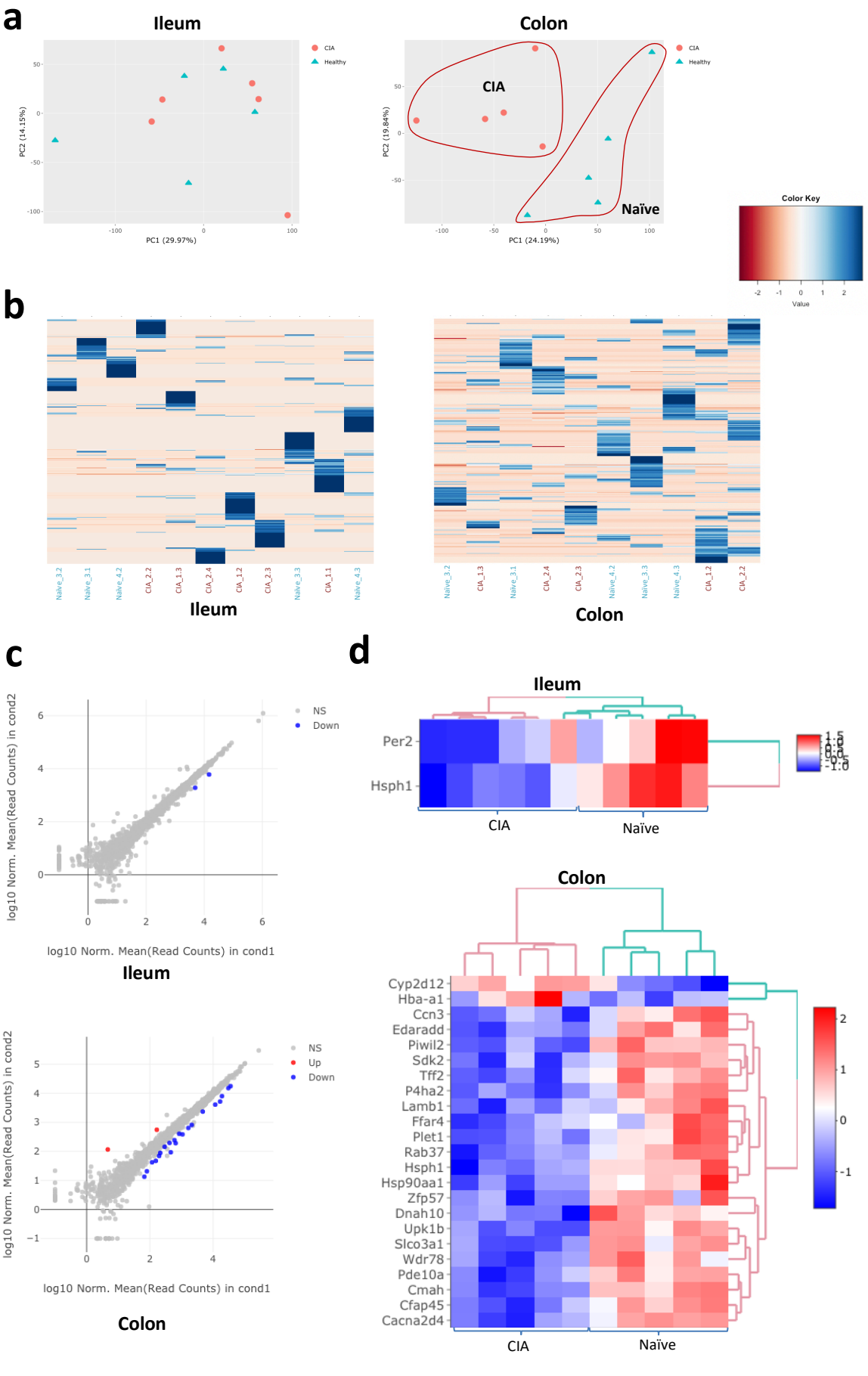
a
Ileum
Colon
CIA
Healthy
PC1 (29.97%)
PC2 (14.15%)
PC1 (24.19%)
PC2 (19.84%)
CIA
Naïve
Color Key
Value
b
Ileum
Colon
c
NS
Up
Down
log10 Norm. Mean(Read Counts) in cond1
log10 Norm. Mean(Read Counts) in cond2
Ileum
Colon
d
Ileum
Per2
Hsph1
CIA
Naïve
Colon
Cyp2d12
Hba-a1
Ccn3
Edaradd
Piwil2
Sdk2
Tff2
P4ha2
Lamb1
Ffar4
Plet1
Rab37
Hsph1
Hsp90aa1
Zfp57
Dnah10
Upk1b
Slco3a1
Wdr78
Pde10a
Cmah
Cfap45
Cacna2d4
CIA
Naïve

Figure 6-4 Significant genes analysis of epithelial cells in ileum and colon of naïve and arthritic mice.

RNA was extracted from epithelial cells in ileum and colon tissue from naïve and CIA mice, and subjected to bulk RNAseq (75 bp paired-end, 30 M reads). a) Principal component analysis (PCA) is shown that the plots (red, CIA; blue, healthy). b) Heatmap of all detected genes (unsupervised). c) All detected genes were plotted in a scatter plot in ileum and colon, genes that pass the threshold of padj < 0.01 and |log2Foldchange| > 2 were considered as differentially expressed genes. In CIA samples, upregulated genes are coloured in red and downregulated genes are coloured in blue. d) Heatmap shows the differentially expressed genes detected in scatter plot.

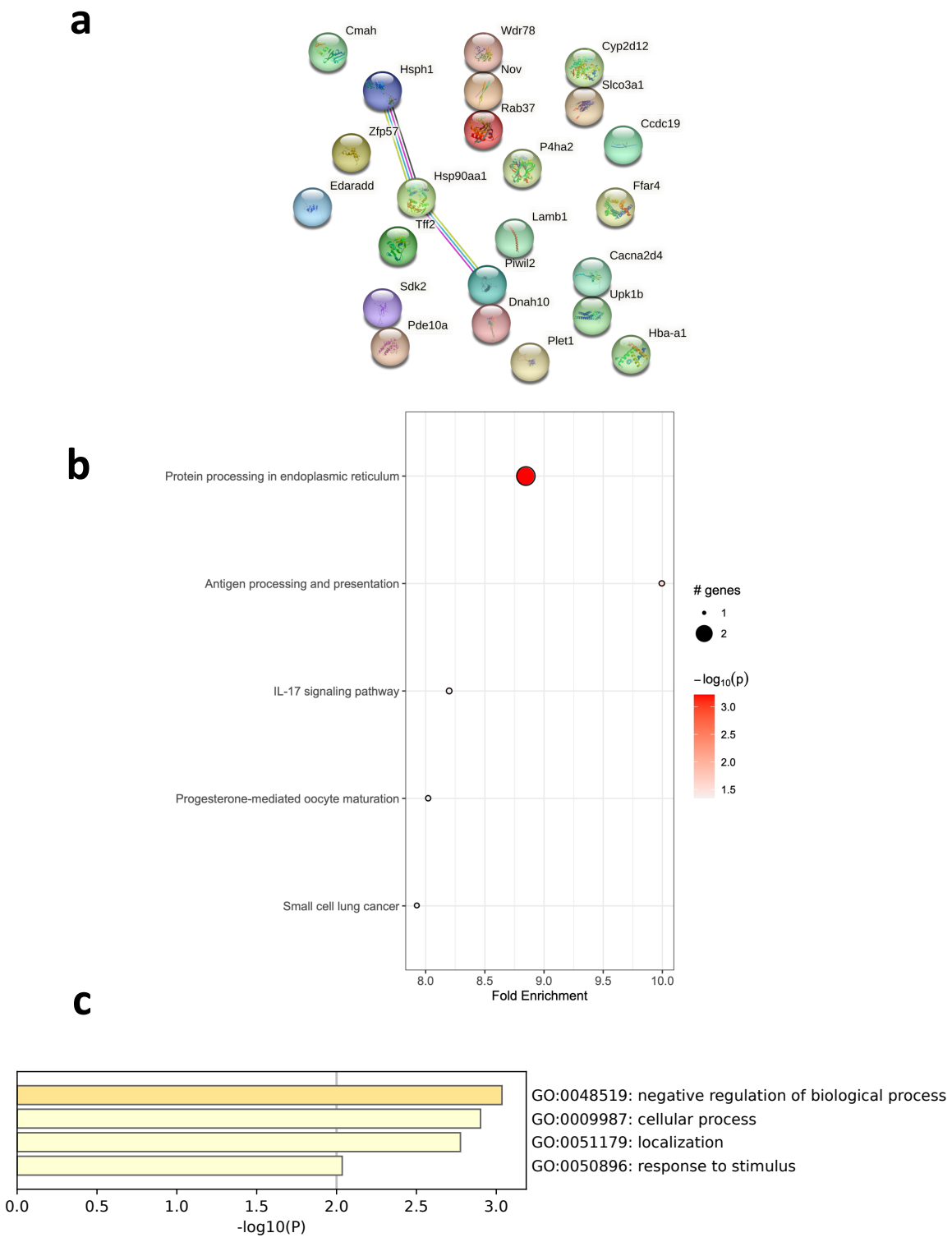

Figure 6-5 Functional enrichment and network analysis of epithelial cells in colon of naïve and arthritic mice.

a) Differentially expressed genes identified in colon were used for pathway enrichment analysis of the KEGG pathway. **b)** KEGG pathways were plotted in bubble charts using the Pathfind R package, with fold change on the X-axis and -log10 p-value on the coloured scale. The size of the bubble is proportional to the number of differentially expressed genes. **c)** GO biological process pathways of genes identified in colon. GO-biological process pathways were plotted in bar charts using Metascape (https://metascape.org).

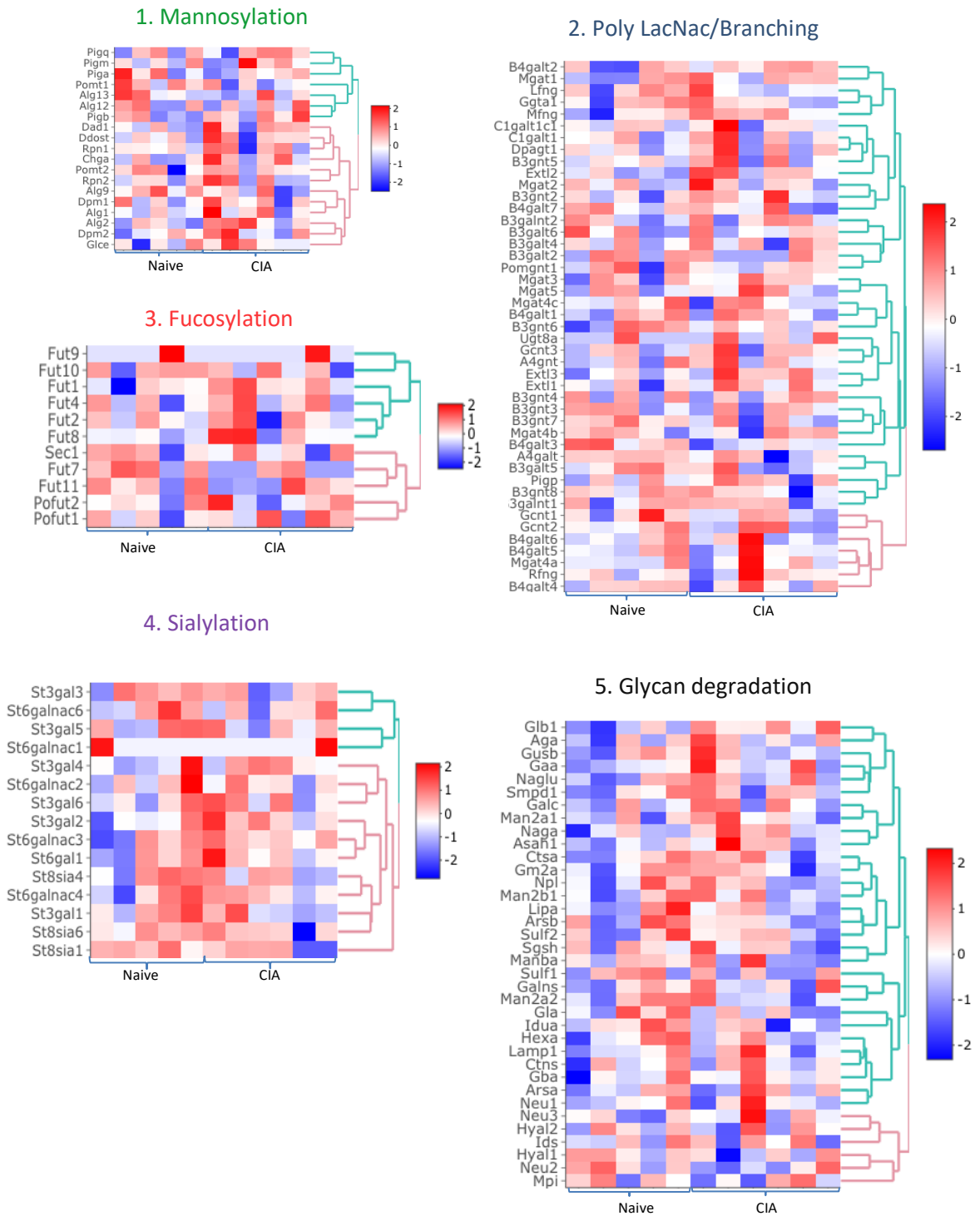

Figure 6-6 Expression of genes involved in glycosylation pathways in ileal epithelial cells.

Heatmap of expression of genes involved in glycosylation pathways in the ileum epithelial cells, including mannosylation, Poly LacNac/Branching, fusosylation, sialylation and Glycan degradation.

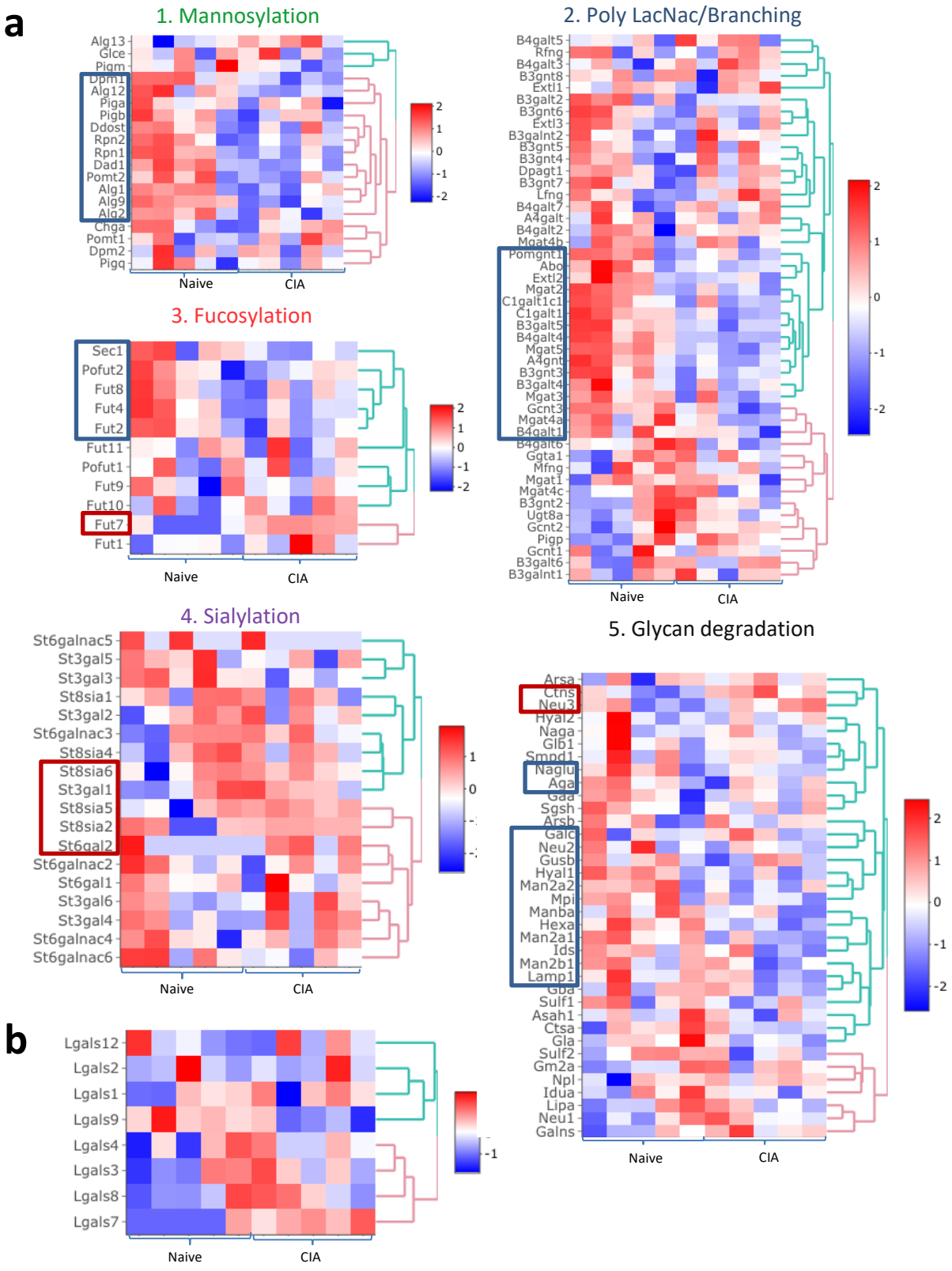

Figure 6-7 Expression of genes involved in glycosylation pathways in colonic epithelial cells.

a) Heatmap of expression of genes involved in glycosylation pathways in the colon epithelial cells, including mannosylation, Poly LacNac/Branching, fusosylation, sialylation and Glycan degradation. **b)** Galectin involved genes expression in the colon. Upregulated genes (red box) and downregulated genes (blue box) in the CIA sample compared to Naïve sample.

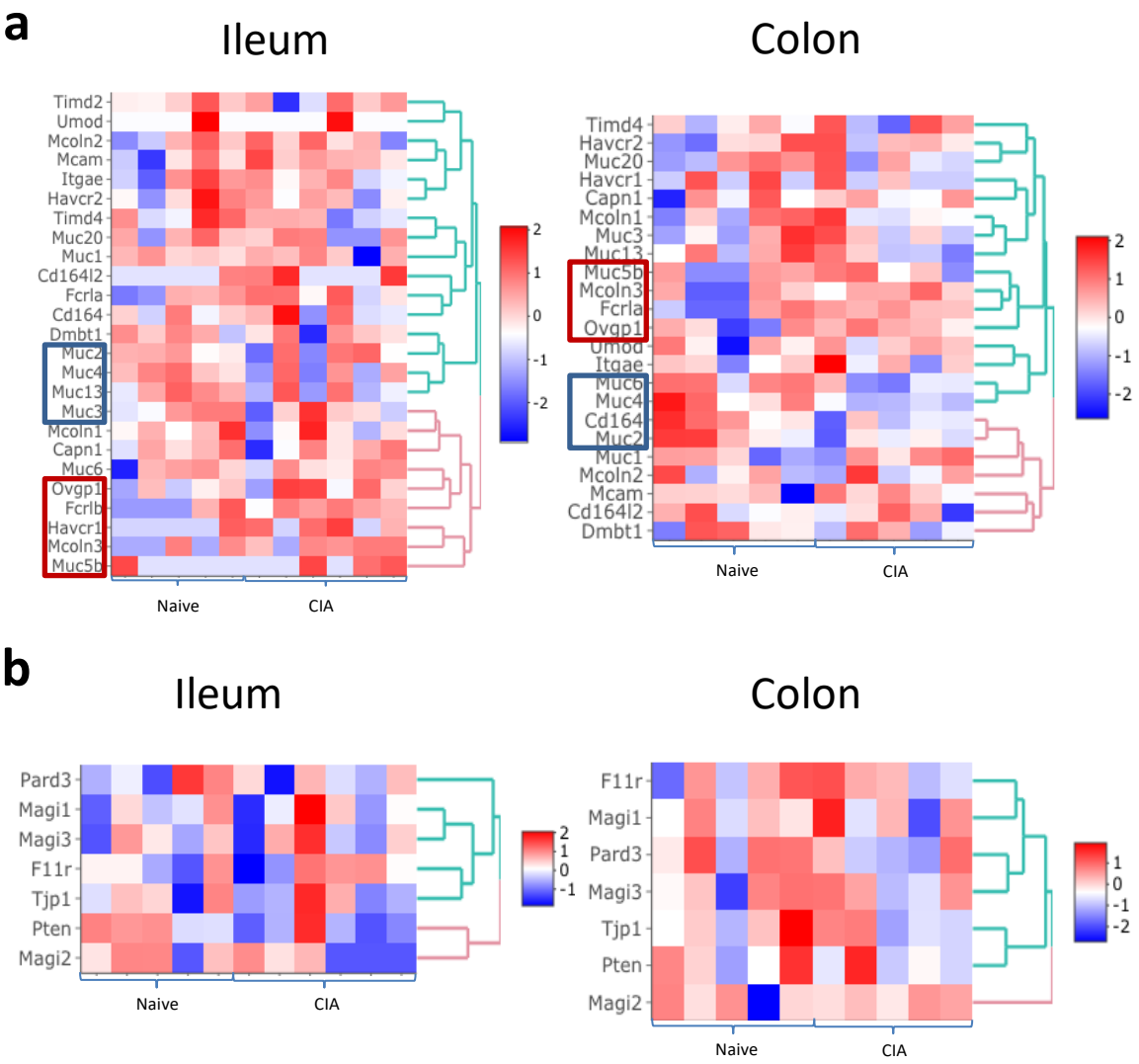

Figure 6-8 Heatmap of expression of genes involved in gut barrier in the ileum and colon epithelial cells.

a) Heatmap of expression of genes involved in mucins production. **b)** Heatmap of expression of genes involved tight junction.

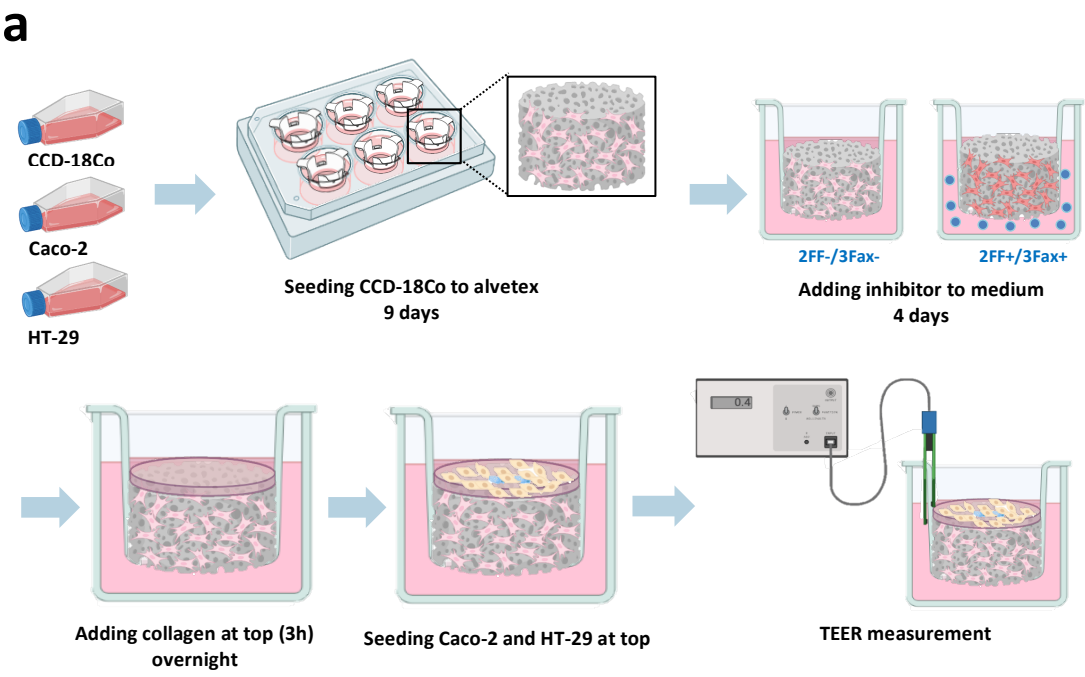

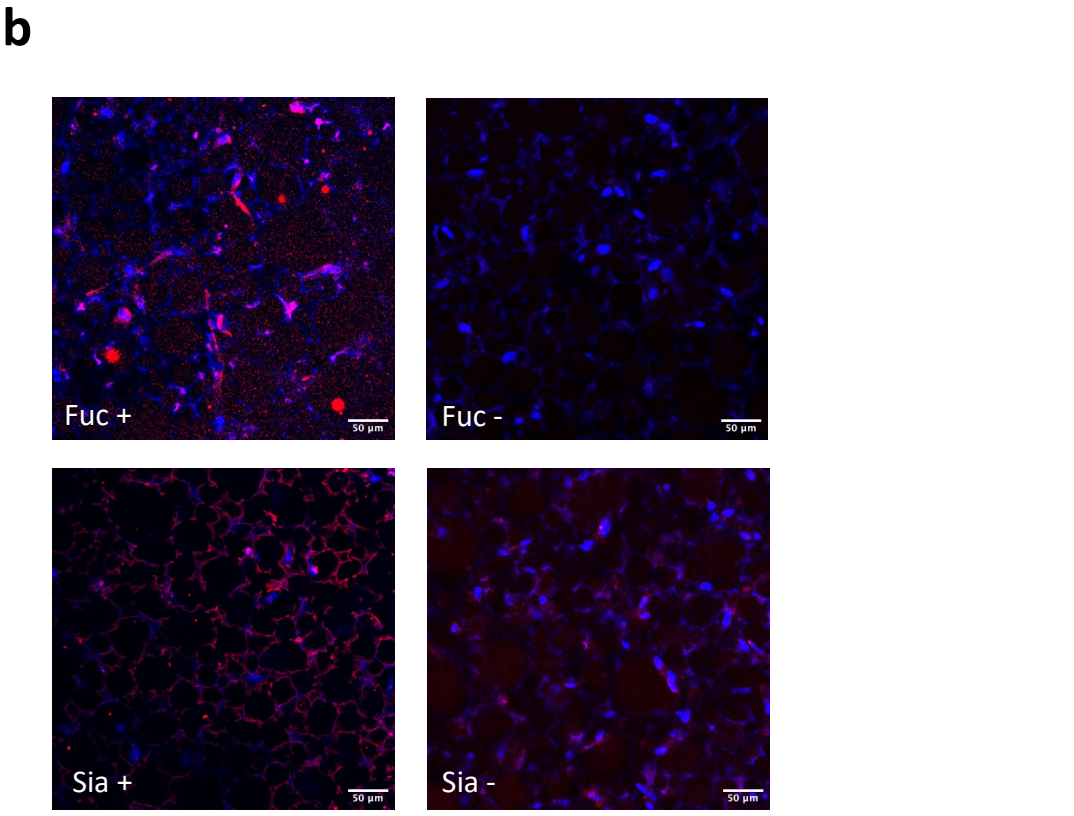

Figure 6-9 Three-dimensional (3D) system cell culture.

a) Procedure of 3D cell culture system. CCD-18Co, Caco-2, and HT-29 cell lines were cultured maintained in flask. CCD-18Co cells were seeded on the Alevetex Scaffold (1×10^6 cells/well) and cultured for 9 days and treated sialytransferase inhibitor (3 Fax) and fucosyltransferase inhibitor (2FF) for 4 days. After which, 2 mg/mL rat tail collagen I solution was added on the Alvetex Scaffold surface and incubated for 3 hours to set, topped up the medium overnight. The following day, seeded Caco-2 and HT-29 (9:1, 0.5×10^6 cells/well) on the surface of Scaffold and incubated for 3-4 hours to allow cells to settle. After which the plates were ready to perform Transepithelial Electrical Resistance (TEER) potential test. **b)** Representative immunofluorescence images of Alvetex Scarffold with/without inhibitor treatment, slides were stained with UEA I (binds fucose) and SNA (binds with sialic acid). lectin, red; DAPI, blue. Scale bar = 50 µm. Fuc, fucose; Sia, sialic acid.

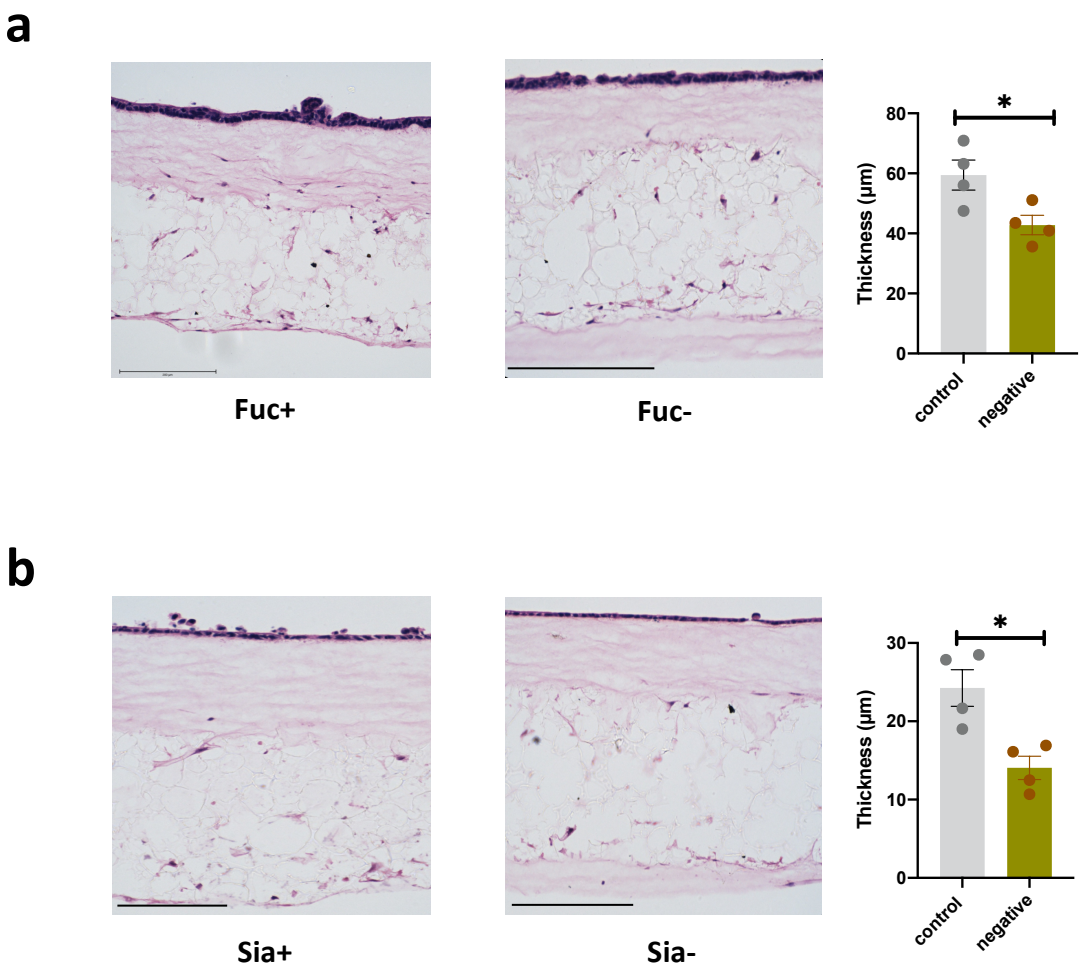

Figure 6-10 Measurement of epithelial layer thickness.

Representative HE images of Alvetex Scaffold treat with/without fucosyltransferase inhibitor (a) or sialyltransferase inhibitor (b). Scale bar = 200 μm. The thickness of epithelial layer were measured by Image J software. Each dot represents individual sample. Statistical significance was determined using Unpaired t-test. Significance is indicated by asterisks, *p < 0.05. Fuc, fucose; Sia, sialic acid.

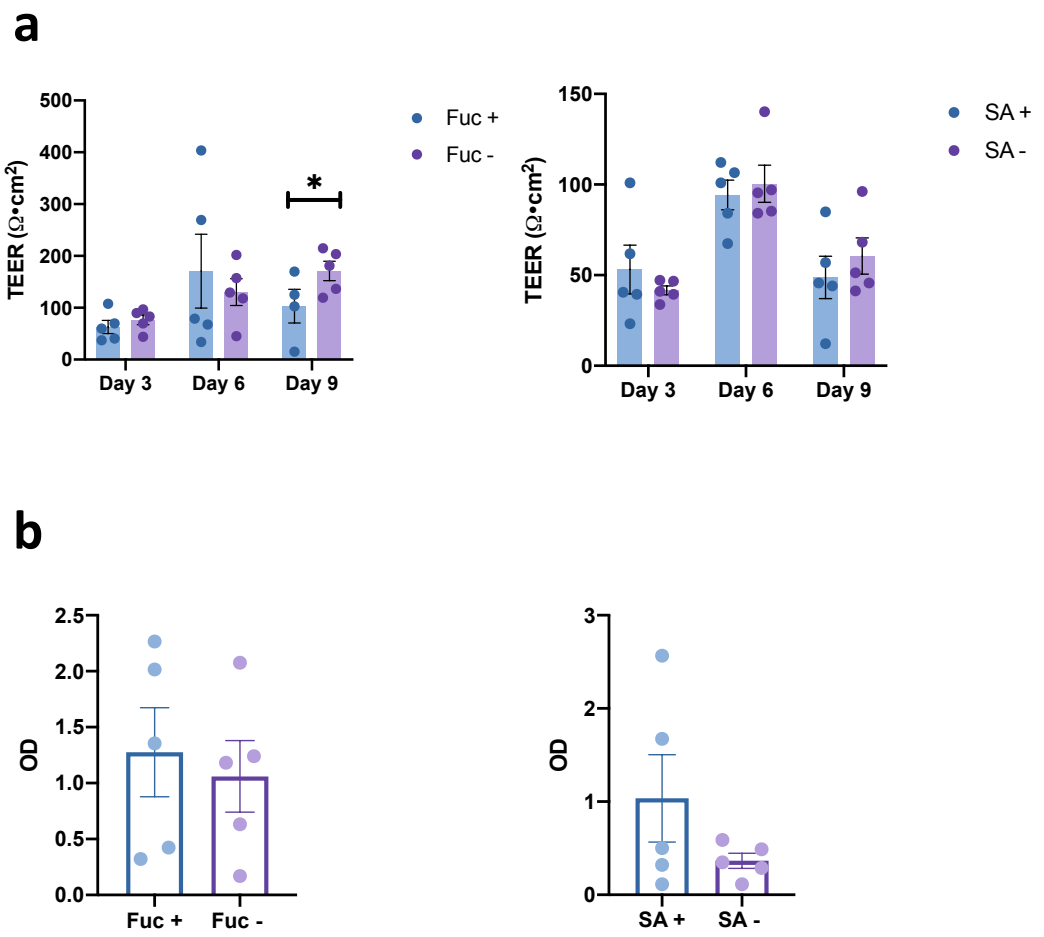

Figure 6-11 Measurement of integrity of monolayer.

a) After Caco-2 and HT-29 cells were added on the surface of Alvetex Scaffold (day 0), TEER measurement was conducted at day 3, day 6, and day 9. The TEER value ($\Omega \cdot cm^2$) was calculated by subtracting the resistance of the blank insert from that of the sample and multiplying it with the surface area of the insert (cm^2). Statistical significance was determined using Unpaired t-test. Significance is indicated by asterisks, *$p < 0.05$. **b)** Permeability was evaluated by Horseradish peroxidase (HRP) permeability Assay. The medium was collected after 1 hour and examined by spectrophotometer (450 nm). Each dot represents individual sample. Fuc, fucose; SA, sialic acid.

Chapter 7 General discussion

7.1 Future perspectives for the therapeutic use of UC-II in RA.

7.1.1 The regulator between oral tolerance and glycomics

Rheumatoid arthritis (RA) is a chronic autoimmune inflammatory disorder affecting synovial joints. Oral tolerance is a fascinating immunoregulation for RA treatment. Collagen-derived products have been used to induce oral tolerance and undenatured Type II collagen (UC-II) from Lonza, which preserves the physiological structure of collagen fibres, has shown an enhanced ability to induce tolerance (Bagi et al., 2017, Bagchi D., 2002), although its protective mechanism is not yet fully understood. Most research has focused on the modulation of immune and tolerogenic responses in the gut, while less attention has been given to stromal cells within the local microenvironment. However, in this study, the focus was not only on the immune responses in the joint and gut but also on mucosal tissue, such as barrier integrity and microbiome diversity due to the gut-joint axis hypothesis.

In this thesis, two doses of UC-II (0.66 mg/kg and 7.33 mg/kg) were applied to experimental arthritis, and both of them showed a protective effect to some degree. In fact, the higher dose of UC-II showed better protection against disease incidence and severity, which is associated with the regulation of IL-17 and IL-22 cytokines in the joint and rewiring of associated $\gamma\delta$ T cell and ILC cytokine networks in the gut. Moreover, these results confirmed the ability of UC-II to rewire gut glycosylation profile and gut microbiome composition.

Stromal cells like intestinal fibroblasts (FB) in the gut are essential to intestinal homeostasis and the data presented here indicated the PDGFRα^{hi} FB subset expanded during arthritis and its fucosylation was downregulated. Since FB are able to affect the intestinal condition, and its glycan profile was changed during arthritis, it is possible FB may have the ability to affect local inflammation by glycans as glycans can work as ‘cell communication tools’. In fact, many studies have reported the role of glycans in immunity and cancer. For example, loss of

fucosylation leads to inflammation in the gut (Wang et al., 2017b, Garber et al., 2021).

However, it is still not clear whether these changes of fibroblasts are associated with oral tolerance. For example, changes in intestinal fibroblasts's glycan profile could also affect the induction of oral tolerance as fibroblasts are involved in intestinal epithelial integrity, and glycans are involved in cell communication. Thereby, the data have led to the hypothesis that UC-II could act as a regulator between glycosylation of intestinal fibroblasts and oral tolerance since UC-II is able to reshape the microenvironment in the gut. To answer these questions, it was therefore checked whether UC-II have an influence on the intestinal fibroblast subsets and their glycosylation profile. Surprisingly, UC-II reduced the expansion of PDGFRα^{hi} FB subset during CIA (Figure 7-1). Meanwhile, UC-II recovered the fucosylation level of the PDGFRα^{hi} FB subset (Figure 7-2). Interestingly, it can also alter the core fucosylation of PDGFRα^{lo} CD34^{hi} FB and galactose expression of the CD81+CD90+ FB subset, cells which are enriched in the colon. All these data confirmed that UC-II is able to regulate the glycosylation profile of intestinal fibroblasts, suggesting it could be involved in the communication between fibroblasts and epithelial cells in the gut.

However, these data do not provide proof of causality since UC-II could reshape the gut microbiome composition at the same time. There is a possibility that the mechanisms triggered by UC-II led to IL-17/IL-22 networks in the gut and restored the increased abundance of *Lachnospirales* and *Candidatus Saccharimonas* in the gut, and also specifically increased the abundance of *Parasutterella* in the ileum, subsequently affecting the glycan profile, especially fucose expression in the gut. This type of change promotes the gut immune response to the bacteria in the gut as well, which forms an effective cycle to protect against gut damage and introduce oral tolerance during experimental arthritis, ultimately reducing inflammation in the joint due to the gut-joint axis (Figure 7-3). Or it could be another possibility that UC-II regulates the glycan expression in the gut, which initiates the regulation of microbial composition. The changes in bacteria promote the effectiveness of oral tolerance to rewire the cytokines expression. It can further affect gut immunity and responses to stimuli, which can help with intestinal homeostasis (Figure 7-3).

To further understand the protective effects of UC-II and the relationship between the microbiome and crosstalk between intestinal fibroblast and epithelial cells via the glycan-mediated pathway, more investigations involving antibiotic application (to deplete the gut microbiome) and co-housing models are needed in the future. Overall, the performance of UC-II in this study is encouraging, with the results enriching the understanding of mechanisms underlying oral tolerance induction by UC-II, paving the way for novel therapeutic interventions targeting glycosylation/microbiota-related pathways in RA.

7.1.2 Limitations and Future Application of UC-II

Despite the protective effects observed in this study, we also noticed some limitations of UC-II during the process as the lack of effect in some mice. This can be caused by some factors. For example, UC-II powder is not soluble in water, which means our UC-II suspension may have affected the amount of UC-II being administered to the animals. Less accurate dosing could affect the protective effect since we noticed the dose of UC-II is one of the main factors affecting oral tolerance. In addition, poor solubility can lead to low bioavailability resulting in suboptimal drug delivery. This could be one of the factors that account for some mice not responding to UC-II in this study.

Many techniques could be adapted to improve the solubility of UC-II. For example, converting a crystalline form of a compound into its amorphous form can enhance solubility by spray drying (Alamilla-Beltrán et al., 2005). Nanoparticles are another option to improve solubility and bioavailability by solid dispersion, milling media, and high-pressure homogenization (Sareen et al., 2012, Kalepu et al., 2015). A study on water-soluble UC-II found it ameliorates experimental arthritis (Yoshinari et al., 2015, Yoshinari et al., 2013), which suggests that improved solubility of UC-II may enhance the protective effect of UC-II in RA.

In this study, only the prophylactic effect of UC-II was investigated throughout the research, however some studies have reported the therapeutic effect of UC-II (Yoshinari et al., 2013, D'altilio et al., 2007, David E. Trentham, 2002). There are some limitations although the efficacy is encouraging. To improve the prophylactic and therapeutic effect of UC-II, a glycan-modified UC-II could be explored in the future based on our findings. For example, we observed

downregulation of fucosylation in the gut tissue, hence we could modify the epitope of UC-II to a fucose-rich format. Fucosylated UC-II may ameliorate the loss of fucose in the gut, and change the specific composition of bacteria in the intestine. In addition, antigen epitope glycosylation plays an important role in T cell recognition and B cell responsiveness (Alexandrecorthay, 1998, Backlund et al., 2002, Schulte et al., 1998). This recognition effectively suppresses the heightened immune response, thereby diminishing inflammation, pain, and swelling mediated by T cells. For example, glycosylation can affect the presentation of antigens on the surface of APCs via MHC II molecules. The addition of glycans to antigen epitopes can impact the binding of antigens to MHC II, influencing T cell recognition. T cell recognition relies on the interaction between the T cell receptor (TCR) on CD4+ T cells and the peptide-MHC II complex. Glycosylation of antigens can modulate this interaction, influencing the activation of CD4+ T cells. Therefore, glycosylation-modified UC-II could be a promising alternative and maximise the effectiveness of RA, although more research and clinical studies are needed to confirm the feasibility.

Overall, the evidence presented here supported the effectiveness of UC-II in CIA as a potential RA treatment. It can regulate the immune responses in the joint and reshape the microbiome composition and glycomic pathways in the gut. Collectively, UC-II showed a very positive potential for RA treatment in the future even though it has some limitations right now.

7.2 Microbiota – nexus of glycomic and inflammation networks underlying oral tolerance

7.2.1 Imbalance of microbiota in inflammatory diseases

Much work has highlighted the importance of the microbiota ito human health n recent decades. Human microbiota composition varies in different locations. Predominant bacterial sites in the body are the oral cavity, respiratory tract, skin, gut, and vagina (Hou et al., 2022). Microbiota in the gut are considered the most significant as they are involved in food fermentation, pathogen protection, immune response stimulation and vitamin production (Hou et al., 2022, Hillman et al., 2017, Rajilic-Stojanovic, 2013, Jandhyala et al., 2015). Generally, the majority of the gut microbiota is mostly composed of two types: the *Bacteroidetes*

and the *Firmicutes*, whereas *Proteobacteria*, *Verrucomicrobia*, *Actinobacteria*, *Fusobacteria*, and *Cyanobacteria* are present in minor proportions (Sekirov et al., 2010, Hou et al., 2022). The microbial numbers and diversity increase from the proximal to the distal gastrointestinal tract. The colon is where the majority of microbiota reside, reaching 10^{11} to 10^{12} bacteria per gram (Sekirov et al., 2010). In addition, the microbiota present in the intestinal lumen differs significantly from the microbiota in the mucus layer as well as in the epithelium (Sekirov et al., 2010, Swidsinski A, 2005).

The microbiota exhibits stability, resilience, and symbiotic interaction with the host in a healthy state. However, microbiota dysbiosis can lead to dysregulation of bodily functions and diseases including cardiovascular diseases (CVDs), cancers, respiratory diseases, IBD, brain disorders, obesity, and chronic kidney diseases (Hou et al., 2022, Sekirov et al., 2010, Wang et al., 2017a). For example, we found an increased abundance of *Lachnospirales* and *Candidatus Saccharimonas* and a decreased abundance of *Mucispirllum* in the mouse gut during experimental arthritis. Supporting this, recent studies of preclinical and early-stage of onset of arthritis indicate that alteration of intestinal microbial composition accelerates the development of RA (Matei et al., 2021, Gracey et al., 2020, Scher et al., 2013). Studies reported an increase of *Collinsella aerofaciens, Lactobacillus,* and *Prevotella copri* in RA patients (Chen et al., 2016, Scher et al., 2013, Alpizar-Rodriguez et al., 2019, Zhao et al., 2022, Zhang et al., 2015), and the data here present similar results. By contrast, a decrease of *Bacteroidetes* and *Bifidobacteria* was noticed in the composition of bacteria in the RA patients (Scher et al., 2013, Jussi Vaahtovuo Evelina Munukka, 2008). Additionally, evidence shows that chronic liver disease is usually accompanied by intestinal dysbiosis, which is characterized by the increase of *Enterobacteriaceae* and the decrease of *Bifidobacterium* (Wang et al., 2017a).

In addition to the gut microbiota, changes in the skin microbiota composition are highly associated with many common skin diseases, such as acne, a chronic inflammatory skin condition mediated by *Propionibacterium acnes* (Hou et al., 2022). Research also reported levels of *Actinomyces*, *Veillonella*, *Streptococcus*, *Megasphaera*, and *Mycobacterium* were more abundant in lung cancer patients compared with healthy individuals. Therefore, the imbalanced composition of microbiota in the body is closely relevant to inflammatory diseases.

7.2.2 Microbiota on the regulation of immune response via interaction with glycans

As described beforehand in the general introduction, intestinal integrity and homeostasis are pivotal in RA due to the gut-joint axis hypothesis, which is also supported by the results presented here. Dysbiosis in the gut will cause the dislocation of gut microbiota, followed by the activation of immune system cells. However, the process of the interaction between microbiota and immune cells is yet not fully understood.

In this study, we examined the glycosylation profile of the epithelial layer in gut tissue by different techniques. Interestingly, we found the changes in glycosyltransferase mRNA did not explain the actual gut glycome (resolved by MS), suggesting that factors in the environment were involved in the regulation of glycans expression. In fact, glycan synthesis is not a one-way pathway, and it is far more dynamic and susceptible to environmental changes (diet, enzymes produced by local microbiota, smoking, etc.) (Moran et al., 2011). Actually, pathogenic infections are usually initiated by sugar recognition, pathogens like bacteria and viruses would like to synthesize or obtain glycans from host cells such as IECs to escape from immune surveillance and survive (Severi et al., 2007, Khatua et al., 2010). Therefore, the gut microbiota is one of the main factors that interact with glycans and affects the glycosylation in the gut, therefore setting the immune tone in the intestine.

For example, we noticed a downregulation tendency of fucosylation in the ileum, although the expression of fucosyltransferases was not significantly changed. What factors could be inducing these changes? The bacteria in the intestine could produce fucosidase which cleaves fucose from host cells and uses it as energy and therefore affects intestinal fucosylation (Comstock et al., 2006, Goto et al., 2016, Pickard et al., 2015). In our results, we found dysregulation of *Mucispirllum* and *Candidatus Saccharimonas* in the colon, which are involved in the mucin degradation process (Herp et al., 2021, Gryaznova et al., 2022). These bacteria can cleave glycans including fucose in the mucus layer as a nutrient source, subsequently affecting glycosylation in the gut. In addition, research reported that *segmented filamentous bacteria* (SFB) enriched in the epithelial surface of the ileum stimulated ILC3 to produce IL-22, and therefore induce the fucosylation of

the epithelial layer. The epithelial fucosylation could inhibit infection by *Salmonella typhimurium* (Goto et al., 2014).

In addition, loss of sialic acid will result in damage to mucus integrity and increase the sensitivity of cells to microenvironmental stimuli, which makes the bacteria access the intestine easily (Yao et al., 2022, Zhao et al., 2023). An increase of sialylated glycans in mucus correlated with a higher diversity of microbiome and lower inflammation and microbial translocation (Giron et al., 2020).

We also found the microbiota to be highly involved in immunological tolerance, although this process is expected likely to be achieved via Foxp3+ regulatory T (Treg) cells, which release tolerogenic cytokines including IL-10 and TGF-ß. However,in this study, the upregulation of *Parasutterella* was associated with the tolerance induced by UC-II, which was associated with the changes in fucosylation profile of intestinal epithelial cells and subsequently affected the gut barrier integrity and change effectiveness of tolerance (Figure 7-3). Combined with the glycomic results, the mechanisms underlying tolerance may involve alteration of glycosylation caused by gut microbiota.

Similar to the glycosylation of the gastrointestinal tract, human cervicovaginal fluid (CVF) is a complex, functionally important and glycan-rich biological fluid, where vaginal microbiota resides. A higher abundance of *Lactobacillus spp*. is associated with a higher percentage of sialylation and fucosylated glycans in CVF of Community State Type (CST) IV-B (characterised by *G. vaginalis* and *A. vaginae* dominance) people compared to CST I-A/B sample (mostly dominated by *L. crispatus* but also containing low abundance *of L. gasseri, L. jensenii* and *G. vaginalis*) (Wu et al., 2022). The interaction between glycans and microbiota could affect cervicovaginal homeostasis, playing an important role in its health.

Collectively, microbiota play an important role in the regulation of immune responses during disease, which involves in recognition and interaction of glycans expressed in the host and their selves. They can also affect immunological processes like tolerance by reshaping the glycosylation profile in the gut.

7.2.3 Microbiota and disease treatment

With an appreciation of the importance of microbiota and their role in disease development and immune responses, manipulating microbiota in the body can be key for disease treatment.

The most effective way to modulate the microbial composition is through a balanced diet, as imbalanced nutrition can lead to changes such as intestinal permeability and metabolic processes (Valdes-Ramos et al., 2010, Pascale et al., 2018, Maslowski et al., 2011). In this study, alteration of microbial composition in the ileum and colon is associated with the induction of oral tolerance. The upregulation of *Parasutterella* could alter the intestinal environment and enhance the effect of tolerance, possibly by affecting the glycosylation profile in the gut. In this case, changing a diet to transform the intestine into a *Parasutterella*-friendly environment could benefit the arthritis treatment.

In addition, oral administration of probiotics and prebiotics are widely used in microbiota modulation as a dietary supplement for clinical intervention (Hou et al., 2022). Administration of probiotics can restore microbial dysbiosis by occupying host tissue to prevent colonization of other pathogenic bacteria. Probiotic species engineered to produce therapeutic biomolecules have been used against infection, reduce inflammation, and treat diet-induced obesity (Mimee et al., 2016). The most well-known prebiotics are inulin, fructo-oligosaccharides (FOS), lactulose, and galacto-oligosaccharides (GOS), most of which are predominantly glycans (Hou et al., 2022). Prebiotics are primarily employed for the regulation of *Bifidobacterium* and *Lactobacillus* strains, known for their production of lactic acid and acetate, which are used in the treatment of gastroenteritis. This modulation helps sustain host health through the fermentation of prebiotics (Pascale et al., 2018). Moreover, antibiotics are widely used to treat bacteria-mediated diseases in clinics to manipulate the composition of microbiota (Hou et al., 2022).

Overall, microbiota work as a nexus of glycomic and inflammation networks underlying oral tolerance. They help ensure that the immune system responds appropriately to real threats while maintaining tolerance to harmless substances. Dysbiosis, or an imbalance in the microbiota, can lead to immune dysregulation

and may contribute to various health conditions, including inflammatory disorders and autoimmune diseases.

7.3 Glycan therapeutics

7.3.1 Glycans - hidden players in health and disease

As mentioned in the general introduction, glycans play an essential role in human health, it being inevitable to involve glycans communication during disease development as every living cell is endowed with a glycan coat (Varki, 2011). Glycan works as a kind of 'biolanguage' mediating/regulating human life. In fact, they serve as essential components in numerous cellular processes. Glycans have been traditionally overshadowed by other biomolecules such as cytokines and chemokines, but recent research has illuminated their pivotal role in health and disease. Glycans are involved in cell signalling, immune responses, host-pathogen interactions, and many more physiological processes.

RA is one of the most intractable diseases in the world with a large economic burden for the whole world, since its exact pathogenesis is still unknown. The role of gut integrity and intestinal homeostasis have recently attracted attention leading to the gut-joint axis hypothesis. In this study, it was shown that in addition to the "traditional" immunological responses, the glycosylation profile was altered in the gut during experimental arthritis, suggesting glycan changes may be a factor causing RA, which has been neglected over the years. For example, fucosylation of epithelial cells and intestinal fibroblast subsets is a key change in CIA mice. This is because, as mentioned before, fucose on intestinal epithelial plays an essential role in integrating host, microbial, and environmental cues to maintain mucosal homeostasis suggesting that the microbiota in the gut could communicate with immune system cells by interacting with fucose.

Moreover, a decrease in Cmah gene expression was observed in the whole colon tissue and colonic epithelial cells in arthritic mice. The enzyme CMP-N-acetylneuraminic acid hydroxylase (Cmah) is responsible for the synthesis of N-glycolylneuraminic acid (Neu5Gc), a sialic acid present on the cell surface proteins of most deuterostomes (Peri et al., 2018). However, in humans, Cmah was inactivated by a 92 bp deletion that occurred 2–3 million years ago (Perota et al.,

2019). Loss of Neu5Gc greatly increases the levels of N-acetylneuraminic acid (Neu5Ac) in human cells (Brinkman-Van Der Linden et al., 2000). This change could alter the sialic acid composition and affect glycoprotein and glycolipid function. Microbes or viruses approaching the surface of a human cell are likely to first encounter sialic acids which include Neu5Ac and Neu5Gc, therefore loss of Cmah could enhance the success of some pathogens which are preferable binding to Neu5Ac (Varki, 2001). Interestingly, animals do not develop RA as it is seen in humans, which suggests RA might related to some microbes or virus infection caused by the evolutionary loss of Cmah in humans.

7.3.2 Dysregulation of glycosylation of fibroblast across tissue in RA?

Intestinal fibroblasts (FB) are important for gut health and integrity. They play a key role in epithelial and endothelial homeostasis, and also affect immune system cell localization and function. In this study, dysregulation of fucosylation was observed in the PDGFRα^{hi} FB subset of arthritic mice, which could be associated with dysbiosis in the gut. Interestingly, a recent study found that loss of α2-6 sialylation promotes the synovial fibroblast transformation into an inflammatory phenotype in RA (Wang et al., 2021). In addition, some research reported the importance of glycosylation in skin fibroblast and cardiac fibroblast during disease (Yamazaki et al., 2012, Scott M. Wilhelm, 1987). Considering RA is a systemic inflammatory disease impacting various organs, it is possible that the dysregulation of glycosylation of fibroblast happened across tissue in RA.

Actually, a similar hypothesis was confirmed by the study of Korsunsky's group (Korsunsky et al., 2022). They found CXCL10+CCL19+ immune-interacting and SPARC+COL3A1+ vascular-interacting fibroblasts, were expanded in all inflamed tissue across the salivary gland, lung, synovium and gut, sharing pathological fibroblast phenotypes. Regarding this, the glycosylation profile of fibroblasts could regulate the disease development. Therefore, investigating the glycosylation signature of stromal cells could benefit the complex systemic disease.

7.3.3 Glycan-based therapies

Glycan-based therapeutics, a burgeoning field within the realm of biochemistry and medicine, holds immense promise for addressing various diseases and medical

conditions. Unlike traditional small-molecule drugs and biologics, glycan-based therapies target complex sugar molecules that play critical roles in numerous physiological processes.

7.3.3.1 Cancer treatment

One of the most promising applications of glycan-based therapy lies in cancer treatment. Many studies have reported the nonrandom alteration of glycosylation in cancer cells, for example, overexpression of MGAT5 (responsible for N-glycan branching) and FUT8 (transfer core fucose to N-glycan), and an increase of sialylation (Dube et al., 2005, Varki A, 2022, Pinho et al., 2015). Therefore, glycan-based biomarkers are currently used for diagnoses of cancers and monitoring of malignant progression (Adamczyk et al., 2012, Hu et al., 2019, Pinho et al., 2015). Targeting defective glycosylation pathways has the potential to be a novel approach to cancer treatment and metastasis prevention (Beheshti Zavareh et al., 2008). With the development of new techniques and knowledge of vaccine design, fully synthetic anti-vaccines targeting tumour-associated carbohydrates have been an attractive approach for cancer treatment (Li et al., 2010, Danishefsky et al., 2000).

7.3.3.2 Neurological disorders treatment

Glycans also play a crucial role in neurological disorders. Changes in glycosylation are associated with various neurological disorders, including Alzheimer’s disease, Parkinson’s disease, autism spectrum disorder, and schizophrenia (Pradeep et al., 2023). Emerging research indicates that glycan-based therapies may hold the key to treating neurodegenerative conditions like Alzheimer's and Parkinson's diseases (Pradeep et al., 2023, Burgi et al., 2021, Wang et al., 2019). Glycan modification of proteins involved in these diseases may offer a new avenue for disease modification and symptom management.

7.3.3.3 Glycan-based therapy in other diseases

The development of glycan-based therapeutics extends to other diseases including autoimmune diseases and infectious diseases as well. The ability to manipulate glycan structures to modulate immune responses opens new possibilities for treating diseases like RA, multiple sclerosis, and IBD (Dube et al., 2005, Hu et al.,

2019, Li et al., 2018, De Kivit et al., 2011). In addition, glycan-based therapy can disrupt the binding of pathogens to host cells or interfere with the replication cycle, offering an effective treatment against infectious diseases (Anderluh et al., 2021, Geissner et al., 2014, Echeverri et al., 2022).

7.3.4 Future and challenges

Looking ahead, the application of glycan-based strategies to current medical frameworks offers the potential for healthcare solutions that are not only more efficient but could also be tailored to individual patients. Glycan therapeutics are undoubtedly a frontier worth watching as they continue to shape the future of medicine (Paderi et al., 2018). The development of the combination of nanotechnology and glycans has shown a promising future of glycan-based immunotherapies (Anderluh et al., 2021).

Despite the immense promise of glycan-based therapeutics, several challenges remain. The complexity of glycans and the need for precise targeting present hurdles in drug development. The biosynthesis of glycans is not template-driven. The combination of the action of glycosyltransferases and glycosidases, and environmental factors (diet, lifestyle, and social factors) make the delineation of glycan function very slow and complex. Additionally, glycan-based therapies may require personalized approaches, given the variability in glycan structures among individuals. Tailoring therapies to an individual's specific glycan profile is a complex task that requires advances in diagnostics and treatment design. Developing standardized approaches for customization is challenging.

To sum up, glycan-based therapeutics have the potential to bring about a paradigm shift in the field of medicine. As our comprehension of glycans grows deeper, the promise of precision medicine and highly targeted therapies becomes more apparent. Collaborations between researchers, clinicians, and the pharmaceutical industry are driving innovation in this field, offering new hope for patients with a wide range of conditions.

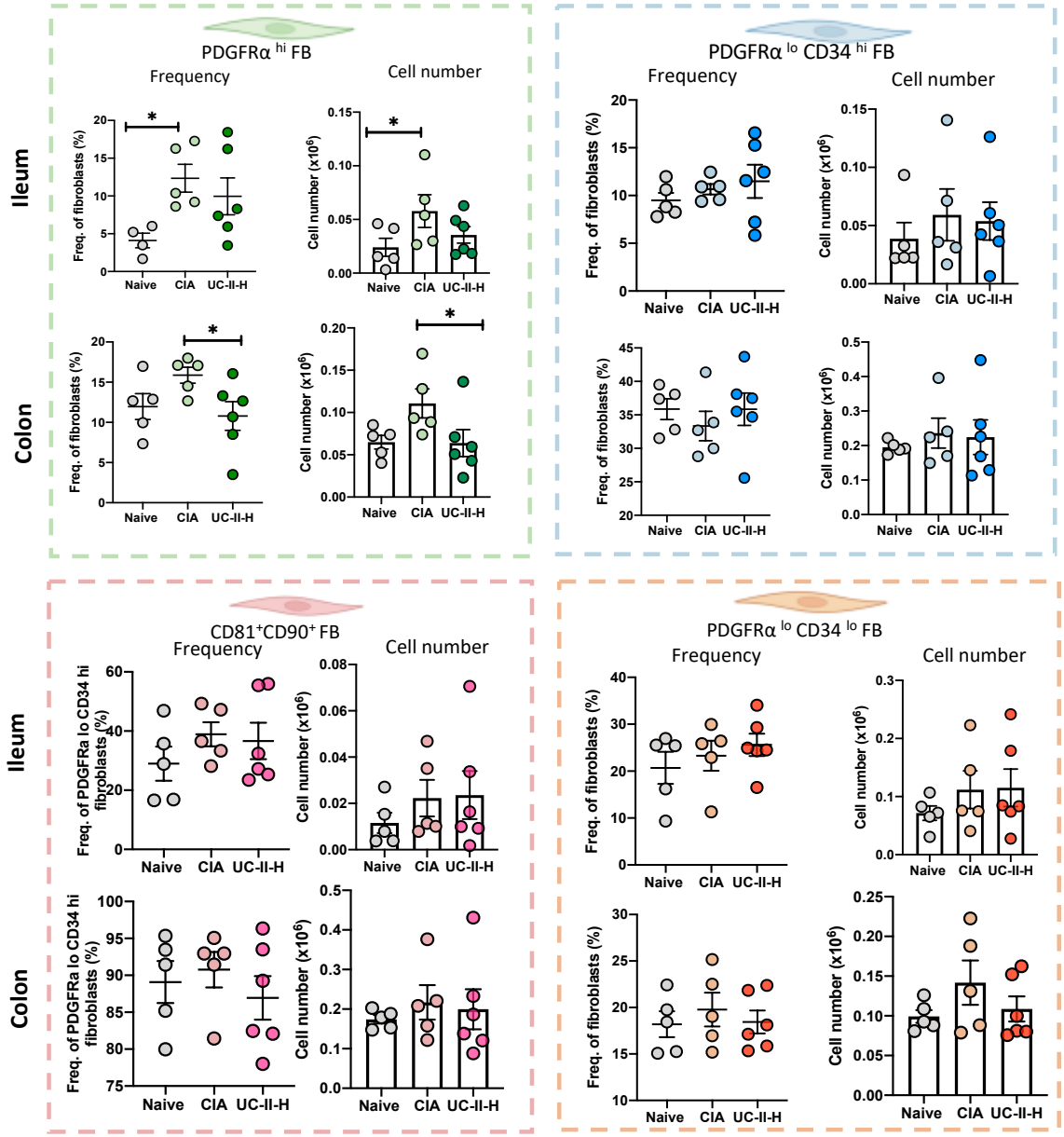

Figure 7-1 UC-II reduce PDGFRαhi fibroblast subset expansion in CIA.

Frequency and cell number of different fibroblast subsets in PDPN^{+} fibroblast in the ileum and colon. Each dot represents individual mouse. Statistical significance was determined using One-way ANOVA. Significance is indicated by asterisks, *p < 0.05. CIA, collagen induced arthritis; UC-II-H, UC-II higher dose.

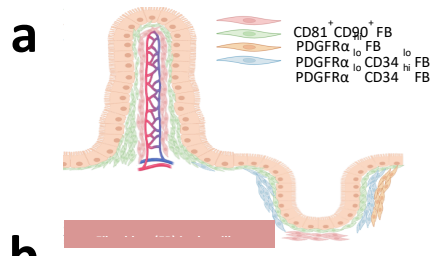
a
CD81+CD90+ FB
PDGFRα lo FB
PDGFRα lo CD34 lo hi FB
PDGFRα - CD34 lo hi FB

b

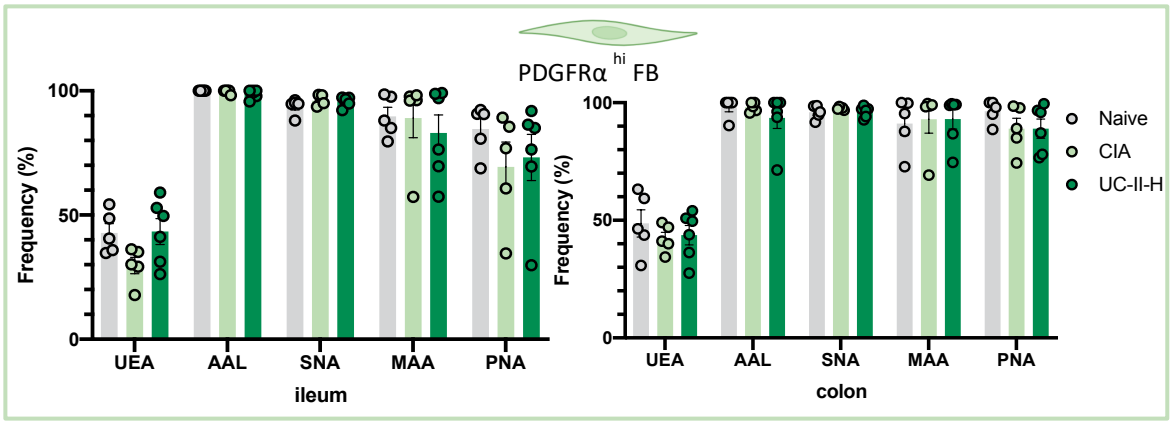
PDGFRα hi FB
Frequency (%)
100
50
0
UEA
AAL
SNA
MAA
PNA
ileum
colon
Naive
CIA
UC-II-H

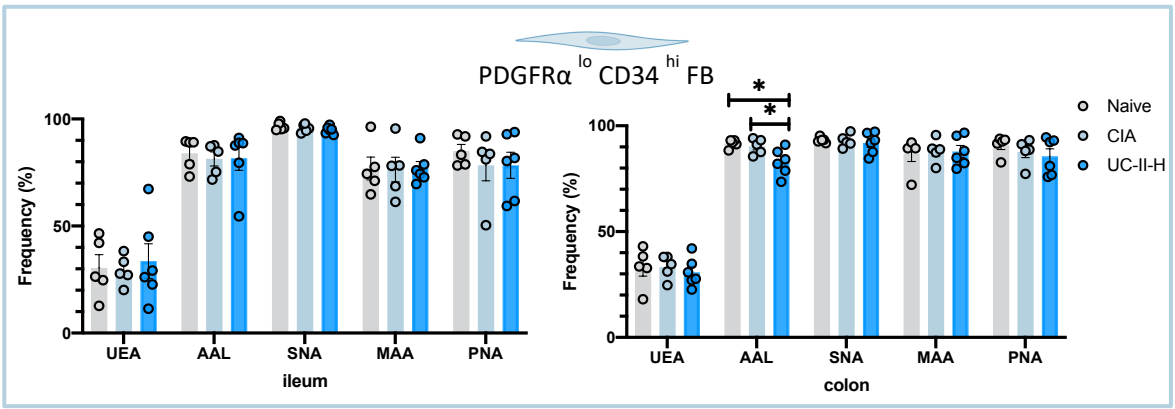
PDGFRα lo CD34 hi FB
Frequency (%)
100
50
0
UEA
AAL
SNA
MAA
PNA
ileum
colon
*
*
Naive
CIA
UC-II-H

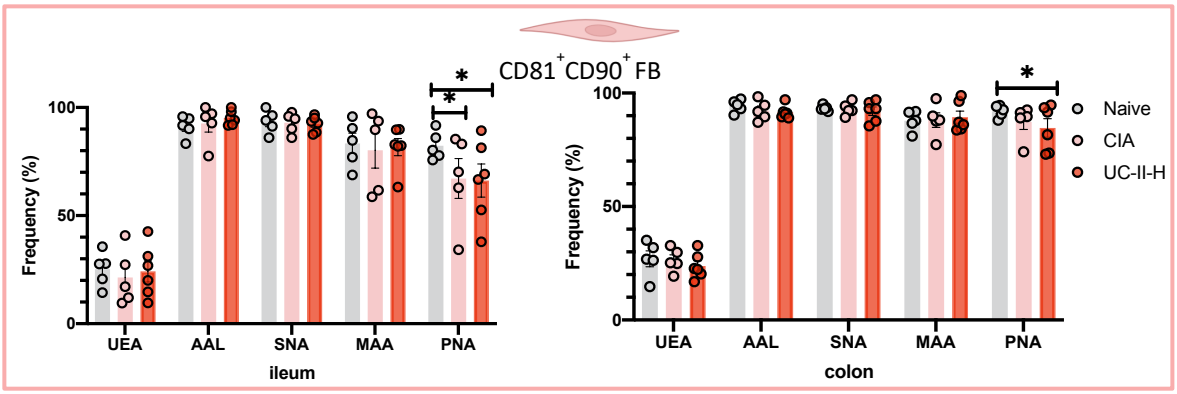
CD81+CD90+ FB
Frequency (%)
100
50
0
UEA
AAL
SNA
MAA
PNA
ileum
colon
*
*
*
Naive
CIA
UC-II-H

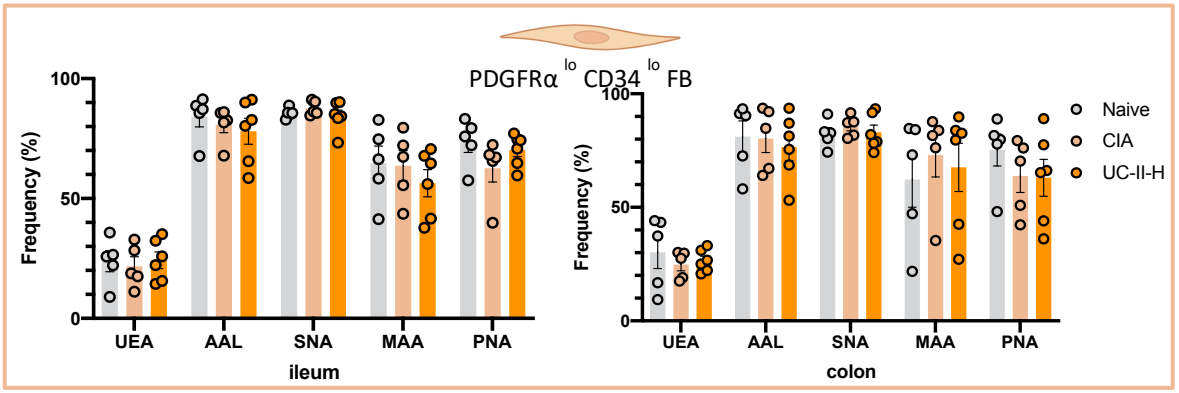
PDGFRα lo CD34 lo FB
Frequency (%)
100
50
0
UEA
AAL
SNA
MAA
PNA
ileum
colon
Naive
CIA
UC-II-H

Figure 7-2 Alteration of lectin binding expression of intestinal fibroblast subsets in UC-II treated mice during CIA.

a) Diagram of location of intestinal fibroblast subset. **b)** Frequency of lectin+ cells of each intestinal fibroblast subset in the ileum and colon. Each dot represents individual mouse. Statistical significance was determined using two-way ANOVA. Significance is indicated by asterisks, *p < 0.05. CIA, collagen induced arthritis; UC-II-H, UC-II higher dose; UEA, *Ulex Europaeus Agglutinin I*; AAL, *Aleuria aurantia lectin;* SNA, *Sambuccus nigra agglutinin*; MAA, *Maackia aurensis lectin II*; PNA, *Peanut agglutinin.*

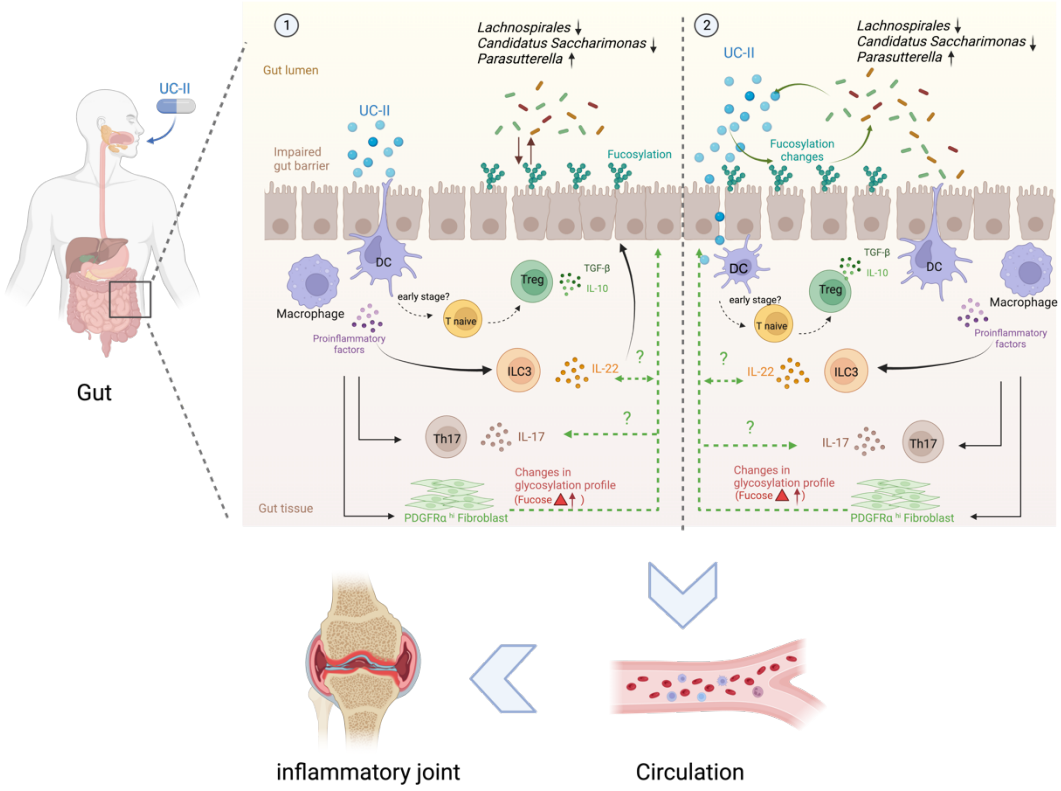

Figure 7-3 Potential mechanisms upon UC-II administration.

Possible mechanisms happened after UC-II administration. 1. It is possible that uptaking UC-II by APCs led to arthritis IL-17/IL-22 networks in the gut and reduced expansion of PDGFRα^{hi} intestinal fibroblast and changed its glycosylation. These changed the fucosylation profile of epithelial cells and therefore reduced abundance of *Lachnospirales* and *Candidatus Saccharimonas* in the gut, and also specifically increased the abundance of Parasutterella, subsequently affecting the glycan profile, especially fucose expression in the gut. This type of change promotes the gut immunity response to the bacteria in the gut as well, which forms an effective cycle to protect against gut damage and introduce oral tolerance during experimental arthritis, ultimately reducing inflammation in the joint due to the gut-joint axis. 2. Another possibility is that UC-II regulates the glycan expression in the gut, which initiates the regulation of microbial composition. The changes in bacteria promote the effectiveness of oral tolerance to rewire the cytokines expression. It can further affect gut immunity and responses to stimuli, which can help with intestinal homeostasis.

Chapter 8 Reference

Adamczyk, B., Tharmalingam, T. & Rudd, P. M. 2012. Glycans as cancer biomarkers. *Biochim Biophys Acta,* 1820**,** 1347-53.

Adrian Youings, S.-C. C., Raymond A. Dwek and Ian G. Scragg 1996. Site-specific glycosylation of human immunoglobulin G is altered in four rheumatoid arthritis patients. *Biochem. J,* 314**,** 621-630.

Alamilla-Beltrán, L., Chanona-Pérez, J. J., Jiménez-Aparicio, A. R. & Gutiérrez-López, G. F. 2005. Description of morphological changes of particles along spray drying. *Journal of Food Engineering,* 67**,** 179-184.

Alessio Ceroni, K. M., Hildegard Geyer, Rudolf Geyer, Anne Dell, and Stuart M. Haslam 2008. GlycoWorkbench: A Tool for the Computer-Assisted Annotation of Mass Spectra of Glycans. *Journal of Proteome Research***,** 1650-1659.

Alexandrecorthay, J. C., Johanbroddefalk, Erikmichae¨Lsson, Tomj. Goldschmidt, Jan Kihlberg and Rikard Holmdahl 1998. Epitope glycosylation plays a critical role for T cell recognition of type II collagen in collagen-induced arthritis. *Eur J Immunol,* 28**,** 2580-2590.

Alpizar-Rodriguez, D., Lesker, T. R., Gronow, A., Gilbert, B., Raemy, E., Lamacchia, C., Gabay, C., Finckh, A. & Strowig, T. 2019. Prevotella copri in individuals at risk for rheumatoid arthritis. *Ann Rheum Dis,* 78**,** 590-593.

Anderluh, M., Berti, F., Bzducha-Wrobel, A., Chiodo, F., Colombo, C., Compostella, F., Durlik, K., Ferhati, X., Holmdahl, R., Jovanovic, D., Kaca, W., Lay, L., Marinovic-Cincovic, M., Marradi, M., Ozil, M., Polito, L., Reina-Martin, J. J., Reis, C. A., Sackstein, R., Silipo, A., Svajger, U., Vanek, O., Yamamoto, F., Richichi, B. & Van Vliet, S. J. 2021. Emerging glyco-based strategies to steer immune responses. *FEBS J,* 288**,** 4746-4772.

Backlund, J., Carlsen, S., Hoger, T., Holm, B., Fugger, L., Kihlberg, J., Burkhardt, H. & Holmdahl, R. 2002. Predominant selection of T cells specific for the glycosylated collagen type II epitope (263-270) in humanized transgenic mice and in rheumatoid arthritis. *Proc Natl Acad Sci U S A,* 99**,** 9960-5.

Bagchi, D., Misner, B., Bagchi, M., Kothari, S. C., Downs, B. W., Fafard, R. D. & Preuss, H. G. 2002. Effects of orally administered undenatured type II collagen against arthritic inflammatory diseases: a mechanistic exploration. *Int J Clin Pharmacol Res,* 22**,** 101-10.

Bagchi D., M. B., Bagchi M., Kothari S.C., Downs B.W., Fafard.R.D., Preuss H.G. 2002. EFFECTS OF ORALLY ADMINISTRATION UNDENATURED TYPE II COLLAGEN AGAINST ARTHRITIC INFLAMMATORY DISEASES: A MECHNISTIC EXPLORATION. *INT.J.CLIN.PHARM.RES,* 22**,** 101-110.

Bagi, C. M., Berryman, E. R., Teo, S. & Lane, N. E. 2017. Oral administration of undenatured native chicken type II collagen (UC-II) diminished deterioration of articular cartilage in a rat model of osteoarthritis (OA). *Osteoarthritis Cartilage,* 25**,** 2080-2090.

Bann, J. G., Peyton, D. H. & Bachinger, H. P. 2000. Sweet is stable: glycosylation stabilizes collagen. *FEBS Lett,* 473**,** 237-40.

Bansil, R. & Turner, B. S. 2018. The biology of mucus: Composition, synthesis and organization. *Adv Drug Deliv Rev,* 124**,** 3-15.

Barbi, E., Longo, G., Berti, I., Matarazzo, L., Rubert, L., Saccari, A., Lenisa, I., Ronfani, L., Radillo, O. & Ventura, A. 2012a. Adverse effects during

specific oral tolerance induction: in home phase. *Allergol Immunopathol (Madr),* 40**,** 41-50.

Barbi, E., Longo, G., Berti, I., Neri, E., Saccari, A., Rubert, L., Matarazzo, L., Montico, M. & Ventura, A. 2012b. Adverse effects during specific oral tolerance induction: in-hospital "rush" phase. *Eur Ann Allergy Clin Immunol,* 44**,** 18-25.

Bauche, D. & Marie, J. C. 2017. Transforming growth factor beta: a master regulator of the gut microbiota and immune cell interactions. *Clin Transl Immunology,* 6**,** e136.

Beheshti Zavareh, R., Lau, K. S., Hurren, R., Datti, A., Ashline, D. J., Gronda, M., Cheung, P., Simpson, C. D., Liu, W., Wasylishen, A. R., Boutros, P. C., Shi, H., Vengopal, A., Jurisica, I., Penn, L. Z., Reinhold, V. N., Ezzat, S., Wrana, J., Rose, D. R., Schachter, H., Dennis, J. W. & Schimmer, A. D. 2008. Inhibition of the sodium/potassium ATPase impairs N-glycan expression and function. *Cancer Res,* 68**,** 6688-97.

Belkaid, Y. & Hand, T. W. 2014. Role of the microbiota in immunity and inflammation. *Cell,* 157**,** 121-41.

Bennett, E. P., Mandel, U., Clausen, H., Gerken, T. A., Fritz, T. A. & Tabak, L. A. 2012. Control of mucin-type O-glycosylation: a classification of the polypeptide GalNAc-transferase gene family. *Glycobiology,* 22**,** 736-56.

Bergstrom, K. S. & Xia, L. 2013. Mucin-type O-glycans and their roles in intestinal homeostasis. *Glycobiology,* 23**,** 1026-37.

Beswick, E. J., Johnson, J. R., Saada, J. I., Humen, M., House, J., Dann, S., Qiu, S., Brasier, A. R., Powell, D. W., Reyes, V. E. & Pinchuk, I. V. 2014. TLR4 activation enhances the PD-L1-mediated tolerogenic capacity of colonic CD90+ stromal cells. *J Immunol,* 193**,** 2218-29.

Beumer, J., Puschhof, J., Yengej, F. Y., Zhao, L., Martinez-Silgado, A., Blotenburg, M., Begthel, H., Boot, C., Van Oudenaarden, A., Chen, Y. G. & Clevers, H. 2022. BMP gradient along the intestinal villus axis controls zonated enterocyte and goblet cell states. *Cell Rep,* 38**,** 110438.

Bevins, C. L. & Salzman, N. H. 2011. Paneth cells, antimicrobial peptides and maintenance of intestinal homeostasis. *Nat Rev Microbiol,* 9**,** 356-68.

Birchenough, G. M., Johansson, M. E., Gustafsson, J. K., Bergstrom, J. H. & Hansson, G. C. 2015. New developments in goblet cell mucus secretion and function. *Mucosal Immunol,* 8**,** 712-9.

Bokers, S., Urbat, A., Daniel, C., Amann, K., Smith, K. G., Espeli, M. & Nitschke, L. 2014. Siglec-G deficiency leads to more severe collagen-induced arthritis and earlier onset of lupus-like symptoms in MRL/lpr mice. *J Immunol,* 192**,** 2994-3002.

Bottini, N., Vang, T., Cucca, F. & Mustelin, T. 2006. Role of PTPN22 in type 1 diabetes and other autoimmune diseases. *Semin Immunol,* 18**,** 207-13.

Bowman, C. C. & Selgrade, M. K. 2008. Failure to induce oral tolerance in mice is predictive of dietary allergenic potency among foods with sensitizing capacity. *Toxicol Sci,* 106**,** 435-43.

Brand, D. D., Marion, T. N., Myers, L. K., Rosloniec, E. F., Watson, W. C., Stuart, J. M. & Kang, A. H. 1996. Autoantibodies to murine type II collagen in collagen-induced arthritis: a comparison of susceptible and nonsusceptible strains. *J Immunol,* 157**,** 5178-84.

Brazil, J. C. & Parkos, C. A. 2021. Finding the sweet spot: glycosylation mediated regulation of intestinal inflammation. *Mucosal Immunol*.

Brennan-Olsen, S. L., Cook, S., Leech, M. T., Bowe, S. J., Kowal, P., Naidoo, N., Ackerman, I. N., Page, R. S., Hosking, S. M., Pasco, J. A. & Mohebbi, M. 2017. Prevalence of arthritis according to age, sex and socioeconomic

status in six low and middle income countries: analysis of data from the World Health Organization study on global AGEing and adult health (SAGE) Wave 1. *BMC Musculoskelet Disord,* 18**,** 271.
Brinkman-Van Der Linden, E. C., Sjoberg, E. R., Juneja, L. R., Crocker, P. R., Varki, N. & Varki, A. 2000. Loss of N-glycolylneuraminic acid in human evolution. Implications for sialic acid recognition by siglecs. *J Biol Chem,* 275**,** 8633-40.
Brugger, M. D. & Basler, K. 2023. The diverse nature of intestinal fibroblasts in development, homeostasis, and disease. *Trends Cell Biol*.
Burgi, M., Aparicio, G. I., Dorella, A., Kratje, R., Scorticati, C. & Oggero, M. 2021. Novel erythropoietin-based therapeutic candidates with extra N-glycan sites that block hematopoiesis but preserve neuroplasticity. *Biotechnol J,* 16**,** e2000455.
C Trollmo, M. V., A Tarkowski 1997. Fasting enhances mucosal antigen specific B cell responses in rheumatoid arthritis. *Ann Rheum Dis,* 56**,** 130-134.
Caio, G., Volta, U., Sapone, A., Leffler, D. A., De Giorgio, R., Catassi, C. & Fasano, A. 2019. Celiac disease: a comprehensive current review. *BMC Med,* 17**,** 142.
Campbell, I. K., Hamilton, J. A. & Wicks, I. P. 2000. Collagen-induced arthritis in C57BL/6 (H-2b) mice: new insights into an important disease model of rheumatoid arthritis. *Eur J Immunol,* 30**,** 1568-75.
Canavan, C., West, J. & Card, T. 2014. The epidemiology of irritable bowel syndrome. *Clin Epidemiol,* 6**,** 71-80.
Castenmiller, C., Keumatio-Doungtsop, B. C., Van Ree, R., De Jong, E. C. & Van Kooyk, Y. 2021. Tolerogenic Immunotherapy: Targeting DC Surface Receptors to Induce Antigen-Specific Tolerance. *Front Immunol,* 12**,** 643240.
Chalkidi, N., Paraskeva, C. & Koliaraki, V. 2022. Fibroblasts in intestinal homeostasis, damage, and repair. *Front Immunol,* 13**,** 924866.
Chen, J., Wright, K., Davis, J. M., Jeraldo, P., Marietta, E. V., Murray, J., Nelson, H., Matteson, E. L. & Taneja, V. 2016. An expansion of rare lineage intestinal microbes characterizes rheumatoid arthritis. *Genome Med,* 8**,** 43.
Cheroutre, H., Lambolez, F. & Mucida, D. 2011. The light and dark sides of intestinal intraepithelial lymphocytes. *Nat Rev Immunol,* 11**,** 445-56.
Choudhary, N., Bhatt, L. K. & Prabhavalkar, K. S. 2018. Experimental animal models for rheumatoid arthritis. *Immunopharmacol Immunotoxicol,* 40**,** 193-200.
Clevers, H. C. & Bevins, C. L. 2013. Paneth cells: maestros of the small intestinal crypts. *Annu Rev Physiol,* 75**,** 289-311.
Comstock, L. E. & Kasper, D. L. 2006. Bacterial glycans: key mediators of diverse host immune responses. *Cell,* 126**,** 847-50.
Cone, R. A. 2009. Barrier properties of mucus. *Adv Drug Deliv Rev,* 61**,** 75-85.
Connors, J., Dawe, N. & Van Limbergen, J. 2018. The Role of Succinate in the Regulation of Intestinal Inflammation. *Nutrients,* 11.
Cook, A. D., Rowley, M. J., Mackay, I. R., Gough, A. & Emery, P. 1996. Antibodies to type II collagen in early rheumatoid arthritis. Correlation with disease progression. *Arthritis Rheum,* 39**,** 1720-7.
Coombes, J. L. & Powrie, F. 2008. Dendritic cells in intestinal immune regulation. *Nat Rev Immunol,* 8**,** 435-46.
Coombes, J. L., Siddiqui, K. R. R., Arancibia-CáRcamo, C. V., Hall, J., Sun, C.-M., Belkaid, Y. & Powrie, F. 2007. A functionally specialized population of mucosal CD103+ DCs induces Foxp3+ regulatory T cells via a TGF-β-

and retinoic acid–dependent mechanism. *The Journal of Experimental Medicine,* 204**,** 1757-1764.

Corfield, L., Sylvester, Et Al 2000. Mucins and mucosal protection in the gastrointestinal tract: new prospects for mucins in the pathology of gastrointestinal disease. *Gut,* 47**,** 589-594.

Cornick, S., Tawiah, A. & Chadee, K. 2015. Roles and regulation of the mucus barrier in the gut. *Tissue Barriers,* 3**,** e982426.

Corthay, A., Backlund, J., Broddefalk, J., Michaelsson, E., Goldschmidt, T. J., Kihlberg, J. & Holmdahl, R. 1998. Epitope glycosylation plays a critical role for T cell recognition of type II collagen in collagen-induced arthritis. *Eur J Immunol,* 28**,** 2580-90.

Cosovanu, C. & Neumann, C. 2020. The Many Functions of Foxp3(+) Regulatory T Cells in the Intestine. *Front Immunol,* 11**,** 600973.

Courtenay, J. S. & Margaret J. Dallman, A. D. D., Angela Martin, Betty Mosedale 1980. Immunisation against heterologous

type II collagen induces arthritis in mice. *Nature,* 283**,** 666-668.

Crespo, H. J., Lau, J. T. & Videira, P. A. 2013. Dendritic cells: a spot on sialic Acid. *Front Immunol,* 4**,** 491.

Croft, A. P., Campos, J., Jansen, K., Turner, J. D., Marshall, J., Attar, M., Savary, L., Wehmeyer, C., Naylor, A. J., Kemble, S., Begum, J., Durholz, K., Perlman, H., Barone, F., Mcgettrick, H. M., Fearon, D. T., Wei, K., Raychaudhuri, S., Korsunsky, I., Brenner, M. B., Coles, M., Sansom, S. N., Filer, A. & Buckley, C. D. 2019. Distinct fibroblast subsets drive inflammation and damage in arthritis. *Nature,* 570**,** 246-251.

Cummings, R. D. & Pierce, J. M. 2014. The challenge and promise of glycomics. *Chem Biol,* 21**,** 1-15.

D'altilio, M., Peal, A., Alvey, M., Simms, C., Curtsinger, A., Gupta, R. C., Canerdy, T. D., Goad, J. T., Bagchi, M. & Bagchi, D. 2007. Therapeutic Efficacy and Safety of Undenatured Type II Collagen Singly or in Combination with Glucosamine and Chondroitin in Arthritic Dogs. *Toxicol Mech Methods,* 17**,** 189-96.

Dang, H., Harryvan, T. J. & Hawinkels, L. 2021. Fibroblast Subsets in Intestinal Homeostasis, Carcinogenesis, Tumor Progression, and Metastasis. *Cancers (Basel),* 13.

Daniel Mucida, Y. P., Gisen Kim, Olga Turovskaya, Iain Scott, Mitchell Kronenberg, Hilde Cheroutre 2007. Reciprocal T 17 and Regulatory T Cell Differentiation Mediated by Retinoic Acid. *Science,* 317**,** 256-260.

Danishefsky, S. J. & Allen, J. R. 2000. From the Laboratory to the Clinic: A Retrospective on Fully Synthetic Carbohydrate-Based Anticancer Vaccines. *Angewandte Chemie International Edition,* 39**,** 836-863.

Darling, N. J., Mobbs, C. L., González-Hau, A. L., Freer, M. & Przyborski, S. 2020. Bioengineering Novel in vitro Co-culture Models That Represent the Human Intestinal Mucosa With Improved Caco-2 Structure and Barrier Function. *Front Bioeng Biotechnol,* 8**,** 992.

David E. Trentham, A. H., Roselyn Trentham, Manashi Bagchi, Shil Kothari, Harry G. Preuss, Debasis Bagchi 2002. Treatment of Rheumatoid Arthritis Using Undenatured Type II Collagen. *THE ORIGINAL INTERNIST*.

Dayer, J. M., Oliviero, F. & Punzi, L. 2017. A Brief History of IL-1 and IL-1 Ra in Rheumatology. *Front Pharmacol,* 8**,** 293.

De Kivit, S., Kraneveld, A. D., Garssen, J. & Willemsen, L. E. 2011. Glycan recognition at the interface of the intestinal immune system: target for immune modulation via dietary components. *Eur J Pharmacol,* 668 Suppl 1**,** S124-32.

De Silva, N. S. & Klein, U. 2015. Dynamics of B cells in germinal centres. *Nat Rev Immunol,* 15**,** 137-48.

Deaglio, S., Dwyer, K. M., Gao, W., Friedman, D., Usheva, A., Erat, A., Chen, J. F., Enjyoji, K., Linden, J., Oukka, M., Kuchroo, V. K., Strom, T. B. & Robson, S. C. 2007. Adenosine generation catalyzed by CD39 and CD73 expressed on regulatory T cells mediates immune suppression. *J Exp Med,* 204**,** 1257-65.

Degirmenci, B., Valenta, T., Dimitrieva, S., Hausmann, G. & Basler, K. 2018. GLI1-expressing mesenchymal cells form the essential Wnt-secreting niche for colon stem cells. *Nature,* 558**,** 449-453.

Demetriou M, G. M., Quaggin S, Dennis Jw 2001. Negative regulation of T-cell activation and autoimmunity by Mgat5 N-glycosylation. *Nature,* 409**,** 733-739.

Dennis Jr, G., CéCile Tj Holweg, Sarah K Kummerfeld, David F Choy, a Francesca Setiadi, Jason a Hackney, Peter M Haverty, Houston Gilbert, Wei Yu Lin, Lauri Diehl, S Fischer, an Song, David Musselman, Micki Klearman, Cem Gabay, Arthur Kavanaugh, Judith Endres, David a Fox, Flavius Martin and Michael J Townsend 2014. Synovial phenotypes in rheumatoid arthritis correlate with response to biologic therapeutics. *Arthritis Research & Therapy,* 16**,** R19.

Dias, A. M., Pereira, M. S., Padrao, N. A., Alves, I., Marcos-Pinto, R., Lago, P. & Pinho, S. S. 2018. Glycans as critical regulators of gut immunity in homeostasis and disease. *Cell Immunol,* 333**,** 9-18.

Dokoshi, T., Seidman, J. S., Cavagnero, K. J., Li, F., Liggins, M. C., Taylor, B. C., Olvera, J., Knight, R., Chang, J. T., Salzman, N. H. & Gallo, R. L. 2021. Skin inflammation activates intestinal stromal fibroblasts and promotes colitis. *J Clin Invest,* 131.

Doonan, J., Tarafdar, A., Pineda, M. A., Lumb, F. E., Crowe, J., Khan, A. M., Hoskisson, P. A., Harnett, M. M. & Harnett, W. 2019. The parasitic worm product ES-62 normalises the gut microbiota bone marrow axis in inflammatory arthritis. *Nat Commun,* 10**,** 1554.

Dube, D. H. & Bertozzi, C. R. 2005. Glycans in cancer and inflammation--potential for therapeutics and diagnostics. *Nat Rev Drug Discov,* 4**,** 477-88.

Duca, M., Malagolini, N. & Dall'olio, F. 2023. The story of the Sd(a) antigen and of its cognate enzyme B4GALNT2: What is new? *Glycoconj J,* 40**,** 123-133.

E.Trentham, D. 1998. ORAL TOLERIZATION AS A TREATMENT OF RHEUMATOID ARTHRITIS. *RHEUMATIC DISEASE CLINICS OF NORTH AMERICA,* 24**,** 525-536.

Echeverri, D. & Orozco, J. 2022. Glycan-Based Electrochemical Biosensors: Promising Tools for the Detection of Infectious Diseases and Cancer Biomarkers. *Molecules,* 27.

Fawkner-Corbett, D., Antanaviciute, A., Parikh, K., Jagielowicz, M., Geros, A. S., Gupta, T., Ashley, N., Khamis, D., Fowler, D., Morrissey, E., Cunningham, C., Johnson, P. R. V., Koohy, H. & Simmons, A. 2021. Spatiotemporal analysis of human intestinal development at single-cell resolution. *Cell,* 184**,** 810-826 e23.

Fergusont, A. 1977. Intraepithelial lymphocytes of the small intestine. *Gut,* 18**,** 921-937.

Fermin Lee, A., Chen, H. Y., Wan, L., Wu, S. Y., Yu, J. S., Huang, A. C., Miaw, S. C., Hsu, D. K., Wu-Hsieh, B. A. & Liu, F. T. 2013. Galectin-3 modulates Th17 responses by regulating dendritic cell cytokines. *Am J Pathol,* 183**,** 1209-1222.

Fernandez-Veledo, S. & Vendrell, J. 2019. Gut microbiota-derived succinate: Friend or foe in human metabolic diseases? *Rev Endocr Metab Disord,* 20**,** 439-447.

Fleischmann, R., Mysler, E., Hall, S., Kivitz, A. J., Moots, R. J., Luo, Z., Demasi, R., Soma, K., Zhang, R., Takiya, L., Tatulych, S., Mojcik, C., Krishnaswami, S., Menon, S., Smolen, J. S. & Investigators, O. S. 2017. Efficacy and safety of tofacitinib monotherapy, tofacitinib with methotrexate, and adalimumab with methotrexate in patients with rheumatoid arthritis (ORAL Strategy): a phase 3b/4, double-blind, head-to-head, randomised controlled trial. *Lancet,* 390**,** 457-468.

Furuya, S. & Furuya, K. 2007. Subepithelial Fibroblasts in Intestinal Villi: Roles in Intercellular Communication.

Gabriel A. Rabinovich, M. I. M. I., Nidia M. Modesti, Leonardo F. Castagna, Carlota Wolfenstein-Todel, Clelia M. Riera, and Claudia E. Sotomayor 1998. Activated rat macrophages produce a galectin-1-like protein that induces apoptosis of T cells: biochemical and functional characterization. *The Journal of Immunology,* 160**,** 4831-4840.

Garber, J. M., Hennet, T. & Szymanski, C. M. 2021. Significance of fucose in intestinal health and disease. *Mol Microbiol,* 115**,** 1086-1093.

Garside, K., Mowat 1999. Oral tolerance in disease. *Gut,* 44**,** 137-142.

Geboes, L., Dumoutier, L., Kelchtermans, H., Schurgers, E., Mitera, T., Renauld, J. C. & Matthys, P. 2009. Proinflammatory role of the Th17 cytokine interleukin-22 in collagen-induced arthritis in C57BL/6 mice. *Arthritis Rheum,* 60**,** 390-5.

Geissner, A., Anish, C. & Seeberger, P. H. 2014. Glycan arrays as tools for infectious disease research. *Curr Opin Chem Biol,* 18**,** 38-45.

Giron, L. B., Tanes, C. E., Schleimann, M. H., Engen, P. A., Mattei, L. M., Anzurez, A., Damra, M., Zhang, H., Bittinger, K., Bushman, F., Kossenkov, A., Denton, P. W., Tateno, H., Keshavarzian, A., Landay, A. L. & Abdel-Mohsen, M. 2020. Sialylation and fucosylation modulate inflammasome-activating eIF2 Signaling and microbial translocation during HIV infection. *Mucosal Immunol,* 13**,** 753-766.

Go, M. F., Schrohenloher, R. E. & Tomana, M. 1994. Deficient galactosylation of serum IgG in inflammatory bowel disease: correlation with disease activity. *J Clin Gastroenterol,* 18**,** 86-7.

Gonzalo-Gil, E. & Galindo-Izquierdo, M. A. 2014. Role of Transforming Growth Factor-Beta (TGF) Beta in the Physiopathology of Rheumatoid Arthritis. *Reumatol Clin,* 10**,** 174-179.

Goto, Y., Obata, T., Kunisawa, J., Sato, S., Ivanov, Ii, Lamichhane, A., Takeyama, N., Kamioka, M., Sakamoto, M., Matsuki, T., Setoyama, H., Imaoka, A., Uematsu, S., Akira, S., Domino, S. E., Kulig, P., Becher, B., Renauld, J. C., Sasakawa, C., Umesaki, Y., Benno, Y. & Kiyono, H. 2014. Innate lymphoid cells regulate intestinal epithelial cell glycosylation. *Science,* 345**,** 1254009.

Goto, Y., Uematsu, S. & Kiyono, H. 2016. Epithelial glycosylation in gut homeostasis and inflammation. *Nat Immunol,* 17**,** 1244-1251.

Gracey, E., Vereecke, L., Mcgovern, D., Frohling, M., Schett, G., Danese, S., De Vos, M., Van Den Bosch, F. & Elewaut, D. 2020. Revisiting the gut-joint axis: links between gut inflammation and spondyloarthritis. *Nat Rev Rheumatol,* 16**,** 415-433.

Groux-Degroote, S., Cavdarli, S., Uchimura, K., Allain, F. & Delannoy, P. 2020. Glycosylation changes in inflammatory diseases. *Adv Protein Chem Struct Biol,* 119**,** 111-156.

Gryaznova, M., Dvoretskaya, Y., Burakova, I., Syromyatnikov, M., Popov, E., Kokina, A., Mikhaylov, E. & Popov, V. 2022. Dynamics of Changes in the Gut Microbiota of Healthy Mice Fed with Lactic Acid Bacteria and Bifidobacteria. *Microorganisms,* 10.

Guo, Z., Jang, M. H., Otani, K., Bai, Z., Umemoto, E., Matsumoto, M., Nishiyama, M., Yamasaki, M., Ueha, S., Matsushima, K., Hirata, T. & Miyasaka, M. 2008. CD4+CD25+ regulatory T cells in the small intestinal lamina propria show an effector/memory phenotype. *Int Immunol,* 20**,** 307-15.

Hayday, A. & Gibbons, D. 2008. Brokering the peace: the origin of intestinal T cells. *Mucosal Immunol,* 1**,** 172-4.

Herp, S., Durai Raj, A. C., Salvado Silva, M., Woelfel, S. & Stecher, B. 2021. The human symbiont Mucispirillum schaedleri: causality in health and disease. *Med Microbiol Immunol,* 210**,** 173-179.

Higgins, P. J. & Weiner, H. L. 1988. Suppression of experimental autoimmune encephalomyelitis by oral administration of myelin basic protein and its fragments. *J Immunol,* 140**,** 440-5.

Hiki, Y., Odani, H., Takahashi, M., Yasuda, Y., Nishimoto, A., Iwase, H., Shinzato, T., Kobayashi, Y. & Maeda, K. 2001. Mass spectrometry proves under-O-glycosylation of glomerular IgA1 in IgA nephropathy. *Kidney Int*, 59**,** 1077-85.

Hillman, E. T., Lu, H., Yao, T. & Nakatsu, C. H. 2017. Microbial Ecology along the Gastrointestinal Tract. *Microbes Environ,* 32**,** 300-313.

Holers, V. M. 2013. Autoimmunity to citrullinated proteins and the initiation of rheumatoid arthritis. *Curr Opin Immunol,* 25**,** 728-35.

Holers, V. M., Demoruelle, M. K., Kuhn, K. A., Buckner, J. H., Robinson, W. H., Okamoto, Y., Norris, J. M. & Deane, K. D. 2018. Rheumatoid arthritis and the mucosal origins hypothesis: protection turns to destruction. *Nat Rev Rheumatol,* 14**,** 542-557.

Hong, S. P., Yang, M. J., Cho, H., Park, I., Bae, H., Choe, K., Suh, S. H., Adams, R. H., Alitalo, K., Lim, D. & Koh, G. Y. 2020. Distinct fibroblast subsets regulate lacteal integrity through YAP/TAZ-induced VEGF-C in intestinal villi. *Nat Commun,* 11**,** 4102.

Hou, K., Wu, Z. X., Chen, X. Y., Wang, J. Q., Zhang, D., Xiao, C., Zhu, D., Koya, J. B., Wei, L., Li, J. & Chen, Z. S. 2022. Microbiota in health and diseases. *Signal Transduct Target Ther,* 7**,** 135.

Hoytema Van Konijnenburg, D. P., Reis, B. S., Pedicord, V. A., Farache, J., Victora, G. D. & Mucida, D. 2017. Intestinal Epithelial and Intraepithelial T Cell Crosstalk Mediates a Dynamic Response to Infection. *Cell,* 171**,** 783-794 e13.

Hu, M., Lan, Y., Lu, A., Ma, X. & Zhang, L. 2019. Glycan-based biomarkers for diagnosis of cancers and other diseases: Past, present, and future. *Prog Mol Biol Transl Sci,* 162**,** 1-24.

Hu, Y., Shen, F., Crellin, N. K. & Ouyang, W. 2011. The IL-17 pathway as a major therapeutic target in autoimmune diseases. *Ann N Y Acad Sci,* 1217**,** 60-76.

Human Microbiome Project, C. 2012. Structure, function and diversity of the healthy human microbiome. *Nature,* 486**,** 207-14.

Hyun, J. G. & Barrett, T. A. 2006. Oral tolerance therapy in inflammatory bowel disease. *Am J Gastroenterol,* 101**,** 569-71.

Ignacio, A., Shah, K., Bernier-Latmani, J., Koller, Y., Coakley, G., Moyat, M., Hamelin, R., Armand, F., Wong, N. C., Ramay, H., Thomson, C. A., Burkhard, R., Wang, H., Dufour, A., Geuking, M. B., Mcdonald, B.,

Petrova, T. V., Harris, N. L. & Mccoy, K. D. 2022. Small intestinal resident eosinophils maintain gut homeostasis following microbial colonization. *Immunity,* 55**,** 1250-1267 e12.

Ilarregui, J. M., Croci, D. O., Bianco, G. A., Toscano, M. A., Salatino, M., Vermeulen, M. E., Geffner, J. R. & Rabinovich, G. A. 2009. Tolerogenic signals delivered by dendritic cells to T cells through a galectin-1-driven immunoregulatory circuit involving interleukin 27 and interleukin 10. *Nat Immunol,* 10**,** 981-91.

Iozzo, R. V. & Schaefer, L. 2015. Proteoglycan form and function: A comprehensive nomenclature of proteoglycans. *Matrix Biol,* 42**,** 11-55.

Ismail, A. S., Severson, K. M., Vaishnava, S., Behrendt, C. L., Yu, X., Benjamin, J. L., Ruhn, K. A., Hou, B., Defranco, A. L., Yarovinsky, F. & Hooper, L. V. 2011a. Gammadelta intraepithelial lymphocytes are essential mediators of host-microbial homeostasis at the intestinal mucosal surface. *Proc Natl Acad Sci U S A,* 108**,** 8743-8.

Ismail, M. N., Stone, E. L., Panico, M., Lee, S. H., Luu, Y., Ramirez, K., Ho, S. B., Fukuda, M., Marth, J. D., Haslam, S. M. & Dell, A. 2011b. High-sensitivity O-glycomic analysis of mice deficient in core 2 beta1,6-N-acetylglucosaminyltransferases. *Glycobiology,* 21**,** 82-98.

Jacob, J. M., Di Carlo, S. E., Stzepourginski, I., Lepelletier, A., Ndiaye, P. D., Varet, H., Legendre, R., Kornobis, E., Benabid, A., Nigro, G. & Peduto, L. 2022. PDGFRalpha-induced stromal maturation is required to restrain postnatal intestinal epithelial stemness and promote defense mechanisms. *Cell Stem Cell,* 29**,** 856-868 e5.

Jakobsson, H. E., Rodriguez-Pineiro, A. M., Schutte, A., Ermund, A., Boysen, P., Bemark, M., Sommer, F., Backhed, F., Hansson, G. C. & Johansson, M. E. 2015. The composition of the gut microbiota shapes the colon mucus barrier. *EMBO Rep,* 16**,** 164-77.

Jandhyala, S. M., Talukdar, R., Subramanyam, C., Vuyyuru, H., Sasikala, M. & Nageshwar Reddy, D. 2015. Role of the normal gut microbiota. *World J Gastroenterol,* 21**,** 8787-803.

Jennifer A. Fulcher, S. T. H., Ernest L. Levroney, Mabel Pang, Kevin B. Gurney, Linda G. Baum, and Benhur Lee 2006. Galectin-1-Matured Human Monocyte-Derived Dendritic Cells Have Enhanced Migration through Extracellular Matrix. *The Journal of Immunology,* 177**,** 216-226.

Jianjun Li, J. C. R. 2010. *Functional Glycomics*.

Johannes A. Romijn, E. P. C., Louis M. Havekes and Hanno Pijl 2008. Gut-brain axis. *Current Opinion in Clinical Nutrition and Metabolic Care,* 11**,** 518-521.

Johansson, M. E., Larsson, J. M. & Hansson, G. C. 2011. The two mucus layers of colon are organized by the MUC2 mucin, whereas the outer layer is a legislator of host-microbial interactions. *Proc Natl Acad Sci U S A,* 108 Suppl 1**,** 4659-65.

Johnson, J. L., Jones, M. B., Ryan, S. O. & Cobb, B. A. 2013. The regulatory power of glycans and their binding partners in immunity. *Trends Immunol,* 34**,** 290-8.

Jones, C., Virji, M. & Crocker, P. R. 2003. Recognition of sialylated meningococcal lipopolysaccharide by siglecs expressed on myeloid cells leads to enhanced bacterial uptake. *Mol Microbiol,* 49**,** 1213-25.

Ju, T., Kong, J. Y., Stothard, P. & Willing, B. P. 2019. Defining the role of Parasutterella, a previously uncharacterized member of the core gut microbiota. *ISME J,* 13**,** 1520-1534.

Jubair, W. K., Hendrickson, J. D., Severs, E. L., Schulz, H. M., Adhikari, S., Ir, D., Pagan, J. D., Anthony, R. M., Robertson, C. E., Frank, D. N., Banda, N. K. & Kuhn, K. A. 2018. Modulation of Inflammatory Arthritis in Mice by Gut Microbiota Through Mucosal Inflammation and Autoantibody Generation. *Arthritis Rheumatol,* 70**,** 1220-1233.

Jussi Vaahtovuo Evelina Munukka, M. K., Reijo Luukkainen, and Paavo Toivanen 2008. Fecal Microbiota in Early Rheumatoid Arthritis. *The Journal of Rheumatology,* 35.

Kalepu, S. & Nekkanti, V. 2015. Insoluble drug delivery strategies: review of recent advances and business prospects. *Acta Pharm Sin B,* 5**,** 442-53.

Kaneko Y, N. F., Ravetch Jv 2006. Anti-Inflammatory Activity of Immunoglobulin G Resulting from Fc Sialylation. *Science,* 313**,** 670-673.

Kannan, K., Ortmann, R. A. & Kimpel, D. 2005. Animal models of rheumatoid arthritis and their relevance to human disease. *Pathophysiology,* 12**,** 167-81.

Karpus, O. N., Westendorp, B. F., Vermeulen, J. L. M., Meisner, S., Koster, J., Muncan, V., Wildenberg, M. E. & Van Den Brink, G. R. 2019. Colonic CD90+ Crypt Fibroblasts Secrete Semaphorins to Support Epithelial Growth. *Cell Rep,* 26**,** 3698-3708 e5.

Kastele, V., Mayer, J., Lee, E. S., Papazian, N., Cole, J. J., Cerovic, V., Belz, G., Tomura, M., Eberl, G., Goodyear, C., Maciewicz, R. A., Wall, D., Cupedo, T., Withers, D. R. & Milling, S. 2021. Intestinal-derived ILCs migrating in lymph increase IFNgamma production in response to Salmonella Typhimurium infection. *Mucosal Immunol,* 14**,** 717-727.

Katie Lynn Mason, G. B. H., Mairi C. Noverr Andjohn Y. Kao 2008. Overview of Gut Immunology.

Kelm, M., Quiros, M., Azcutia, V., Boerner, K., Cummings, R. D., Nusrat, A., Brazil, J. C. & Parkos, C. A. 2020. Targeting epithelium-expressed sialyl Lewis glycans improves colonic mucosal wound healing and protects against colitis. *JCI Insight,* 5.

Khatua, B., Ghoshal, A., Bhattacharya, K., Mandal, C., Saha, B., Crocker, P. R. & Mandal, C. 2010. Sialic acids acquired by Pseudomonas aeruginosa are involved in reduced complement deposition and siglec mediated host-cell recognition. *FEBS Lett,* 584**,** 555-61.

Kim, K. W., Kim, H. R., Park, J. Y., Park, J. S., Oh, H. J., Woo, Y. J., Park, M. K., Cho, M. L. & Lee, S. H. 2012. Interleukin-22 promotes osteoclastogenesis in rheumatoid arthritis through induction of RANKL in human synovial fibroblasts. *Arthritis Rheum,* 64**,** 1015-23.

Kim, S. H., Cho, B. H., Kiyono, H. & Jang, Y. S. 2017. Microbiota-derived butyrate suppresses group 3 innate lymphoid cells in terminal ileal Peyer's patches. *Sci Rep,* 7**,** 3980.

Kim, Y. S. & Ho, S. B. 2010. Intestinal goblet cells and mucins in health and disease: recent insights and progress. *Curr Gastroenterol Rep,* 12**,** 319-30.

Klose, C. S., Kiss, E. A., Schwierzeck, V., Ebert, K., Hoyler, T., D'hargues, Y., Goppert, N., Croxford, A. L., Waisman, A., Tanriver, Y. & Diefenbach, A. 2013. A T-bet gradient controls the fate and function of CCR6-RORgammat+ innate lymphoid cells. *Nature,* 494**,** 261-5.

Kong, S., Yanhui H. Zhang, and Weiqiang Zhang 2018. Regulation of Intestinal Epithelial Cells Properties and Functions by Amino Acids. *BioMed Research International***,** 1-10.

Kononova, S., Litvinova, E., Vakhitov, T., Skalinskaya, M. & Sitkin, S. 2021. Acceptive Immunity: The Role of Fucosylated Glycans in Human Host-Microbiome Interactions. *Int J Mol Sci,* 22.

Korsunsky, I., Wei, K., Pohin, M., Kim, E. Y., Barone, F., Major, T., Taylor, E., Ravindran, R., Kemble, S., Watts, G. F. M., Jonsson, A. H., Jeong, Y., Athar, H., Windell, D., Kang, J. B., Friedrich, M., Turner, J., Nayar, S., Fisher, B. A., Raza, K., Marshall, J. L., Croft, A. P., Tamura, T., Sholl, L. M., Vivero, M., Rosas, I. O., Bowman, S. J., Coles, M., Frei, A. P., Lassen, K., Filer, A., Powrie, F., Buckley, C. D., Brenner, M. B. & Raychaudhuri, S. 2022. Cross-tissue, single-cell stromal atlas identifies shared pathological fibroblast phenotypes in four chronic inflammatory diseases. *Med,* 3**,** 481-518 e14.

Kościelak, J. 2012. The Hypothesis on Function of Glycosphingolipids and ABO Blood Groups Revisited. *Neurochemical Research,* 37**,** 1170-1184.

Kosinski, C., Li, V. S., Chan, A. S., Zhang, J., Ho, C., Tsui, W. Y., Chan, T. L., Mifflin, R. C., Powell, D. W., Yuen, S. T., Leung, S. Y. & Chen, X. 2007. Gene expression patterns of human colon tops and basal crypts and BMP antagonists as intestinal stem cell niche factors. *Proc Natl Acad Sci U S A,* 104**,** 15418-23.

Kostopoulos, I., Aalvink, S., Kovatcheva-Datchary, P., Nijsse, B., Backhed, F., Knol, J., De Vos, W. M. & Belzer, C. 2021. A Continuous Battle for Host-Derived Glycans Between a Mucus Specialist and a Glycan Generalist in vitro and in vivo. *Front Microbiol,* 12**,** 632454.

Kotake, S., Udagawa, N., Takahashi, N., Matsuzaki, K., Itoh, K., Ishiyama, S., Saito, S., Inoue, K., Kamatani, N., Gillespie, M. T., Martin, T. J. & Suda, T. 1999. IL-17 in synovial fluids from patients with rheumatoid arthritis is a potent stimulator of osteoclastogenesis. *J Clin Invest,* 103**,** 1345-52.

Kucukural, A., Yukselen, O., Ozata, D. M., Moore, M. J. & Garber, M. 2019. DEBrowser: interactive differential expression analysis and visualization tool for count data. *BMC Genomics,* 20**,** 6.

Kudelka, M. R., Stowell, S. R., Cummings, R. D. & Neish, A. S. 2020. Intestinal epithelial glycosylation in homeostasis and gut microbiota interactions in IBD. *Nat Rev Gastroenterol Hepatol,* 17**,** 597-617.

Kwong, P. D. & Mascola, J. R. 2018. HIV-1 Vaccines Based on Antibody Identification, B Cell Ontogeny, and Epitope Structure. *Immunity,* 48**,** 855-871.

Lefferts, A. R., Norman, E., Claypool, D. J., Kantheti, U. & Kuhn, K. A. 2022. Cytokine competent gut-joint migratory T Cells contribute to inflammation in the joint. *Front Immunol,* 13**,** 932393.

Lerman, R. H., Chang, J. L., Konda, V., Desai, A. & Montalto, M. B. 2015. Nutritional Approach for Relief of Joint Discomfort: A 12-week, Open-case Series and Illustrative Case Report. *Integr Med (Encinitas),* 14**,** 52-61.

Li, M., Song, L. & Qin, X. 2010. Glycan changes: cancer metastasis and anti-cancer vaccines. *J Biosci,* 35**,** 665-73.

Li, R. E., Van Vliet, S. J. & Van Kooyk, Y. 2018. Using the glycan toolbox for pathogenic interventions and glycan immunotherapy. *Curr Opin Biotechnol,* 51**,** 24-31.

Liang, C. C., Li, C. S., Weng, I. C., Chen, H. Y., Lu, H. H., Huang, C. C. & Liu, F. T. 2018. Galectin-9 Is Critical for Mucosal Adaptive Immunity through the T Helper 17-IgA Axis. *Am J Pathol,* 188**,** 1225-1235.

Lin, C. Y., Nozawa, T., Minowa-Nozawa, A., Toh, H., Hikichi, M., Iibushi, J. & Nakagawa, I. 2020. Autophagy Receptor Tollip Facilitates Bacterial

Autophagy by Recruiting Galectin-7 in Response to Group A Streptococcus Infection. *Front Cell Infect Microbiol,* 10**,** 583137.

Lindemans, C. A., Calafiore, M., Mertelsmann, A. M., O'connor, M. H., Dudakov, J. A., Jenq, R. R., Velardi, E., Young, L. F., Smith, O. M., Lawrence, G., Ivanov, J. A., Fu, Y. Y., Takashima, S., Hua, G., Martin, M. L., O'rourke, K. P., Lo, Y. H., Mokry, M., Romera-Hernandez, M., Cupedo, T., Dow, L., Nieuwenhuis, E. E., Shroyer, N. F., Liu, C., Kolesnick, R., Van Den Brink, M. R. M. & Hanash, A. M. 2015. Interleukin-22 promotes intestinal-stem-cell-mediated epithelial regeneration. *Nature,* 528**,** 560-564.

Liu, F. T. & Stowell, S. R. 2023. The role of galectins in immunity and infection. *Nat Rev Immunol,* 23**,** 479-494.

Liu, J., Zhang, X., Cheng, Y. & Cao, X. 2021. Dendritic cell migration in inflammation and immunity. *Cell Mol Immunol,* 18**,** 2461-2471.

Liu, X., Zou, Q., Zeng, B., Fang, Y. & Wei, H. 2013. Analysis of fecal Lactobacillus community structure in patients with early rheumatoid arthritis. *Curr Microbiol,* 67**,** 170-6.

Luan, J., Hu, Z., Cheng, J., Zhang, R., Yang, P., Guo, H., Nan, G., Guo, N. & Gou, X. 2021. Applicability and implementation of the collagen-induced arthritis mouse model, including protocols (Review). *Exp Ther Med,* 22**,** 939.

Lubbers, J., Rodriguez, E. & Van Kooyk, Y. 2018. Modulation of Immune Tolerance via Siglec-Sialic Acid Interactions. *Front Immunol,* 9**,** 2807.

Lugo, J. P., Saiyed, Z. M. & Lane, N. E. 2016. Efficacy and tolerability of an undenatured type II collagen supplement in modulating knee osteoarthritis symptoms: a multicenter randomized, double-blind, placebo-controlled study. *Nutr J,* 15**,** 14.

Lugo, J. P., Saiyed, Z. M., Lau, F. C., Molina, J. P., Pakdaman, M. N., Shamie, A. N. & Udani, J. K. 2013. Undenatured type II collagen (UC-II(R)) for joint support: a randomized, double-blind, placebo-controlled study in healthy volunteers. *J Int Soc Sports Nutr,* 10**,** 48.

Mabbott, N. A., Donaldson, D. S., Ohno, H., Williams, I. R. & Mahajan, A. 2013. Microfold (M) cells: important immunosurveillance posts in the intestinal epithelium. *Mucosal Immunol,* 6**,** 666-77.

Macauley, M. S., Crocker, P. R. & Paulson, J. C. 2014. Siglec-mediated regulation of immune cell function in disease. *Nat Rev Immunol,* 14**,** 653-66.

Marinova-Mutafchieva, L. & R. O. Williams, L. J. M., C. Mauri, M. Feldmann, and R. N. Maini 1997. Dynamics of proinflammatory cytokine expression in the joints of mice with collagen-induced arthritis (CIA). *Clin Exp Immunol,* 197**,** 507-512.

Marko Salmi, D. P. A., Eugene C. Butcher, & Jalkanen, A. S. 1995. Dual Binding Capacity of Mucosal Immunoblasts to Mucosal and Synovial Endothellum in Humans: Dissection of the Molecular Mechanisms. *J. Exp. Med,* 181**,** 137-149.

Martins Dos Santos, V., Muller, M. & De Vos, W. M. 2010. Systems biology of the gut: the interplay of food, microbiota and host at the mucosal interface. *Curr Opin Biotechnol,* 21**,** 539-50.

Masahata, K., Umemoto, E., Kayama, H., Kotani, M., Nakamura, S., Kurakawa, T., Kikuta, J., Gotoh, K., Motooka, D., Sato, S., Higuchi, T., Baba, Y., Kurosaki, T., Kinoshita, M., Shimada, Y., Kimura, T., Okumura, R., Takeda, A., Tajima, M., Yoshie, O., Fukuzawa, M., Kiyono, H., Fagarasan, S., Iida, T., Ishii, M. & Takeda, K. 2014. Generation of colonic IgA-secreting cells in the caecal patch. *Nat Commun,* 5**,** 3704.

Maslowski, K. M. & Mackay, C. R. 2011. Diet, gut microbiota and immune responses. *Nat Immunol,* 12**,** 5-9.

Matei, D. E., Menon, M., Alber, D. G., Smith, A. M., Nedjat-Shokouhi, B., Fasano, A., Magill, L., Duhlin, A., Bitoun, S., Gleizes, A., Hacein-Bey-Abina, S., Manson, J. J., Rosser, E. C., Consortium, A., Klein, N., Blair, P. A. & Mauri, C. 2021. Intestinal barrier dysfunction plays an integral role in arthritis pathology and can be targeted to ameliorate disease. *Med (N Y),* 2**,** 864-883 e9.

May, E., Marker-Hermann, E., Wittig, B. M., Zeitz, M., Meyer Zum Buschenfelde, K. H. & Duchmann, R. 2000. Identical T-cell expansions in the colon mucosa and the synovium of a patient with enterogenic spondyloarthropathy. *Gastroenterology,* 119**,** 1745-55.

Mccarthy, N., Kraiczy, J. & Shivdasani, R. A. 2020a. Cellular and molecular architecture of the intestinal stem cell niche. *Nat Cell Biol,* 22**,** 1033-1041.

Mccarthy, N., Manieri, E., Storm, E. E., Saadatpour, A., Luoma, A. M., Kapoor, V. N., Madha, S., Gaynor, L. T., Cox, C., Keerthivasan, S., Wucherpfennig, K., Yuan, G. C., De Sauvage, F. J., Turley, S. J. & Shivdasani, R. A. 2020b. Distinct Mesenchymal Cell Populations Generate the Essential Intestinal BMP Signaling Gradient. *Cell Stem Cell,* 26**,** 391-402 e5.

Mcinnes, I. B., Leung, B. P., Harnett, M., Gracie, J. A., Liew, F. Y. & Harnett, W. 2003. A novel therapeutic approach targeting articular inflammation using the filarial nematode-derived phosphorylcholine-containing glycoprotein ES-62. *J Immunol,* 171**,** 2127-33.

Mcinnes, I. B. & Schett, G. 2007. Cytokines in the pathogenesis of rheumatoid arthritis. *Nat Rev Immunol,* 7**,** 429-42.

Mcinnes, I. B. & Schett, G. 2011. The Pathogenesis of Rheumatoid Arthritis. *The new england journal of medicine,* 365**,** 2205-19.

Meimei Shan, M. G., John R. Yeiser, A. Cooper Walland, Victor U. Bornstein, Kang Chen, Bing He, Linda Cassis, Anna Bigas, Montserrat Cols, Laura Comerma, Bihui Huang, J. Magarian Blander, Huabao Xiong, Lloyd Mayer, Cecilia Berin, Leonard H. Augenlicht, Anna Velcich, Andrea Cerutti 2013. Mucus Enhances Gut Homeostasis and Oral Tolerance by Delivering Immunoregulatory Signals. *Science,* 342**,** 447-453.

Meresse, B., Curran, S. A., Ciszewski, C., Orbelyan, G., Setty, M., Bhagat, G., Lee, L., Tretiakova, M., Semrad, C., Kistner, E., Winchester, R. J., Braud, V., Lanier, L. L., Geraghty, D. E., Green, P. H., Guandalini, S. & Jabri, B. 2006. Reprogramming of CTLs into natural killer-like cells in celiac disease. *J Exp Med,* 203**,** 1343-55.

Mimee, M., Citorik, R. J. & Lu, T. K. 2016. Microbiome therapeutics - Advances and challenges. *Adv Drug Deliv Rev,* 105**,** 44-54.

Moore, R., King, N. & Alroy, J 1988. Differences in cellular glycoconjugates of quiescent, inflamed, and neoplastic colonic epithelium in colitis and cancer-prone tamarins. *Am. J. Pathol,* 131**,** 484-489.

Moran, A. P., Gupta, A. & Joshi, L. 2011. Sweet-talk: role of host glycosylation in bacterial pathogenesis of the gastrointestinal tract. *Gut,* 60**,** 1412-25.

Morris, A. D. a. H. R. 2001. Glycoprotein Structure Determination by Mass Spectrometry. *Science,* 291**,** 2351-2356.

Moseley, T. A., Haudenschild, D. R., Rose, L. & Reddi, A. H. 2003. Interleukin-17 family and IL-17 receptors. *Cytokine & Growth Factor Reviews,* 14**,** 155-174.

Mowat, A. M. & Agace, W. W. 2014. Regional specialization within the intestinal immune system. *Nat Rev Immunol,* 14**,** 667-85.

Muller, S. & Radic, M. 2015. Citrullinated Autoantigens: From Diagnostic Markers to Pathogenetic Mechanisms. *Clin Rev Allergy Immunol,* 49**,** 232-9.

Murphy, T. L. & Murphy, K. M. 2022. Dendritic cells in cancer immunology. *Cell Mol Immunol,* 19**,** 3-13.

Nagao-Kitamoto, H., Leslie, J. L., Kitamoto, S., Jin, C., Thomsson, K. A., Gillilland, M. G., 3rd, Kuffa, P., Goto, Y., Jenq, R. R., Ishii, C., Hirayama, A., Seekatz, A. M., Martens, E. C., Eaton, K. A., Kao, J. Y., Fukuda, S., Higgins, P. D. R., Karlsson, N. G., Young, V. B. & Kamada, N. 2020. Interleukin-22-mediated host glycosylation prevents Clostridioides difficile infection by modulating the metabolic activity of the gut microbiota. *Nat Med,* 26**,** 608-617.

Nam, J. L., Takase-Minegishi, K., Ramiro, S., Chatzidionysiou, K., Smolen, J. S., Van Der Heijde, D., Bijlsma, J. W., Burmester, G. R., Dougados, M., Scholte-Voshaar, M., Van Vollenhoven, R. & Landewe, R. 2017. Efficacy of biological disease-modifying antirheumatic drugs: a systematic literature review informing the 2016 update of the EULAR recommendations for the management of rheumatoid arthritis. *Ann Rheum Dis,* 76**,** 1113-1136.

Nancy L. Perillo, K. E. P. & Jeffrey J. Seilhamer, L. G. B. 1995. Apoptosis of T cells mediated by galectin-1. *Nature,* 378**,** 736-739.

Natoli, M., Leoni, B. D., D'agnano, I., Zucco, F. & Felsani, A. 2012. Good Caco-2 cell culture practices. *Toxicol In Vitro,* 26**,** 1243-6.

Nielen, M. M., Van Schaardenburg, D., Reesink, H. W., Van De Stadt, R. J., Van Der Horst-Bruinsma, I. E., De Koning, M. H., Habibuw, M. R., Vandenbroucke, J. P. & Dijkmans, B. A. 2004. Specific autoantibodies precede the symptoms of rheumatoid arthritis: a study of serial measurements in blood donors. *Arthritis Rheum,* 50**,** 380-6.

O'connor, W., Jr., Zenewicz, L. A. & Flavell, R. A. 2010. The dual nature of T(H)17 cells: shifting the focus to function. *Nat Immunol,* 11**,** 471-6.

Olivares-Villagomez, D. & Van Kaer, L. 2018. Intestinal Intraepithelial Lymphocytes: Sentinels of the Mucosal Barrier. *Trends Immunol,* 39**,** 264-275.

Orhan, C., Juturu, V., Sahin, E., Tuzcu, M., Ozercan, I. H., Durmus, A. S., Sahin, N. & Sahin, K. 2021. Undenatured Type II Collagen Ameliorates Inflammatory Responses and Articular Cartilage Damage in the Rat Model of Osteoarthritis. *Front Vet Sci,* 8**,** 617789.

Osaka, T., Moriyama, E., Arai, S., Date, Y., Yagi, J., Kikuchi, J. & Tsuneda, S. 2017. Meta-Analysis of Fecal Microbiota and Metabolites in Experimental Colitic Mice during the Inflammatory and Healing Phases. *Nutrients,* 9.

Paderi, J., Prestwich, G. D., Panitch, A., Boone, T. & Stuart, K. 2018. Glycan Therapeutics: Resurrecting an Almost Pharma-Forgotten Drug Class. *Advanced Therapeutics,* 1.

Pærregaard, S. I., Schussek, S., Wulff, L., Niss, K., Mörbe, U., Jendholm, J., Wendland, K., Andrusaite, A. T., Brulois, K. F., Nibbs, R. J. B., Sitnik, K., Mowat, A. M., Butcher, E. C., Brunak, S. & Agace, W. W. 2021. The small and large intestine contain transcriptionally related mesenchymal stromal cell subsets that derive from embryonic Gli1+ mesothelial cells.

Paone, P. & Cani, P. D. 2020. Mucus barrier, mucins and gut microbiota: the expected slimy partners? *Gut,* 69**,** 2232-2243.

Park, K. S., Park, M. J., Cho, M. L., Kwok, S. K., Ju, J. H., Ko, H. J., Park, S. H. & Kim, H. Y. 2009. Type II collagen oral tolerance; mechanism and role

in collagen-induced arthritis and rheumatoid arthritis. *Mod Rheumatol,* 19**,** 581-9.

Parks, O. B., Pociask, D. A., Hodzic, Z., Kolls, J. K. & Good, M. 2015. Interleukin-22 Signaling in the Regulation of Intestinal Health and Disease. *Front Cell Dev Biol,* 3**,** 85.

Pascale, A., Marchesi, N., Marelli, C., Coppola, A., Luzi, L., Govoni, S., Giustina, A. & Gazzaruso, C. 2018. Microbiota and metabolic diseases. *Endocrine,* 61**,** 357-371.

Patnaude, L., Mayo, M., Mario, R., Wu, X., Knight, H., Creamer, K., Wilson, S., Pivorunas, V., Karman, J., Phillips, L., Dunstan, R., Kamath, R. V., Mcrae, B. & Terrillon, S. 2021. Mechanisms and regulation of IL-22-mediated intestinal epithelial homeostasis and repair. *Life Sci,* 271**,** 119195.

Paulson, J. C., Blixt, O. & Collins, B. E. 2006. Sweet spots in functional glycomics. *Nat Chem Biol,* 2**,** 238-48.

Pelaseyed, T. & Hansson, G. C. 2020. Membrane mucins of the intestine at a glance. *J Cell Sci,* 133.

Per Brandtzaeg, F.-E. J. 2005. Mucosal B cells: phenotypic characteristics, transcriptional regulation, and homing properties. *Immunological Reviews,* 206**,** 32-63.

Pereira, M. S., Alves, I., Vicente, M., Campar, A., Silva, M. C., Padrao, N. A., Pinto, V., Fernandes, A., Dias, A. M. & Pinho, S. S. 2018. Glycans as Key Checkpoints of T Cell Activity and Function. *Front Immunol,* 9**,** 2754.

Peri, S., Kulkarni, A., Feyertag, F., Berninsone, P. M. & Alvarez-Ponce, D. 2018. Phylogenetic Distribution of CMP-Neu5Ac Hydroxylase (CMAH), the Enzyme Synthetizing the Proinflammatory Human Xenoantigen Neu5Gc. *Genome Biol Evol,* 10**,** 207-219.

Perota, A. & Galli, C. 2019. N-Glycolylneuraminic Acid (Neu5Gc) Null Large Animals by Targeting the CMP-Neu5Gc Hydroxylase (CMAH). *Front Immunol,* 10**,** 2396.

Persson, E. K., Scott, C. L., Mowat, A. M. & Agace, W. W. 2013a. Dendritic cell subsets in the intestinal lamina propria: ontogeny and function. *Eur J Immunol,* 43**,** 3098-107.

Persson, E. K., Uronen-Hansson, H., Semmrich, M., Rivollier, A., Hagerbrand, K., Marsal, J., Gudjonsson, S., Hakansson, U., Reizis, B., Kotarsky, K. & Agace, W. W. 2013b. IRF4 transcription-factor-dependent CD103(+)CD11b(+) dendritic cells drive mucosal T helper 17 cell differentiation. *Immunity,* 38**,** 958-69.

Pham, T. A., Clare, S., Goulding, D., Arasteh, J. M., Stares, M. D., Browne, H. P., Keane, J. A., Page, A. J., Kumasaka, N., Kane, L., Mottram, L., Harcourt, K., Hale, C., Arends, M. J., Gaffney, D. J., Sanger Mouse Genetics, P., Dougan, G. & Lawley, T. D. 2014. Epithelial IL-22RA1-mediated fucosylation promotes intestinal colonization resistance to an opportunistic pathogen. *Cell Host Microbe,* 16**,** 504-16.

Phillips A.D., S. N., S Hicks, G Dougan, T Wallis, G Frankel 2000. Enterohaemorrhagic Escherichia coli O157:H7 target Peyer's patches in humans and cause attaching/eVacing lesions in both human and bovine intestine. *Gut,* 47**,** 377-381.

Pickard, J. M. & Chervonsky, A. V. 2015. Intestinal fucose as a mediator of host-microbe symbiosis. *J Immunol,* 194**,** 5588-93.

Pickert, G., Neufert, C., Leppkes, M., Zheng, Y., Wittkopf, N., Warntjen, M., Lehr, H. A., Hirth, S., Weigmann, B., Wirtz, S., Ouyang, W., Neurath, M.

F. & Becker, C. 2009. STAT3 links IL-22 signaling in intestinal epithelial cells to mucosal wound healing. *J Exp Med,* 206**,** 1465-72.

Pineda, M. A., Mcgrath, M. A., Smith, P. C., Al-Riyami, L., Rzepecka, J., Gracie, J. A., Harnett, W. & Harnett, M. M. 2012. The parasitic helminth product ES-62 suppresses pathogenesis in collagen-induced arthritis by targeting the interleukin-17-producing cellular network at multiple sites. *Arthritis Rheum,* 64**,** 3168-78.

Pineda, M. A., Rodgers, D. T., Al-Riyami, L., Harnett, W. & Harnett, M. M. 2014. ES-62 protects against collagen-induced arthritis by resetting interleukin-22 toward resolution of inflammation in the joints. *Arthritis Rheumatol,* 66**,** 1492-503.

Ping Zhu, X. L., Hongkun Wang, Junfeng Jia, Zhaohui Zheng, Jin Ding, Chunmei Fan 2007. Oral administration of type-II collagen peptide 250--270 suppresses specific cellular and humoral immune response in collagen-induced arthritis. *Clinical Immunology***,** 75-84.

Pinheiro-Rosa, N., Torres, L., Oliveira, M. A., Andrade-Oliveira, M. F., Guimaraes, M. a. F., Coelho, M. M., Alves, J. L., Maioli, T. U. & Faria, A. M. C. 2021. Oral tolerance as antigen-specific immunotherapy. *Immunother Adv,* 1**,** ltab017.

Pinho, S. S. & Reis, C. A. 2015. Glycosylation in cancer: mechanisms and clinical implications. *Nat Rev Cancer,* 15**,** 540-55.

Powell, D. W., Pinchuk, I. V., Saada, J. I., Chen, X. & Mifflin, R. C. 2011. Mesenchymal cells of the intestinal lamina propria. *Annu Rev Physiol,* 73**,** 213-37.

Pradeep, P., Kang, H. & Lee, B. 2023. Glycosylation and behavioral symptoms in neurological disorders. *Transl Psychiatry,* 13**,** 154.

Qiu, Y. & Yang, H. 2013. Effects of intraepithelial lymphocyte-derived cytokines on intestinal mucosal barrier function. *J Interferon Cytokine Res,* 33**,** 551-62.

Querol Cano, L., Tagit, O., Dolen, Y., Van Duffelen, A., Dieltjes, S., Buschow, S. I., Niki, T., Hirashima, M., Joosten, B., Van Den Dries, K., Cambi, A., Figdor, C. G. & Van Spriel, A. B. 2019. Intracellular Galectin-9 Controls Dendritic Cell Function by Maintaining Plasma Membrane Rigidity. *iScience,* 22**,** 240-255.

R.Pabst 1987. The anatomical basis for the immune function of the gut. *Anatomy and Embryology,* 176**,** 135-144.

Rabinovich, G. A. 2010. A sweet path toward tolerance in the gut. *Nat Med,* 16**,** 1076-7.

Rabinovich, G. A., Van Kooyk, Y. & Cobb, B. A. 2012. Glycobiology of immune responses. *Ann N Y Acad Sci,* 1253**,** 1-15.

Rajilic-Stojanovic, M. 2013. Function of the microbiota. *Best Pract Res Clin Gastroenterol,* 27**,** 5-16.

Rantapaa-Dahlqvist, S., De Jong, B. A., Berglin, E., Hallmans, G., Wadell, G., Stenlund, H., Sundin, U. & Van Venrooij, W. J. 2003. Antibodies against cyclic citrullinated peptide and IgA rheumatoid factor predict the development of rheumatoid arthritis. *Arthritis Rheum,* 48**,** 2741-9.

Rausch, P., Rehman, A., Kunzel, S., Hasler, R., Ott, S. J., Schreiber, S., Rosenstiel, P., Franke, A. & Baines, J. F. 2011. Colonic mucosa-associated microbiota is influenced by an interaction of Crohn disease and FUT2 (Secretor) genotype. *Proc Natl Acad Sci U S A,* 108**,** 19030-5.

Reily, C., Stewart, T. J., Renfrow, M. B. & Novak, J. 2019. Glycosylation in health and disease. *Nat Rev Nephrol,* 15**,** 346-366.

Reparaz, D., Hommel, M., Navarro, F. & Llopiz, D. 2022. The role of dendritic cells in the immune niche of the peritoneum. *Int Rev Cell Mol Biol,* 371, 1-14.

Rindi, G., Leiter, A. B., Kopin, A. S., Bordi, C. & Solcia, E. 2004. The "normal" endocrine cell of the gut: changing concepts and new evidences. *Ann N Y Acad Sci,* 1014, 1-12.

Rohani, M., Noohi, N., Talebi, M., Katouli, M. & Pourshafie, M. R. 2015. Highly Heterogeneous Probiotic Lactobacillus Species in Healthy Iranians with Low Functional Activities. *PLoS One,* 10, e0144467.

Roulis, M. & Flavell, R. A. 2016. Fibroblasts and myofibroblasts of the intestinal lamina propria in physiology and disease. *Differentiation,* 92, 116-131.

Rui, F., Jiawei, K., Yuntao, H., Xinran, L., Jiani, H., Ruixue, M., Rui, L., Na, Z., Meihong, X. & Yong, L. 2021. Undenatured type II collagen prevents and treats osteoarthritis and motor function degradation in T2DM patients and db/db mice. *Food Funct,* 12, 4373-4391.

Ryan, S. O., Bonomo, J. A., Zhao, F. & Cobb, B. A. 2011. MHCII glycosylation modulates Bacteroides fragilis carbohydrate antigen presentation. *J Exp Med,* 208, 1041-53.

Sahin, E., Orhan, C., Erten, F., Saiyed, Z., Azari, E. K., Durkee, S. & Sahin, K. 2023. The effect of oral administration of undenatured type II collagen on monosodium iodoacetate-induced osteoarthritis in young and old rats. *Sci Rep,* 13, 6499.

Sandya, S. & Sudhakaran, M. a. a. a. P. R. 2009. MULTIPLE MATRIX METALLOPROTEINASES IN TYPE II COLLAGEN INDUCED ARTHRITIS. *Indian Journal of Clinical Biochemistry,* 24.

Sareen, S., Mathew, G. & Joseph, L. 2012. Improvement in solubility of poor water-soluble drugs by solid dispersion. *Int J Pharm Investig,* 2, 12-7.

Scheiman, J. M. 2016. NSAID-induced Gastrointestinal Injury: A Focused Update for Clinicians. *J Clin Gastroenterol,* 50, 5-10.

Scher, J. U., Sczesnak, A., Longman, R. S., Segata, N., Ubeda, C., Bielski, C., Rostron, T., Cerundolo, V., Pamer, E. G., Abramson, S. B., Huttenhower, C. & Littman, D. R. 2013. Expansion of intestinal Prevotella copri correlates with enhanced susceptibility to arthritis. *Elife,* 2, e01202.

Schnaar, R. L. 2016. Glycobiology simplified: diverse roles of glycan recognition in inflammation. *J Leukoc Biol,* 99, 825-38.

Schon, C., Knaub, K., Alt, W., Durkee, S., Saiyed, Z. & Juturu, V. 2022. UC-II Undenatured Type II Collagen for Knee Joint Flexibility: A Multicenter, Randomized, Double-Blind, Placebo-Controlled Clinical Study. *J Integr Complement Med,* 28, 540-548.

Schroeder, B. O. 2019. Fight them or feed them: how the intestinal mucus layer manages the gut microbiota. *Gastroenterol Rep (Oxf),* 7, 3-12.

Schulte, S., Unger, C., Mo, J. A., Wendler, O., Bauer, E., Frischholz, S., Von Der Mark, K., Kalden, J. R., Holmdahl, R. & Burkhardt, H. 1998. Arthritis-related B cell epitopes in collagen II are conformation-dependent and sterically privileged in accessible sites of cartilage collagen fibrils. *J Biol Chem,* 273, 1551-61.

Schulze-Koops, H. & Kalden, J. R. 2001. The balance of Th1/Th2 cytokines in rheumatoid arthritis. *Best Pract Res Clin Rheumatol,* 15, 677-91.

Scott M. Wilhelm, I. E. C., Annemarie Kronberger, Arthur Z. Eisen, Barry L. Marmer, Gregory A. Grant, Eugene A. Bauer, Gregory I.Goldberg 1987. Human skin fibroblast stromelysin: structure glycosylation substrate specificity and differential. *Proc Natl Acad Sci U S A,* 84, 6725-6729.

Sekirov, I., Russell, S. L., Antunes, L. C. & Finlay, B. B. 2010. Gut microbiota in health and disease. *Physiol Rev,* 90**,** 859-904.

Severi, E., Hood, D. W. & Thomas, G. H. 2007. Sialic acid utilization by bacterial pathogens. *Microbiology (Reading),* 153**,** 2817-2822.

Shan, M., Gentile, M., Yeiser, J. R., Walland, A. C., Bornstein, V. U., Chen, K., He, B., Cassis, L., Bigas, A., Cols, M., Comerma, L., Huang, B., Blander, J. M., Xiong, H., Mayer, L., Berin, C., Augenlicht, L. H., Velcich, A. & Cerutti, A. 2013. Mucus enhances gut homeostasis and oral tolerance by delivering immunoregulatory signals. *Science,* 342**,** 447-53.

Shi, N., Li, N., Duan, X. & Niu, H. 2017. Interaction between the gut microbiome and mucosal immune system. *Mil Med Res,* 4**,** 14.

Smolen, G. N. S. a. J. 2002. Autoantibodies in rheumatoid arthritis and their clinical significance. *Arthritis Research,* 4**,** S1-S5.

Smolen, J. S., Aletaha, D., Barton, A., Burmester, G. R., Emery, P., Firestein, G. S., Kavanaugh, A., Mcinnes, I. B., Solomon, D. H., Strand, V. & Yamamoto, K. 2018. Rheumatoid arthritis. *Nat Rev Dis Primers,* 4**,** 18001.

Smolen, J. S., Landewe, R., Bijlsma, J., Burmester, G., Chatzidionysiou, K., Dougados, M., Nam, J., Ramiro, S., Voshaar, M., Van Vollenhoven, R., Aletaha, D., Aringer, M., Boers, M., Buckley, C. D., Buttgereit, F., Bykerk, V., Cardiel, M., Combe, B., Cutolo, M., Van Eijk-Hustings, Y., Emery, P., Finckh, A., Gabay, C., Gomez-Reino, J., Gossec, L., Gottenberg, J. E., Hazes, J. M. W., Huizinga, T., Jani, M., Karateev, D., Kouloumas, M., Kvien, T., Li, Z., Mariette, X., Mcinnes, I., Mysler, E., Nash, P., Pavelka, K., Poor, G., Richez, C., Van Riel, P., Rubbert-Roth, A., Saag, K., Da Silva, J., Stamm, T., Takeuchi, T., Westhovens, R., De Wit, M. & Van Der Heijde, D. 2017. EULAR recommendations for the management of rheumatoid arthritis with synthetic and biological disease-modifying antirheumatic drugs: 2016 update. *Ann Rheum Dis,* 76**,** 960-977.

Srinivasan, B., Kolli, A. R., Esch, M. B., Abaci, H. E., Shuler, M. L. & Hickman, J. J. 2015. TEER measurement techniques for in vitro barrier model systems. *J Lab Autom,* 20**,** 107-26.

Stabile, M., Girelli, C. R., Lacitignola, L., Samarelli, R., Crovace, A., Fanizzi, F. P. & Staffieri, F. 2022. (1)H-NMR metabolomic profile of healthy and osteoarthritic canine synovial fluid before and after UC-II supplementation. *Sci Rep,* 12**,** 19716.

Stamp, L. K., James, M. J. & Cleland, L. G. 2005. Diet and rheumatoid arthritis: a review of the literature. *Semin Arthritis Rheum,* 35**,** 77-94.

Stefka, A. T., Feehley, T., Tripathi, P., Qiu, J., Mccoy, K., Mazmanian, S. K., Tjota, M. Y., Seo, G. Y., Cao, S., Theriault, B. R., Antonopoulos, D. A., Zhou, L., Chang, E. B., Fu, Y. X. & Nagler, C. R. 2014. Commensal bacteria protect against food allergen sensitization. *Proc Natl Acad Sci U S A,* 111**,** 13145-50.

Stephen-Victor, E. & Chatila, T. A. 2019. Regulation of oral immune tolerance by the microbiome in food allergy. *Curr Opin Immunol,* 60**,** 141-147.

Stojanov, S., Berlec, A. & Strukelj, B. 2020. The Influence of Probiotics on the Firmicutes/Bacteroidetes Ratio in the Treatment of Obesity and Inflammatory Bowel disease. *Microorganisms,* 8.

Strehl, C., Bijlsma, J. W., De Wit, M., Boers, M., Caeyers, N., Cutolo, M., Dasgupta, B., Dixon, W. G., Geenen, R., Huizinga, T. W., Kent, A., De Thurah, A. L., Listing, J., Mariette, X., Ray, D. W., Scherer, H. U., Seror, R., Spies, C. M., Tarp, S., Wiek, D., Winthrop, K. L. & Buttgereit, F. 2016. Defining conditions where long-term glucocorticoid treatment has

an acceptably low level of harm to facilitate implementation of existing recommendations: viewpoints from an EULAR task force. *Ann Rheum Dis,* 75**,** 952-7.

Stzepourginski, I., Nigro, G., Jacob, J. M., Dulauroy, S., Sansonetti, P. J., Eberl, G. & Peduto, L. 2017. CD34+ mesenchymal cells are a major component of the intestinal stem cells niche at homeostasis and after injury. *Proc Natl Acad Sci U S A,* 114**,** E506-E513.

Sugimoto, K., Ogawa, A., Mizoguchi, E., Shimomura, Y., Andoh, A., Bhan, A. K., Blumberg, R. S., Xavier, R. J. & Mizoguchi, A. 2008. IL-22 ameliorates intestinal inflammation in a mouse model of ulcerative colitis. *J Clin Invest,* 118**,** 534-44.

Suwandi, A., Alvarez, K. G., Galeev, A., Steck, N., Riedel, C. U., Puente, J. L., Baines, J. F. & Grassl, G. A. 2022. B4galnt2-mediated host glycosylation influences the susceptibility to Citrobacter rodentium infection. *Front Microbiol,* 13**,** 980495.

Swidsinski A, L.-B. V., Lochs H, Hale Lp 2005. Spatial organization of bacterial flora in normal and inflamed intestine: A fluorescence in situ hybridization study in mice. *World J Gastroenterol,* 11**,** 1131-1140.

Tang, F., Chen, Z., Ciszewski, C., Setty, M., Solus, J., Tretiakova, M., Ebert, E., Han, J., Lin, A., Guandalini, S., Groh, V., Spies, T., Green, P. & Jabri, B. 2009. Cytosolic PLA2 is required for CTL-mediated immunopathology of celiac disease via NKG2D and IL-15. *J Exp Med,* 206**,** 707-19.

Terahara, K., Nochi, T., Yoshida, M., Takahashi, Y., Goto, Y., Hatai, H., Kurokawa, S., Jang, M. H., Kweon, M. N., Domino, S. E., Hiroi, T., Yuki, Y., Tsunetsugu-Yokota, Y., Kobayashi, K. & Kiyono, H. 2011. Distinct fucosylation of M cells and epithelial cells by Fut1 and Fut2, respectively, in response to intestinal environmental stress. *Biochem Biophys Res Commun,* 404**,** 822-8.

Thomson, C. A., Van De Pavert, S. A., Stakenborg, M., Labeeuw, E., Matteoli, G., Mowat, A. M. & Nibbs, R. J. B. 2018. Expression of the Atypical Chemokine Receptor ACKR4 Identifies a Novel Population of Intestinal Submucosal Fibroblasts That Preferentially Expresses Endothelial Cell Regulators. *J Immunol,* 201**,** 215-229.

Thurston, T. L., Wandel, M. P., Von Muhlinen, N., Foeglein, A. & Randow, F. 2012. Galectin 8 targets damaged vesicles for autophagy to defend cells against bacterial invasion. *Nature,* 482**,** 414-8.

Tizaoui, K., Terrazzino, S., Cargnin, S., Lee, K. H., Gauckler, P., Li, H., Shin, J. I. & Kronbichler, A. 2021. The role of PTPN22 in the pathogenesis of autoimmune diseases: A comprehensive review. *Semin Arthritis Rheum,* 51**,** 513-522.

Tong, T., Zhao, W., Wu, Y. Q., Chang, Y., Wang, Q. T., Zhang, L. L. & Wei, W. 2010. Chicken type II collagen induced immune balance of main subtype of helper T cells in mesenteric lymph node lymphocytes in rats with collagen-induced arthritis. *Inflamm Res,* 59**,** 369-77.

Tordesillas, L. & Berin, M. C. 2018. Mechanisms of Oral Tolerance. *Clin Rev Allergy Immunol,* 55**,** 107-117.

Toussirot, E. R. A. 2002. Oral Tolerance in the Treatment of Rheumatoid Arthritis. *Current Drug Targets - Inflammation & Allergy,* 1**,** 45-52.

Turner, J. D. & Filer, A. 2015. The role of the synovial fibroblast in rheumatoid arthritis pathogenesis. *Curr Opin Rheumatol,* 27**,** 175-82.

Turner, J. E., Stockinger, B. & Helmby, H. 2013. IL-22 mediates goblet cell hyperplasia and worm expulsion in intestinal helminth infection. *PLoS Pathog,* 9**,** e1003698.

Ueda, Y., Kayama, H., Jeon, S. G., Kusu, T., Isaka, Y., Rakugi, H., Yamamoto, M. & Takeda, K. 2010. Commensal microbiota induce LPS hyporesponsiveness in colonic macrophages via the production of IL-10. *Int Immunol,* 22**,** 953-62.

Ulgen, E., Ozisik, O. & Sezerman, O. U. 2019. pathfindR: An R Package for Comprehensive Identification of Enriched Pathways in Omics Data Through Active Subnetworks. *Front Genet,* 10**,** 858.

Valdes-Ramos, R., Martinez-Carrillo, B. E., Aranda, G., Ii, Guadarrama, A. L., Pardo-Morales, R. V., Tlatempa, P. & Jarillo-Luna, R. A. 2010. Diet, exercise and gut mucosal immunity. *Proc Nutr Soc,* 69**,** 644-50.

Valle-Noguera, A., Gomez-Sanchez, M. J., Girard-Madoux, M. J. H. & Cruz-Adalia, A. 2020. Optimized Protocol for Characterization of Mouse Gut Innate Lymphoid Cells. *Front Immunol,* 11**,** 563414.

Van Den Broeck, W., Derore, A. & Simoens, P. 2006. Anatomy and nomenclature of murine lymph nodes: Descriptive study and nomenclatory standardization in BALB/cAnNCrl mice. *J Immunol Methods,* 312**,** 12-9.

Van Der Laarse, S. a. M., Leney, A. C. & Heck, A. J. R. 2018. Crosstalk between phosphorylation and O-GlcNAcylation: friend or foe. *FEBS J,* 285**,** 3152-3167.

Van Der Sluis, M., De Koning, B. A., De Bruijn, A. C., Velcich, A., Meijerink, J. P., Van Goudoever, J. B., Buller, H. A., Dekker, J., Van Seuningen, I., Renes, I. B. & Einerhand, A. W. 2006. Muc2-deficient mice spontaneously develop colitis, indicating that MUC2 is critical for colonic protection. *Gastroenterology,* 131**,** 117-29.

Vang, T., Congia, M., Macis, M. D., Musumeci, L., Orru, V., Zavattari, P., Nika, K., Tautz, L., Tasken, K., Cucca, F., Mustelin, T. & Bottini, N. 2005. Autoimmune-associated lymphoid tyrosine phosphatase is a gain-of-function variant. *Nat Genet,* 37**,** 1317-9.

Varki, A. 2001. Loss of N-glycolylneuraminic acid in humans: Mechanisms, consequences, and implications for hominid evolution. *Am J Phys Anthropol,* Suppl 33**,** 54-69.

Varki, A. 2011. Evolutionary forces shaping the Golgi glycosylation machinery: why cell surface glycans are universal to living cells. *Cold Spring Harb Perspect Biol,* 3.

Varki A, C. R., Esko Jd, Et Al 2022. *Essentials of Glycobiology, 4th edition*, Cold Spring Harbor Laborotory Press.

Varney, J. L., Fowler, J. W. & Coon, C. N. 2021. Undenatured type II collagen mitigates inflammation and cartilage degeneration in healthy Labrador Retrievers during an exercise regimen. *Transl Anim Sci,* 5**,** txab084.

Vonarbourg, C., Mortha, A., Bui, V. L., Hernandez, P. P., Kiss, E. A., Hoyler, T., Flach, M., Bengsch, B., Thimme, R., Holscher, C., Honig, M., Pannicke, U., Schwarz, K., Ware, C. F., Finke, D. & Diefenbach, A. 2010. Regulated expression of nuclear receptor RORgammat confers distinct functional fates to NK cell receptor-expressing RORgammat(+) innate lymphocytes. *Immunity,* 33**,** 736-51.

Wachten, D. & Mick, D. U. 2021. Signal transduction in primary cilia - analyzing and manipulating GPCR and second messenger signaling. *Pharmacol Ther,* 224**,** 107836.

Wang, B., Yao, M., Lv, L., Ling, Z. & Li, L. 2017a. The Human Microbiota in Health and Disease. *Engineering,* 3**,** 71-82.

Wang, C. C., Huang, Y. L., Ren, C. T., Lin, C. W., Hung, J. T., Yu, J. C., Yu, A. L., Wu, C. Y. & Wong, C. H. 2008. Glycan microarray of Globo H and

related structures for quantitative analysis of breast cancer. *Proc Natl Acad Sci U S A,* 105**,** 11661-6.
Wang, J., Manni, M., Barenwaldt, A., Wieboldt, R., Kirchhammer, N., Ivanek, R., Stanczak, M., Zippelius, A., Konig, D., Rodrigues Manutano, N. & Laubli, H. 2022. Siglec Receptors Modulate Dendritic Cell Activation and Antigen Presentation to T Cells in Cancer. *Front Cell Dev Biol,* 10**,** 828916.
Wang, W., Gopal, S., Pocock, R. & Xiao, Z. 2019. Glycan Mimetics from Natural Products: New Therapeutic Opportunities for Neurodegenerative Disease. *Molecules,* 24.
Wang, Y., Huang, D., Chen, K. Y., Cui, M., Wang, W., Huang, X., Awadellah, A., Li, Q., Friedman, A., Xin, W. W., Di Martino, L., Cominelli, F., Miron, A., Chan, R., Fox, J. G., Xu, Y., Shen, X., Kalady, M. F., Markowitz, S., Maillard, I., Lowe, J. B., Xin, W. & Zhou, L. 2017b. Fucosylation Deficiency in Mice Leads to Colitis and Adenocarcinoma. *Gastroenterology,* 152**,** 193-205 e10.
Wang, Y., Khan, A., Antonopoulos, A., Bouche, L., Buckley, C. D., Filer, A., Raza, K., Li, K. P., Tolusso, B., Gremese, E., Kurowska-Stolarska, M., Alivernini, S., Dell, A., Haslam, S. M. & Pineda, M. A. 2021. Loss of alpha2-6 sialylation promotes the transformation of synovial fibroblasts into a pro-inflammatory phenotype in arthritis. *Nat Commun,* 12**,** 2343.
Wang, Z., Zhang, H., Liu, R., Qian, T., Liu, J., Huang, E., Lu, Z., Zhao, C., Wang, L. & Chu, Y. 2018. Peyer's patches-derived CD11b(+) B cells recruit regulatory T cells through CXCL9 in dextran sulphate sodium-induced colitis. *Immunology,* 155**,** 356-366.
Ward, A. B. & Wilson, I. A. 2017. The HIV-1 envelope glycoprotein structure: nailing down a moving target. *Immunol Rev,* 275**,** 21-32.
Webster, H. C., Andrusaite, A. T., Shergold, A. L., Milling, S. W. F. & Perona-Wright, G. 2020. Isolation and functional characterisation of lamina propria leukocytes from helminth-infected, murine small intestine. *J Immunol Methods,* 477**,** 112702.
Wei, J., Zhang, C., Gao, Y., Li, Y., Zhang, Q., Qi, H., Jin, M., Yang, X., Su, X., Zhang, Y. & Yang, R. 2022. Gut Epithelial-derived CXCL9 Maintains Gut Homeostasis Through Preventing Overgrown E. coli. *J Crohns Colitis,* 16**,** 963-977.
Weiner, H. L. 1997. Oral tolerance: immune mechanisms and treatment of autoimmune diseases. *MMUNOLOGY TODAY,* 18**,** 335.
Weiner, H. L., Da Cunha, A. P., Quintana, F. & Wu, H. 2011. Oral tolerance. *Immunol Rev,* 241**,** 241-59.
Wershil, B. K. & Furuta, G. T. 2008. 4. Gastrointestinal mucosal immunity. *J Allergy Clin Immunol,* 121**,** S380-3; quiz S415.
Wheway, G., Nazlamova, L. & Hancock, J. T. 2018. Signaling through the Primary Cilium. *Front Cell Dev Biol,* 6**,** 8.
Williams, A. E. 2011. *Immunology Mucosal and Body Surface Defences*.
Williams, R. O. 2004. Collagen-induced arthritis as a model for rheumatoid arthritis. *Methods Mol Med,* 98**,** 207-16.
Withers, D. R. & Hepworth, M. R. 2017. Group 3 Innate Lymphoid Cells: Communications Hubs of the Intestinal Immune System. *Front Immunol,* 8**,** 1298.
Wong, Z. Y., Nee, E., Coles, M. & Buckley, C. D. 2023. Why does understanding the biology of fibroblasts in immunity really matter? *PLoS Biol,* 21**,** e3001954.
Worbs, T., Hammerschmidt, S. I. & Forster, R. 2017. Dendritic cell migration in health and disease. *Nat Rev Immunol,* 17**,** 30-48.

Wu, G., Grassi, P., Macintyre, D. A., Molina, B. G., Sykes, L., Kundu, S., Hsiao, C. T., Khoo, K. H., Bennett, P. R., Dell, A. & Haslam, S. M. 2022. N-glycosylation of cervicovaginal fluid reflects microbial community, immune activity, and pregnancy status. *Sci Rep,* 12**,** 16948.

Wu, N., Sun, H., Zhao, X., Zhang, Y., Tan, J., Qi, Y., Wang, Q., Ng, M., Liu, Z., He, L., Niu, X., Chen, L., Liu, Z., Li, H. B., Zeng, Y. A., Roulis, M., Liu, D., Cheng, J., Zhou, B., Ng, L. G., Zou, D., Ye, Y., Flavell, R. A., Ginhoux, F. & Su, B. 2021. MAP3K2-regulated intestinal stromal cells define a distinct stem cell niche. *Nature,* 592**,** 606-610.

Xu, X., Wang, M., Wang, Z., Chen, Q., Chen, X., Xu, Y., Dai, M., Wu, B. & Li, Y. 2022. The bridge of the gut-joint axis: Gut microbial metabolites in rheumatoid arthritis. *Front Immunol,* 13**,** 1007610.

Yamazaki, K. G., Gonzalez, E. & Zambon, A. C. 2012. Crosstalk between the renin-angiotensin system and the advance glycation end product axis in the heart: role of the cardiac fibroblast. *J Cardiovasc Transl Res,* 5**,** 805-13.

Yao, Y., Kim, G., Shafer, S., Chen, Z., Kubo, S., Ji, Y., Luo, J., Yang, W., Perner, S. P., Kanellopoulou, C., Park, A. Y., Jiang, P., Li, J., Baris, S., Aydiner, E. K., Ertem, D., Mulder, D. J., Warner, N., Griffiths, A. M., Topf-Olivestone, C., Kori, M., Werner, L., Ouahed, J., Field, M., Liu, C., Schwarz, B., Bosio, C. M., Ganesan, S., Song, J., Urlaub, H., Oellerich, T., Malaker, S. A., Zheng, L., Bertozzi, C. R., Zhang, Y., Matthews, H., Montgomery, W., Shih, H. Y., Jiang, J., Jones, M., Baras, A., Shuldiner, A., Gonzaga-Jauregui, C., Snapper, S. B., Muise, A. M., Shouval, D. S., Ozen, A., Pan, K. T., Wu, C. & Lenardo, M. J. 2022. Mucus sialylation determines intestinal host-commensal homeostasis. *Cell*.

Yoshinari, O., Moriyama, H. & Shiojima, Y. 2015. An overview of a novel, water-soluble undenatured type II collagen (NEXT-II). *J Am Coll Nutr,* 34**,** 255-62.

Yoshinari, O., Shiojima, Y., Moriyama, H., Shinozaki, J., Nakane, T., Masuda, K. & Bagchi, M. 2013. Water-soluble undenatured type II collagen ameliorates collagen-induced arthritis in mice. *J Med Food,* 16**,** 1039-45.

Zaia, J. 2011. At last, functional glycomics. *Nat Methods,* 8**,** 55-7.

Zaiss, M. M., Joyce Wu, H. J., Mauro, D., Schett, G. & Ciccia, F. 2021. The gut-joint axis in rheumatoid arthritis. *Nat Rev Rheumatol,* 17**,** 224-237.

Zhang, T., De Waard, A. A., Wuhrer, M. & Spaapen, R. M. 2019a. The Role of Glycosphingolipids in Immune Cell Functions. *Front Immunol,* 10**,** 90.

Zhang, X., Liu, S., Wang, Y., Hu, H., Li, L., Wu, Y., Cao, D., Cai, Y., Zhang, J. & Zhang, X. 2019b. Interleukin-22 regulates the homeostasis of the intestinal epithelium during inflammation. *Int J Mol Med,* 43**,** 1657-1668.

Zhang, X., Zhang, D., Jia, H., Feng, Q., Wang, D., Liang, D., Wu, X., Li, J., Tang, L., Li, Y., Lan, Z., Chen, B., Li, Y., Zhong, H., Xie, H., Jie, Z., Chen, W., Tang, S., Xu, X., Wang, X., Cai, X., Liu, S., Xia, Y., Li, J., Qiao, X., Al-Aama, J. Y., Chen, H., Wang, L., Wu, Q. J., Zhang, F., Zheng, W., Li, Y., Zhang, M., Luo, G., Xue, W., Xiao, L., Li, J., Chen, W., Xu, X., Yin, Y., Yang, H., Wang, J., Kristiansen, K., Liu, L., Li, T., Huang, Q., Li, Y. & Wang, J. 2015. The oral and gut microbiomes are perturbed in rheumatoid arthritis and partly normalized after treatment. *Nat Med,* 21**,** 895-905.

Zhang, Y. Z. & Li, Y. Y. 2014. Inflammatory bowel disease: pathogenesis. *World J Gastroenterol,* 20**,** 91-9.

Zhao, C., Hu, X., Qiu, M., Bao, L., Wu, K., Meng, X., Zhao, Y., Feng, L., Duan, S., He, Y., Zhang, N. & Fu, Y. 2023. Sialic acid exacerbates gut dysbiosis-

associated mastitis through the microbiota-gut-mammary axis by fueling gut microbiota disruption. *Microbiome,* 11**,** 78.

Zhao, T., Wei, Y., Zhu, Y., Xie, Z., Hai, Q., Li, Z. & Qin, D. 2022. Gut microbiota and rheumatoid arthritis: From pathogenesis to novel therapeutic opportunities. *Front Immunol,* 13**,** 1007165.

Zheng, Y., Valdez, P. A., Danilenko, D. M., Hu, Y., Sa, S. M., Gong, Q., Abbas, A. R., Modrusan, Z., Ghilardi, N., De Sauvage, F. J. & Ouyang, W. 2008. Interleukin-22 mediates early host defense against attaching and effacing bacterial pathogens. *Nat Med,* 14**,** 282-9.

Zhou, Y., Zhou, B., Pache, L., Chang, M., Khodabakhshi, A. H., Tanaseichuk, O., Benner, C. & Chanda, S. K. 2019. Metascape provides a biologist-oriented resource for the analysis of systems-level datasets. *Nat Commun,* 10**,** 1523.

Zhu, P., Li, X. Y., Wang, H. K., Jia, J. F., Zheng, Z. H., Ding, J. & Fan, C. M. 2007. Oral administration of type-II collagen peptide 250-270 suppresses specific cellular and humoral immune response in collagen-induced arthritis. *Clin Immunol,* 122**,** 75-84.

Zhu, W., London, N. R., Gibson, C. C., Davis, C. T., Tong, Z., Sorensen, L. K., Shi, D. S., Guo, J., Smith, M. C., Grossmann, A. H., Thomas, K. R. & Li, D. Y. 2012. Interleukin receptor activates a MYD88-ARNO-ARF6 cascade to disrupt vascular stability. *Nature,* 492**,** 252-5.

Ziff, M. 1974. Relation of cellular infiltration of rheumatoid synovial membrane to its immune response. *Arthritis Rheum,* 17**,** 313-9.

Appendix

Table S 1Statistics of Alpha Diversity Indices in ileum

Sample_Name	chao1	dominance	goods coverage	observed otus	pielou_e	shannon	simpson
Naive.1.2	113	0.028	1	113	0.848	5.785	0.972
Naive.1.3	94	0.106	1	94	0.7	4.588	0.894
Naive.1.4	112	0.076	1	111	0.709	4.817	0.924
Naive.1.5	110	0.045	1	110	0.778	5.275	0.955
CIA.3.1	142.333	0.039	1	142	0.799	5.71	0.961
CIA.3.5	91.857	0.073	0.999	91	0.702	4.572	0.927
CIA.4.4	175.25	0.058	0.999	174	0.712	5.296	0.942
CIA.3.4	86	0.079	1	86	0.701	4.505	0.921
CIA.4.1	159	0.05	1	159	0.764	5.589	0.95
CIA.4.5	103.375	0.075	1	103	0.711	4.753	0.925
UC-II.7.3	47	0.093	1	47	0.72	3.998	0.907
UC-II.8.1	15	0.204	1	15	0.731	2.855	0.796
UC-II.8.5	158	0.103	1	158	0.68	4.964	0.897
UC-II.7.4	178.2	0.112	1	178	0.664	4.967	0.888
UC-II.7.5	93	0.026	1	93	0.869	5.683	0.974
UC-II.8.2	109	0.08	0.999	105	0.678	4.552	0.92

Table S 2 Statistics of Alpha Diversity Indices in colon

Sample_Name	chao1	dominance	goods coverage	observed otus	pielou_e	shannon	simpson
Naive.1.2	175.303	0.033	0.979	163	0.814	5.98	0.967
Naive.1.3	165.143	0.251	0.978	143	0.597	4.276	0.749
Naive.1.4	188.5	0.044	0.98	178	0.794	5.938	0.956
Naive.1.5	106.1	0.038	0.999	106	0.871	5.858	0.962
CIA.3.1	114.84	0.036	0.995	114	0.843	5.758	0.964
CIA.3.5	200.941	0.029	0.972	178	0.833	6.228	0.971
CIA.4.4	257.182	0.011	0.972	243	0.906	7.179	0.989
CIA.3.4	38	0.043	1	38	0.922	4.837	0.957
CIA.4.1	58.2	0.141	0.999	58	0.723	4.237	0.859
CIA.4.5	120.75	0.033	0.993	117	0.863	5.931	0.967
UC-II.7.3	163.938	0.052	0.986	158	0.793	5.789	0.948
UC-II.8.1	172.676	0.021	0.988	169	0.868	6.425	0.979
UC-II.8.5	59.333	0.047	0.999	59	0.855	5.03	0.953
UC-II.7.4	74.143	0.044	0.996	72	0.834	5.145	0.956
UC-II.7.5	188.111	0.044	0.982	177	0.83	6.2	0.956
UC-II.8.2	67.429	0.068	0.998	67	0.794	4.819	0.932

Table S 3 Top 200 significant gene list in among DCs subsets in the same location

DIFFERENT DCs IN THE SAME LOCATION													
UP-REGULATED							DOWN-REGULATED						
ML	LP			MLN			ML	LP			MLN		
CD103 vs DP	CD11b vs CD	CD11b vs DP	CD103 vs DP	CD11b vs CD	CD11b vs DP	CD103 vs DP	CD103 vs DP	CD11b vs CD	CD11b vs DP	CD103 vs DP	CD11b vs CD	CD11b vs DP	CD103 vs DP
Ighv13-2	Col25a1	L3mbtl4	D930020B18	Mybpc1	Rgs13	Aicda	Sh3gl3	Ighv1-36	Igkv9-123	Col25a1	S100a9	Ppbp	Cwh43
Ighv3-1	Tcrg-C4	Gp2	St18	Gm43914	Tcrg-C1	Marco	Thbs4	Ighv13-2	Tfec	Tmem27	Pdilt	Etos1	1700024P16
I830127L07R	Penk	D930020B18	Btnl7-ps	Bglap3	Endou	Klrc1	Ace2	Ighv1-77	Slc1a2	Cyp26b1	Lrg1	Slc27a2	Ppbp
Ighv1-63	Ptgis	Angpt4	Cnga2	Cwh43	Pax5	Rgs13	Tmprss2	Lingo4	Igkv4-62	Tnfaip8l3	S100a8	Serpina3i	Npr1
Ighv1-84	Cel	Murc	Scel	Spock1	Il22	Ncr1	C77370	Pla2g2d	C1qb	Ptgis	Klrc1	Sult1a1	Mybpc1
Igkv7-33	Gcg	Osbpl10	Cd209b	Napb	Scn4a	Cd163l1	Itgb8	Bex6	Itga9	Gm11837	Etos1	Ifitm1	Slc27a3
Camp	H2-M5	Itgae	Upk1b	Bace2	Cpne7	Zcchc18	Gm9745	Igkv9-123	C1qc	Cadm1	Rem2	Pdilt	Mfsd7c
Ighv1-36	Gm973	Plet1	Igkv4-54	Eva1a	5830411N06	Prdm8	Eva1a	Tfec	Acod1	Gm17057	Gm17944	Abcg4	Scnn1g
Ighv1-12	Cyp26b1	Ppp1r1a	Ighv1-56	Cpne8	Cntn1	Fgd5	Itgae	Retnlg	C1qa	Tulp3	Fgd5	1700011B04	Oit1
Ly6i	Tcrg-C2	Entpd3	Fam189a2	Sh3gl3	Klrb1c	Lhx2	Napb	Upk1b	Uchl1	Fzd6	Htra1	Cdk15	Pou4f1
Cyp4f37	Gm11837	Slc5a11	5730435O14	Shroom3	Dll1	Lipc	Rbm11	Rem2	Pla2g2d	Gm43914	Mmp8	Clec4b2	Gm28706
Igkv3-1	Tmem27	Gm44205	Adgrl3	Tmprss2	Gm43914	Ighg1	Cd200r4	Ighv2-6	Cd209d	Gramd2	Rasd2	Gp2	Gm9992
Igkv6-13	Gm44448	Apol10b	Gp2	Abca17	Aicda	Tnfrsf8	Arhgap8	Ighv2-6-8	P2ry13	Cd8a	Bmp8a	Phkg1	Ch25h
Ighv9-2	Ttc39a	D330045A2(	Ighv1-36	Thbs4	Mef2b	Il17f	P3h2	Mmp9	Sell	Arhgef9	2610528A11	Bcl2l15	Gabrr1
Igkv4-90	Crtam	Cd209b	Cd101	Asphd2	Ighg1	Bambi-ps1	Gm13589	Ighv1-56	Mertk	Shroom4	Clec4n	Timd4	Syt7
Sirpb1c	Esyt3	Slc44a5	Clec4a4	Arhgap8	Cr2	Cecr2	Mab21l3	Cnga2	Cst7	H2-M6-ps	Prdm8	Ms4a6d	Casc1
Igkv4-58	Cadm1	Vit	Dmkn	Alox15	Lipc	Emid1	Tgfb2	C1qa	Fam20c	Plpp1	Dkk2	Entpd3	Fut2
Ngp	Gpr33	Fndc5	Rem2	Cd81	Ifng	Cr2	Fgfbp3	St18	Apoe	Tlr12	Peli2	H2-Q10	Wfdc13
Ighv1-76	Myh7b	Siglecf	Clec4n	Galc	Ncr1	Ttn	BC016579	C1qc	Adgrg3	Clec9a	Ffar2	Clec4n	Lurap1
Igkv4-69	Xcr1	Tmeff1	Ptger3	Fzd6	Fam71a	Pax5	Gm17057	C1qb	Retnla	Cxcr3	Ptk6	Mospd4	Gm37010
Igkv4-59	Foxj1	Clec4b2	1810011H11	Ccer2	Igkv15-103	Rimkla	Ttc39a	Msr1	Cx3cr1	Itga8	2900052N01	Ccr1	Bace2
Igkv4-53	Themis	Xlr	Gm15448	Clec9a	Prf1	Scn4a	Mtss1l	Clec4e	Mafb	Gm43011	Cdk15	Ccl17	Scin
Igkv2-112	1700009J07I	Scel	Slc27a2	Cadm1	Ntrk3	B3gnt7	Trgv2	Cd209d	C5ar1	Gpr33	Lilra5	Ffar2	Gm7694
Tnfrsf17	Cd8a	Ptger3	Ptgs2os	Ptgis	Psd2	Cpne7	Cpne8	Igkv1-122	Pi16	Ffar4	Nlrp10	Clec4a4	Dpysl5
Ighv1-80	Gzmk	5730435O14	Igkv1-122	Rab42	Igkv4-70	Ikzf3	Plppr4	Ms4a4c	Fcgr1	Bvht	Stra6l	Gda	Adh4
Clec4d	Tulp3	Map9	Cd209a	Agpat3	Tnfsf11	Timd2	Idi2	Csf3r	Igkv4-57-1	H2-M5	Rgs7bp	Mgl2	Cxcl3
Igkv6-20	4932438H23	Cpm	Trem1	Aff3	Clnk	S100a9	Ttc39aos1	Trim29	Ccr2	Zmat4	Bpifa6	Gm11413	Kcp
Cd300e	Iqch	Mylk	Cxcr2	Fgd6	Fcer2a	Spns2	Spata31d1b	Treml2	Bex6	Tcrg-C4	Gm14207	Vdr	Ass1
Spink2	E330020D12	Cntnap2	Gm45055	Gabrr1	Igkv3-12	Cntn1	Ocln	Acod1	Msr1	Xcr1	Timd2	Nectin2	Ces2c
Ighv8-5	Ptprh	Ocln	Pilra	Oit1	Nuggc	Xcl1	Lima1	Igkv3-1	Npl	Arhgap42	Grpr	Hpcal4	Glis3
Igkv1-88	H2-M6-ps	AW822252	Clec4g	Ifnlr1	Sgca	Fcer2a	Tcrg-C1	Mafb	Tlr7	Rab7b	Atf7ip2	RP24-167A1	Ank2
Igkv8-27	A530099J19	1700003E16	Itgam	Henmt1	Dkkl1	Bank1	Ncoa7	Cd209a	Tnfsf11	A530099J19	Slc27a2	Gm19434	Sult1a1
Igkv12-41	Gm17057	Fndc4	Ehf	Arhgap42	Xcl1	Vpreb3	Ndrg2	Gm15448	AB124611	Dapk2	Cecr2	E230029C05	Cdkn2c
F10	Cxcr3	Pianp	Ppm1n	P3h2	Nlrc3	Klrb1c	Tcrg-C2	Ptgs2os	Klrb1f	Ptprh	Nlrc4	Oas2	Met
Ighv1-34	Gm29151	Gpr4	Clec4a2	Rhobtb1	Tcrg-C4	Tlr7	Bvht	Adgre4	Tnfaip8l3	Proser2	Ttn	A4galt	F5
Igkv8-19	Gzma	Ppm1j	Siglece	Kcng2	Fcmr	2610528A11	Bcl2l14	Prr29	Chst2	Galc	Hpcal4	Cxcl3	Sh3pxd2b
Slc27a2	Plpp1	Agbl2	Cd209c	Scnn1g	Tmem121	Mef2b	Hdac11	Dmxl2	Ccl9	R74862	Cygb	Nrep	Gm5424
Igkv12-44	Arhgef9	Gm8221	Cd33	Nos1ap	Egln3	Cxcl13	Serpinb9b	Igkv1-133	Tgfbi	Ptger2	Nrep	Rasd2	Stk39
Ighv1-72	Proser2	Serpinb6b	Ptgs2	R74862	Ikzf3	Nuggc	Tanc1	Igkv5-45	Ighg1	Trdc	Gp2	Stxbp6	Tcn2
Nodal	Itgae	Gm12159	Skint3	Fgfbp3	Pla2g2d	Capn12	Laptm4b	Ms4a4a	Clec4a3	Irf8	Stra6	Olfm1	Afap1
Ighv5-17	Trdc	Gm19434	Ccr1	Gpr33	Colq	Ifng	Gm44448	Csf1r	Igkv3-1	Penk	Ifitm1	Slc27a3	Gm26902
Anxa8	Ppef2	Serpinb9	Ighv13-2	E330020D12	Bspry	Atf7ip2	Tcrg-C4	Itgam	Rarg	Ttc39a	Chst10	Adgrl3	Napb
Ighv14-3	Cd160	Pgf	Cdh1	Mab21l3	Gzma	Tnfsf11	Cd163l1	Abcd2	S100a9	Ppef2	Il1f9	Cldn12	Klra5
Igkv13-85	Gzmb	Fam189a2	Pltp	Xcr1	Dcbld1	Ngp	Sh2d5	Apoe	Gdf15	4932438H23	Clec4a4	RP24-167A1	Vdr
Trem3	Nkg7	Apol7e	Atp1a3	Gramd3	Il17f	Cd19	Mgll	1810011H11	Colq	Itga3	Sirpa	Cyp7b1	Gpr33
Ighv1-53	Apol10b	Slc27a2	Slc44a5	Spire2	Gm4759	Calm4	Scin	Nxpe1-ps	Lmo1	Esyt3	Tarm1	Ap1s2	Gm37535
Ighv1-69	Ighg2c	Tmem52b	Gm43753	D630045J12	Rgcc	Myo5b	Afap1	Atp1a3	Dab2	Gm44448	Slc6a12	Plek2	Ccl17
Ighv1-50	Tlr3	A630072L19	Nxpe1-ps	Rad51b	Gm19585	Gm17944	Wtip	Dmkn	Tmem26	Crtam	Gm11413	Adora2b	Wtip
Igkv1-135	Ffar4	Egfl8	Il23a	Cd247	Siglech	Crmp1	Aldh1a2	Nr1h3	G0s2	Xcl1	Gm8773	Siglece	Pkib
Ighv1-74	Plce1	2510009E07	Cd300a	Plce1	Bambi-ps1	Fcmr	Crtam	Gm45055	Gbp2b	Aoah	Adgre4	Glis3	Ints3
Ighv5-6	Gm19569	Cd101	Cd300ld	Ank2	Blk	Ltf	Net1	Fxyd2	Vipr1	Mab21l3	St18	Ccdc162	Slc9a4
Pkd1l2	Fndc5	Notch4	RP23-240G3	Lrrc3	Tox	Endou	Gpr33	Clec4n	Tlr4	P3h2	Gm15925	Gm4956	Pdcd1lg2
Gm8890	4931406G06	St18	Mmp12	Zdhhc2	Ltf	Grpr	Zdhhc14	Cd300lb	Zbtb32	Unc13b	Tgm1	Zfp971	Rnaset2a
Igkv5-45	Fzd1	Plet1os	Siglecf	Sgca	Igkv4-61	Ip6k3	Ptgis	Aif1l	Smad3	Nfe2l3	Grin2c	Oas1g	Ppl
Igkv12-46	Dapk2	Nme9	Tgm2	6430562O15	Cd163l1	Siglec1	Tmie	Klra2	Padi2	Tlr3	Pltp	Ifitm2	Tmem131
Igkv14-100	Arhgap42	Myom1	Ifit1bl1	Syt7	Rnf144a	Crispld2	Gclc	Cd209e	Il12rb2	Fzd1	Gbp7	Amica1	Snx24
Ighv2-3	Skap1	Robo4	Peli2	Itga6	Il2rb	St6galnac3	Gzmb	Irak3	Hebp1	Gm43727	Oas2	Tcn2	Ifit1bl1
Igkv10-94	Snx22	Cdh1	Angpt4	Ldlrad3	Gm37711	Cdh22	Rims3	Gm9733	Egln3	Ppt1	RP24-167A1	Npr1	Flt1
Ighv9-1	Sh2d2a	Bmp8a	Mmp9	Ctnnal1	Emid1	Pou2af1	Exoc3l4	Clec4g	Nr1h3	RP24-531B2	Cyp7b1	RP24-167A1	Acot6
Igkv4-92	Gm44205	Tvp23a	Il1rl2	Itga3	Igkv8-24	Rgcc	Fndc5	Sirpb1b	Blk	Synpo	St6galnac3	Btbd16	Map3k15
Gm5086	Tcrg-C1	9530059O14	Hacd4	Plpp1	Rab37	Blk	Sh3d19	Il1rn	Ms4a4a	Snx22	Siglecg	Stra6	Sphk1
Ace	Chsy3	Cxcr2	Robo4	Scin	Bank1	1500009L16	Fbxo2	Sirpb1a	Pdgfa	Lif	Spns3	Dpysl5	Gm11724
Igkv3-5	Bvht	Gpr55	Cd300lf	Nfe2l3	Crtam	Cd79a	Apol10b	Tgm1	AI839979	Agpat3	Mefv	Tmem51os1	Cds1
Clec4a1	Synpo	Fmo5	Cntnap2	Klf5	Fcrla	Blnk	Vwa5a	Plaur	Irak3	Ppt2	H2-Q10	Prdm1	P4ha2
Ighv1-59	Sh3gl3	Bfsp1	Gm16553	Ppp1r1c	Shroom3	Igkv3-12	Fam83h	Adgrl3	Mrc1	Sh3gl3	Foxred2	Dapk1	Mycl
Ighv1-66	Gm43914	Cdh17	Myo15	Npr1	Ighd	Btbd11	Gcnt4	1700071M1(	Lingo4	Tcrg-C2	Adora2b	St7	Il12rb2
Sirpb1b	Tlr11	Gm42962	Il1r2	Zfp618	CR974586.5	Iglv2	Synpo2	Itga9	Cpxm1	Erc1	Gm15448	Tmem131	Ncoa7
Ighv1-61	Itm2a	Adgrl3	Clec4a1	Mpeg1	Cd19	Pla2g2d	Rragd	Sell	Ighv5-17	Slc7a8	Mospd4	Pilra	Bcl2l14
Igkv1-117	Ppt1	Hepacam2	L3mbtl4	Afap1	Cd79a	Ighg2b	Sptb	Stab1	Ikbke	Cd81	St8sia1	Plcd3	Mab21l3
Stac2	Gm14597	Rasgrf2	Cyp4f18	Gm12407	Sytl3	Penk	Kcnk13	Clec4a3	Nos1ap	E330020D12	Clec4b2	Tpm2	E330020D12
Ighv1-78	P3h2	Ear2	Sirpa	Tnik	Btbd11	Krt7	Heatr9	Clec4a4	Treml2	P2ry14	Fabp5	Tgtp1	Pacsin2
Gm9733	Fndc7	Pdlim3	Gm43814	BC016579	Oprd1	Cd22	Pi4k2b	Skint3	Lrp8	Kcng2	Cd1d2	Sh3pxd2b	Abtb2
Ighv1-58	Mab21l3	Ccdc162	Cybb	Ighg2c	Pou2af1	Gm45153	Tnik	Gm16553	Cd163	Adamts6	Tyrobp	Htr7	B3gnt5
Igkv6-14	Baiap3	Gpr82	Gm15925	Gm9992	Hs3st1	Tmem158	Src	Serinc2	Art2b	Itm2a	Gm19434	Gm28100	Gm9776
Fcgr4	Fam149a	Arpin	Ddx60	Gcm1	Gzmb	Siglech	Ccdc120	Fam189a2	Cp	Kif5a	Rbpms2	Oasl2	Gm10441
Ighv1-31	Agpat3	Kif17	Nxpe5	Gcsam	Gm8818	Serpinc1	Oprd1	Sirpb1c	Cxcl3	Gm38248	Cgnl1	Tlr13	Nid2
Cyp4f16	Asap2	Pilra	Hcar2	Src	Ighg2b	Sh2d2a	Slc22a23	Il23a	Gpm6b	Foxj1	Bcl2l15	4930426L09	Tcea3
Clec4a2	Mpzl2	Gm33370	Il18rap	Dnah6	Zfp618	Gzmb	Slc18a1	Clec4a1	Siglech	Gcg	Gprc5d	Serpina3g	4931406C07
Cadm3	Lrrc3	Serpinb1b	Plet1	Perp	Marco	Gm14207	Tmeff1	Fam20c	Slc11a1	Iqch	Bcas1	Pkib	Rnaset2b
Igkv3-10	Itga3	Gsg1	Ptgfrn	Slc16a1	Rhobtb1	Ly6d	Trdc	Ptgs2	Ms4a4c	Akr1b8	Nfe2	Casc1	Ppfia3
Ighv8-8	Clec9a	Ttc39b	Kcne3	Aqp11	Sh2d2a	A630023P12	Gbp4	Cx3cr1	Dmxl2	Tcrg-C1	Cd72	Gpr82	Itga3
Gdf15	Cxx1c	Scd1	9830107B12	Slc8b1	Capn5	Gzma	Glce	Scel	Pla2g15	Lrrc3	Cyp4f18	Ifit3	Gm17767
Igkv19-93	Gm8221	Irf6	Aif1l	Scx	Rab42	E230020D15	Rnf152	Sele	Itgb5	Nkg7	Ear2	Car2	Prelid2
Ighv10-1	Cd36	Ifit1bl1	Smox	Oosp1	Asphd2	Pgap1	Me1	Rtp4	Plpp2	Plce1	Gm14328	Pltp	Tnik
Igkv12-38	Cgref1	Scd4	Pgf	Cd8a	Lif	Kcnk5	Arc	Gm43753	Mmp13	Cd160	Lilra6	Ext1	Stard10
AI839979	Zmat4	Epcam	Hrh1	Trpm2	Ip6k3	Smpd5	Camk4	Clec4a2	Gm7694	Lima1	Ppp1r14a	Gm6166	Aldh1a2
Csf3r	Lrrc1	Mmp12	Clec4b1	Gm26902	5830444F18	Slc35f2	Themis	Cybb	Mmp14	Mras	Tbc1d16	Vwa3b	Nos1ap
Ighv1-64	Lima1	Mical2	Lifr	Zdhhc14	Serpinc1	Mctp2	Slc9a3r2	Klra17	Gpnmb	Gzma	Stab1	Fdps	C030037D09
Igkv4-61	Perm1	Trem1	Gbp8	Slc41a2	Crmp1	Fam71a	Pbld2	Fcgr1	Il17f	Pdgfa	Fam84b	Gm12606	Gm26809
Gm8879	Klra5	Mfsd2a	Kcnh4	Itga1	Iglc1	Tox	Msrb3	Hcar2	Stk26	Med12l	Nod1	Ifitm3	Rnf217
Igkv8-24	Efcc1	Calml4	Rtp4	Ch25h	Ly6d	Dscam	Rnaset2b	Cd209c	Tln2	4931406G06	Gda	Bcas1	Dnah6
Igkv1-122	Med12l	Dip2c	Mylk	Cttnbp2	Rasd1	Ebf1	Fam160a1	S100a9	Ccl6	Serpinb8	Dll4	Tspan2	Chpt1
Ighv1-77	Mras	Foxr1	Cxcl2	Wtip	Dnah8	Susd1	Spo11	Mrc1	Aoah	Igf2r	9430076C15	Rac3	Serpind1
Igkv3-2	Akr1b8	RP24-94F12.	Ccdc180	Itgb8	B3gnt7	Iglc3	Megf9	Cd300a	Adgre4	Lrrc1	Igf2bp2	Gm20703	Plppr4
Igkv17-127	Naaa	Dcun1d4	Ms4a6d	Sort1	Lax1	Arhgap24	Oasl1	Ltb4r1	Vcam1	Rgs9	Gpr183	Hvcn1	Gpr85
Ighv5-9-1	Cxx1b	Rell1	Pygl	Ttc39c	Focad	Txk	Xlr	Abca9	Synj2	Fgd6	Ms4a4a	Gm5602	Mkrn1

Igkv4-79	R74862	A530064D06	Adora2b	B3gnt5	Themis	Usp2	Rhoc	Uchl1	Prkar1b	Gm973	Il1bos	1600010M0	Itpripl1
Ighv1-82	Gm26520	Nid2	Hpgd	Met	Abca17	Tesc	Met	Sirpa	Stxbp6	Eva1a	Fcer1g	4933404O12	Ptprf
Mzb1	Erc1	Gm8817	Stra6l	Irf8	E230020D15	Egln3	Ppm1j	Slc16a7	Ppt2	Gm42549	Erbb3	Chst10	Vwa3b
Igha	Eva1a	Sash1	Wls	Igf2r	Cnr2	Cd79b	Slamf1	Rorc	Trim29	Ifi205	Ccr1	Dthd1	Fzd6
Cd300lg	Cd3g	Lad1	Plaur	Clec1b	Gm45153	Gnaz	Insm1	Slc1a2	Slc7a4	Gcsam	Arhgef10l	Rpl3l	Slc25a42
Ighv5-4	Trbc2	Gm14597	Hilpda	Ak7	Nkg7	St6galnac2	Hc	Ehf	Ccdc109b	Gzmk	Tmem158	Ccdc102a	Atl1
Igkv8-21	Irf8	Chac1	Rilpl1	Csrp2	Zdhhc2	Dkkl1	Ptpn21	Igkv4-57-1	Spn	Smad3	Hrh1	Gbp7	Itgae
Igkv9-124	Tanc1	Qpct	Slc15a3	Gm13994	Stk26	St8sia1	Cd247	Dab2	Pld3	Naaa	Fam189a2	Ifit1bl1	Ap1s2
Ccl2	Rab7b	Hgfac	Ctnnd2	Sema4f	Cd28	Sntb1	Baiap3	Npl	Ighv1-5	Rnf217	Sntb1	Mylk	Nectin2
Ifitm3	Zfp57	Tspan8	Ceacam19	Enpp5	Xylt1	Tdrp	Lmntd2	Tgm2	Arhgef10l	Trat1	Cdh26	Dram1	Prkar2b
S100a8	Serpinb6b	Cystm1	Rgl1	F5	Vpreb3	Rapgef3	Fscn1	Fcer1g	Plxdc2	Fbxo4	Glycam1	Pik3r6	Dock5
Igkv10-96	Shroom3	Ltf	Osbpl10	Adh4	Sspo	Bspry	Gm37711	Gm15987	Ly6i	Eml5	Icam5	Cd300a	Tlr13
Ighv14-4	Scd4	Stra6l	Pglyrp2	Flt1	Cd55	Cd93	Parp16	Siglece	Klra17	Ifi211	Frrs1	Ms4a7	Pex11a
S100a4	Itk	Styxl1	Upb1	Sgms1	Msc	Gimap6	Rnaset2a	Gm43388	Eng	Sarm1	Rab9b	Tmem106a	08-Sep
Ccr10	Morn1	Ttc39a	Esr1	Enpp4	Icam2	Cd28	Rab13	Hacd4	Serpine1	Cd226	Gm6166	Bmp8a	Acsf3
Ifitm6	Nfe2l3	Plagl1	Abca9	Gng12	Nptx2	Trp53i11	Kpna3	Alox5	Epb41l3	Gm26603	Cybb	A530076I17	Alox15
Gm5150	03-Sep	Cyp2s1	Ffar2	A530099J19	Gm20696	Snap91	Cttnbp2nl	Cd209b	Tmem176a	Plcb4	Tgtp2	Fabp5	Oosp1
S100a9	Lif	Cwc25	Rasd2	Thnsl2	Dusp14	Cd2	Cptp	Fcer2a	Prr29	Efcc1	Abcd2	Stbd1	Ifi205
Fcgr1	Scd3	Sec24d	Plet1os	Ighv10-1	Blnk	Cxcr6	Serpinb6b	Cd101	Gm20559	Fnip2	Pcdh1	Tacc2	Med17
Mgst1	Cd3e	Ffar2	Etos1	2310030G06	Dusp4	Podnl1	Nqo1	Gm14548	C230085N15	Spry4	A4galt	Nme9	Sqrdl
Tspan15	Arpin	Ppp1r14a	Lair1	Rnf217	E430014B02	C3	Reck	Vipr1	Gda	Fam160a2	Myo5b	Gm38345	Ece1
Igkv8-16	Tnik	Ltc4s	Clec4e	Reck	Cd37	Nptx2	Parp3	Cd33	Gm28875	Shroom3	Il1rn	Gm11724	Ntn4
Ms4a6c	2310031A07	Slc52a3	Gm15987	Pbx1	Sla2	Sit1	Pik3r3	Wfdc17	Tmem176b	Pbx1	Srms	Syngr3	Hc
Cd300c2	Gm42962	Ptprv	Sirpb1b	Oxct1	Treml2	Gimap7	Pigg	Blk	Ccr5	Gzmb	Cpm	Gpx1	Lrrk2
Igkv2-109	Gm44950	Cxx1c	Pla2g2d	Asb11	Kcnk5	Xrcc5	Ehd3	Ppm1n	Aff3	Ncoa7	Tnni1	Zyx	Etnk2
Igkv6-23	E130102H24	Itgad	Zfp667	Il12rb2	Gimap7	Nlrc4	Idi1	Ccr1	Il22ra2	Bag2	Gm15922	Mxra7	Cttn
Mir99ahg	Slc22a23	Anpep	RP24-167A1	Snx22	Zcchc18	Pxdc1	Rnf180	Pla2g7	Cd209e	Chsy3	RP24-167A1	Ppp1r14a	Lima1
Igkv4-86	Fgd6	Gzmb	Csf3r	Pde4c	Cd8a	Dtx1	Prkcq	Cyp4f18	Csf1r	Clnk	Zfp773	Tnfrsf18	Gclc
Igkc	Slc22a18	Rgs1	Krt80	Foxj1	Igkv4-59	Il23a	Mturn	Cd300lg	Abca1	Zdhhc2	Prdm1	2600006K01	Suox
Cd209a	Ccser1	Mxra7	Mefv	Oprd1	Cadm1	Igkv8-24	Itk	C5ar1	Fkbp11	Pdia5	Abcc3	Gm13546	Cd36
Ighv1-55	Tlr12	Nedd9	B4galt6	Bvht	Rnf125	Il2rb	Rab23	Hbegf	Rorc	Ispd	Tmem51os1	Cotl1	Gm13994
Ighv1-22	Lck	Pald1	Pcyt1b	Bcl2l14	Bend5	Dmwd	Arhgap28	Lifr	Osm	BC037032	Olfm1	2310009B15	Mpeg1
Mmp12	Reck	Fam149a	Fgfr1	P2ry14	Hspa1b	Gm19585	Sh3bp4	Ccdc180	Syne3	Zap70	Tmem176b	Ccnd2	Snx22
Igkv14-111	Notch4	Havcr2	Gm9733	Spag4	Ly6c2	Cygb	Catsperg1	Ighv3-8	H2-M2	Sh2d2a	Meis1	Pyurf	Map3k10
Ctnnd2	Gm12551	Apol7c	Acy1	Hspb1	Vipr1	Adgre4	Epsti1	Trem1	Gria3	Klf2	Gm17641	Gm14328	Gm28100
Klra2	Gm37648	Tnni2	Arl5c	Gstm5	Gimap1	Atcay	Glipr2	C3ar1	Ddit4	Mpeg1	Pira2	Gm11423	Galc
Itgam	Dbn1	5031425F14	Sh2d1b1	9630013D21	Iglc2	Nt5e	Cttn	Rgl1	Clec4e	Gm3336	Gm15987	Trpv4	P3h2
Sspn	Zap70	Clec4a4	Irf4	Wfdc13	Fam160a1	Stx1a	Sorbs1	Gm15925	Clnk	Cd36	Oas1b	Gpr183	Fbxo46
Krt80	Ly75	Pcdh1	Pira2	Rab7b	Cd247	Focad	Aplp1	Gda	Gm15848	Fndc7	Rem1	Flywch2	Sfxn2
Bhlhe41	Slc6a9	Enho	Oas1c	Hk3	Cd2	Ankrd37	Dock9	Retnla	Mmp9	Hc	Bco2	1810006J02	Gm13546
Lpl	Ncoa7	Plekha5	Oas1a	Fbxo4	Penk	Il9r	Slc27a3	Cd300ld	S100a6	Dbn1	Acp5	Rcl1	AA467197
Jchain	Cldn1	Rhof	RP23-220F2	Slc27a3	Fosb	Spns3	Il27	Hrh1	Itga8	F2r	Pou2f2	Gm20939	Ifi211
Siglece	Slc7a8	B3gnt3	Fcgr3	Gm37711	Ighv1-80	Mzb1	2510009E07	Iglv2	Serinc2	Adrb2	Fgr	Cdkn2b	Adam19
Igkv6-17	Gm26603	Trim13	Vit	Plppr4	Sit1	Msc	Myo6	Lilra6	Selenop	2310031A07	Ddr1	Tgtp2	Rab13
Ccl4	Xcl1	Ppm1n	Trem3	Kif3c	Usp2	Gm13589	Cd3e	Ccl6	Axl	Ccno	Gnmt	Chst14	Stbd1
Ffar2	RP24-531B2	Abcb1a	Gm15513	Otud7b	Tesc	Cryaa	Ly75	Klri2	Col17a1	Dync2li1	Tacc2	Ifitm6	Hvcn1
Mafb	Lat	1700086O06	Plau	Hc	Cxcr3	Igkv4-80	Thnsl2	Cd300lf	Tns1	Nck2	Igsf3	Slc36a3os	Acadm
C1qb	Mospd1	Actn1	Ggt5	Pxmp2	Hspa1a	Gfpt2	Palld	Nxpe5	Igkv14-111	Tanc1	Tvp23a	Plet1	Syngr2
Epb41l4b	Sema4f	Gm8113	Spns3	Maml2	Hsd11b1	Nrgn	Bdkrb2	Sv2b	Tbc1d2	B3gnt5	Oas1a	Tgm1	Shc1
Ccl3	Plcb4	Spsb1	Arhgap10	Oasl1	Ighv14-3	Phlda2	Jag1	Ms4a6d	Fam129b	Gm26762	Col5a3	Gm44135	Gpr55
Clec10a	Abca17	Bcl2l1	Fcer1g	Sdc1	Igkv8-28	Ggt1	Galnt7	Ptpro	Il22	Pi4k2a	Cd300a	Hsd17b4	Acsf2
a	Qpct	Sema7a	Pecam1	Hdac11	Gimap6	Colq	Txndc17	Osm	Cd37	Parvb	Fcgr3	Mmp14	Dgkh
Derl3	Fam160a2	Pygl	Slc16a3	Glipr2	Pdgfa	Hspa1a	Ccl22	Pltp	Prss16	Cgref1	Ifi47	Zfp52	Slc52a2
Ighv1-75	Kif5a	Zfp831	Ltb4r1	2310031A07	Ighv1-18	Xylt1	Kif3c	Lair1	Il1rn	Mpzl2	Rasgrf1	Smox	Trpm2
Oas1g	Gramd2	Klk8	Clec7a	Sqrdl	Ctsw	Nkg7	Morn1	Upb1	Sema4a	Gm14051	Mgl2	Tmem51	1700011B04
Ighv1-38	Sult1a1	Ltbp1	Mgl2	Clec12a	Tlr7	Serpina3f	Rnf144b	Pilra	Sox4	Scd3	Apobec1	Aldh1b1	Mesdc1
Ptprv	Myo6	Tspan2	Cpm	RP23-421N2	Ehd3	Tnfrsf13c	Emp2	Peli2	Gm43388	Ccser1	Dmxl2	Zfp229	Zfp128
Dab2ip	Hoga1	Tmem231	Arhgef3	Rnaset2b	Gimap5	Fasl	Nol4l	Oas2	Ptgs1	08-Mar	Arap3	Ccl22	Rap1gap
Iglv1	Gm13571	Tnfaip2	Emb	Il23r	Gm22748	Trbv1	Cd96	Ceacam19	Spon1	Mycl	Piwil2	Sphk1	Tbc1d14
Ighv5-16	BC055308	Slamf1	Ddr1	Ighv14-3	Iglv1	Trim43b	Suox	Apobec1	Nupr1	Btla	Klrd1	Il31ra	Ddit4
Fstl3	Nck2	Pltp	Gbp7	Ctla4	Igkv1-110	Gimap8	Kcnn1	Tnip3	Fam65b	Alms1	Palm	Zfp951	Purg
1600010M0	Gm43011	Rps6ka2	Scml4	Slc7a8	Ighv1-2	Zfp507	Fbxw10	Hebp1	Klra2	Fhl2	Abcg3	Cish	Sestd1
Mgl2	Ltbp2	Cd33	A530064D06	Glce	Ighv7-3	Hspa1b	Arhgap31	Myo15	Mzb1	Atg9b	Adgrl3	Il13ra1	Fnip2
Retnlg	Cd3d	Agmo	Ifit3	Gm44448	Iglv2	Tcrg-C4	Gca	Ddx60	Rab3il1	Gpt2	Ms4a7	Pdcd1lg2	Zbtb42
Igkv6-15	P2ry14	Ly75	Ddx58	Plcb4	Kcnn4	Sbk1	Mapre3	Cxcr2	E130012A19	Gm26520	RP24-167A1	Hmgcs1	Gm28884
A4galt	Fasl	RP24-502J3.	Tnfsf8	Laptm4b	1500009L16	Tbxa2r	Il12b	Fcgr3	Igkv4-59	Asap2	Fxyd2	Fkbp5	Pla1a
Trem1	Pi4k2a	Ier5l	Ptgs2os2	Map3k15	Trbv1	Sh2d1a	Sema4c	Hilpda	Ccl2	Gpr171	Mylk	Fbxo46	Fam83h
Ighv2-2	Slc25a26	Tpm2	Abcd2	Macc1	Nt5e	Ighd	Sema6d	Il17f	Rgs9	Ltbp2	Dscam	Tmem173	Cnnm2
Igkv16-104	Noxred1	Mospd4	Tgm1	Lif	Cd79b	Fam65b	Ttyh2	Tmem26	Irf7	Mgll	Igsf6	Mkrn1	Glipr2
Ptgr1	Gm14051	Rilpl1	1700003E16	Gm37535	Itgal	Rem1	Serpinb9	Xkrx	Cd19	Gm19569	Nupr1	Gm14326	Gga2
Ccl7	Cd8b1	Nabp1	Pald1	Cnnm2	Trbv12-2	Sytl1	Slc41a2	Pxdc1	Cd300lb	Cpq	Il18	Rundc3b	Cmc2
C5ar1	Atg9b	Stk32c	Tarm1	Klra5	Perp	Ighv7-3	Yes1	Ddr1	Emp3	Aff3	Trim43b	Hfe	Gcnt2
Ighv10-3	Ptger2	Tnfsf8	Oasl2	Erc1	Klf2	Ly6c2	Nbl1	Ank	Lrp1	Il12b	Gbp3	Itga5	Vat1
Iglc1	Btla	Sult1a1	Zfyve28	Txndc17	Agpat3	Igkv14-111	Fnbp1l	Il17re	L1cam	Popdc2	Tctex1d2	RP24-502J3.	1700025G04
C1qa	Rab13	Cd274	Abcb1a	Il12b	Ighv1-81	Ptprcap	Dscaml1	Pi16	Heg1	Casp6	Oas1g	Klri1	Irf6
Klrb1	Pianp	Htr7	Pilrb2	Rab34	Sema4b	Slc1a4	Mocos	Nfe2	Al504432	Gm42466	1700011B04	Arsa	1700030J22
Ms4a4a	Bcl2l14	Cd86	Zcwpw1	Insm1	Ighv1-72	Apoe	Phf21b	Clec4b1	Csf3r	Fhad1	Btbd16	Zbtb8a	Gnptab
Plaur	Egr4	Amacr	Ptpro	Cds1	Ighv10-1	Itk	Gnb4	Gm15848	Sirpb1a	Sgms1	Upb1	Irf6	Ndrg4
Tmem26	Bag2	Ppp1r3b	Ccrl2	Cdc14a	Phgdh	Gm45552	Mylk	Mcemp1	Slc4a11	Trbc2	Kctd14	Acbd4	Fgd6
Clec4n	Mycl	Arap3	Gm5150	Gm38340	Zap70	Rnf125	Cblb	Ighv1-59	Cd226	Slc6a9	Zcchc3	Cd36	Slc25a24
Iglc3	Gm38228	Zfp770	Stab1	Rasd1	Ctnnal1	Abcb9	Zc3h12d	Oas1a	Sirpb1c	Ubtd2	Crispld2	BC049352	Rac3
Cd14	Adam8	Cxx1b	Cd300lg	Ubash3b	Fam65b	Dusp8	Dpy19l3	Ighg1	Fcrls	Stbd1	Ctrc	Ctrc	Macc1
Ighv2-9-1	Mpeg1	Adgre1	Gbp4	Ncoa7	Foxc1	Rorc	Mtmr1	Krt80	Gm45153	Cd3g	Abcg2	Wfdc17	Lonrf1
Igkv17-121	4930404I05	Tbc1d4	2210406H18	Klhdc8a	Baiap3	Mgst2	Endod1	Tnfsf9	Trib2	Gpsm2	Tmem14a	Relt	Oasl1
Cd300lf	Ctsw	Ccr1	Tnip3	Abca3	Tspan32	Lca5	Pdgfa	Gpnmb	Galc	Zfp57	Mfsd2a	Gm42547	Trim30d
Ckap4	Dync2li1	Tlr11	Il1b	Epsti1	Ephx1	Gimap1	Cpne2	AB124611	Ccr6	6530409C15	Ms4a6d	Gm28884	Ctnna1
Alox5ap	Dpy19l3	Gm11545	Fgr	Hs3st1	Clec9a	Crtam	Zfp873	Ptgfrn	Nr1d1	BC055308	Gm4651	2510009E07	Zdhhc12
Adgrl3	Pde1b	2010300C02	Cd72	Sdc3	Sik1	St18	Trat1	Mefv	Cdyl2	Snx24	Myo1e	Slc35f5	Gls2
Fkbp11	Hgfac	Zbtb42	Sorl1	Ppt2	Angptl4	Dpp10	Tmtc4	Il18rap	Hacd1	Lck	Dpp10	Rin3	Dapk1
Prss57	Afap1	Ssx2ip	Tnfaip3	Myo6	Srpk3	Trbv12-2	St6galnac2	Ptafr	Maml2	D630045J12	Ddx60	Ass1	Mospd1
Gm5547	Cxx1a	Pglyrp2	Gm17944	Gm10441	Inpp4b	Trbc1	Perm1	Il1rl2	P2ry6	Ctsw	Fcgr2b	Ppp1r21	Osbpl1a
Gm45055	Igf2r	Dgke	Tlr5	Atxn1	Cdca7	Iglc2	Ahrr	Adora2b	Whrn	Skap1	Car2	Oas1a	Sort1
Tgfbi	Enho	Als2cl	Slc2a3	Prelid2	Aff3	Peli2	Mtmr4	Slc27a2	Cnr2	Gm37648	Scn2b	Kcp	Pde1b
Hacd4	Apol7c	Spire1	2010300C02	Slc9a4	Grap2	Aqp3	Abtb2	Slc15a3	Ahnak	Oasl1	Ptpro	Gm20257	Pkdcc
Ifitm1	Rhpn1	Zkscan5	Ncf2	Ifi205	Gm12260	Ighm	Rnf24	Gm5150	Bahcc1	Pdlim7	Ptgs2os2	Tlr6	Gm37560
Pilrb1	Trbc1	Msmo1	Zfp658	Ccnd3	Atp2a3	Abcd2	Actn1	Cp	Kctd14	Tmem86a	Camkmt	Ramp3	Dnajb13
Hcar2	Itga8	Pilrb2	Mcemp1	Tpst2	Mef2c	Eaf2	Frmd4a	Nccrp1	Ctsd	Itk	Ints6l	Stat4	Nfe2l3
Cd300lb	Gnb4	Marveld2	Rasgrf2	Lurap1	Cd3d	Pgf	Gal3st2	Arl5c	Klre1	Mllt3	Slc7a7	Rras	Rtn4
Gm5861	Gm44401	Cd84	Prdm1	Tmem27	Iglc3	Efnb2	Aff3	Slc7a11	Tnfrsf12a	Gm1965	Rnf186	Irgm2	Slc33a1
Igkv6-25	Actn1	Siglece	Slc7a11	Ccser1	Nefh	Ets1	Pfkfb3	Tmem176b	Itgal	RP23-292C5	Wls	Bmf	Htr7
Gm43201	Galc	Slc36a3os	Ifit3b	Fbxo17	Nsg2	Adm	Lnx2	Mertk	Fam26f	Mospd1	Siglece	Msmo1	Map4k5
Hbegf	Il12b	Slc16a3	F11r	Fam160a2	Arhgap24	Dkk2	Serpinc1	Ppm1l	Oas3	Tlr11	H2-DMb2	Eepd1	Dock9
Cdhr3	Cst3	Rab30	Ceacam1	Synpo	S1pr1	Gm9994	D17Wsu92e	Ighv1-76	Ighg2b	Crim1	1600010M0	Gm7665	Cpt2
Smim5	Gm3336	Mpzl3	Ank	Cyb561	Cd8b1	Gm43291	Pls3	Clec10a	Kcna3	Met	Ifi27	Prosc	Zyx
Cfp	Chst11	Net1	Trim47	Pou4f1	Slc35f2	Cd37	Llgl2	Il1r2	Myo1e	Oxct1	Cabp4	Foxn3	Itpr1

Table S 4 Top 200 significant genes of same DCs subset in different locations

SAME DCs IN DIFFERENT LOCATIONS														
UP-REGULATED								DOWN-REGULATED						
CD11b	CD103				DP			CD11b	CD103				DP		
LP vs MLN	ML vs MLN	LP vs MLN	LP vs ML	ML vs MLN	LP vs MLN	LP vs ML		LP vs MLN	ML vs MLN	LP vs MLN	LP vs ML	ML vs MLN	LP vs MLN	LP vs ML
Rab9b	1700024P16	Pou4f1	Rgs13	Sh3gl3	Gm12407	Igkv7-33		Ighv1-34	Klrc1	Ptprh	Col25a1	Igkv11-125	Robo4	Reg3g
RP24-161A2	Cwh43	Fut2	Atf7ip2	Ccdc36	Gm9994	Spic		Ighv3-8	Cd163l1	Ighv2-5	Ighv1-37	Igkv1-99	Muc13	Fcgbp
Gm43636	Slc27a3	Mybpc1	Foxh1	Ace2	Gm13589	Tfec		Ighv1-47	Aicda	Igkv4-90	Igkv4-90	Igkv4-79	Psma8	Cdh1
Gm4956	Npr1	Slc27a3	Prg3	Cnga2	Pax5	Pax5		Ighv1-78	Gzmk	Gm973	H2-M6-ps	Igkv10-95	Lypd8	Lypd8
Foxh1	Wfdc13	Npr1	Ifi208	Patl2	Aicda	E430014B02		Igkv1-88	Gzmc	Gzmk	Lypd8	Cadm3	D930020B18	Reg3b
Stra6	Ch25h	Gm9745	Aicda	Gm13589	E430014B02	Krt83		Ighv1-74	Tnfrsf8	Xcl1	Krt19	9830107B12	Gpx2	Dmbt1
Cbln3	Gm9992	Gabrr1	Nptx2	Tgfb2	Ccdc33	Serpina12		Ighv9-2	Zcchc18	Cel	Ighv2-4	Ighv5-9-1	A630091E08	Cntnap2
1700011B04	Pou4f1	Gcm1	Gm14085	BC016579	Atp8b3	Camp		Ighv7-1	Cr2	Klrc1	Ighv1-31	Ighv1-77	Tff3	Entpd3
Atcay	Casc1	Spata31d1b	Oprd1	Itgb8	Lhx2	Klra8		Igkv1-132	Eomes	Cxcl11	Ptprh	Ly6i	Reg3b	Robo4
Tnnt2	Syt7	Gm37535	Cntn1	Ocln	Hgd	Igkv8-34		Igkv15-103	Ccr8	Ighv2-4	Cps1	Ighv1-34	Ighv1-56	Itgae
Cdkn2a	Dpysl5	Casc1	Lpo	Ttc39a	Cpne7	Tmem132c		Ighv14-4	Rgs13	Zcchc18	Cyp26b1	Ighv5-17	Gm14851	Clca3b
Ptk6	Adh4	Stx1b	Ankrd35	Fgfbp3	CR974586.5	Prph		Igkv3-7	Lhx2	Penk	Pnlip	Ighv14-4	Ppp1r1b	Gpx2
Tdh	Gm28706	Etnk2	Gm20465	Hdac11	Tmprss11d	Tmprss11d		Igkv4-79	Emid1	Gm38346	Cwh43	Igkv4-68	Asgr2	Vit
Cdkn2b	Oit1	1700024P16	Gal3st2	Spata31d1b	Gm37711	Aicda		Agr2	B3gnt7	Tmem163	Ighv2-5	Igkv10-94	Defa24	Lgals2
Gprc5d	Asb11	Gm26902	Gm9745	Tmie	1810064F22	Scn3a		Igkv4-91	Epha8	Serpina3f	Ighv3-1	Igkv4-92	Spink4	Tspan8
Gm37223	Gm5424	1700016F12	Aire	Mab21l3	Fam71b	Cacna1i		Ighv10-1	Tmem163	Tlr3	Igkv5-37	Sirpb1b	Vit	Ckmt1
1810064F22	Ass1	Plekhs1	Rimkla	Idi2	Gal3st2	4930426D05		Igkv6-25	Cilp2	Ighv1-31	Ighv1-20	Igkv19-93	D330045A20	Gm14851
Gm37712	Vdr	Spock1	Cfap58	Fndc5	Gm5541	Spink2		Krt18	Ifng	Ighv1-37	Igkv2-109	Igkv9-124	Reg3g	Agr2
Serpinb9b	Sult1a1	Tmprss11d	Tmprss11d	P3h2	Gm16685	Dpp10		Ighv13-2	Cntn1	Gm45014	Ighv1-12	Igkv14-130	Nlrp6	Olfm4
Gm17641	Tcn2	Kcnn1	Gm9994	Serpinb9b	Oprd1	Prg3		Cacna1h	1600012P17	Tnfrsf8	Reg3g	Retnla	Ighv5-15	Spink4
Lad1	Scnn1g	Ido2	Cdhr1	Itgae	Snap91	Zdbf2		Ighv5-15	Tnfsf14	Ighv4-1	Spon2	Bex6	Dmbt1	Gm19434
Dlgap3	Ccl17	Gm5541	2610528A11	Mtss1l	Rgs13	Ip6k3		Ighj4	Prdm8	Cd163l1	Tnfaip8l3	Igkv4-91	Siglecf	Muc2
Ccdc33	Fut2	Gm20465	Il5ra	Kcnk13	Krt83	Mir9-3hg		Serpinb2	Ttn	Rhpn1	Ighv1-53	Ighv1-61	Fcgbp	Muc13
Spata31d1b	Kcp	Foxh1	Insm1	Plppr4	Serpina12	Fcmr		Reg3b	Crmp1	Tnfsf14	Aldob	Sirpb1a	Clca3b	D330045A20
Gm11413	Cdkn2c	Dpysl5	Cr2	Laptm4b	Marco	Gm9994		Muc13	Ecel1	Gzmb	Scd3	Igkv1-88	Ighv5-9-1	Krt19
Cacnb3	Ddit4	Gal3st2	Gm37711	Mgll	Rab42	Gm5541		Ighv1-5	Gm42870	Ighv6-3	Tlr3	Clec4a3	Gm43121	Murc
Dscaml1	AW046200	Gm37712	Epha8	Bcl2l14	Scn4a	F2		Fcgbp	Xcl1	Egr3	Gm973	Ighv1-36	Pilra	Btnl7-ps
Pdilt	Ifit1bl1	Snn	Sec1	Slc9a3r2	Gm14085	1500009L16		Ighv1-36	Il22	Ighv1-81	Ighv5-12	Igkv12-38	Slc5a11	Cdhr5
Nudt17	Cxcl3	Insm1	Hgd	Pbld2	Psca	Cfap58		Ighv14-3	Trbj1-1	Ifng	Defa24	Trem3	Pilrb1	Podxl
Gal3st2	Gm26902	Fscn1	Kcnn1	Exoc3l4	Gm20465	Hgd		Spink4	Cpne7	Ighv14-1	Plce1	Igkv6-20	Cd209a	Angpt4
1110032F04	Ank2	RP24-94F12.	1600012P17	Mylk	Prph	Cpne7		Igkv4-61	Rimkla	Igkv5-43	Ighv1-74	Sirpb1c	Clec4a2	Myh11
Hpcal4	Scin	Dnah2	Gprc5d	Sh2d5	Trbv12-2	Rgs13		Ighv1-59	Klrb1c	Pnlip	Gm38346	Gm9733	Ighv5-4	Plet1
Gm13546	Sphk1	Ankrd35	Ighg3	Lima1	Cfap58	2610528A11		Igkv4-57-1	Fcer2a	Egr2	Ighv14-3	Igkv6-14	Ighv1-49	Car12
1700016F12	Ntn4	Coch	Dscaml1	Ndrg2	Heatr9	Lhx2		Igkv3-2	Bank1	Igkv4-55	Gm42962	Igkv13-85	Ighv5-12	Qpct
Dnajc22	Klra5	Lpo	Spata31d1b	Tmeff1	Dscaml1	1810064F22		Igkv4-70	Ikzf3	Igkv2-109	Igkv4-58	Clec4a2	Ighv1-34	Myo1a
Cd1d2	Alox15	Papss2	Stx1b	Aldh1a2	F2	Marco		Elf3	Timd2	Col23a1	Igkv8-27	Ighv9-1	Ccr1	Ptprb
Gm12606	Stard10	Pla2g4f	Pla2g4f	Ppm1j	Spic	Gm6166		Ighv5-6	Mapk10	Susd1	Ighv5-6	Clec4a1	Krt19	Sparcl1
Rgs6	Mybpc1	Wfdc13	Gm8773	Catsperg1	Serpinc1	H2-M2		Igkv11-125	Spns2	Atg9b	Sparcl1	Igkv8-21	9830107B12	Krt8
Syngr3	Nid2	Dscaml1	Serpinc1	Apol10b	Ccl5	Ceacam15		Ighv1-82	Capn12	Gm26802	Ocstamp	Klra2	Ighv5-6	Adgrf5
Car2	Gstm5	Dthd1	Scube3	Fam160a1	Aire	Mir99ahg		Ighv1-61	Pax5	Igkv8-30	Parvb	Csf3r	Lgals2	Gp2
Extl1	Serpind1	Syt7	Gm13387	Xlr	Kcnh3	CR974586.5		Igkv4-74	Gpr174	Igkv10-94	Ighv1-85	Ighv5-6	Gp2	Cnga2
Pla2g4f	Acot6	Gm9847	Mapk10	Rhoc	Asprv1	Gm12407		Ighv5-12	Gzmb	Serpinb8	Rhpn1	Gm5150	Slc27a2	Agbl2
Dnah2	Wtip	Gng4	Pax5	Tnnt2	Atcay	Eomes		Cldn3	Kcnk1	Iglc1	Igkv12-46	Ighv2-9-1	Ighv9-4	Slc5a11
Tnfrsf4	Pkib	Plppr4	Gspt2	Pik3r3	Il23r	Tdo2		Ighv1-72	Tnfsf11	Lgals2	Ptprv	Ighv3-1	Gsg1	Tff3
Atf7ip2	Gm11724	Ndrg4	Plekhs1	Ccdc120	Tdrp	Klra4		Ighv1-20	Gpr15	Sarm1	Ighv5-15	Igkv12-98	Ighv9-1	Siglecf
Gm26535	Tmem131	Tmem150c	Asprv1	Afap1	Bambi-ps1	Gm16685		Clca3b	Cecr2	Eomes	Ighv1-69	Gdf15	Aldob	Kcne3
Ikzf4	Rnaset2a	Slc25a29	Gm12407	Spo11	Fcmr	Ngp		Ighv1-77	Il17a	Cps1	Ighv5-17	Igkv2-112	Ctnnd2	St18
Ceacam15	Stk39	Cfap58	Fcmr	Rragd	Insm1	Wdr95		Cps1	Trp73	Cacna1e	Ighv1-61	Igkv3-10	Siglece	Dpt
Nipal1	Glis3	Zfp872	Cilp2	Crtam	Trim43b	Ighd		Endou	Cd19	Plvap	Qpct	Ighv6-3	Cdh1	Fut1
Adcy6	Gm43201	Lamc2	H2-M2	Slamf1	Ankrd35	Gal		Ighv9-4	Gzma	Cyp26b1	Lgals2	Tmem26	Reg1	Lepr
Tnfrsf9	Plce1	Tnfrsf4	Dpp10	Cd247	Myh7	E230020D15		Upk1b	Ighg1	Igkv9-120	Reg3b	Tnfrsf17	Cd209c	C1s1
Stx1b	Tcea3	Dlgap3	Ankrd33b	Gm9574	4930426D05	F10		Igkv17-127	Fcmr	Ptprv	Tmem150b	Ighv1-63	Mmp12	Gsg1
Efna2	Ints3	Thbs4	Gm9847	Gm16712	Ip6k3	Gm37121		Ighv1-18	Ret	Bank1	Ighv1-78	Igkv6-15	Ocstamp	Pianp
Arpin	Pdcd1lg2	Ccer2	Slco5a1	Fbln5	Cacna1i	Scn4a		Slc16a5	2610528A11	Gzma	Igkv12-44	Clec4b1	Trem1	Fbln1
Fscn1	Afap1	Ccr7	Card14	Serpinb6b	Tnnt2	Trim43b		Igkv12-41	Prg3	Igkv8-27	Ighv5-4	Cyp4f37	Entpd3	Bmp4
Idi2	Apcdd1	Gm13546	Ido2	Rab13	Tmem150c	Gm20465		C130089K02	Mctp2	Ikzf3	Igkv10-94	Ighv5-4	Ighv1-61	Sema6b
Gm8221	Gm26809	Cacnb3	Serpinb9b	Foxc1	Cdh26	Gm37711		Ighv1-64	Rgs16	Ighv1-22	H2-M5	Cd300lg	Tie1	Fam189a2
Gm10851	RP23-421N2	Gm37696	Fcer2a	Gclc	Ceacam15	Gm21188		Igkv12-46	Siglech	Mmp28	Nlrp1c-ps	Igkv4-55	Cps1	Ighv1-49
Gm20465	Gm9776	Oprd1	Gcm1	Heatr9	Arc	Slc6a1		Ighv5-17	Iglv2	Igkv5-39	Igkv8-19	Ifitm6	Pilrb2	5730435O14
Gm16685	Mycl	2310030G06	Sowahd	Msrb3	Lpo	Asprv1		Ighv1-39	Btbd11	Igkv1-117	Ighv1-63	Fcgr1	Ighv1-77	Gm33280
Cib3	Sh3pxd2b	Ankrd33b	D330050G23	Slc18a1	Tmem132c	Ighg1		Gpx2	Cxcr6	Nuggc	Pilrb1	Cyp4f16	Clec4b1	Tmeff1
Tmem150c	Il31ra	Gm43636	Gm13589	Synpo2	Gspt2	Slc1a2		Igkv3-4	Cdh22	Dusp18	Tbxas1	Igkv5-45	Myh11	Cdx1
Apol10b	9630013D21	Nudt17	Treml2	Arc	H2-M2	Cldn10		Igkv12-44	Trgv2	Iglv1	Gm26520	Igkv6-25	Cntnap2	Spon2
Tm4sf5	Dnah6	Cdkn2b	1110032F04	2510009E07	Fah	Gal3st2		Igkv8-28	Rgcc	Fosb	Ltbp4	Trp73	Ifitm6	Ppp1r1b
Eno3	Vwa3b	Tmie	Eno2	Ncoa7	Fam89a	Dscam		Ighv1-37	Klrb1f	Igkv6-17	1700009J07	Gucy2c	Cd101	Pgf
Stap2	Gm10441	Gm37223	Tnnt2	Rnaset2a	Hcn3	Cadm3		Ighv3-6	Serpinc1	Gm7580	Naaa	Ighv5-16	Il1a	Acot6
Ppp1r1a	E330020D12	D330050G23	Snap91	Zdhhc14	Ndnf	Bambi-ps1		Igkv4-72	Nuggc	Ighv1-85	Gsg1	Oas2	Cd33	A530064D06
Smim22	Ap1s2	Rgs6	Tdh	Syngr3	Eomes	Cdh22		Igkv4-58	Mef2b	Rapgef3	Dpt	Ighv1-42	Clec4g	Kif17
Hcn3	Gm28100	Rnaset2a	CR974586.5	Gbp4	Spata31d1b	Anxa8		Ighv1-76	Trdc	Ighv5-16	Olfm4	Scn3a	Kcne3	AW822252
Nme9	Nectin2	Gspt2	Tmem150c	Tcrg-C1	Slco5a1	Blk		Muc2	Myo5b	Naaa	Ighv1-76	Igkv4-53	Plet1	Ltbp4
Arc	Map3k10	Cd63	Spic	Fbxw10	Synpo2	Cd19		Krt19	Cd22	Gm42870	Gm26802	Ighv8-5	5730435O14	Cd101
Ankrd35	Plcd3	Adcy6	Tmie	Arap3	Atf7ip2	Ly6i		Igkv5-45	Tcrg-C4	Rgs16	RP23-312B1	Nodal	Muc2	Cyp2s1
D330050G23	Snx24	Tdh	Clu	Scin	E230020D15	Adam11		Igkv13-84	Xrcc5	Gas7	Igkv4-61	F10	Ighv1-5	Clec4b2
Phkg1	Gpr55	Hcn3	Ndnf	Ccl22	Ighd	Oprd1		Igkv16-104	Blnk	Igkv6-15	Cxx1b	Pkd1l2	Igkv12-98	Cd200r4
Snn	Scd4	Synpo2	Zfp872	Slc22a23	Dapl1	Zbtb32		Ighv1-54	Grpr	Egr4	Serpinb8	Msr1	Ighv14-1	Eln
Apol7c	Mkrn1	Glipr2	Gm16685	Sptb	Calm4	Uchl1		Ighv1-7	St6galnac2	Olfr433	Ighv1-22	Ighv1-69	Igkv6-14	Cysltr1
Ccl22	Hvcn1	Adgrg6	Rnf152	Pcbp4	Nudt17	Clec4a3		Igkv8-19	Atf7ip2	Cxcr3	Ighv1-72	Ifitm3	Gm37347	Ccr1
Mreg	Gm13546	Scin	Cd19	Ido1	Ido2	Cdhr3		Ighv1-42	Sh2d2a	Tctn2	Igkv1-117	Clec10a	Gm45014	1810011H11
Icam5	Cds1	Asphd2	Map6d1	Net1	Dpp10	Nrgn		Igha	Txk	Ighv5-9-1	Tifab	Igkv8-27	Mgl2	Cd209c
Zfp872	Syngr2	Cnga2	Dthd1	Src	Phlda2	Fam20c		Ighv1-69	Ip6k3	Qpct	Igha	Abca9	Ighv1-74	Cd33
Gm6166	Bcl2l14	Itgb8	Synpo2	Epsti1	Pbld2	Mdk		Ighv2-2	Crispld2	Igkv4-86	Hic1	Ighv1-74	Igkv3-2	Atp8b1
Serpina3i	Pacsin2	Serpinb9b	Atcay	Fscn1	Icam5	Mid2		Jchain	Foxs1	Hes1	Rasgrp4	Igkv4-90	Mrvi1	Camkk1
Gm9847	Prelid2	Arc	Lhx2	Vwa5a	Kctd19	Kcnh3		Igkv5-43	Blk	Adrb2	Ighv1-5	Ccl2	Gm13373	Ccdc162
Kcnh3	Slc25a42	Asprv1	Fut2	Dscaml1	1500009L16	Ccdc184		Aoah	Psd2	Parvb	Mrvi1	Ltb4r1	Dpt	Vwa1
Gm14328	4930426L09	Mreg	Lef1	Pdgfa	Fam160a1	Gm6637		Igkv1-122	Gm45153	Ighv2-9-1	Igkv6-20	Ace	1810011H11	Col23a1
Rhoc	4931406C07	Ch25h	Ip6k3	Gm8221	Cd19	Serpinc1		Igkv13-85	Egln3	Igkv1-110	Gm13373	Igkv12-46	Gm14023	Scd4
Il7r	Slc52a2	Scnn1g	Tcf7	Rnaset2b	Gm37712	S100a4		Igkv4-55	Podnl1	C4b	Igkv6-17	Plxna4os1	Igkv4-68	Tmprss2
Plek2	Etnk2	Gm10851	Ehf	Zc3h12d	Gcnt4	Aire		Ighv2-6	Ly6d	Adamdec1	Igkv5-48	Ighv1-59	A530064D06	Nlrp6
Socs2	Itga3	Acvr1c	Chst3	Pla2g16	Pla2g4f	Ndnf		Ighv6-6	Il2rb	Ptger2	Eln	Tgfbi	Etos1	Tie1
Gm44950	Ctif	Adh4	Heatr9	Sema6d	Ighg1	Foxs1		Ighv9-3	Kcnk5	Acyp1	01-Mar	Mertk	Ighv1-26	Gm44860
Gm8773	Gm17767	1110032F04	Stra6	Parp3	Cryaa	P2ry13		Igkv5-48	Pou2af1	Igkv3-10	A530064D06	a	Itgam	Mfap4
Fabp5	Pkdcc	Sec1	Blk	Fam83g	Thbs4	Gm14085		Igkv4-59	Cd79a	Dusp6	Ighv1-81	Igkv6-17	Ighv1-36	Dcn
Ctrc	P4ha2	Gm37975	Kndc1	Myom1	Klra4	Fut7		Ighv1-26	Pgap1	Ighv1-53	Igkv4-79	Ighv9-4	Igkv13-84	C4b
Gm42601	Mfsd2b	Jag1	Spock1	Tnik	Extl1	Retnla		Igkv17-121	Msc	Emid1	Ighv1-64	Gm8890	Ighv5-17	Siglece
Ndrg4	B230354K17	Ighg3	Spib	AW112010	Cacnb3	Ccl5		Ighv8-12	A630023P12	Akr1b8	Gm7580	Ms4a6c	Adgrl3	Fgfr1
Slc25a29	Prodh	Ifi208	Etnk2	Perm1	Anxa3	Tdrp		Plvap	Nptx2	Ighv1-69	Sash1	Ptgir	Ltbp4	Pdlim3

Mylk	Gm37560	Adora2a	Papss2	Ido2	Scube3	Gm45552	Igkv14-126	Slc35f2	Focad	Ighv5-9-1	Cd209a	Ighv1-47	Cd209b
Syne4	Rgag4	Socs2	Acvr1c	Bcl2l1	Slc4a8	Fah	Ighv1-9	Tdrp	Dhrs9	Olfr433	Igkv3-2	Ighv8-12	Slc52a3
Lima1	Cmc2	Idi2	Itgb8	Ikzf4	Rgs6	Atcay	Igkv4-57	Fasl	Olfm4	Ighv10-3	Ccr10	Gucy2c	Pilra
Mmp25	Oosp1	AW112010	Cryaa	Ppp1r1a	Gm10851	Fabp5	Igkv6-15	Tcrg-C2	Igkv1-135	Ighv1-52	Mmp12	Fabp2	Ms4a4d
Slc4a8	Map3k15	Fxyd2	Socs2	Cmtm8	Tcf7	Il9r	Igkv10-94	Igkv4-80	Egr1	Slc9a9	Cx3cr1	Olfm4	Fhl1
Timm8a2	Rap1gap	Ikzf4	Arc	Nbl1	Cd70	Lpo	Tie1	Serpina3f	Spry1	Shroom4	Igkv8-16	Cfh	Xlr
Slco5a1	Sqrdl	Map6d1	Anxa3	Tmem200b	Gm6166	Myh7	Mmrn2	Susd1	Disc1	2310040G24	Bhlha15	Cd244	Arap3
Gm28884	Met	Rnf152	Asphd2	Cptp	Cdh22	Tlr7	Ighv1-53	Arhgap24	Igkv5-48	Wdfy4	Igkv17-121	Ighv2-4	Calml4
Eno2	Acsf3	Slc18a1	Cacnb3	Ahrr	Tnfrsf9	C1qb	Plxna4os1	Bspry	Ighv10-3	Itgae	Ighv1-53	Igkv4-91	Dapk1
Tcf7	Zbtb42	Gm12407	Tnfrsf4	Icam5	Clu	Clu	Sparcl1	Gimap6	Ighv1-75	Cfh	C1qb	Sparcl1	2900026A02
Gm28100	Rnaset2b	Vdr	1700016F12	Lad1	Zfp872	Rgs6	Igkv9-124	Dkkl1	Ighv8-12	Ppef2	Mgst1	2900026A02	Epcam
Casc1	Cd14	Tcn2	Extl1	Palld	2610528A11	Insm1	Igkv6-23	Iglc3	Slc39a8	Lrrc18	Igkv6-23	Qpct	Gm42962
Dpysl5	Tlr13	Dnajc12	Cxcr5	Fam89a	Chst3	Ncr1	Ighv5-16	Tox	Igkv13-85	Sult1a1	Fcgr4	Nxpe5	Ighv1-56
Rragd	Aldh1a2	Il7r	Nudt17	Large1	Sptb	S100a8	Ighv8-8	Il23a	Impa2	Igkv10-96	Cd300ld	Igkv6-20	Gm11870
Strip2	Rab13	Rhbdl3	Ccl5	Pygl	Gm12260	Ccl9	Ighv1-63	Itk	Prss57	Slc6a9	Ccl4	Apob	L3mbtl4
RP24-502J3.	C030037D09	Marcksl1	Capn12	Tanc1	5033430I15F	Gspt2	Igkv4-53	Usp2	Trib3	Itln1	S100a4	Angpt4	Dennd2c
Slamf1	Sfxn2	Zmynd15	Fscn1	Gm11613	Sh2d1a	Cdhr1	Aatk	Colq	Ighv6-6	Scd4	Ighv1-55	Misp	Fgd1
Catsperg1	1700016F12	Gm37711	Mreg	Cpne2	Tnfrsf4	Ankrd35	Bex6	Tnfsf10	Itga8	Ppfia4	Mafb	Ighv2-5	Cfh
2210408F21	Snx22	Fam89a	Ptgs2os	Adcy6	Mef2b	Carmil3	Tff3	Gm19585	2610318N02	Cxcl11	Igkv8-30	Cysltr1	Trem1
Ces2c	Gm5602	Nipal1	Il7	Cacnb3	Tmem158	Ms4a1	Igkv4-69	Atcay	Iglc3	03-Sep	Clec4n	Tspan8	Irf6
Igsf3	Cpne8	Sowahd	Jag1	Ttyh2	Gm37975	Calm4	Igkv6-32	Sytl1	Gm43291	Ighv1-75	Clgn	Serpinb2	Ighv5-15
H2-Q10	Gga2	Slco5a1	Gzmc	Rnf24	Mdk	Tmem158	Igkv4-68	C3	Igkv3-12	Igkv13-85	Rgs18	Ighv1-39	Gm16185
Tspan3	Adam19	Gm11724	Cd70	Glipr2	Epsti1	Chst3	Ighv1-15	Gimap7	Cd93	Mctp1	Igkv16-104	Ighv1-59	Pilrb2
Gm42602	BC049352	Spib	Rapgef4	Sema4c	Eno2	S100a9	Igkc	Baiap3	Slc35f2	Slc7a8	Adgrl3	Trem3	Zcwpw1
H2-Eb2	Tmem35b	Scn4b	Cxcl13	Cttn	Zmynd15	Mex3a	Ighv1-56	Kif21a	Ighv1-20	Slco3a1	Clec5a	Ighv1-78	Mical2
Insl6	Ppfia3	Stap2	Ntn5	D17Wsu92e	Fgfr3	Dscaml1	Ighv1-22	Nkg7	KIAA1683	Med12l	Cd300lf	Igkv6-17	Pilrb1
Tnni1	Gpr85	Tspan3	Hcn3	Tmem8	Ccdc184	Klrb1f	Ighv1-55	Cd28	Nr4a1	Slc25a43	Clec4a4	Cd300lf	Gm33370
Large1	Rap2b	Lad1	Cd63	Oprd1	Ace2	Cdh26	C1qa	Zfp507	Jchain	Xcr1	Ms4a4a	Igkv12-46	Nlrp1c-ps
Mmp23	Acsf2	Gm17767	Gm37712	Morn1	Plppr4	Gpr174	Igkv1-110	Cd79b	Ighv14-2	Ighv1-80	Mzb1	Itgae	D930020B18
Scn4b	Bcl2a1a	RP24-502J3.	Phlda2	Insl6	Gm13994	Fxyd2	Sele	Crtam	Ighv3-6	Mical2	Igkv12-44	Camkk1	Pcyt1b
Insm1	Gm7694	Rragd	Slc4a8	Sh3bp4	A430093F15	1300017J02	Igkv3-1	Stx1a	Nfatc2	Anxa1	Gm8879	Igkv4-57	Mxra7
Anxa3	Hc	Scube3	Cc2d2a	Ndrg4	Lef1	Tmem176a	Igkv1-117	Tmem158	Angptl4	Igkv6-14	Fabp1	Agr2	Col14a1
Ccl17	Zbtb8a	Fas	Adcy6	Cttnbp2nl	Tdh	Sh2d4a	Ighv1-31	Cd93	Fos	Ighv1-66	Cd300c2	Igkv17-121	Dip2c
Ido1	Camk2b	Gm10441	Cecr2	Fnbp1l	Zdbf2	Gm37975	Ighv5-4	Ighd	Gm37352	Vwa1	Cd300e	Igkv8-21	Slco3a1
Id2	Mmp25	Rhoc	Cpne7	Arhgef40	Cecr2	Tmem150c	Igkv6-17	Sbk1	Osgin1	Igkv1-135	Igkv17-127	Ighv5-16	Dtx4
Papss2	Mesdc1	Mfsd6l	Idi2	Oasl1	Fgfbp3	Adm	Ighv10-3	Abcb9	Igkv4-79	Camkk1	Gm5086	Clec10a	Gpr161
Ccr7	Zfp358	Aire	Zmynd15	Cd8b1	Laptm4b	Gm12260	C1qc	Gimap8	Srgap3	Ighv10-1	Clec4d	Igkv10-94	Sdk1
Synpo2	Csrp2	Gm44293	Arhgap28	Trpv4	Pdgfa	Mef2b	Igkv6-20	St6galnac3	Gna15	Serpinb2	Itgam	Pkd1l2	Arhgap18
Ttc39a	Ndrg4	Gm37856	Sell	Extl1	Cdkn2a	Heatr9	Igkv12-98	Trp53i11	Cln8	Ighv1-50	Igkv1-133	Abca9	Klk8
Piwil4	Gpr33	Extl1	Slc25a29	Zscan20	Colq	AB124611	Pde9a	Fam65b	Tnfaip8l3	Atg9b	Csf1r	C130089K02	Tlr3
Nqo1	Lrrc3	Gm4956	Gm37223	Gm2065	Dscam	Klrg2	Ighv1-75	Bcat1	Crtam	Gm15964	Hes1	Ighv1-53	Garnl3
Il2ra	Zyx	Fgfbp3	Ccr7	Mmp25	Serpinb9b	Fcrl5	Ighv1-50	Nrgn	Inpp1	Ighv1-82	Ighv1-78	Ms4a6d	Plvap
Kctd19	Purg	Ace2	Dlgap3	Reck	Mab21l3	B3gnt7	Itln1	Sntb1	Gm36933	Gcg	A4galt	Clec4b2	Pigr
Map6d1	Gng4	Alox15	Cdkn2b	Gbp5	Spo11	C1qc	Igkv8-21	Sit1	Msh5	Ighv3-6	Ccl3	Styxl1	Rps6ka2
Cd1d1	Csf2rb	Anxa3	Myo5b	Arhgap22	Gm43636	Gm8773	Igkv19-93	Rorc	Ltbp4	Gm45014	C1qa	Ighv3-1	Gcnt1
Pcbp4	Abtb2	Gls2	Mtss1l	B3galnt1	Mmp23	Timd2	Igkv12-89	Tcrg-C1	Acss1	Tbkbp1	Igkv6-32	Ighv5-9	Micall2
Aldh1a2	0610009L18	Spsb1	Il9r	Mapre3	Cmpld2	Lpar3	Ighv1-80	Tmem121	Mns1	Igkv4-59	Cfp	Gm33280	Ppm1j
Ccl5	Mettl21a	Gatsl3	Ecel1	Prkcq	Naprt	2900052N01	Igkv10-96	Rnf144a	Plk3	Igkv4-53	Prss57	Igkv19-93	Lpar1
Cdk15	Med17	Samsn1	Slc30a2	Endod1	Papss2	Gm4956	Reg3g	Dtx1	Tnfrsf17	Styxl1	Ctnnd2	Il1r2	Rnf144b
Chdh	AA467197	Pbld2	1810064F22	Uhrf1bp1	Ms4a1	Cx3cr1	Ighv2-9-1	Phlda2	Serpinb2	Igkv3-2	Lyz1	Cd300lg	Kcnk13
Esam	Tnr	Laptm4b	Snn	Ly75	RP24-254O2	5033430I15F	Ighv4-1	Ebf1	Entpd1	Unc119b	Ms4a6d	Rnf128	Il1a
Mras	Bcl2a1c	Ppl	Ighd	Gm9994	Insl6	Dapl1	Bhlha15	Bcl11b	Muc13	Ifi205	AI839979	Slc36a3os	Rnf128
D130040H23	Ucp2	Dnajc22	Fam184b	Cmc2	Cr2	Gdf15	Ighv1-58	Dusp18	Hivep3	Igkv17-127	Igha	Galnt3	Pald1
Myom1	1700025G04	Pdcd1lg2	Samsn1	Amot	Patl2	Cryaa	Igkj5	Ankrd37	Ighv7-3	Fhl1	Pilrb1	Atp8b1	2510016D11
Kcnn1	Ifit3	Efna2	Slc22a4	Pfkfb3	Adcy6	Cd37	Ighv1-12	Rnf125	Sdad1	Ckb	Lyz2	Clec4a4	Gpr141
AI480526	Rnf217	Insl6	Tmem200b	Hcn3	Mx1	Igsf3	Kcnk1	Gm13589	Igkv17-121	Dapk1	Igkc	Nlrp3	Nlrp1a
Plppr4	RP24-94F12.	Stat4	Efna2	Apol7c	Sell	Izumo1r	Egfl7	Mgst2	Tet1	Unc119	Lpl	Ckmt1	Zfhx3
Ido2	Npas2	Patl2	Gm43636	Serpind1	Fscn1	Chil3	Igkv2-112	Gfpt2	Dynlt1a	Plbd1	Plaur	Ighv1-7	Clec4g
N4bp2l1	Fbxo46	Sphk1	Ace2	Mtmr4	1700025B11	Pla2g2d	Adamdec1	Il9r	Chac1	Zfp57	Ighv1-26	Gpr141	Serping1
Tmem19	Gatsl3	Rab42	A430093F15	Cd3e	Ncr1	Crispld2	Igkv9-123	Ctse	Tfrc	Gm43011	Tspan15	B430306N03	C1ra
Sult1a1	Gls2	1700011B04	Srpk3	Mocos	Trbv1	Gm42602	Igkv2-109	Ighg2b	Slc6a9	Igkv12-41	Iglc3	Ccdc162	Ocstamp
Fam89a	Chpt1	Rpl10a-ps2	AW112010	Ttc39c	Tnni1	Sell	Ccr10	Cacna1e	Trgv2	Cd34	Fkbp11	Sdk1	2510009E07
Slc22a23	Dock5	H2-Eb2	Gbp8	Serpinb9	Slc25a29	Slco5a1	Igkv8-30	Apol7e	Igkv10-96	Ighv5-16	Stk32c	Ptger3	Gm13373
Ankrd33b	Plek2	Tm4sf5	Lad1	Tcp11	Idi2	Bex6	Lypd8	Gm14207	Camkk1	Rab7b	Ccl7	Sh2d1b1	Eps8
Lpar3	Rhoc	Sod3	Gm37696	Suox	Lipc	Sucnr1	Ighv1-62-2	Cd2	Cacna1h	Gm44205	Ighv1-39	Dapk1	Kifc3
Asprv1	Itpr1	Tcf7	Scn4b	Cd3g	Il9r	Dtx1	Ighv1-19	Rasgrp2	Igha	Ppt1	Alox5ap	Ifitm3	Htra3
Eid2	Ifitm2	Slc4a8	Gm15931	Arhgap31	Cdkn2b	C1qa	Ighv1-81	Rgl3	Ighv1-78	Tlr12	Nfe2	Igkv3-10	Cpm
Exoc3l4	Dgcr6	Strip2	Kcnh4	Tapbpl	Cd247	Siglech	Epha2	Xylt1	Iigp1	Sftpc	Cd300c	Svip	Mylk
Fam3b	Vat1	Gclc	Il7r	Tnfrsf4	Igsf3	Lrp8	Hes1	Nt5e	Tlr12	Gm8113	Il1r2	Atp1a3	Svip
Fndc5	Acadm	Gm43690	Stap2	Aplp1	Strip2	Smad3	Iglv1	Ets1	Ighv1-12	Dmbt1	Tnfsf14	Ltb4r1	Rasgrf2
Gng4	Trim30d	Eno2	Pglyrp2	Lnx2	Blk	Tdh	Ighv5-9-1	Acod1	Gucy2c	Snx22	Prss16	Cd300ld	Rapgef3
Adora2a	Zdhhc12	Gm26535	Tmem123	Gal3st2	Sh2d4a	Tmem176b	Igkv6-14	Sytl3	Kazn	Igkv6-13	Rasgef1c	Spon2	Ctnnd2
Gm37975	Htr7	Car13	Bdkrb2	Pi4k2b	Gm42602	Ube2e2	Ighv1-85	Flt3l	Igkv12-98	Pigr	Sh2d1b1	Plau	Gpr82
Rpl3l	Zbtb7b	Il15ra	Tdrp	Gm37712	Gal	Cd2	Itga9	Tesc	Gm8113	Dynlt1a	Ighv1-72	Cd300c2	Nxpe5
Htra1	Txnip	Rap2b	Ttn	Gm12216	Rragd	Klrb1c	Ighv9-1	Zfp831	Ighv1-55	Ighv1-26	Fstl3	Ms4a4d	A630091E08
Fnbp1l	Cst3	N4bp2l1	Pbld2	Zmynd15	Cd8b1	Cdc42ep3	Iglc1	Tmem71	Spon2	Gm12892	Derl3	Calml4	Hic1
Timd4	Rad51b	RP24-94F12.	Eno3	Glce	Cd63	Cecr2	Igkv3-12	Trbv12-2	Mir212	Hoga1	Ccr2	Cyp2s1	Agmo
Sema6d	Bcl2a1d	Nuak1	Gbp4	Tyk2	Gm9847	Ighv1-38	Igkv12-38	D8Ertd82e	Nrg2	Unc13b	Emilin2	Igkv9-124	Ppp1r3b
Mrc2	Pxmp2	Gm16685	Fas	Nol4l	Sh3gl3	5830444F18	Igkv14-100	Hspa1b	Gm38248	Gm10484	Pilra	Cd300a	B430306N03
Gm43413	Mitf	Arl5c	Adgrg6	Gm26603	Il22	Cst7	Gm16553	St8sia1	01-Mar	Gm2a	Ocstamp	Hpgd	Cd209a
Ocln	F830112A20	Dnah6	Fah	Micall1	Gm37215	Mctp2	Lgals2	Itgb3	Ighv1-58	Ighv1-55	Npl	Igha	Gm38140
Tnr	Trpm2	Tcea3	Colq	Uba7	Chst2	Nuak1	Igkv3-10	Themis	Igkc	Dhrs9	Igkv1-135	Hic1	Il1rl2
Mpzl2	Cttn	Hgd	Cdh22	Arhgap28	Gjb2	Lipc	Pla2g2d	Slc40a1	Igkv4-70	Cysltr1	0610040J01	Eln	Spint1
Ace2	Gm43323	Csf2rb2	Adora2a	Kpna3	Sgca	Gm14328	Nlrp3	Ms4a4c	Ptpn7	Slamf8	Ighv8-12	Gm16894	Gsn
Serpinb6b	Tnik	Gm42601	Ppm1l	Cblb	Slc1a2	Npl	Ighv1-66	Hspa1a	Igkv12-46	Cass4	Esr1	Igkv6-15	Cxx1b
Itgb8	Epb41	Cib3	Il15ra	Ube2l6	Trbc2	Ebf1	Prss16	Trbc1	Eln	Gm37309	Fcgr3	Cd34	Dip2a
Rac3	Tusc1	Ramp3	Crispld2	Gnb4	Ankrd33b	Tnni1	Ighv1-52	Myo1e	Ighv3-1	Psma8	Clec4e	Cd300e	Aldoc
Slc27a3	Stbd1	Rftn1	Gm37856	Acsf3	Prkcq	Colq	Igkv1-135	Cdh2	Mef2c	Pianp	7330423F06	Clec4n	Gm26835
2600006K01	Lrrk2	Slc30a2	Eya2	Tmem150c	Rhbdl3	A430093F15	Fosb	Tbxa2r	Ppef2	Gm43914	Egr2	Lepr	Asgr2
Chst10	Ccdc149	Ifit1bl1	Cib3	Cdkn2b	Col27a1	Itga9	KIAA1683	Ablim1	Igkv8-24	Pilrb2	Jchain	Nlrp1c-ps	Scel
Rnaset2a	Trim25	Il7	Pcbp4	Actn1	Mctp2	Cr2	Fam83f	Atp2a3	Ighv1-74	Hk3	Cd14	Igkv13-85	Lpar5
2200002D01	Map3k14	Slamf1	Prdm8	Ptpn21	Prkg1	Rem1	Igkv3-5	Il5ra	Ighv1-26	Egr1	Ffar2	Adamdec1	Ptger3
Nck2	Ifi211	Sez6l	RP24-94F12.	Dnah2	Lck	Gm8369	Fcgr1	Muc1	Dnph1	Igkv4-72	Klrb1	Milr1	Cxcl2
Pdcd1lg2	Tmem198b	Gm5424	Rasl11a	Ccl5	Exoc3l4	Scube3	Igkv8-27	Sytl2	Ighv1-52	Tmem27	Mag	Cd209b	Gm14023
Il7	Snn	Mmp23	Mdk	Mrc2	Spib	Anxa3	Igkv5-39	Rapgef3	Tm6sf1	Entpd1	C1qc	Ighv1-69	Prkd3
Syn3	Pik3cg	1810064F22	Gm10399	Rgmb	Fas	Col27a1	Fosl1	Dscam	Hspa1a	Itga8	Igkv14-111	Gpr82	Rasd2
Dkk2	Ttll1	Ass1	B3gnt7	Idi1	Stap2	Vcam1	C4b	Iglc2	Tbxas1	Asb2	Slc36a3os	Mfap4	Kif9
Zfp606	Gm38115	Stxbp6	Irak3	Gm44950	Sema6d	1700016F12	Igkv4-62	Apoe	Gm1965	Igkv3-10	Prg3	Plet1os	Gm37347
E130311K13	Cxcl2	Catsperg1	Plppr4	Ankrd35	Efna2	Tubb2b	Igkv4-90	Sh2d1a	Plbd1	Adgra2	Ckap4	Ms4a6c	Rab39
Tnfrsf18	Ikzf4	Pik3r3	Gjb2	Wdr90	Trat1	Lrp8os2	Cd163	Ccdc184	Igkv4-58	Dennd2c	Mgl2	Col14a1	Plau
Gatsl2	Suox	Dock9	Rpl10a-ps2	Dock9	Itgb8	Ldhb	Atp1a3	Slco2b1	Hpgds	Mycl	Ryr1	Ighv1-18	Gm45221
Tmem120b	Pde1b	Serpind1	Tmem176a	Frmd4a	Slc22a23	Sh2d1a	Igkv8-24	Slc1a4	Derl3	Egr3	Gm37347	Rasgrp4	Nlrp1b
Gm37267	Slc39a1	Slc22a4	Dusp14	Elmo3	Bdkrb2	Apoe	Igkv4-50	Nlrc3	Hspa1b	Havcr2	Cln8	Ighv2-9-1	Nlrp3
Tmem123	Bak1	Plxnc1	Arg2	Bzrap1	Rasd1	Gm45153	C1qb	St3gal6	H2-DMb1	Gm43201	Bhlhe41	Pianp	1700003E16
Laptm4b	St7	Vwa3b	Gpc1	Slc22a4	Tmem121	Zfp872	Cd209d	Gm43291	Ighv9-3	Clec4b2	Ighv1-12	Igkv2-109	Nrep

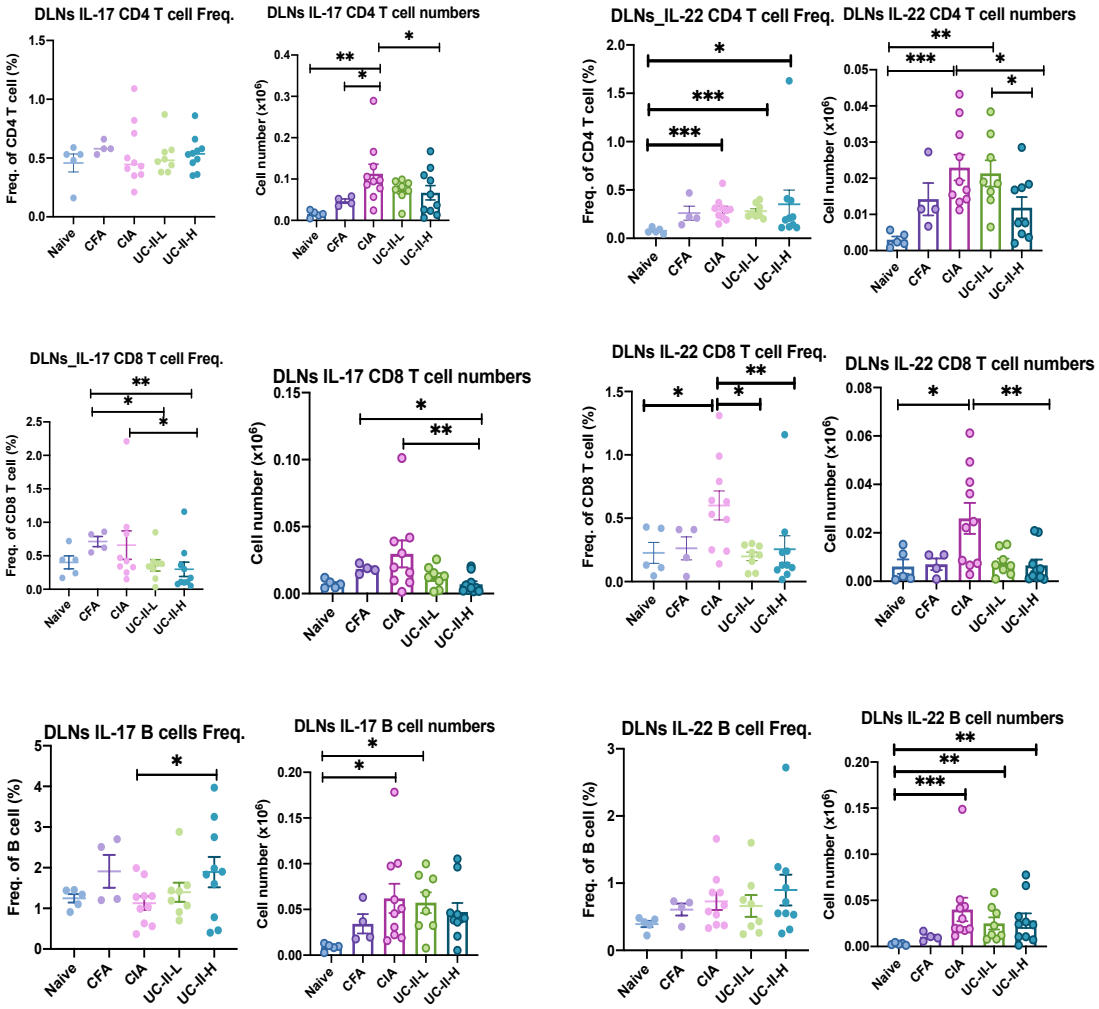

Figure S 1 Individual bar chart for Figure 3-8.

Raw data for radar chart in Figure 3-8. Regulation of IL-17 and IL-22 producer in the draining lymph nodes upon UC-II administration. Cell frequency and total cell numbers of IL-17+ and IL-22+ CD4 T cells, CD8 T cells and B cells in DLNs. Each dot represent one individual mouse. Statistical significance was determined using Ordinary one-way ANOVA. Significance indicated by asterisks, *p < 0.05, **p < 0.01, and ***p < 0.001. CFA, Complete Freund's Adjuvant; CIA, collagen induced arthritis; UC-II-L, UC-II lower dose; UC-II-H, UC-II higher dose.

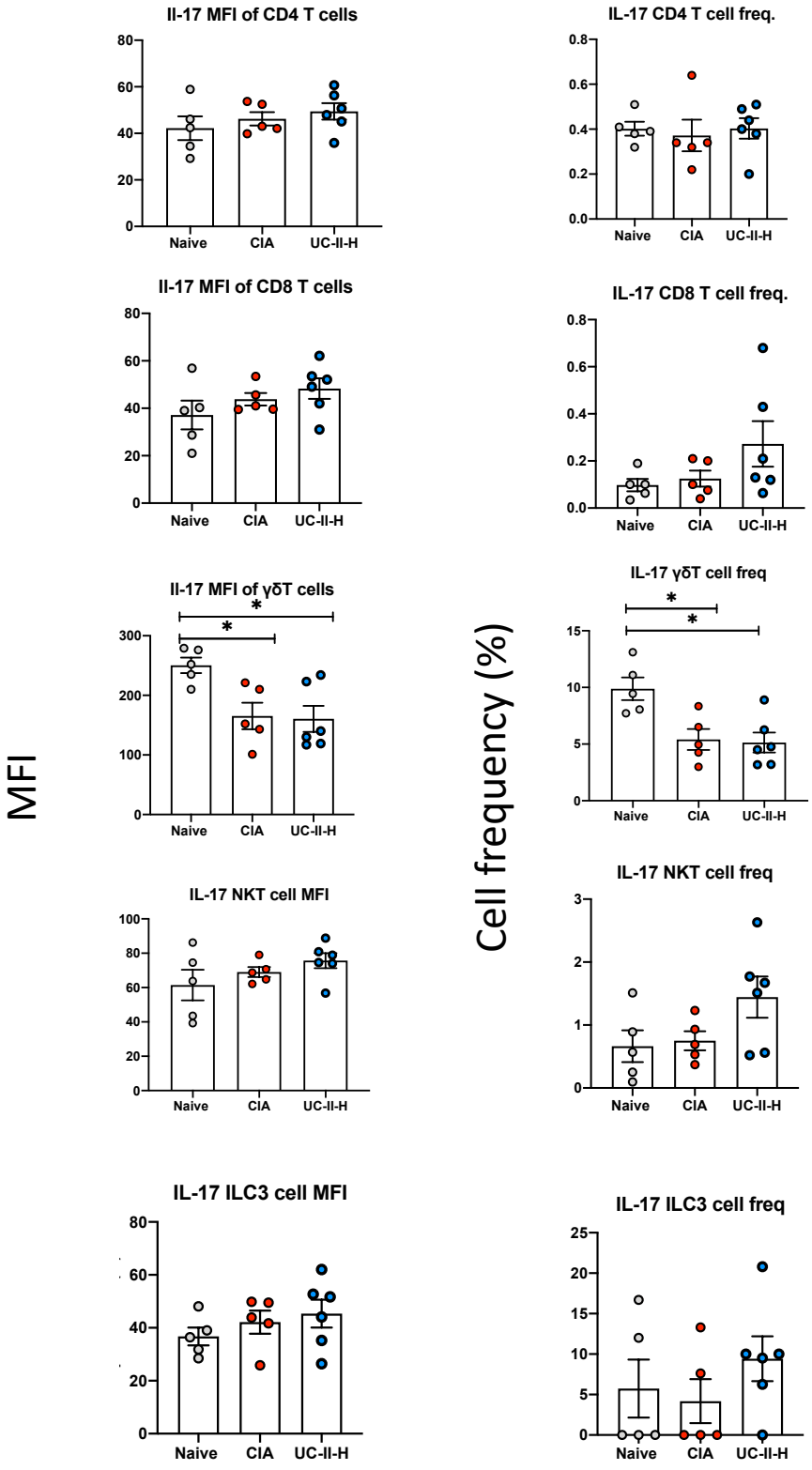

Figure S 2 IL-17 expression in mLNs.

Raw data for radar chart in Figure 3-14. Regulation of IL-17 producer in the mesenteric lymph nodes upon UC-II administration. Cell frequency and mean fluorescence intensity (MFI) of IL-17+ Producers. Each dot represents one individual mouse. Statistical significance was determined using Ordinary one-way ANOVA. Significance indicated by asterisks, *p < 0.05.CIA, collagen induced arthritis; UC-II-H, UC-II higher dose.

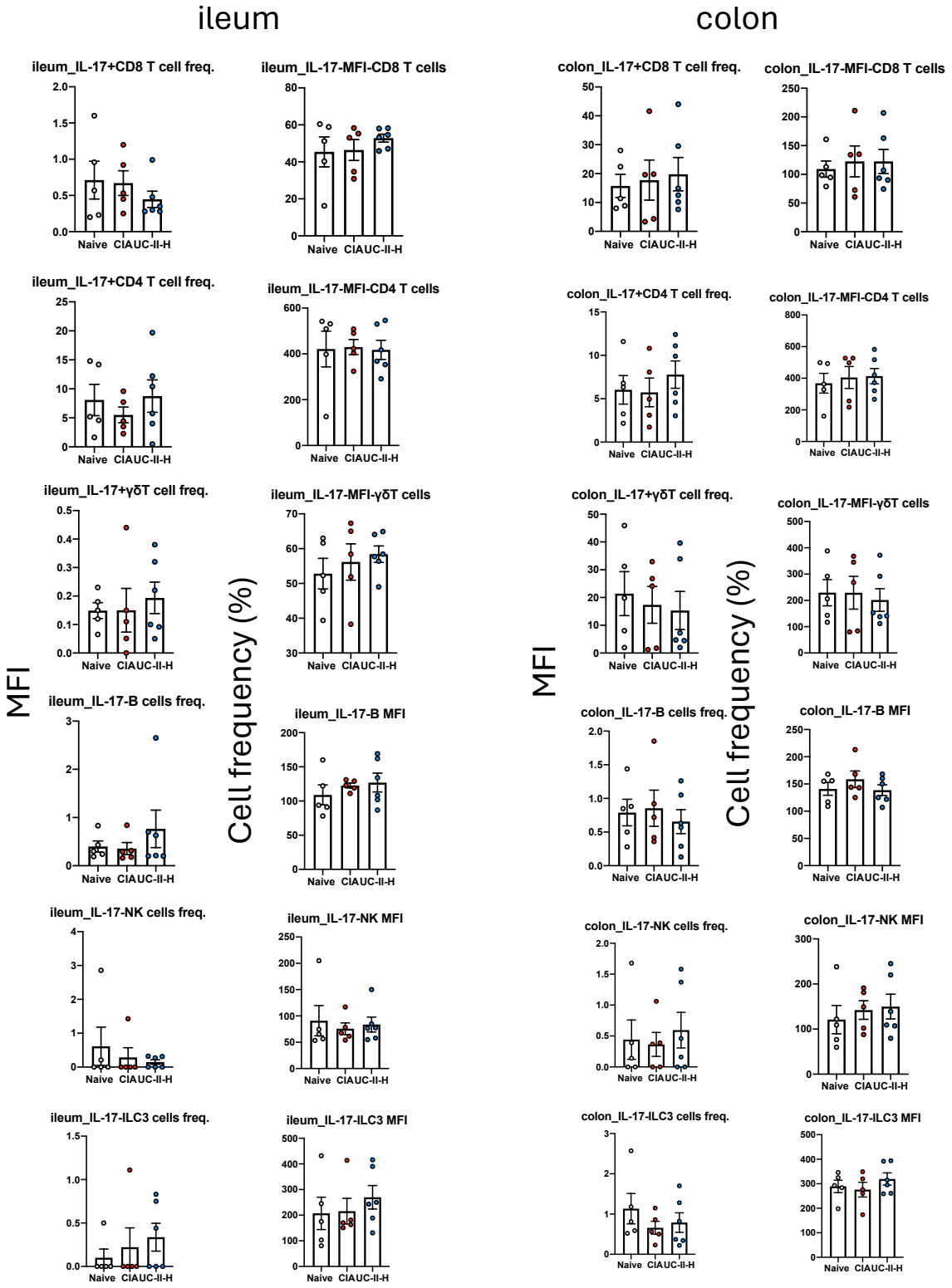

Figure S 3 IL-17 expression in the ileum and colon

Raw data for radar chart in Figure 3-14. Regulation of IL-17 producer in the ileum and colon upon UC-II administration. Cell frequency and mean fluorescence intensity (MFI) of IL-17+ Producers. Each dot represents one individual mouse. Statistical significance was determined using Ordinary one-way ANOVA.CIA, collagen induced arthritis; UC-II-H, UC-II higher dose.

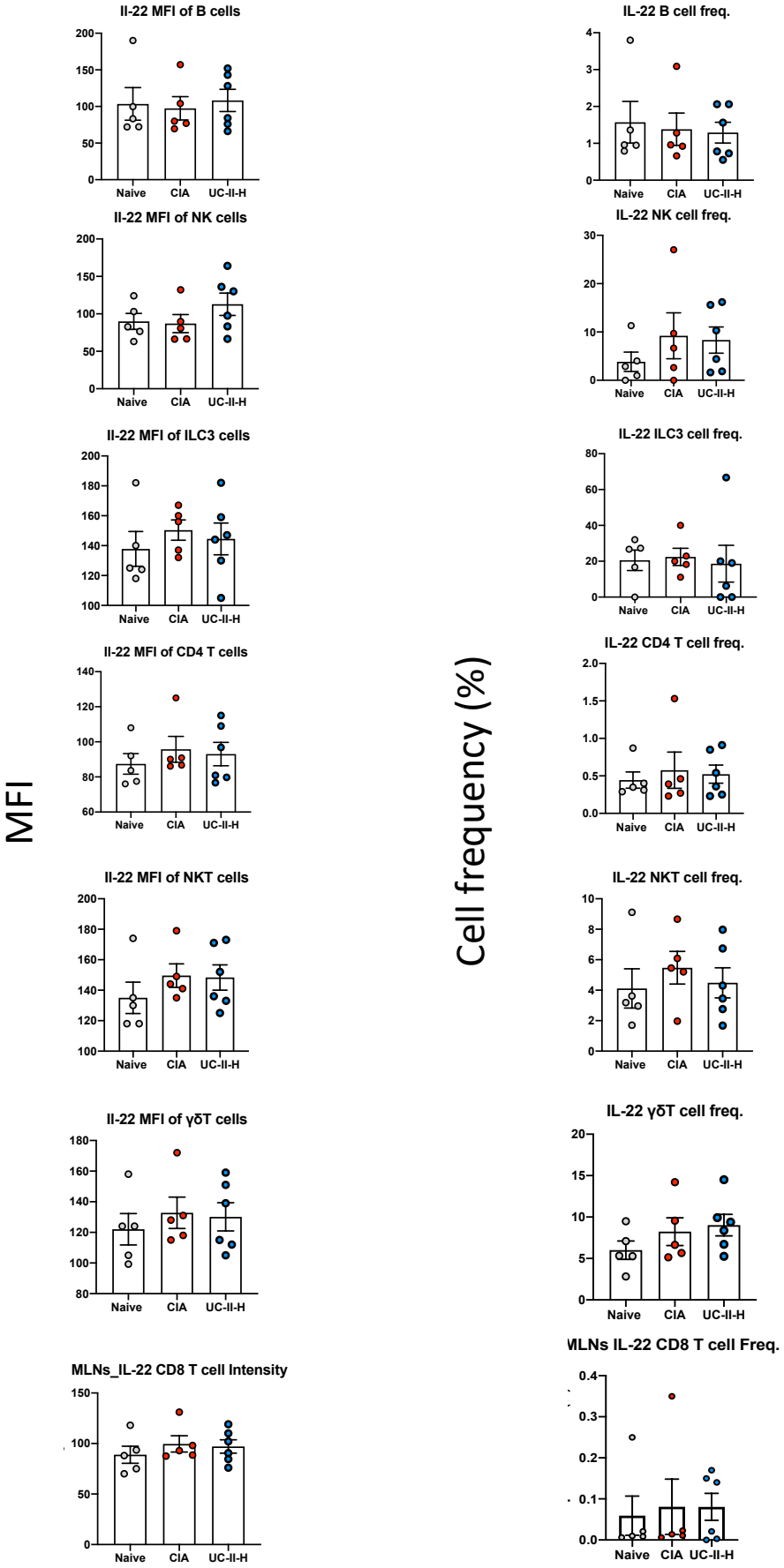

Figure S 4 IL-22 expression in mLNs

Raw data for radar chart in Figure 3-15. Regulation of IL-22 producer in the mesenteric lymph nodes upon UC-II administration. Cell frequency and mean fluorescence intensity (MFI) of IL-22+ Producers. Each dot represents one individual mouse. Statistical significance was determined using Ordinary one-way ANOVA. CIA, collagen induced arthritis; UC-II-H, UC-II higher dose.

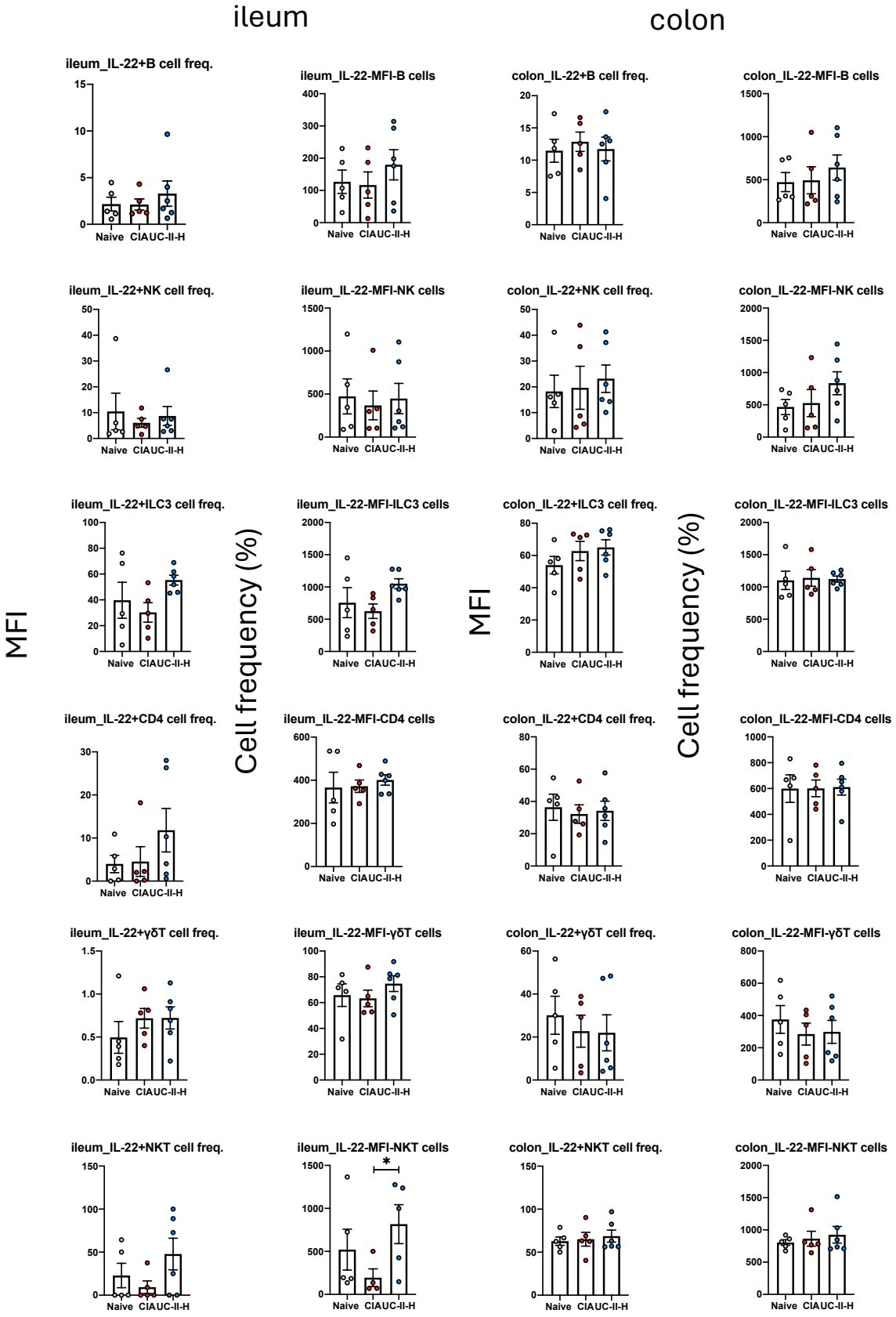

Figure S 5 IL-22 expression in thel ileum and colon.

Raw data for radar chart in Figure 3-15. Regulation of IL-22 producer in the ileum and colon upon UC-II administration. Cell frequency and mean fluorescence intensity (MFI) of IL-22+ Producers. Each dot represents one individual mouse. Statistical significance was determined using Ordinary one-way ANOVA. Significance indicated by asterisks, *p < 0.05. CIA, collagen induced arthritis; UC-II-H, UC-II higher dose.

Data of RNA-seq in Chapter 4

The data used in Chapter 4 is accessible on OneDrive (within the University of Glasgow) at:

https://gla-my.sharepoint.com/:f:/g/personal/xxxxxxxx_student_gla_ac_uk/ElPnkjyN431lqsnijdLlXl0B-mtokgfZoevCpebi3Wl4kg

Data is available externally upon reasonable request to the author:

Email:XXXXXXXX@student.gla.ac.uk